Toward single motor driven biped robot

Li, Mingjian

2006

Li, M. (2006). Toward single motor driven biped robot. Doctoral thesis, Nanyang Technological University, Singapore.

https://hdl.handle.net/10356/6547

https://doi.org/10.32657/10356/6547

TOWARD SINGLE MOTOR DRIVEN BIPED ROBOT

By

Li Mingjian

M.Eng, Hunan University, China (2000)
B.S., Harbin Institute of Technology, China (1997)

A thesis submitted in partial fulfillment of
the requirements for the degree of
Doctor of Philosophy

at the
Division of Mechatronics and Design
School of Mechanical and Aerospace Engineering
NANYANG TECHNOLOGICAL UNIVERSITY
January 2005

Author……..
School of Mechanical and Aerospace Engineering, NTU
January 20, 2005

Certified by……..
Xie Ming
Associate Professor of Mechanical and Aerospace Engineering, NTU
Thesis Supervisor

Toward Single Motor Driven Biped Robot
by
Li Mingjian
Submitted to the School of Mechanical and Aerospace Engineering
on January 20, 2005, in partial fulfillment of the requirements for the degree of
Doctor of Philosophy

Abstract

Biped robot system as a mobile mechanical system must consider the energy efficiency problem in addition to other traditional performance requirements. Many researches show that a lightweight and low inertia mechanism is the predominant solution. Since actuators often contribute to a significant portion of the biped robot's weight, this thesis addresses the issue through the way of reducing the number of actuators in a biped robot. In the extreme situation, a scheme of biped robot powered by only one motor is prompted.

To achieve the goal, this thesis presents a modular robot actuation technology called Single Motor Driven (SMD) which can power an articulated robot as well as parallel one with only one motor. Drive torque for the module is tapped from a central rotating shaft using clutch. The position and velocity of the modules are regulated by controlling the engagement time of the clutches using the Pulse Width Modulation (PWM) technique. With experiments, SMD technology proved its ability to transmit and distribute mechanical energy.

Elastic Actuation (EA) technology, as the complementary technology to SMD, is proved to have the ability to modulate and control the mechanical energy flow. It has a spring intentionally placed between the SMD mechanism and robot link. Measuring the spring strain gives an accurate measurement for closed-loop joint torque control. The low spring stiffness allows for high control gain while maintaining system stability. This gives EA many desirable properties including high bandwidth at moderate torque amplitudes, low output impedance, large dynamic range, internal error rejection, and tolerance to shock loading.

The combination of SMD and EA to the so called "Advanced SMD" is very suitable for biped robots, which interact with the environment very often and are required to have as small total weight as possible. This thesis investigated the detailed properties of both SMD and EA. Their combination and application in biped robots are demonstrated as well. An experimental Purposeful Elastic Joint (PEJ) robot based on the SMD and EA concept has been designed and fabricated. The mathematical model of the PEJ is developed. Experimental and simulation results are compared. Based on the theory of variable structure systems and nonlinear PWM control, a local controller is designed and tested on the PEJ. In the modeling and simulation of SMD biped robot walking, an effective gait planning method is developed to generate the stable walking gait only based upon several simple walking parameters. The local controllers and gait planning algorithm are integrated and tested with an SMD biped robot in ADAMS. The experimental and simulation results show that the combined actuation approach of Advanced SMD for biped robot is viable and promising. With brief discussion on future work of SMD biped robot, the thesis predicts that real walking SMD biped robot will come to world soon.

Thesis Supervisor: Xie Ming
Title: Associate Professor of Mechanical and Aerospace Engineering, NTU

Acknowledgements

Without the support of my family, completion of this thesis certainly would not have been possible. I am grateful to their tremendous patience, understanding, and care which they have shown during my academic endeavours. I would like to specially thank my wife for her bearing with me spending so little time with her during my doctorate program.

I am thankful to my supervisors, A/P Xie Ming, who had a cruicial role in my PhD study. He was a source of valuable guidance and assistance for conducting research and overcoming it's numerous, and often unexpected obstacles. His insights and experience had a positive influence on my work, particularly, in terms of providing proper research directions, and developing ideas for writing papers and this thesis. The time and efforts he had devoted to my PhD topic are truly appreciated.

I am grateful to all the technicians at the Robotics Research Centre of Nanyang Technological University, especially Mr. Lim and Ms. Egnas for their support during the manufacturing of the PEJ. I also would like to achnowledge the financial support of the Singapore Technologies Kinetics (STK) and Singapore-MIT Alliance (SMA).

I am indebted to Chia Hon Fai and Hendra for their help in writing the thesis.

Finally, last but certainly not least, I am thankful to all my friends such as Jaya, Tan Huai, Zhou Yuan, Ronaldo, Ten Min Hai, Mahesh, Arun and many others for all their assistance (too numerous to mention), enlightening discussions and enjoyable occasions.

Contents

List of Figures

List of Tables

1 Introduction

In the future, it is believed that human being will coexist with robots in the same society and environment. In order to move in such an environment, the robots must have legs and arms and most important, walk like a human [1].

Walking machine can be tracked back to 1960's. The first biped locomotion mechanism was developed by Kato and Tsuiki [2][1]. Since then, more and more robot researchers have focused there attention into this challenging field. Human being, which has hundreds of bones and hundreds of muscles, can be thought of over-actuated and super redundant from view of robotics, therefore we are able to do very complicated tasks. Currently biped walking mechanism, however, limited by actuation/control engineering and technology, are always under-actuated. For such an under-actuated mechanism, the first thing to do is always defining the feasible motion, or gait planning when walking alone is considered.

Zero Moment Point (ZMP), initially proposed by Vukobratovic and Juricic [3], is the most used concept in biped gait planning. It is formally presented and completely explained in [4]. Based on the ZMP method, Hirai *et al*. [1] proposed the concept of Center of Actual Total Ground Reaction Force (C-ATGRF) in the Honda Humanoid Robot; Goswami used concept of Foot Rotation Indicator (FRI) in analysis of biped postural stabiltiy [5]. These concept/criteria are to describe the feature of dynamic stability for bipedal walking. The static stability criteria are mainly used with Center of Mass (CoM) or Center of Gravity (CoG). Because static walking is usually too slow and has little application potential, this thesis will only consider the biped robot that can dynamically walk.

1.1 Inspiration

Some walking robot, like the 5-link biped introduced by Furusho and Masubuchi [6], the biped model in [7] and [8], did not consider the ankle joint. However more and more

[1] In 1971 the research team of Professor Vukobratovic in the Mihajlo Pupin Institute, first in the world, developed an active exoskeleton that enabled walking of the paraplegics.

researchers realized that foot with certain shape and functional device such as sensor is very important for complex and stable walking. Two feet transformed the 5-link biped into 7-link one, with introducing large power motors in two ankles.

Large power motor exist not only in ankle joint, but also almost every other joint. This is because biped walking mechanism is highly nonlinear. For a predefined stable gait, torque peaks exist in every joint therefore large power motor at every joint is needed. Limited by current engineering and technology, large power DC motor always has bulky size and heavy weight. These drawbacks largely degrade current biped robot's performance. For example, the Honda P2 robot has 20 kg battery on board, but because of the total weight of 210 kg, it can walk only 15 minutes [1][2]. Therefore to minimize biped robot size and weight is a big challenge for biped researcher and engineer.

There are many ways to achieve "lightweight, low inertia" properties, such as modularization, new structure material application, centralized actuator deployment, pre-designed appropriate controller, and so on. This thesis will address this problem through the only way that how biped robots are actuated. With analysis, it is spreaded into two questions: how the actuators are deployed, and how the single actuator works. Two consequent questions are: how to transmit and distribute the mechanical energy to every joint of the biped robot, and how to modulate and control the mechanical energy flow in every joint of the robot. Before the analysis goes on, three sets of comparisons are presented.

1.1.1 Mechanical vs. Electrical

Mechanical system and electrical system have a lot of similar features. They all can be modeled as a second order dynamic system, in which the force F (linear force or torque) and voltage U play the similar role – supply power, either mechanical power or electrical power. The velocity (linear or angular) V and the electrical current I play another similar role – deliver the power. Their product, which is FV for mechanical system and UI for electrical system, is the flow of energy, or simply power.

Mechanical components and electrical components also have similar features. The mechanical friction is similar to the electrical resistance – both have the trend to block energy flow[3]. The mechanical mass or inertia is similar to electrical inductance – both

[2] Present-day powering sources like lithium batteries allow autonomy of longer time usually up to several hours.

[3] In engineering, this feature is called system stiffness.

have the trend to delay energy flow. The mechanical spring is similar to electrical capacitor – both have the property of "storing" energy and then "delivering" it after a short while. Such comparisons can be made more, and point out that mechanical system and electrical system have many similar features and can be made a fair comparison.

Based on these similar features, a domain-independent representation of physical system called "bond graph" was made in [9], and a mechatronic simulation software called "20-sim" was developed in University of Twente [10]. Our focus, however, is to find someway to reduce the overall weight of biped robot, and a question based on the comparison is prompted – Since electrical system usually has one electrical power supplier, can mechanical system like biped robot also has only one mechanical power supplier, or actuator?

Single Motor Driven (SMD) technology, which was brought out in NTU/IVL, is the possible answer to this question. Chapter 3 will discuss SMD technology in detail.

1.1.2 Modular vs. Nonmodular

Current robot designs usually target a specific application, and produce robots that are monolithic in construction. Although successful in the intended application, these robots often become ineffective in other areas. This hinders widespread robot use especially in "3D[4]" and other critical environments where diverse needs must be met. The solution lies in producing highly adaptable robot architectures. This may be achieved by developing a robot architecture based on component modularity. As discussed in [11], such an architecture provides many benefits including

- Improved system versatility by making them reconfigurable
- Easy integration of emerging technologies
- Reduced development costs in the long run
- Selective integration of fault tolerance
- Reduced threat of system obsolescence

Also, developing a standardized modular architecture delivers a great deal of freedom to the design process. Examples of this freedom are apparent in the standardization of computer buses and languages. While the design of the bus structure of many computer systems could be improved with modern technology, the stability afforded by remaining with a standard has produced a significant amount of products to support it. However one must note that a trade-off exists with the use of standards in that

[4] Danger, Dirty, and Dummy environment.

they are introduced at the expense of increased performance. To help alleviate this problem, a set of standards must be developed so that it not only considers current system demands but also predicts future requirements. If this insight can be introduced in the design of the standardized modular robot architecture, the compromise between performance and standardization will be acceptable.

Several modular robots have been recently developed, such as the modular robot system in [12], the Reconfigurable Modular Manipulator System RMMS [13], the modular robot system TOMMS [14], the robot platform SIRIUS [15], and the modular robot in [16]. Below are two successful modular robots which, by means of modularization, achieved relatively light weight.

Bryngelson and Tosunoglu [17] present the development of a 7-DOF robotic manipulator that is based on standardized, modular design philology. This manipulator is referred to as the ALPHA manipulator since it is an Advanced Lightweight Prototype High-performance Arm. The configuration of the component modules of this manipulator consists of a 3-DOF shoulder module, a 1-DOF elbow module, and a 3-DOF wrist module interconnected by link structures. With modular design and particular actuator selection, the total weigh of this arm is less than 160 kg.

DLR's three generations of light weight robots (LWR) are more successful in reducing the overall weight. LWR I [18] with it's 18 kg weight, a nearly 1:2 load to weight ratio and its carbon fiber grid structure links was a highly mechatronic arm, but its double-planetary gearings with a 1:600 reduction turned out to be too critical in terms of tolerance-safe manufacturing. In addition, its inductive torque sensing was critical in terms of complexity and robustness. In LWR II [19], harmonic drive gearings and strain gauge based torque measurement system were embedded into a full state measurement and feedback system, including motor position, link position, and joint torque. Again all electronics, like signal, power, and control, was fully integrated into the arm weighing 17 kg and having the capacity of carrying 8 kg. The third version of LWR was under constructing in DLR. It will be fully built up on all the experiences made in LWR I and LWR II, and one of the main concern is to reduce its overall weight and make it "the lightest robot that has been built so far" [20].

1.1.3 Actuator vs. Actuation

A robot is made up of mechanical segments that are linked by joints, and moved by actuators. In mechanical domain, any motion is produced by the conversion of mechanical energy [21]. For a robot, the actuator is a motor or valve that converts other

kind of power into mechanical power (robot movement). In other words, an actuator is a power converter which converting energy flow between two different power domains. Because the output power is always mechanical power, it can also be considered as a mechanical power supplier.

Currently, only electro-magnetic, hydraulic, and pneumatic actuators have the power and torque capability required for robot tasks. Hydraulic actuators, which have the highest torque and power density characteristics of any of the actuation methods, are capable of performing tasks which involve the application of thousands of Newton-meters of torque and many kilowatts of power output. However, their very high output stiffness characteristics, which make the hydraulic actuator essentially a pure position source, can render it very dangerous. The output impedance, as compared to the driven manipulator and environment, is virtually infinite, generating very high impact loads during collisions. Thus, hydraulic actuators have very poor application cases in robot. Pneumatic actuators on the other hand can be made very compliant. Due to the near zero inductance of the compressible gas, their output impedance is low over a wide frequency range, reducing uncontrolled impact loads to potentially safe levels. However, pneumatic actuators have very low bandwidth capabilities, and thus are only used in such circumstance where mechanical contact occurs, like the robot end-effectors.

As a result of the limitations of pneumatic and hydraulic actuators, most current robots use actuation devices that employ electro-magnetic actuation as their primary torque source. And the mechanical power supplier – electrical motor – plays the key role. This thesis will consider the only situation that using EM motor as mechanical energy source.

1.2 Motivation

The need to build machinery for the purpose of accomplishing automated or semi-automated tasks drives the development of what is sometimes termed application-driven technology [22]. In robotics, a fundamental machine limitation is often directly related to limitations in the actuator technology driving the system. Particularly in larger machines, issues concerned with power density (power-to-mass ratio) and torque density (torque-to-mass ratio) of the actuators can greatly restrict the overall machine payload and power range.

This thesis, with the goal to achieve sole EM motor powered biped robot, is the first investigation toward the development of a new actuation technology (advanced SMD)

for robotics. It should be noted that the amount of available literature on "Single Motor Driven" is all but non-existent, though Serial Elastic Actuator has been proposed for sometime. This work is a pioneering effort toward the advanced SMD technology as well as the new concept of SMD biped robot, and hopefully it will ignite an interest in this exciting new area.

1.2.1 Design Aspects of Biped Robot

Although the end goal of production of a biped robot may at present have few if any industrial or commercial applications, the technology development needed to implement such a system sets challenges which form an excellent test bed and demonstrator for new structures, mechanism, devices and techniques and as such forms an excellent research tool. It is for the many problems to be faced in producing a biped robot that the task has been suggested has one of the major challenges for robotic technology and technologists [23] [24].

In identifying the production of a biped robot as a goal for development it is initially important to determine the level of human like characteristics and components required. Is the aim exact human replication, physical replication or functional replications? Similar functional/physical replication can be identified in the robot structure which may look human but do not use bones, cartilage etc. From this it would seem that the goal of biped robot development is human physical/functional replication and this will be the strategy selected in this work.

The development of any biped robot project requires the blending of a number of areas of technology some of which are well developed, while others still require considerable research. The identifiable components of a biped robot include the following four aspects [23] [24] [25]:

- Mechanical/Skeletal Structure

This concerns both the physical structure/anatomy of the robot and the materials to be used in construction to provide low mass with good strength and flexibility. With regard to the anatomy the usual specified requirement is for a biped walking robot with one trunk, twin thighs, two shanks, and two feet. For the materials it has been suggested that composite materials such as carbon fibres will be optimum. The use of composite material is of course analogous to the human bone.

Clearly there has recently been much work on the area of anatomy and materials, with a range of examples of construction of the components section such as legs, arms, hands, and even some scale and full sized humanoid robot [26] [27] [28].

- Actuators and Power Sources

This aspect of technology concerns the storage, generation and delivery of power to the robot. For most robotic applications the favored power source has been electrical drives with some limited use of hydraulic and pneumatic cylinder drives [29]. Although these systems have been well proven and successful in conventional industrial robot applications the need to operate in unconventional environments will place new constraints on these designs. For these new application domains, actuators will be required which combine controlled motion and high power/weight and power/volume ratios with portability and safety for humans operating close to or in cooperation with the robot (or other systems). These restrictions have prompted work on a variety of new actuation systems with potential for use in generalized as well as specific areas. These new technologies include: Shape Memory Alloys, Electro-Rheological Fluids, Magneto-Astrictive Actuators, Ultrasonic Motors, Polymeric Actuators, and Pneumatic based system [29]. As with the skeletal structure of the robot it has been suggested that a new form of soft actuator may provide a valuable source for biped drives. Among the most promising of the new actuators with these characteristics is a pneumatic system, Pneumatic Muscle Actuators (PMAs) derived from a mechanism, known as the McKibben muscle, pioneered in the 1960's [30].

- Sensory Systems

These sensory systems equal to the human sense of vision, audition, taste, smell and touch. As with previous discussions the need for all these functions can be questioned, but as a generic test system they must be specified. In addition it may be that sense not presently available to humans but available through technology, e.g. x-ray, can be incorporated [31] [32].

Clearly of these sensors, vision and audition are well developed with cameras and microphones able to perform close to, at or above the capacities of the natural analogues. Unfortunately the same cannot be reported for the other senses. As yet there are no good or even barely adequate commercial equivalents to skin, muscle and all their associated nerve responses, while the situation for taste and smell is even worse with only limited research (although some progress) and as yet no viable equivalents to the natural senses [33].

- Intellectual Capacity

The ability to function at an intellectual level similar to a human has long been a subject for debate amongst researchers in AI, and a full discussion is beyond this thesis. It is sufficient to say that at present there are accepted to be no machines with human

intellect [24], however, there are many research activities aimed at developing machines and robots with cognitive abilities both simply as computers and as humanoid type robots.

1.2.2 Actuation and Torque Control

Actuation is the process of converting some form of energy into mechanical force and motion. An actuator is the device or mechanism that accomplishes this energy conversion process. An electro-magnetic motor with a gear transmission is an example of such actuators.

With few exceptions, standard robot actuation systems are poor at creating accurate torques in robot joints. The reasons for this inaccuracy include friction, stick-slip, back lash in transmissions, cogging in motors, and reflected inertia through transmission. All of these real phenomena induce torque noise in the actuator. The effects of torque noise are minimized when controlling the position of trajectory of the robot. The mass of both the robot and the actuators are low-pass filter for torque noise on positional output. This is one reason why robots are so successful at trajectory control even in the face of torque noise. However, for tasks requiring good torque control, the torque noise in the actuators can be problematic.

Good torque-controlled actuators have several important measures: torque bandwidth, mechanical output impedance, dynamic range, power density and torque density. The first three measures are related to one another, and typically an improvement in one yields an overall improvement. An increase in power of torque density usually means that the other three characteristics suffer in performance.

- Bandwith

The torque bandwidth is a measure of how quickly the actuator can generate commanded torques. Bandwidth is the highest frequency at which the actuator creates a near one-to-one output torque to desired torque[5]. The bandwidth must be sufficient to transmit accurate torques through the robot structure. Most torque control tasks only require a few hertz bandwidth as demonstrated by the low bandwidth of human muscle. However, improving the bandwidth of the actuator above the minimal operational level can only improve the overall capabilities of the robot.

[5] A -3dB magnitude of output torque to desired torque is typically considered the bandwidth. -3dB is roughtly 70%.

- Impedance

Mechanical output impedance[6] is defined as the minimum amount of torque an actuator outputs for a given load motion. In the simplest terms it can be thought of as the stiffness of the actuator output. Ideally, the impedance of a torque controlled device is zero. Low impedance means that the actuator appears to the robot as a pure torque source with negligible internal dynamics. An actuator with low impedance is sometimes referred to as being back-driveable.

- Dynamic Range

Dynamic range is the maximum output torque divided by the minimum resolvable output torque increment of the actuator. It gives a measure for how sensitive the actuator is to small torques with respect to its full torque output capability. A large dynamic range is desireable because it permits the actuator to be used in a versatile way in both very sensitive activities and in large torque situations. Humans have very good dynamic range.

- Torque Density and Power Density

Torque density and power density are not necessarily operational characteristics. Nevertheless, these qualities refer to an actuator's ability to generate torque or deliver power to the robot per unit mass and unit volume of the actuator respectively. Having high torque and power density means that a small package can output a lot of energy. Lightweight actuators prevent over-burdening the robot structure with excess mass and allow for quick and responsive robot performance.

Electrical motors with gear reductions are the present-day actuator systems that have high torque and power density and can also achieve moderate to high bandwidth. Unfortunately, neither system possesses low impedance or large dynamic range qualities required for good torque control.

1.3 Problem Statement

1.3.1 EM Motor Has Deficiencies

Electro-magnetic (EM) motors are well understood [22]. They are easy to model and control because they are linear for the most part. In the simplest model, motor torque is proportional to current. EM motors are also typically easy to back-drive and have low impedance. This means that a small external torque on the motor shaft will cause it to

[6] Throughout this thesis mechanical output impedance is referred as impedance or output impedance.

accelerate. There are many other merits for EM motor such as clean, low cost, easy accessibility of electricity for energy source and so on. All these merits make EM motor the first choice for biped robot actuator.

Besides those merits of EM motor, torque density and power density are also important to robotics applications. Unfortunately EM motor usually has low torque density and power density. The fundamental gaps of torque density and power density are the primary "deficiencies" of electric actuators when compared to other kind of actuators such as hydraulic actuators. To implement EM motor in robotics applications, some other means, usually speed reduction mechanism, must adopt. Unfortunately these means will introduce new problem and hinder robot's overall performance.

1.3.2 Actuator Dominates Robot's Performance

The major motivator for this thesis was the traditional design and deployment of EM motors that are used to actuate the biped robot. Many times, the power requirements needed for the design situation are beyond electric actuation feasibility and the problem is that electric actuators just cannot produce the torque as defined in the design space with the speeds required. For instance, if high torque and high speed are required for the design, then fixed gear reducers can help one situation only at the expense of the other. If a high torque range is required, a high gear ratio can help reach the torque requirement, but only at the cost of overall speed range. The converse is also true. As we have seen, the fundamental problem is with the electric actuator and its torque/power density.

At current biped robot research level, more emphasis is put on the torque requirement than the speed; therefore large gear ratio is always a must-have. The result is that the weight of EM motor and speed reduction mechanism accounts for the major share of robot's total weight, and the robot's performance is always degraded by its own weight. For biped robots which usually have more than ten joints, this problem is even worse. Harmonic drive has large reduction ratio but small size and weight. It relieves the problem but does not touch the radical one – Is there anyway to avoid using EM motor at every joint of a robot? In the extreme situation, the problem evolves to the one prompted in Section 1.1.1 – Can biped robot be powered by only one motor?

1.3.3 Single Motor Driven Biped Robot Never Exists

Although having sole EM motor on board may save biped robot's overall weight, none of the previous researches has been focused on this. These researches include some famous

walking robot projects in the world: WL-10RV1 from Waseda University, P2/P3 from Honda, Toddler from University of New Hampshire, the Moscow State University Biped, SD-2 from Clemson and Ohio State University, Biper from University of Tokyo, Meltran II from Mechanical Engineering Lab in Tsukuba, and Timmy from Harvard.

This PhD work is the first one trying to setup a Single Motor Driven biped robot scheme. At the end of thesis, it is concluded that SMD biped robot is viable and will come true one day. The conclusion is based on both experimental results and simulation results. Some of the research highlights are listed in the next section.

1.4 Highlights of Research Results

1.4.1 Idea – Biped Robot Powered by One EM Motor

The property of lightweight is important for walking robot. Reducing the number of actuator is one way to achieve this. In the extreme situation, only one EM motor powered biped robot scheme is prompted. It is inspired by simple comparison between mechanical system and electrical system. The idea is fortified when the analysis goes deep on current EM motor and biped robot design.

1.4.2 Approach – Advanced SMD Technology

Traditional Single Motor Driven (SMD) technology exists several years in NTU/IVL. Elastic Actuation (EA) is not brand new in robotics research. However, these two technologies have not touched each other before, and their combination/complementation is firstly discussed in this thesis. As a result, the "Advanced SMD" is brought out. A one motor powered biped robot scheme just explains the necessity of such new actuation technology. Successful analysis and experiment/simulation show that this actuation approach is viable and promising. Some research highlights of this approach are:

- Bandwidth Analysis for EA

Bandwidth is a measure of how well the actuator can output a load torque or torque in the spring, τ_l, given a desired output torque, τ_d. The closed-loop bandwidth, or the relationship between τ_l and τ_d, changes with frequency and can be written as a transfer function of the form

$$G_{cl}(s) = \frac{\tau_l(s)}{\tau_d(s)}$$

The proposed bandwidth is measured with the load position of the actuator output held constant. This is analogous to when the actuator is in rigid contact with an unyielding environment or if the actuator is connected to an infinite load itertia[7].

Two cases of bandwidth are examined. The first is the small torque closed-loop bandwidth and the second is the large torque bandwidth when the actuator is operating at full torque and velocity saturation limits.

- Output Impedance Analysis for EA

As defined previously, output impedance is the amount of torque an actuator outputs given a moving load position θ_l. This can be written as a transfer function in the form

$$Z_{cl}(s) = \frac{\tau_l(s)}{\theta_l(s)}$$

Ideally the actuator is a pure torque source and has zero output impedance. If this were the case, the dynamics of the actuator would be completely decoupled from that of the load motion. However, since the actuator is a real physic system, it has some output impedance.

Purposeful Elastic Joint (PEJ), because of its elasticity introduced, has very low impedance. The spring's stiffness can be more than two orders of magnitude lower than a standard torque sensor – for example the Six Beam Torque Sensor in [34]. Even without closed-loop control, the spring lowers the impedance. This effect is most noticeable at high frequencies.

The second effect is due to the active control system. With decreased sensor stiffness, the control gain is increased. This effect is noticeable at low frequencies. Consider the following situation

$$T_l = I_{eq} s^2 \Theta_l$$

Equivalent impedance inertia, I_{eq}, can be defined for the actuation mechanism. To give a sense of the equivalent inertia, the following is defined for PEJ

$$I_{eq} = \frac{I_a}{K}$$

where I_a is the reflected actuation mechanism inertia and K is the overall gain in the control system. In PEJ the control system gain, K, is very large. Therefore, the equivalent inertial impedance, I_{eq}, is small relative to the reflected inertia I_a.

[7] This situation will always leads to actuator damage or other unexpected result for conventional actuator which does not have the feature of elasticity.

➢ Load Motion Analysis for EA

PEJ is meant to be used in real world biped robots that contact the environment. However, there are many times when such a robot is simply moving an inertial load in free space, like the swing foot in single-support phase. In this case, the load motion is defined by the inertia of the load, I_l, and the torques through the actuators.

Ideally a PEJ can be considered a pure torque source within the controlled bandwidth independent of the load inertia. However, as just explained, the impedance of the actuator is not perfectly zero. The actuator does have minimal dynamics that must be considered when looking at the torque the actuator applies to a freely moving inertia load.

When $I_l >> I_{eq}$ then the dynamic of the actuator or the actuation mechanism are negligible within the bandwidth and the actuator can be considered a torque source. However, the closed-loop torque transfer function changes at low frequency if the load inertia is close to or less than that of the impedance equivalent inertia, I_{eq}. In the limit, if there were no load inertia, the actuator has nothing to push on and produces no torque.

In summary, PEJ has many desireable properties as torque controllable actuators. The high bandwidth, low impedance, shock tolerance, internal non-linear error rejection and large dynamic range are balanced with reduced large torque bandwidth and reduced load torque response. These tradeoffs are important to successfully apply PEJ in robot systems.

1.4.3 Prototype – Purposeful Elastic Joint

At current technology and financial status, for a PhD work, it's a "Mission Impossible" to design and fabricate a biped robot that has both SMD and EA feature built in. However, this thesis presents a one joint actuator that has both SMD and EA feature fulfilled (Advanced SMD). Figure 1.1 shows CAD picture of the actuator (PEJ) designed, built and tested in this thesis. The actuator has the minimum torque level of about one Nmm[8]. Without elastic characteristics, normal actuators have high output impedance and are poor at open-loop torque control. However, with elasticity, the actuators are very torque sensitive and can achieve high bandwidth at moderate torque amplitudes. The closed-loop actuators have low output impedance. The lowest resolvable torque, which is limited by the noise floor of the sensor, is approximately 0.001 Nmm, giving a dynamic range on the order of 1000:1. The low output impedance also helps to significantly decouple the actuator dynamics from that of an inertial load.

[8] Calculated from spring specifications.

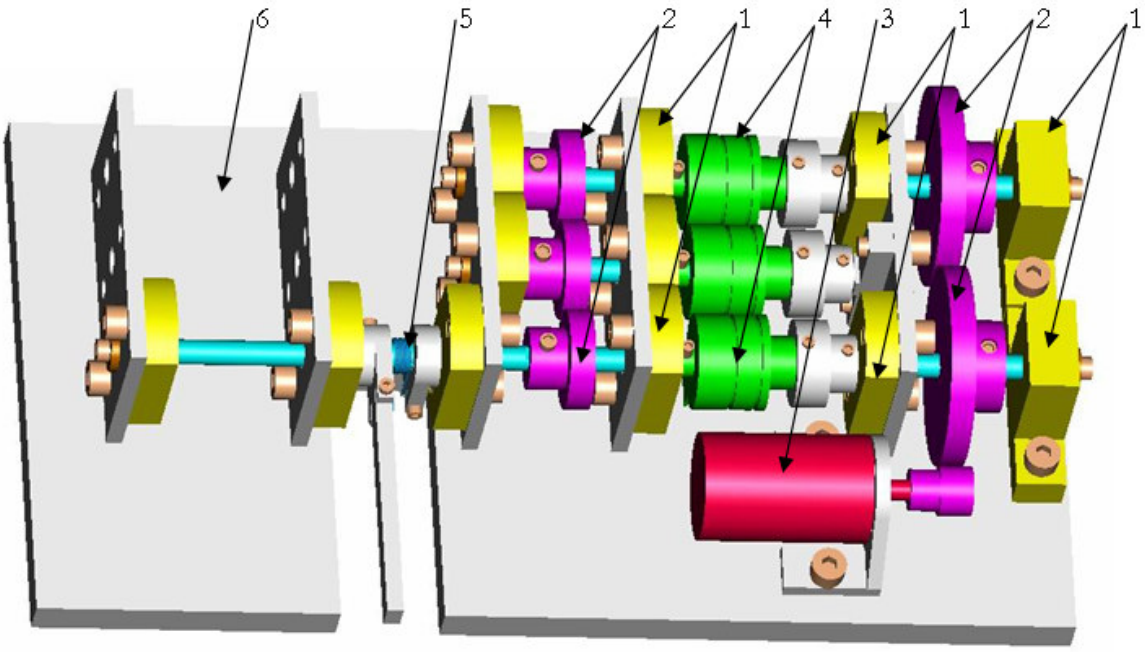

Figure 1.1 CAD Model of PEJ

Labels: 1-Bearing, 2-Gear, 3-DC Motor, 4-Clutch, 5-Torsion Spring, 6-Base/Frame

1.4.4 Simulation – SMD Biped Walking in ADAMS

To build a robot, especially a new concept one like the SMD biped robot, is very costly. It's not a good idea to directly fabricate it without sufficient research and investigation. However, with sophisticated mathematical tools such as MATLAB and ADAMS, we have build a virtual biped robot which has almost all the features to be considered as a real biped robot, such as the kinematics, dynamics, friction, interaction with environment especially foot-ground contact, and so on. Control developed before is used in the simulation to test and find the unique feature of SMD biped robot. The simulation results show that it is possible to make the SMD biped robot walking, and the idea of SMD biped robot is viable. Furthurmore the simulation results verify our believing that the heavier the biped is, the more energy it will consume. This in turn indicates that SMD biped robot is promising.

1.5 Thesis Structure

The thesis is organized as follows:

Chapter 1 starts the thesis with three comparisons, and gives a brief introduction to the background and motivation of the thesis. It also includes a summary of the key results from the research.

Chapter 2 presents detailed background material and related work covering general ideas of torque control, present-day actuator technology, actuators which use compliance, and actuator deployment.

Chapter 3 describes the Single Motor Driven technology in detail. SMD is not firstly proposed by this thesis but it has in-depth description and analysis in this chapter. Some basic idea and formula are developed for later chapters.

Chapter 4 describes the Elastic Actuation technology which is treated as the complementary technology for SMD in this thesis. More theory and formula are developed here for later use.

Chapter 5 applies results of Chapter 3 and Chapter 4 to a case study of the PEJ robot. The theoretical model is compared with experimental results. This model contains all of the key characteristics of the SMD and EA and especially a compliant load sensor used in closed-loop torque control.

Chapter 6 concentrates an SMD biped robot. Though there is no physic prototype available, sophisticated simulation are conducted in ADAMS and MATLAB/Simulink. The results verify the idea of SMD biped robot.

Chapter 7 concludes the thesis with some future works pointed out.

2 Background and Related Work

The goal and approach of this thesis are all about biped robot actuation. This chapter explores the background of current biped robot actuator systems, actuator deployment techniques, and some of the state-of-art control techniques. Compliant actuator, as a relative research topic of Elastic Actuation, is also covered.

2.1 Force Control

Robots are very successful at performing tasks that require movement in free space or known environments under position control. Tasks such as spray painting vehicle exteriors, pick and place of IC chips, arc welding and spot welding fit very well into this paradigm. While many robotic applications that use position control have found their way into the commercial sector, robots that contact the surrounding environment and work within kinematic constraints have for the most part been limited to laboratory research, just like the biped robot. In fact, simple tasks such as driving a screw, turning a crank, assembling toys, and writing on a chalk board are extremely difficult for most robotic manipulators [35]. Instead of position control, these robots require force control. The robots themselves must be capable of accurately modulating and controlling actuator torques and forces.

Force Control is the term used to describe the necessary interaction between a robot and an external unknown environment. The robot must have the capability of sensing and controlling forces in addition to knowing where it is in its work space. The necessity for force control deserves some discussion. Paynter gives a general explanation for maintaining proper causality when any two physical systems interact energetically [36]. The two systems' interaction is defined at the interface by a set of orthogonal variables: flow and effort. In a mechanical system, flow is the velocity or motion and effort is the force/torque. In any power domain (such as mechanical, hydraulic, electric, thermal, etc.) there are equivalent flow and effort variables. The product of these two variables is the power transferred across the system interface. Interestingly, one physical system cannot independently control both the flow and the effort at the point of interface. A system may define and control one of these variables or a relation between the two

variables, but not both. This explanation of general physical system interaction has direct application for why force control is necessary when a robot interacts with an unknown environment. Most workpieces and environments with which a robot will interact are inertially and kinematically constrained. A pallet has mass. A door swings on a hinge. A wall and door are vertical and horizontal barriers respectively. Given these constraints the environment often defines the flow interaction. This leaves the robot with only the option to modulate the effort. In other words, while the robot can push on and give energy to the environment, it cannot specify how the environment will respond. If the robot tries to control the position at a constrained interface, there exists a basic incompatibility between the two physical systems. Therefore, whenever a robot interacts with an environment or workpiece and is not simply moving around in free space, it must use force control. While it is still important for the robot to understand its own sense of position, it also needs some capability of being compliant in order to effectively match the given constraints. As defined in the introduction, the robot must have low impedance. This allows the causality of the robot-environment interface to maintain a proper relationship. It is important to point out that all environments do have some compliance. While most constraints have high stiffness, there are other environments which are very compliant such as sod or carpet. In fact some systems, like water, can exhibit variable compliance depending on the conditions. In these cases it may be necessary to control some linear combination of flow and effort. Nevertheless the robot must be capable of being compliant. It cannot be limited to high stiffness. Therefore, responsive force control is essential. The following three subsections cover different techniques, ideas and algorithms that robot operators use in order to match compliance requirements with the environment. This includes passive methods as well as active control. The discussion also outlines some robotic applications where force control can be very useful.

2.1.1 Passive Compliance

A simple method to achieve pseudo force control and low robot output impedance is to have a robot use conventional position control but incorporate passive compliance. Passive compliance can be found in the robot structure, joints, and at the end effector. It differs from active force control in that passive compliance does not use force information for feedback to modulate the control algorithm. There are two major ideas behind passive compliance: low servo stiffness and passive end effectors. By introducing passive compliance into the joints, the loop gain for the position control loop is effectively softened. A similar effect can be achieved by increasing the compliance in the robot

structure (links). With a combination of low servo stiffness and low structural rigidity, the robot may be able to successfully interact with a work piece or environment simply by using position control schemes. However, the risk of adding too much compliance to a robot is that the robot may be sloppy in its task execution and may fail in its overall goal [37]. Successful examples of passive compliance in robot joints are the bipedal walking robots built by Honda Research and Development called P2 and P3. P3 is slightly smaller than P2. Both robots use a compliant damping material as a coupling between the robot actuators and joints [38] [39]. The coupling protects the robot's actuators from the shock loads in each step and decouples the reflected inertia through the large harmonic drive gear reduction. To compensate for softened servos, P3 has active force sensors in the ankles which give feedback to the control system and are critical to its walking stability. Passive end effectors are another successful strategy for helping robots interact with the environment. This is because many robots only touch the environment at the manipulator endpoint. A robot can use position control to approximately locate the endpoint properly in its workspace. The endpoint then performs its workpiece interaction task. For example, many end effectors have a soft rubber covering. This effectively decouples the robot from the workpiece through the compliance. Biological examples of passive compliance at manipulator end points are human hands and feet. The soft compliant skin compensates for poor positioning accuracy of gross motions, allows for one manipulation and also aids shock reduction in locomotion [40]. Interestingly, soft endpoint covering has also been shown to be an effective tool for active force control [37]. P3 has a compliant foot in addition to compliance in the actuators. It helps to keep the supporting foot securely in contact with the ground during walking. Besides a soft rubber covering, pneumatics is also common end effectors that effectively convert the end of the robot into a force control device. This is because pneumatics is inherently compliant. By controlling the pressure in a pneumatic piston, the piston converts gas pressure into a mechanical force. Pneumatics also maintains relatively low output impedance regardless of the pressure or force at the output. Another clever passive end-effector is the remote center compliance (RCC) that is set up to automatically perform a peg-in-hole assembly [41]. The configuration of the RCC creates a compliance center at a certain point within its structure. Forces acting on the compliance center of the RCC result in pure translation and torques at that point cause pure rotation. By placing a peg tip right at the compliance center, it can be passively dropped into a hole without jamming.

2.1.2 Active Control

Passive methods have limits when trying to increase the capability of force controlled robots. Often passive techniques are task specific, such as RCC being applied to peg-in-hole assembly. In order for the robot to have the capability to perform more general tasks, there is a need for active control and task planning. This leads to the need for active feedback of measurements to modulate the control of forces on either the manipulator endpoint and joint actuators or both. The vast majorities of active force control techniques and algorithms have been developed to control and monitor the end point forces and torques via a force sensor at the robot tip. Mason [42] and Whitney [43] give good summaries of formalized compliance control and other active force control methods.

This thesis deals with single degree of freedom torque controlled actuators first. Then a high level torque control algorithm is used in the coordination and control of the entire robot arm. Therefore, an overview of several force control methods and algorithms for multidegree of freedom robots is presented. Also included are a few general applications which require force control. Various active force control methods include explicit force control, stiffness control and damping control, impedance control, hybrid position/force control and virtual model control.

- Explicit Force Control

Explicit Force Control creates a virtual endpoint force servo. The controller input is the error between the desired force and actual measured endpoint force. The difficulty in this type of controller is that there is no positional feedback on the robot which means that there is no control on the absolute endpoint position. Therefore, this approach is somewhat difficult to apply to a multi-degree of freedom robot without a higher level control system modulating the forces.

- Stiffness Control and Damping Control

Stiffness Control [44] and Damping Control [43] create a virtual six degree of freedom spring or damper in robot end point coordinates respectively. Both techniques are related because they measure the endpoint forces as well as the joint positions and velocities in order to generate a desired force output relating to the virtual spring or damper. Good torque control on the joints is helpful as the endpoint forces are created with the Jacobian transpose. However, no inverse kinematic calculation is needed.

- Impedance Control

Impedance Control [45] generalizes the ideas of stiffness control and damping control. The position and velocity of the robot endpoint is commanded to follow some trajectory. In addition, the control system modulates a manipulator disturbance response

which handles the control of dynamic interactions. The robot disturbance response is modeled after a second order mass-spring-damper behavior. In other words, the robot endpoint will behave as if it is a second order system. Therefore the endpoint forces, joint positions and velocities are used to generate actuator torques. The gain matrices which set the effective stiffness, damping and inertia of the manipulator endpoint correlate directly with stability and bandwidth criteria for the robot.

- Hybrid Position/Force Control

Hybrid Position/Force Control [46] is a method that combines conventional position control and force control. The environment dictates natural constraints (such as being in contact with a surface) where only force control can be used. Similarly, position control is used in the directions where there are no constraints and the robot can move freely. The trajectory and path that the robot follows are called artificial constraints. A systematic method for understanding and defining natural and artificial constraints has been outlined in several places [47] [48] [49] [50]. Once a task has been defined, actuator torques are then commanded to make the robot operate within the given constraints. This technique requires a new control system for each new task.

- Virtual Model Control

Virtual Model Control [51] [52] is a motion control language that allows the control designer to use simulations of virtual mechanical and/or other components, linear or non-linear, to create reaction forces which are transmitted through the robot via joint torques. The robot behaves as if the virtual components are actually attached to the robot. This algorithm can be formulated into a state machine so that different virtual elements control the robot with each change of state. Virtual model control is different from impedance control in that it does not assume a fixed base and allows component connections between any two points on the robot, not just between base and endpoint. While this control language has been applied to legged robots that successfully accomplish their task of locomotion [53], there is currently no formal method for quantifying stability.

2.1.3 Application of Force Control

There are many applications that require real time force control. These applications include: teaching and skill acquisition both for people teaching robots and robots training people, telerobotics, haptics and biomimetic robots. While each application does not have a specific technique associated with it, the following are some of the applications to give emphasis to the importance of force control.

- Teaching and Skill Acquisition

On-line programming has had only partial success in applications in manufacturing such as grinding and deburring. In these cases, interaction forces for the task must be acquired or learned. These skills are often difficult to teach to people, let alone robots. Often it is easiest to train force interaction skill with a teach-by-showing method. It is then possible to embed that information into one of the active control methods listed above such as hybrid force/position control or impedance control. In order for the robot to learn these skills, it must be compliant in the instructor's hands [54]. This requires good force control. Conversely, robots can teach humans. Experiments are being done with robots helping in the rehabilitation process of upper limb control for people recovering from strokes [55]. These robots must be force-sensitive and inherently safe.

- Telerobotics

Telerobotics [56] [57] places a human in the control loop of a robot. One standard form places a human on a master manipulator and the robot slave mimics the motion of the master. To add to the capabilities of the system, a controller will reflect the forces felt by the slave to the master. While it is not recommended that the slave manipulator have endpoint force control from the standpoint of stability, local force control on each individual joint is highly recommended (if not required) for proper teleoperation [58]. Advances in manipulator design and control algorithms have allowed for the development of a teleoperated micro-surgery robot [59].

- Haptics

Haptics [60] [61] is closely related to teleoperation where the only difference is that there is no slave manipulator. A haptic interface will generate forces at its end point as it follows the user's motion. The desired forces are created in a virtual environment rather than reflecting a remote real environment. However, the haptic interface gives the illusion that an environment actually exists. Good force control is critical in haptically representing a virtual environment.

- Biomimetic Robots

Biomimetic Robots are those that try to imitate motions and actions of humans and animals. Robots that walk [53], run [62], catch [63], grasp [60], swim [64], etc. are all currently inferior to their biological counterparts in both structure and technique. These robots interact with the surrounding environment and therefore good actuator force control is very beneficial.

2.2 Biped Robot Actuators

Regardless of the application, algorithm or technique, there is often an assumption made in the control system that high level desired force equals actual force at the robot actuator. For the most part, this assumption is poor, particularly for very low forces when desired force is near zero. There are many reasons why this is the case. Friction, stick-slip, intermittent environment contact (impacts), transmission dynamics, actuator dynamics, actuator saturation, reflected inertia, and noncolocated control are all limiting factors.

Although actuators are often assumed to be black box force devices, the limiting factors above make that assumption invalid. It is important to understand how well various actuation methods generate clean and accurate forces or torques. Studies have been conducted that compare and contrast different actuation domains including internal combustion engines, electro-magnetics, hydraulics and pneumatics as well as other developing technologies such as shape memory alloys (NiTi), electro-active polymers and braided pneumatics (McKibben muscles). In the comparisons, biological muscle is used as a benchmark. These studies focused on characterizing and generalizing different actuators by the shape of their flow-effort relationship [65] and on looking at the power density and force density of each actuation method [66].

This thesis considers only the traditional actuation methods of electric actuation. However as a background investigation and comparison, other actuation methods like the hydraulic actuator are presented in this chapter. The following discussion focuses on how each method performs with respect to force control.

2.2.1 Electro-Magnetic

The vast majority of robotic actuators in use today consist of some form of electro-magnetic (EM) motor with a transmission. EM motors by themselves are well understood. They are fairly easy to model and control because they are linear for the most part. In the simplest model, motor torque is proportional to current. Transmissions, on the other hand, are not linear. They introduce several problems discussed below.

The purpose of having a transmission is to increase the force/torque density of the actuator. This allows the EM motor to run at peak efficiency operating conditions (high speed and low torque) while output power is at the low speed and high torques good for robot operation. While mathematically a transmission works wonderfully, physically it presents problems for both position as well as force control. Non-linearity in the form of

backlash, increased dynamic mass and increased output impedance are all a function of the transmission.

Backlash and other nonlinearities in the transmission are especially problematic at low forces. The actuator may hunt back and forth in the dead zone between gear teeth in an attempt to modulate zero force. It is possible to create and use non-backlash gears to create a stiffer transmission, however they correspondingly increase drive friction [67].

A gear reduction also increases the equivalent dynamic mass of the motor as seen after the transmission by N^2, where N is the reduction ratio. For geared motors, the large reflected inertia leads to broken gear teeth, damaged ball screws and ruined actuators when large unexpected loads appear as the robot interacts with an environment. This is because the large reflected inertia needs time to accelerate in order to store energy. Therefore, the impact energy goes directly into the compliance of the transmission elements until they yield or break. In addition, the motor inertia, as seen through the transmission, will typically be on the same order of magnitude as the robot link inertia and be coupled to the link, significantly altering its dynamic behavior.

EM motors by themselves are typically easy to back-drive and have low impedance. This means that a small external torque on the motor shaft will cause it to accelerate. However, with a large transmission, due to the increased real and apparent friction and increased reflected inertia, an EM motor becomes significantly more difficult to back-drive. With this increased impedance, the actuator becomes much more of a position causal system rather than a force causal one.

To overcome the difficulties associated with linking an EM motor to a transmission, many novel approaches have been tried. Three of these approaches are described below which include: direct-drive, cable transmissions and involute gear sets. In an effort to make a clean, low-friction, low-impedance actuator, Asada and Youcef-Toumi created direct-drive actuators and robots [68]. Direct-drive eliminates the transmission and connects a DC brushless motor directly to a robot link. This construction eliminates friction and backlash and creates a very force sensitive actuator. Advanced torque sensors in the actuators have added to the capabilities of direct-drive robots [69].

From a modeling and control standpoint, direct-drive robots are simple systems. The motor (magnet) mass is included with the link inertia. Unfortunately, to compensate for the loss of transmission, direct-drive motors must be large in order to achieve high torques. High torque requires high current which in turn requires heavy wiring. In weight sensitive and power sensitive applications such as biped robots, direct-drive actuators are often unacceptable. Nevertheless, for ground based robots with few degrees of freedom,

direct-drive actuators have been very successful in both force control applications and position control, particularly in semiconductor manufacturing automation.

In order to improve the force and power density of EM motors without sacrificing force sensitivity, work has also been done to create stiff, low-friction, clean, light-weight cable transmissions [70].

These transmissions have zero backlash and high power efficiency due to high tensioning in the cables. Cable transmissions have been used on novel robots such as the Whole Arm Manipulator [71] used in robot catching [63] and digging, the PHANToM [72] used as a three degree of freedom haptic point interface, Robotuna used to study undersea oscillating foil propulsion [73] [74] and robots for minimally invasive telerobotic surgery [59] [75]. However, because of the size constraints of pulleys, cable transmission can only achieve moderate transmission ratios. Force control with slightly higher ratio gearing has been achieved with very careful actuator design and development in the construction of Artisan, a ten degree-of-freedom manipulator [76]. Instead of using single stage helical gears, Vischer and Khatib used evoloid [77] gear sets for each joint. Evoloid gears have a much coarser pitch than traditional spur gears. These gears have higher load capabilities than helical gears but are still back-drivable and have smooth torque transfer characteristics. This transmission used in conjunction with a novel torque sensor, helped Artisan to demonstrate compliant behavior.

2.2.1.1 DC Electric Motors

To begin, the mechanical equation for a permanent magnet direct current (DC) motor are shown to start the discussion. The mechanical equation relates motor torque to current:

$$T_m(i) = K_T i \tag{2.1}$$

where K_T is the motor torque constant. The electrical equation relates voltage to speed:

$$V(\omega) = K_T \omega + iR \tag{2.2}$$

where R is the winding resistance and $K_T\omega$ is the back electro-motive force (emf)[9]. For a constant voltage V, the torque speed relation is obtained by solving (2.2) for current and using the result in (2.1):

$$T_m(\omega) = \frac{K_T(V - K_T\omega)}{R} = \frac{K_T V}{R} - \frac{K_T^2 \omega}{R} \tag{2.3}$$

Note that torque is a linear function of speed. The constant term defines the stall torque, or the holding torque at zero speed, for the motor at that voltage:

[9] The motor inductance, L, is assumed small.

$$T_o = \frac{K_T V}{R} \tag{2.4}$$

The coefficient of the speed term is related to what is sometimes referred to as the motor constant:

$$K_{motor} \equiv \frac{K_T}{\sqrt{R}}$$

Numerically, the square of K_{motor} represents the slope of the torque-speed curve. Finally, the theoretical "no-load" speed is found to be:

$$\omega_o \equiv \frac{V}{K_T} \tag{2.5}$$

Using (2.4) and (2.5), (2.3) can be written as:

$$T_m(\omega) = T_o\left(1 - \frac{\omega}{\omega_o}\right) \tag{2.6}$$

This torque-speed relation is used several times in this work. By conservation of energy, the mechanical power output of the motor is the difference in the input electrical energy (V_i) and the i^2R losses to heat. This mechanical power is a torque-speed product and has a parabolic form with a maximum power point at half of the free speed:

$$P_{mech} = T(\omega)\omega$$

$$(P_{mech})_{\max} = \frac{T_o}{2}\frac{\omega_o}{2} = \left(\frac{VK_{motor}}{2K_T}\right)^2 \tag{2.7}$$

The achievable amount of torque that can be delivered by a motor depends on the time duration or "duty cycle" that is required. Much larger torques can be delivered for shorter duty cycle times than that for extended or continuous periods. The sustainable current that a motor can handle is fundamentally dependent on both the allowable winding temperatures and the thermal resistance of the motor [22]. An important motor specification is the continuous torque that the motor can provide at stall. It was shown in [22] that the continuous power loss is written as:

$$(P_{loss})_{cont} = \frac{T_\omega - T_a}{R_{therm}} = i_{cont}^2 R \tag{2.8}$$

where T_ω is the winding temperature, T_a is the ambient temperature, and R_{therm} is the thermal resistance of the motor expressed in °C/W. Solving for the current and multiplying by K_T gives the continuous torque available from the motor:

$$(T_m)_{cont} = K_T\sqrt{\frac{(P_{loss})_{cont}}{R}} = K_{motor}\sqrt{(P_{loss})_{cont}} \tag{2.9}$$

This equation shows a fundamental fact: energy must be dissipated in the windings for the production of torque to happen. The resulting heat energy must be dissipated at a rate which avoids overheating of the windings. In many cases, accommodating the heat energy dissipation can be a limiting design factor. Also, heat dissipation sometimes becomes the limiting performance factor during motor operation. In other words, the maximum performance of a motor may be limited by thermal as well as mechanical considerations.

2.2.1.2 Geared Electric Actuators

The available torque density and power density of currently available DC motors are many times limited physically by the magnets themselves. An excellent demonstration of this fact is given in [22] and is summarized here.

For a motor length l with a rotor radius r, the air gap area is given by:

$$A_g = 2\pi rl$$

From the Lorentz relation [78], the maximum tangential force per unit air gap area is given by:

$$\frac{dF}{dA} = i_l B_g$$

where i_l is the effective current per axial length (A/m), and B_g is the effective magnetic field distribution in the air gap (T). The total (continuous) torque is then given by:

$$T_{cont} = \left(\frac{dF}{dA}\right) r A_g = 2\pi r^2 l i_l B_g \tag{2.10}$$

Hollerbach states that a survey of motor specifications indicates that the mass per unit volume for housed motors ranges from 3000-5000 kg/m^3; for purposes of comparison, the density of steel is 8000 kg/m^3. Assuming a mass/volume of ρ =3000 kg/m^3, an upper limit on the torque-to-mass ratio can be calculated as:

$$\frac{T_{cont}}{m} = \frac{2\pi r^2 l i_l B_g}{\rho(\pi r^2 l)} = \frac{i_l B_g}{\rho} \le 12 \frac{Nm}{kg} \tag{2.11}$$

where:

T_{cont} – Total continuous torque generated by motor.

m – Total weight of motor.

r – Rotor radius.

l – Motor length.

i_l – Effective current per axial length (A/m).

B_g – Effective magnetic field distribution in the air gap (T).

ρ – Overal density of motor.

A maximum torque density of 12 Nm/kg is a very low number, especially for high payload systems, and is not subject to much improvement [79]. However, high power density can be achieved with electromechanical motors by allowing the motor to run at higher speeds. As shown earlier, maximum power is achieved at half the free speed of the motor:

$$\omega_{\text{maximum\_power}} = \frac{\omega_o}{2} = \frac{V}{2K_T}$$

where:

ω_o – Theoretical "no-load" speed defined in Equation (2.5).

V – Voltage applied to motor.

K_T – Motor torque constant defined in Equation (2.1).

This shows that mechanical power can be increased at the expense of torque capacity by choosing a lower torque constant K_T. For a selected motor, however, K_T is fixed and may not be used as a parameter for increasing performance. However, the statement – "Higher power density can be achieved by running the motors at higher speeds." – is a true statement in general. Hence, gear reducers (sometimes referred to as speed reducers, torque multipliers, or transmissions) are used to reduce the effective external torque on the motor to a level that allows smaller (hence faster) motors to achieve higher external torques.

Gearing introduces several undesirable characteristics into a robotic system which make accurate control more difficult. Among these, the most prominent are nonlinearities associated with friction (caused by the sliding interfaces between gear teeth), backlash (lost motion due to imperfectly mated gears), and compliance. Research in direct drive machines – those which directly couple motors to the actuated joints without gearing [68] – all but circumvents these problems by eliminating the gearing, but power density and torque density are limiting factors. Torques can be increased somewhat by making the physical size of the motors larger, but the increase comes at the expense of motor size, volume, and weight; hence, increasing motor size alone doesn't address problems with power density and torque density. The final result is that gearing is generally a necessity.

For reasons such as those outlined in this section, the vast majority of commercial electric robots use direct current motors with gear reducers. Further, it is highly unlikely that this situation will change soon. Table 2.1 shows examples of the shoulder pitch reduction ratios seen on a few existing robots.

Table 2.1 Shoulder Pitch Reduction Ratios

Machine	Shoulder pitch gear reduction
Advanced Servo-manipulator	45:1
PUMA 560	50:1
Spar SSRMS[10]	1800:1

2.2.2 Hydraulic

In contrast to electro-magnetic motors, hydraulic systems operate best at high force (high pressure) and low speed (flow rate), which is ideal for robotics. Hydraulic systems also have the highest power density of modern controllable actuation methods [66]. Systems often operate at 3000 psi and higher. Hydraulics can hold large loads indefinitely while consuming minimal power. This is something that would cause electro-magnetic systems to quickly overheat. Hydraulics is particularly useful in high force and high power density situations such as construction machinery, airplanes and automobile steering systems. Nevertheless, there are several downsides to hydraulics which have caused electro-magnetic servos to be favored in the robotics industry. These include potential messiness (catastrophic failure), system complexity, high impedance, sensitivity to contamination, and non-linearity from a control perspective.

There is an inherent messiness with hydraulics especially when hydraulic oil is used. This is especially true for catastrophic system failure such as a tree falling onto hydraulic forestry equipment [80]. Modern system design has alleviated some concerns regarding leakage of hydraulic fluid but the threat is always there.

Since pressure and return lines must be run to hydraulic actuators, there is increased system complexity from a plumbing perspective. The hoses and pipes going to and from the actuator are non-trivial in size. They must be accounted for in robot design and can add significant mass to the robot structure.

Hydraulic systems also have high impedance. This is a result of the low compressibility of hydraulic fluid and the fact that servo valves control fluid flow. All fluids are compressible to some extent, but traditional hydraulic fluids, such as oil or water, can typically be modeled as incompressible. The only way to back-drive (back flow) a hydraulic system is to create a load pressure higher than the source pressure. In this case, fluid reverses flow direction because flow in an open servo valve is a function

[10] Space Station Remote Manipulator System.

of pressure difference. Hydraulics is usually designed for motion control, not force control.

Hydraulics is very sensitive to contamination as foreign particles in the working fluid can cause system failure. In order to limit contamination in the working fluid, hydraulics requires tight seals at the piston cylinder interface. Tight seals increase friction and stiction in the system.

The final downside to hydraulic systems is that they are highly non-linear from a control perspective. Null bias, null shift, hysteresis, threshold, internal leakage, square root flow-load characteristics and unequal piston areas are all non-linear effects in hydraulics. Depending upon the level of precision required by the robot, some or all of these effects need to be accounted for.

The advantages of hydraulics often outweigh the disadvantages. Therefore, hydraulics is used quite frequently in position controlling robots and heavy equipment. Hydraulic actuators typically consist of a pressure source and a flow control valve (i.e., spool valve). A small signal current defects the spool valve which allows the high pressure fluid to flow. In the simplest linear model, the fluid flow rate through the valve is proportional to the small input current. The valve directs high pressure fluid into one of two chambers which drives a piston thus converting fluid flow into a mechanical motion. Thus, in this configuration hydraulics are very good at position control.

It may seem that it would be possible to modulate the piston chamber pressure in order to get good force control. Unfortunately, the pressure in the chamber is not a good representation of the force at the actuator output. A few reasons for this include friction and stiction in the piston and seals, supply pressure variations, non-linear flow characteristics, and high output impedance.

The friction and non-linearity create force noise on the actuator output. High impedance comes from difficulty in back-flowing through a servo valve as well as the fact that hydraulic fluid has great inertia. In general, force control of hydraulic actuators is a difficult problem [81].

There have been attempts to overcome some of the difficulties associated with hydraulics for use in robotic contact tasks. These include mechanically decreasing the seal tolerance of the piston and implementing advanced control algorithms.

In order to reduce the sliding friction and stiction, the seal tolerance can be lifted. However, that has a direct effect on system efficiency, not to mention the problems of keeping the hydraulic fluid and potentially the work environment clean. In Raibert's hopping robots, the legs had two sets of loose seals [62]. The first set allowed leakage

flow from the pressure chambers. The second set of seals simply scavenged the leakage. This configuration helped the piston to slide very smoothly. Even so, using pressure as an estimate of actuator output force proved inaccurate.

Given the natural non-linearity of hydraulic systems, Alleyne created a non-linear Lyapunov based hydraulic piston force controller [82]. This controller also includes adaptive behavior for unknown or varying parameters since many parameters in the hydraulic system are either difficult to measure off-line or are time varying (with temperature).

Hydraulic impedance control has been implemented on an industrial hydraulic robot. The algorithm for control is a specialized one which recognizes that many robot actuators are position causal and is called position-based end-point impedance control [83]. While the implementation was somewhat successful, limitations in the positioning accuracy and the bandwidth of actuators caused the robot to exhibit hunting or chatter behavior when in contact with a semi-stiff environment [84].

It is interesting to note that the hopping robots and the Lyapunov controller also included springs in their actuators. This effect of the compliance will be discussed in the section 2.3.

2.2.3 Pneumatic

Pneumatics typically consists of a piston and a valve connected to a gaseous pressure source. Pressure in a piston chamber converts the piston into a force compliant actuator. Pneumatic actuators have many features similar to hydraulics but with significant differences resulting from the operating fluid.

Inherent compliance from the compressibility of gas makes pneumatics useful as end effectors. Clever design configurations and control schemes have demonstrated that it is possible to achieve moderate positional bandwidths of 21-35 Hz [66].

There are several problems with pneumatics that limit applicability to robotics including safety, thermodynamic effects and potential resonance. First, unlike hydraulics, pneumatic systems run at relatively low pressures (100 psi) for safety reasons. They can operate at higher levels but compressed air stores large amounts of energy. If there is a rupture in the line, pneumatics becomes very dangerous. Thermodynamic effects of compressing and expanding air can heat and cool the system dramatically. Valves and seals can be designed to operate within temperature variations, however, it is usually not recommended. Finally, the natural compliance of pneumatics can also resonate with robot link inertias. Clever damping schemes are often required to maintain stability.

A variation on the standard configuration above is an inflatable elastic tube covered by an flexible braided mesh typically called McKibben muscles [66]. When pressurized, the elastic tube inside expands but is constrained by the mesh. The flexible mesh shortens or contracts like a muscle due to the expanding tube. It has been found that McKibben muscles can exhibit passive behavior very similar to biological muscle [85] since it has both series and parallel elasticity.

2.2.4 Other Actuators

There are many emerging actuator technologies with potential for use in macro scale robots such as shape memory alloy (NiTi), electro-active polymers, polymer gels, piezoelectric and dielectric elastomers [66] [86] [87]. Some of these systems demonstrate moderate force density and look very promising. However, there are some technical hurdles that must still be overcome. These include long actuation time, small scale, low power density and low efficiency.

Several of the systems have very long actuation time constants. This is the case for polymer gels as well as shape memory alloy. Specifically for shape memory alloy, actuation time is thermally limited. The elongation time is fairly short because high current can be pulsed through the actuator. However, in order for shape memory alloy to return to its initial shape, the latent heat in the actuator must be removed which can take a long time.

For the most part, electro-active polymers, piezoelectric actuators and dielectric elastomers have current working prototype systems on a very small scale. This is ideal for actuation of micro robots. In order to work on macro robots, however, work must be done to scale the systems in size.

The final difficulty with many of these actuators is that they have low output power density and are very inefficient. The power density is orders of magnitude lower than electro-magnetic motors and hydraulics. Also, the input power to these systems is still quite high, which gives a poor efficiency rating. One would hope that future development of these systems will make them more competitive with current macro scale robot actuators.

2.3 Compliant Actuators

Each actuation method described above has strengths and weaknesses with respect to force control, force density and power density. The predominant theme for the actuators is that those with high force and high power density typically have high impedance. Therefore these actuators are difficult to use in force control situations regardless of sensory feedback information.

In an attempt to overcome this impasse, it is possible to decouple the dynamics of the actuator from that of the robot by placing a compliant element between the two. This gives passive compliance to the actuators. In addition, by measuring the deflection of the spring, an estimate of torque in the joint is obtained and can be used for active feedback control.

Introducing compliance into the drive system is contrary to conventional machine design wisdom. Traditionally, machines and drive systems are built to be as stiff as possible to increase bandwidth. However, it is interesting to note that the actuator benchmark for force control applications, biological muscle, is connected in series to a link output through an elastic tendon [88]. There are many reasons why this is thought to be the case. Ideas include energy storage and increased efficiency, stability when contacting environments and filtering shock loads to the body. Even though muscles do not have many of the problems inherent to EM motors and hydraulics, elastic elements can be useful to actuation regardless of whether the system is biological or artificial.

Active measurement of a compliant element in an actuator was first applied to electro-magnetic motors with a transmission and called Series Elastic Actuators. This section presents a history of these actuators as well as other systems that use active compliance.

2.3.1 Series Elastic Actuators

Howard [89] built an actuator with a spring in series with an EM motor and transmission. He then measured the relative spring deflection by taking the difference between the motor rotation and output shaft rotation. By controlling this deflection he essentially was controlling the actuator output torque by Hooke's Law:

$$F = kx \tag{2.12}$$

in which:

F – General force (force/torque) produced by spring.

k – Spring constant.

x – Spring deformation.

Unfortunately, use of a differential measurement between motor and output shaft misses the actual strain in the spring due to transmission compliance and is also noise prone. Nevertheless, he was able to show that by using a smaller motor and larger transmission ratio, the output torque and power density increased while maintaining good control over force.

Pratt and Williamson [90] [91] also used elasticity and created an actuator similar to that of Howard's. They showed that to get a better force measurement for closed-loop control, the strain/deflection of the spring should be measured directly and not as the difference of the motor and output shaft. This actuator configuration is called a Series Elastic Actuator. As in Howard's actuator, the series elastic actuator mechanically filters friction and backlash and other non idealities in high ratio transmissions drives. It also filters shock loading from the environment.

In addition to initial prototypes, versions of series elastic actuators have been demonstrated in a few robots.

COG [92] is a humanoid robot with upper torso and head. Series elastic actuators are used in its arms, which have 6 degrees of freedom. Using the natural dynamics of the arms, low noise force controllable actuators and dynamic oscillators for control, COG was able to do many tasks previously thought to be difficult for robots such as hammering and turning a crank [93].

Spring Flamingo is a planar bipedal walking robot with series elastic actuators driving 6 degrees of freedom (three in each leg for hip, knee and ankle) [53]. It can walk at 1.25m/s on flat terrain. It has also walked blindly over terrain of uphill and downhill 15 degree slopes.

Corndog is a planar running robot with one fore and one aft leg [94]. It represents half of a large dog. The actuators used in Corndog are the electro-mechanical series elastic actuators described before.

M2 is a 3 dimensional bipedal walking robot. It has 12 degrees of freedom; 3 at each hip, 1 at each knee and 2 at each ankle. M2 is an extension of the work started with Spring Flamingo. At the time of writing this thesis, the robot could stand on its own.

Series elastic actuators work successfully over a moderate range of spring stiffnesses. Unfortunately no previous work gives design guidelines for choosing an appropriate spring constant in the actuator. The actuators in the robots were mostly designed through trial and error iterations. Most importantly, the compliance is just simply placed between the robot link and the EM motor. Although it gets rid of the heavy

and bulky transmission component, it is still the subject of heavy and bulky EM motor. This problem is more prominent when such actuators are used in multi degree of freedom robots. This thesis firstly combines the compliance of joint (Elastic Actuation) with the Single Motor Driven technology and therefore presents the first SMD biped robot which proved by simulation can walk stably.

2.3.2 Other Electro-mechanical Compliance

There are other examples in which springs have been used in series with transmissions. Elastic transmissions are an integral part of Morrell's parallel coupled micro-macro actuators [95]. In this scheme, a small direct drive actuator is coupled in parallel with a larger geared motor through an elastic transmission. The large motor creates a force with gross sensitivity and the small direct drive motor accounts for the error. While increasing the complexity of the actuator, a substantial increase in dynamic range is achieved.

In the control and handling of arbitrary two dimensional objects, Hanafusa created a three finger gripper with springs at the end of each finger [96]. The fingers were driven by EM motor and by measuring the deflection of each spring, stable grasping forces were achieved.

In the manipulator design for mobile robots to perform cooperative object handling, Sugar built a three degree-of-freedom parallel manipulator which could generate forces in the x and y directions and a moment in the z direction [97]. The actuators for the manipulator have springs between the transmission and load, and the force is controlled by measuring the deflection of the spring. This design is very similar to the series elastic actuators described above.

Sugano designed and build a compliant one degree-of-freedom finger [98]. The finger's compliance could be set by changing the effective length of a leaf spring which was in series with the motor and transmission. The actuator required three motors. One would drive the position and one would set the spring stiffness. An additional motor was required as a brake and used to damp out the residual vibration from the spring.

2.3.3 Hydraulic Compliance

Springs and other compliant mechanisms have also been used in conjunction with hydraulic actuators. Following examples from biological studies of running [40], Raibert's hydraulic legged robots use springs to recover impact energy from each step

during locomotion [62]. Using the stored energy in the springs during stance, these robots were able to perform simple gymnastics such as a flip [99].

These robots were not under force control; however, the springs in the legs are necessary to maintain stability under high shock loading with each step. As discussed previously, Alleyne designed and demonstrated a Lyapunov based controller for hydraulic piston force control [82]. The piston had a standard load cell attached to its output. However, rather than using an inertial load, the force sensor pressed on a spring fixed to ground. The spring compliance dominated over the sensor compliance and essentially lowered the loop gain and allowed the actuator to perform as well as it did.

The first force reflective teleoperated hydraulic manipulator was built by Sarcos, Inc. (Salt Lake City, UT) [100]. Using one of the actuators for this robot, Wells characterized a hydraulic piston with accumulators which give the actuator intrinsic compliance [101]. Instead of a mechanical spring at the actuator output, the piston has a fluid spring on the inside. Wells demonstrated that due to the compliance in the piston chambers, the actuator was much better able to tolerate external disturbances.

2.4 Actuator Deployment

Beside type of actuator, the actuator deployment, or actuation strategy is another important consideration for the final performance of a robot which is supposed to have more than one joint to be actuated.

As mentioned several times, robotics manipulators often require both high speed and high payload operation while minimizing friction and inertia [102]. If it is even possible to implement the system with electric drives, these combined requirements generally result in the use of comparatively high torque drives operating through relatively small gear reductions. That is, generally the motors are made as physically large as it is feasible such that the amount of introduced gear reductions may be as "few" or "small" as possible. Clearly, there is a real trade-off: larger motors require less gearing (hence less friction, etc.), but are physically larger. Therefore, in this example, reduced friction comes at the expense of overall actuator size. This greatly affects the important parameters of torque density and power density, and more importantly, these are limiting design and performance factors. Besides many kinds of new actuator technology, the actuator deployment or actuation strategy is discussed in this section.

2.4.1 Distributed Actuation

Ideally, for overall robot manipulator arm design simplicity, the joint actuators (including the associated gear-reducers) would be coupled directly to the respective joint in what is termed distributed actuation. Distributed actuators tend to minimize overall drive-train complexity. This is not to be confused with a similar idea of direct drive actuators. Direct drive tacitly implies that gear reducer is absent, whereas distributed actuation is a general actuator term. All direct drive robots are distributed actuator systems, but the reverse is not necessarily true. When distributed actuation can be achieved (i.e., the actuators each can meet the necessary performance requirements with all actuators attached at the respective driven joints), the manipulator design does not involve mechanical transmission of torque through the arm joints. Avoiding the transmission of torque through joints greatly simplifies the design. However, for all manipulator classes, it is not generally possible to distribute the joint actuators in the arm extremities because the motor basically would have to lift themselves as well as the arm structure and the payload. Further, if the actuators are direct-drive, the size and weight of the servomotors increase exponentially (actually faster than exponentially) for each upstream joint [103]. It is staggering how fast the payloads go up with distributed actuators. Starting at the most "downstream" joint in an articulated configuration, the first actuator has only to lift itself, the end effector, and the payload. In other words, in general, a joint has to lift itself and everything downstream of it. Moving upstream on the arm not only means a joint has more to lift, but also means that the joint has larger things to lift. Even in the static case this is daunting, but considering even moderate dynamic motion makes distributed actuation a lost cause. Motors with a fixed gear ratio (or no gear ratio at all) simply can't be used in a distributed sense as a general rule (though current robot designs are continuing breaking this rule). With current electric servo actuator technology, the only alternative is to resort to centralized actuators which in essence, positions the actuators such that their contribution to static weight and inertia are minimized [104].

2.4.2 Centralized Actuation

Centralized actuation essentially places all or most of the joint actuators in one local (or "centralized" – hence the name) area that can be used to counterbalance and minimize the local actuator weight with respect to the overall arm design. However, this strategy greatly complicates the specifics of the arm design because extensive engineering design work is involved with the physical specifics of choosing actuators and gear reducers and

integrating them into the overall manipulator topology. With the consideration of back-drivability and the increase of number of DOF, the complexity can be tremendous. In high payload cases, even strategic placement and counterbalancing of the motors is not sufficient. In such instances, with currently available technology, electro-hydraulic actuators are the only remaining choice.

2.4.3 Distributed Macro-Mini Actuation

Recently, a new actuation approach, referred to as the distributed macro-mini actuation approach (DM^2), has been developed to overcome the safety limitations of joint torque control and the performance limitations of normal actuator [105]. As the name implies, the DM^2 approach employs a pair of actuators, connected in parallel and distributed to different locations on the manipulator. The effective inertia of the overall manipulator is substantially reduced by isolating the reflected inertia of the actuator while greatly reducing the overall weight of the manipulator. Performance is maintained with small actuators collocated with the joints. This approach partitions the torque generation into low and high frequency components and distributes these components to the arm location where they are most effective.

The first part of the DM^2 actuation approach is to divide the torque generation into separate low and high frequency actuators whose torque sum in parallel. The effectiveness of this approach can be seen clearly when one considers that most manipulation tasks involve position or force control which are dominated by low frequency trajectory tracking or DC load torques. High frequency torques is almost exclusively used for disturbance rejection. Even haptic device torque profiles, which might require rapid changes approximating a square wave input, have a torque magnitude versus frequency curve that falls off with increasing frequency by $1/\omega$. This partition is even more compelling when one considers power requirements vs. frequency. Using the square wave example above, power versus frequency falls off with $1/\omega^2$. This power versus frequency profile is ideally fit using a large output, low frequency actuator coupled with a high frequency small torque motor.

In order for the DM^2 approach to work properly, both the high and low frequency actuators must have zero or near zero impedance. This is due to the fact that during power transfer the actuator torques will add non-destructively only if their respective impedance is zero. In particular, each actuator must not have significant impedance within the frequency range of the opposing actuator. Only if this condition is true will the DM^2 concept work. For the high frequency actuation, very low impedance is achieved by using

a small low inertia torque motor connected to the manipulator through a low friction, low reduction cable transmission.

The second part of the DM^2 actuation approach, which differs from previous attempts at coupled actuation [106], is to distribute the low and high frequency actuators to locations on the manipulator where their effect on contact impedance is minimized while their contribution to control bandwidth is maximized. This is achieved by locating the low frequency series elastic actuator remotely from the actuated joint. This is particularly advantageous as the low frequency components of most manipulation tasks are considerably larger in magnitude than the high frequency components and consequently require a relatively large actuator. Locating the large DC motor at the base significantly reduces the weight and inertia of the manipulator. The high frequency actuators are located at the manipulator joints and connected through a stiff, low friction transmission, providing the high frequency torque components that the low frequency base actuators cannot. The high frequency torque actuator must be connected to the joint inertia through a connection which produces a high primary mode vibration frequency. By locating the actuator at the joint and by using a low inertia servomotor, this high bandwidth connection with a minimum amount of weight and complexity can be achieved.

The DM^2 approach is analogous to the design of robotic manipulators for use in zero gravity. Under such conditions, gravity induced torques do not exist. Joint actuators provide torques related only to the task, such as trajectory tracking and disturbance rejection, both of which are primarily medium to high frequency in content. Zero gravity analogy can be achieved by compensating for gravity torques and low frequency torques using the low frequency actuators located at the base of the manipulator. With the effects of gravity and low frequency torques compensated, joint torque requirements become similar to those encountered by a zero gravity robotic manipulator. However, unlike robotic manipulators designed for space applications, the DM^2 joint actuators do not require a large gear reducer to achieve the required torque and power densities.

2.5 Summary

For a biped robot design, its actuation is the first issue to be considered. The actuation approach applied to biped robot includes the chosing of actuators' type and their deployment. While there exist lots of suitable actuators for biped robot application, electro-magnetic motor is always the best choice.

Unfortunately, EM motor's performance is especially poor when high torque and power density are required. In order to achieve the high power density, electro-magnetic motors require speed reduction mechanism which introduces many problems including increased friction, large reflected inertia, large total weight, and high impedance. This problem gets worse when the robot's DOF number increases, and this is one of the reasons why current "working" biped robots always have simple DOF design and thus can hardly perform complicate behavior like dancing or climbing[11].

Using less motor and speed reduction mechanism, while maintaining the required number of DOF, is one way to get rid of the problems such as large friction, large reflected inertia, high impedance, and most importantly the large total weight. The following chapters of the thesis describe and quantify this idea. Two complementary actuation approaches, SMD and EA, are introduced first. Then a single joint prototype – PEJ is presented. SMD biped walking is simulated in ADAMS. Finally a single motor driven biped robot concept is proved.

[11] Latest biped robots from Japanese industries, like Honda and Sony, can perform complicate behavior like climbing and dancing. However, most bipeds from academic institute cannot do this.

3 Analysis and Design of SMD Mechanism

Traditional robot has every joint powered by an actuator, usually electro-magnetic motor. These heavy and bulky motors account for a major share of the root weight. The idea of this thesis, however, is to drive all the joints with only one motor. The mechanical power output from the sole motor is delivered to each joint by means of specially designed mechanical transmission. This is named Single Motor Driven (SMD) technology.

The core issue in SMD technology is the mechanical transmission system. Unlike automobile and other machine, biped robot has its unique feature and requires unique mechanism. From view of topology, biped robot has two kinds of structures: articulated structure like the arm and leg, and radiation[12] structure like the palm and hip (Figure 3.1). Correspondently, there are two kinds of SMD mechanism: Serial mechanism and Parallel mechanism. Both come with the form of modularity.

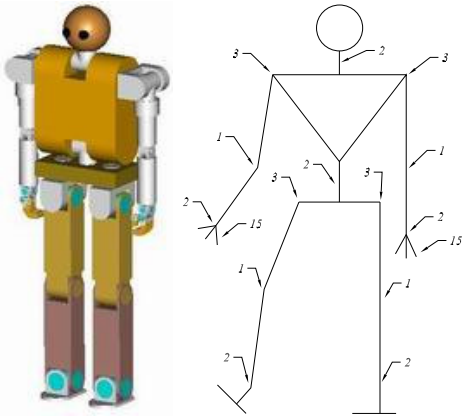

Figure 3.1 Typical Biped Robot and Its Topology Structure
The number means number of DOF in that joint

3.1 Feasibility Analysis

3.1.1 Redundant Manipulators

Industrial robots are typically designed with six degrees of freedom so that the end-effector can impart general rigid body motion to grasp objects. Generally speaking, a

[12] Link in articulated structure has two joints attached, one with the previous link and one with the next link. Link in radiation structure however may have more than two joints.

redundant manipulator is one that has more degrees of freedom than the minimum number required to perform a given task. In the context of industrial manipulators, a redundant manipulator would have seven or more degree of freedom. In a broader view, redundancy should really be determined relative to the task. For example, a six degree of freedom manipulator can be redundant with respect to a task with symmetry about one axis. In engineering contexts, redundancy usually implies a duplication or repetition of electromechanical elements and subsystems to provide alternate means for continued functionality in the event of failure in one or more subsystems. A human arm is a good example of a redundant manipulator.

The motion planning of robot manipulators is one of the most challenging problems encountered in the field of robotics. This problem can be treated either in joint or task space. Motion planning in task space for a desired end-effector trajectory is usually considered as an inverse kinematics problem. The closed-form solution to this problem is available only for certain types of robot manipulators, and in general is difficult to obtain. This is particularly true in the case of a robot with a redundant DOF, that is, the dimension of the joint-space is larger than that of the task space. The inverse kinematics computation for a redundant robot can be very complex, and there is no unique solution to a certain end-effector position without extra design or performance criteria. In many applications, the extra DOFs of the robot are used to achieve supplementary design objectives, such as:

- Geometric Dexterity

The addition of a seventh joint, either at or near the wrist, can overcome a joint motion limitation problem, and permits full end-effector orientation capability in a sub-volume of the workspace called the dexterous or primary workspace [107].

- Workspace Volume

In general, additional joints can significantly improve workspace volume [108].

- Singularity Avoidance

Non-redundant manipulators are not actually capable of performing all general tasks due to kinematic, mechanical, and other design limitations. Redundancy can be used in manipulator design to overcome some of these limitations [109] [110].

- Obstacle Avoidance

Extra degrees of freedom can be used during real time manipulator operations to simultaneously achieve end-effector trajectory control while satisfying additional constraints such as obstacle avoidance [111].

- Ability to Use Bracing Strategies

Bracing is the strategy that is used when people rest his forearm against the desk while writing. Implementing such a strategy requires a manipulator with more than six degrees of freedom [112].

- Reach Inside Capability

The problem of "reach inside" capability is similar to that of bracing. If the manipulator must reach through a restricted opening, the motion range of the joints inboard of the opening are effectively restricted. Therefore, in order to provide increased capability for this type of operation, an additional joint should be located as distantly as possible [113].

- Structure Limitations

Due to hardware limitations, physical constraints such as maximum joint rate and angle always exist. In order to remove these restrictions, redundant manipulators can be utilized [114].

- Joint Failure or Fault Tolerance

Obviously, a complete joint failure in a non-redundant manipulator automatically results in the loss of full end-effector control. However, with a kinematically redundant manipulator, one can use the extra degree of freedom to compensate for a failure [115] [116].

- Torque Minimization

Joint torque minimization can be considered for resolving kinematic redundancies of manipulators. When the generalized inverse dynamics are formulated in terms of accelerations and are incorporated into the dynamic equations, the effect of redundancy resolution on joint torque can be directly reflected. One method uses the joint acceleration null-space vector to minimize the least-squares of the joint torques, while the least-squares are weighted by the allowable torque range. The joint torques then tend to be kept within their limits [117].

- Task Priority Control

Most of the complicated tasks given to robots with many degrees of freedom could be decomposed into several subtasks according to their priorities. For example, in the case of welding, the task could be divided into the hand position and orientation control. The former is more important than the latter. The task, in which the position and orientation of hand should track a desired trajectory while the arm should avoid the obstacle in the working area, is another example for task prioritization. For these tasks, it is natural to first try to satisfy the subtask with the lightest priority. If there is any ability

left to the manipulator after achieving the first subtask, it is supposed to try to perform the second subtask as much as possible. Likewise, a third subtask is performed if there is any ability left. The existence of remaining ability at any stage means the robot is redundant for subtasks up to that stage [118].

Although redundancy in robots can be used to satisfy other objectives, redundant robots may not be repeatable. This phenomenon is known as the non-repeatability or drift of the joint motion [119]. Also when the end-effector of a redundant manipulator traces a closed path in the workspace, the path in the joint-space is not necessarily closed.

Before proceeding further with a discussion on joint-space drift, it is appropriate to add a short comment concerning another type of potential drift in the workspace. Occasionally, Jacobian control is criticized because it is formulated in terms of velocities. Because approximations are involved, it is argued that the end-effector may drift away from the desired trajectory over time. Such a potential problem can be entirely eliminated by augmenting the original desired workspace velocity with a position error term to correct the previous approximation error [120]. Thus, workspace drift in Jacobian control, whether for redundant or non-redundant systems, does not exist for all practical purpose, and must not be confused with joint-space drift in the null space of redundant systems, which does not affect the end-effector position.

The importance of joint-space drift in motion control of redundant manipulators is raised when obstacle avoidance, or joint angle limits exist. Klein and Kee [119] studied the drift properties by performing numerical experiments. They observed that the drift has predictable and numerically stable limits in some situations. Klein and Huang [120] analyzed the non-repeatability phenomenon for a three degree-of-freedom revolute joint planar arm, in terms of the integrability condition of a Pfaffian differential equation[13].

As mentioned so far, the use of redundancy can enhance manipulator performance in complicated environments. The focus of the earliest investigations has been on what might be called the "redundancy control problem". In these studies, different algorithms were developed to provide stable end-effector motion control while additionally optimizing a set of constraints. These investigations might also be termed "redundancy resolution" problems, since the principal problem is finding ways to "resolve" or determine the motion of the joints to simultaneously achieve end-effector trajectory control while optimizing additional constraints.

---

[13] A kind of partial differential equation with the form of: $adx + bdy + cdz = 0$

3.1.2 Hyper-Redundant Manipulators

The term "hyper-redundant" refers to redundant manipulators with a very large (theoretically infinite) number of degrees of freedom. These manipulators are analogous in morphology and operation to "snakes", "elephant trunks", and "tentacles".

A new approach to solve the inverse kinematic problem of hyper-redundant planar manipulators has been introduced in [121]. This method is singularity free, and provides a robust solution even in the event of mechanical failure of some of the robot actuators. The approach is based on defining virtual layers and dividing these into virtual/real three link or four link sub-robots. The approach starts by solving the inverse kinematic problem for the sub-robot located in the lowest virtual layer. The data obtained from the solution of this sub-robot is used to solve the inverse kinematic equations of the sub-robots located in the upper virtual layers. The data in different virtual layers are used in an algorithm which provides a singularity free solution by observing a drop in the configuration index. The configuration index can be interpreted as the average of the determinants of the Jacobians of the sub-robots. This approach guarantees that the robot reaches a fully extended configuration near the outer boundaries of the robot's workspace.

A technique has been presented to effectively optimize the configuration of hyper-redundant multiple-link planar manipulators in [122]. Different kinematic and static criteria, such as the manipulability and the kinematic index, are utilized but the emphasis is given to the joint torques minimization. It is shown that these criteria produce configurations that can easily be recognized and expressed in terms of simple mathematical functions.

A novel kinematic algorithm has been presented for implementing planar hyper-redundant manipulator obstacle avoidance in [123]. "Tunnels" are defined in a workspace in which obstacle are present. Methods of differential geometry are then used to formulate equations, which guarantee that sections of the manipulator are confined to the tunnel, and therefore avoid the obstacles.

3.1.3 Modular Robots

The Modular Robot (MR) concept and technique have been of interest in the robotics area since the 1980s. In robotics, modularity has been studied by many researchers [124] [125] [126] [127] [128] [129]. A fully modular re-configurable robot consisting of a set of standardized modules can be configured to different structures and DOFs for different task requirements. The feasibility of the modular approach has been carried out in

different prototypes built at several research institutes [124] [126] [127] [129] [130] [131] [132]. Modules may have different output powers to provide a wide variety of configurations [126] [129] [133]. This approach provides many benefits, some of which are as follows:

- Modularity introduces flexibility to robots by making them reconfigurable and adding more modules.
- Provides an excellent test bed for emerging component technologies.
- Encourages development and integration of new technologies.
- Reduces development and maintenance costs in the long run.
- Speeds up design turnaround.
- Prevents system obsolescence.
- Allows selective integration of fault tolerance[14] with minimum additional effort.

In order to develop a standardized modular architecture, some basic mechanical elements of a robotic system need to be identified:

Table 3.1 Basic Mechanical Elements of a Robotic System

Base Unit	base part of a robot
Joints	with one or more degrees of freedom
Links	with actuator and electronics enclosure capability
End-effector	for tool and payload handling

This table divides the robot into functional elements and may be used as a basis for module development. The basic approach is then to design each of the modules (in different scales if necessary) that enables quick assembly of a variety of robots.

One example of a modular robot is Polypod [134]. This modular robot is constructed using two different modules. The first module is called a segment, which is capable of providing 2 DOFs, and the second is called a nodded, which supplies the power to the segments. The capability of the Polypod was demonstrated by constructing different configurations, such as a caterpillar, earthworm, and a slinky using these two modules.

In most modular robots, the "building block" principle in used. The joint modules are assumed to be self-actuated, and can generate rotary or translational motions. For instance, in [135], a general framework for solving an optimal assembly configuration

[14] Fault tolerance leans towards sophisticated designs by building as many redundancies as possible to avoid faults.

(arrangement of modules) problem has been introduced. Assuming the fixed set of modules at planning time, the only freedom available for optimization is the recombination and rearrangement of modules. By having the total mummer of possible assembly configurations and the robot task requirements, a task related objective function is defined. This function evaluates a modular robot assembly configuration for a given task while avoiding sub-assemblies with undesirable kinematic properties. A genetic algorithm was employed for optimization because of the discrete nature of the search space. Different types of revolute, prismatic, helical, and cylindrical modules were considered for 1-DOF or 2-DOF joint modules. Joint modules are connected to the link modules through connecting ports and link modules possess multiple joint connections. Link modules are symmetrical. The symmetry allows the link modules to be re-oriented without altering the robot kinematics.

This research was continued for generating the robot forward kinematics in [125]. In this work, a forward kinematics for a modular robot with specific configuration and cubical modules is derived. Both revolute and prismatic types of joint modules are considered. There are connecting interfaces (ports) on all faces of the cubes so that different kinematic configurations can be achieved by just reconnecting the modules into different ports. This design is proposed for electronics assembly tasks and biomedical applications.

This research was continued for generating the robot equation of motion in [136]. In this work, an algorithm for generating the closed-form equation of motion of a modular robot is presented using the kinematics of the assembly configuration. Modular robots with a branching geometry are considered for this research. The formulation of the dynamic model is started with recursive Newton-Euler algorithm. The equivalence between the recursive formulation and the closed-form Lagrangian formulation is used to construct the closed-form equation of motion of the robot.

It was continued for generating the robot inverse kinematics in [137]. In this work, the formulation of a generic numerical inverse kinematics model is addressed for an arbitrary robot with serial and branching type geometry. Both revolute and prismatic joint modules are considered. The inverse kinematics is obtained through the differential kinematic equations based on the Product-of-Exponential (POE) formulas. The Newton-Raphson iteration method is employed for obtaining the solution.

3.1.4 PWM Control Technique

The Pulse Width Modulation (PWM) technique has been successfully used to control many dynamic systems. DC-to-DC power converters and voltage control of DC motor are well known examples. The PWM control technique is a discontinuous feedback control strategy, which classifies as a nonlinear control. Early contribution to the study of PWM controllers are those of Kadota and Bourne [138], Delfed [139], and Murphy [140]. Further developments were contributed later by Skoog [141], Skoog and Blankenship [142]. In all these works, the emphasis was placed primarily on the discrete-time aspects of such controllers. The proposed discrete-time analysis technique fitted the problem quite naturally due to the inherent sampling process associated with every PWM control scheme. In these works the analysis was also limited to the case of linear plants.

In more recent work (Sira-Ramirez [143] [144]) a different approach has been taken by using the geometric properties of average PWM controlled responses. The average PWM is obtained by an infinite PWM frequency assumption. The results, aside from allowing a simpler analysis of nonlinear PWM controlled systems through their average responses, also disclosed that actual PWM controlled responses exhibit sliding mode trajectories about integral manifolds of the average PWM controlled system model.

Application of the PWM control technique to mechanical systems has been recently reported. The discontinuous PWM controller design of a robotic manipulator [145] is an example of this application. In this work, the discontinuous (on-off) stabilizing controller was determined from a continuous controller designed for the nonlinear average model of the PWM controlled system. The combination of a sliding mode controller with PWM has also been reported for controlling an anti-lock brake system (ABS) and position control of an *x-y* table mechanism [146] [147].

In the next section, the multi-agent control technique will be reviewed. This technique has been introduced recently and it can be used to control of redundant and hyper-redundant robots.

3.1.5 Multi-agent Control

In this section, a recent approach to the control of manipulators is reviewed. Monckton [148] proposes a new manipulator control approach based on a multi-agent technique and suggests that this new control architecture is ideal for redundant systems. For global trajectory tracking, the approach utilizes the Jacobian transpose decentralization method, which decomposes the transpose of the Jacobian matrix into its *n* rows. It can be proven

that this approach, under certain assumptions, is essentially equivalent to a Centralized Pseudo-inverse Jacobian (CPJ) that uses null space methods to assign auxiliary behaviors to joint controllers. One of the advantages of this method is that it is less computationally intensive than that of the CPJ. In the following, a summary of an agent based and Jacobian transpose control are explained as a fundamental approach for the multi-agent manipulator control problem.

Traditionally, a robot controller is designed to function within a "sense-think-act" cycle. In this prototypical cycle, sensory data is incorporated into a world model from which task plans are generated and executed as trajectories by a single supervisory controller. The agent control method replaces the single supervisor with multiple sensory driven processes or agents. The following review of multi-agent control technique is mainly from [149].

3.1.5.1 Agent Control

Agent control has been applied primarily to mobile robot in the investigation of navigational and emergent behaviors. Indeed, a definition of the term "agent" is built around the following two hypotheses [149]:

- Hypothesis: H1 (Agent Control) *Given a goal, G, in an unstructured environment and a set of uncontrolled environmental events (observable, unpreventable and abrupt), Σ_u, a control arbitration process or agent, A, can be designed to observe and respond to Σ_u and, in so doing, fulfill G autonomously.*

In particular terms, an agent is a control process that employs a variety of sensory and control inputs from which a final control action is assembled and output. For the behavior of a system composed of multiple autonomous agents, a second multiagent control hypothesis has also emerged:

- Hypothesis: H2 (Multi-agent Control) *An H1-agent, A, can be designed such that a set of such agents will fulfill a group objective without explicit coordination.*

While some theoretical techniques prescribed the response of an agent to particular hazards, there is little or not theoretical treatment of the agent's internal structure [149]. The common denominator among these pragmatic robotics systems is the use of a variety of control strategies or goals, each designed to cope with a particular environmental hazard or objective. So far, the transition from one controller to another through discrete switching logic and simple summation to establish a hybrid controller objective are employed.

Given H1, it seems reasonable to model *A* as a nonlinear mechanism resolving the output of *m* distinct controllers rather than modeling the system as a single integrated controller. In a simple model, *A* manipulates the magnitude of a set of *m* gains as a function of environmental events, Σ_u. Each gain, k_i: $0 \le k_i \le 1$ modifies the ouput, $y_i(t)$: $\{1 \ldots m\}$, of the continuously active control processes. The final output, τ, of the j^{th} agent becomes a simple linear combination of the *m* control actions

$$\tau_j(t) = k^T(t)\, y(t) \tag{3.1}$$

where $k(t)=[k_1(t), \ldots, k_m(t)]^T$ and $y(t)=[y_1(t), \ldots, y_m(t)]^T$. As k_i: $0 \le k_i \le 1$, the i^{th} control strategy might be excluded from, or completely dominate the agent's output. The gain vector, *k*, evolves as nonlinear function of environmental events, time and possibly its current state

$$k(t) = f(k(t), \Sigma_u, t) \tag{3.2}$$

The behaviors evolving through $f(\cdot)$ must result in a stable system. Further, one cannot assume that the isolated stability of *A* guarantees the combined stability of *n* such agents within a coupled nonlinear system. Multi-agent manipulators in particular will be greatly influenced by the design of the behaviors, $k(t)$, arbitration functions, $f(\cdot)$, and control inputs $y(t)$.

3.1.5.2 Jacobian Transpose Control

The Jacobian transpose arises from virtual work

$$\tau^T \delta q = f^T \delta x = f^T J \delta q \tag{3.3}$$

$$\tau = J^T f \tag{3.4}$$

where τ and f are generalized force vectors in configuration and Cartesian space respectively[15]. Thus Equation (3.4) is the map of end-effector force f to joint forces and torques τ. The Jacobian transpose is related to the Jacobian through the familiar rules of linear algebra. The range of the Jacobian transpose, $R(J^T) \subseteq \tau$, is the orthogonal complement of the null space of the Jacobian, $N(J) \subseteq \dot{q}$, while the null space of the Jacobian transpose, $N(J^T) \subseteq f$, is the orthogonal complement of the range of the Jacobian, $R(J^T) \subseteq \dot{x}$.

[15] Here, $x(t)$ is used to show Cartesian trajectory.

3.1.5.3 Links as Agents

There are two properties which identify Jacobian transpose control as an important foundation for multi-agent manipulator control

- The Jacobian transpose can be decentralized amongst *n* control processes.
- The set point for all *n* control processes is a single force vector.

Examination of the Jacobian transpose reveals that the i^{th} row of this matrix is a function of the end-effector and i^{th} actuator positions, x and x_i respectively or

$$\tau_i = J_i^T(x_i, x) f \tag{3.5}$$

By assuming that the values of x, x_i and f are available either through inter-agent communication or sensor data streams, the Jacobian transpose may be decomposed row-wise into n separate processes.

Unlike most decentralized controllers in which each controller pursues a unique joint set point, distributed Jacobian transpose control enables all the controllers to use the same set point, transforming this set point into a global goal. $J_i^T(x_i, x)$ simply identifies that portion of the global goal required from the i^{th} joint. Therefore, if multiple actuators participate in the generation of a force vector component (i.e. the manipulator is redundant in that coordinate), alternate controllers may be used to influence these actuators towards secondary global or local goals.

These elements provide support for hypothesis H2. If appropriate link based sensors (as suggested by Khatib [150]) and link based local controllers are designed to detect and respond to events in Σ_u, then hypothesis H1 suggests that a global goal can be fulfilled autonomously in an unstructured environment. Furthermore, H2 implies that emergent behavior may be observed by a set of such agents.

3.1.5.4 Stability

Asymptotic stability of both local and global goals, while necessary, is not a sufficient condition to guarantee a multi-agent system's simultaneous asymptotic convergence towards goals. For the case $N(J) \neq 0$ that means the dimension of the configuration space n exceeds the unconstrained dimension of Cartesian space m, a configuration space subset will lie in $N(J)$, where $N(J) \cup R(J^T) = 0$. In this case, an infinite number of joint-space velocity solutions and, by implication, joint-space torques, $\tau \notin R(J^T)$, will produce identical end-effector velocities. Therefore, agent motions within $N(J)$ are convergent; asymptotic stability of both configuration and Cartesian space goal systems is thus realizable [149].

3.2 Concept Model

As mentioned in the beginning of this chapter, there are two kinds of SMD mechanism: Serial mechanism and Parallel mechanism. They all have a key component called Motion Splitter, which has a single input shaft but multiple output shafts. Serial SMD and Parallel SMD differ in the shaft arrangement of Motion Splitter. For Serial SMD the input shaft is perpendicular with the output shafts, while for Parallel SMD they are parallel.

3.2.1 Serial SMD Mechanism

Serial SMD mechanism is to accept the unique input (rotational) while generate several perpendicular outputs deployed along the input shaft. For the engineering capability, it is always designed in modular form. So the problem for Serial SMD is how to relay the input (rotational) to every module which is articulated in series.

Karbasi *et al*. demonstrate a uni-drive mechanism in [151] and [152]. They use flexible shaft for mechanical energy relay. This mechanism has poor accuracy since the inherent soft property of flexible shaft.

The Serial SMD mechanism in NTU/IVL however employs a set of bevel gear for motion replay. Bevel gear mechanism was studied for decades for their wide applications in robot spherical wrist [153] [154]. Here 2D bevel-gear mechanism is used to relay the single input motion from robot base to end-effector while generating branches of output motion for each individual joint (Figure 3.2 and Figure 3.6).

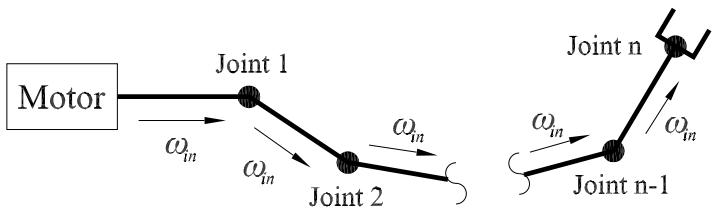

Figure 3.2 Concept Model of Serial SMD

3.2.2 Parallel SMD Mechanism

Parallel SMD mechanism uses Parallel Motion Splitter (Figure 3.3) to generate "axis-parallel" rotational motion. Usually spur-gear was used for this mechanism. Depend on needs, the branch gears can be arranged along the contour of the input gear. The branch gears usually are the same, thus has the same gear ratio G_{ratio} (greater than 1).

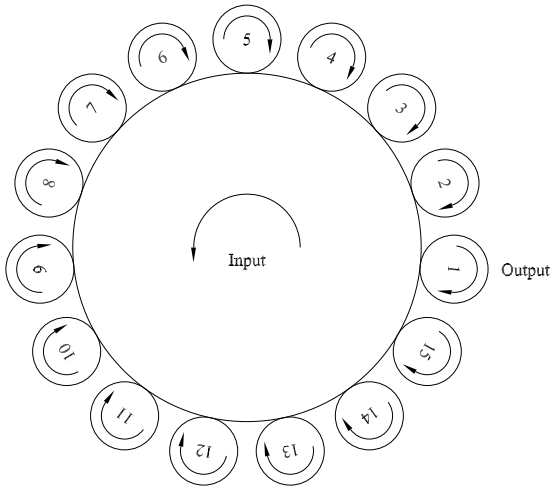

Figure 3.3 Concept Model of Parallel SMD

3.2.3 Bidirectional Clutch

The only function of bidirectional clutch, as normal clutch, is to produce different rotational motion stage with the single rotational motion input. Normal clutch can produce two stages, ON and OFF, or 1 and 0 ratio of input motion. The bidirectional clutch however can produce additional ratio of -1. That means if the input motion is kept constant, say ω_{in}, the output motion ω_{out} can be equal to ω_{in}, 0, or $-\omega_{in}$. The extra stage of $-\omega_{in}$ (inverse of input motion) makes bidirectional clutch an important component for the new SMD technology.

With different shaft arrangement, bidirectional clutch can be classified into two categories: coaxial bidirectional clutch and non-coaxial bidirectional clutch (Figure 3.4).

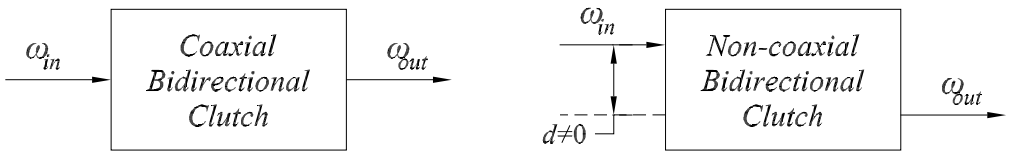

Figure 3.4 Coaxial and Non-coaxial Bidirectional Clutch

Consider the transmission inside "bidirectional clutch". If it has compliant component like "belt" then it is termed as "compliant bidirectional clutch". If all the transmission are rigid (like gear mate) then it is termed as "rigid bidirectional clutch". This classification will be termed in detailed in Section 3.3 and it makes the main difference of Bidirectional Clutch I and Bidirectional Clutch II.

3.2.4 General SMD Model

With the proper integration of mechanism, control, and sensor, a general diagram can be got to describe the key idea of SMD mechanism. As shown in Figure 3.5, each

joint of SMD module has the unique rotational input ω_{in} tapped from the central rotating shaft. ω_{in} can be easily set constant by the PID controller on EM motor [(further refer Figure 6.2 (a)]. With the PWM controller in j_{th} joint, the rotational velocity after the bidirectional clutch ω_{cj} varies from $-\omega_{in}$ to $+\omega_{in}$ continuously. Generally speaking, the PWM controller and bidirectional clutch "divide" the unique velocity ω_{in} into continuous velocity ω_{cj}. With another speed reducer in each joint, the drive velocity ω_{oj} becomes strong enough to drive that joint/DOF. Obviously these joints/DOFs are independent because of the "division" function of PWM controller and bidirectional clutch.

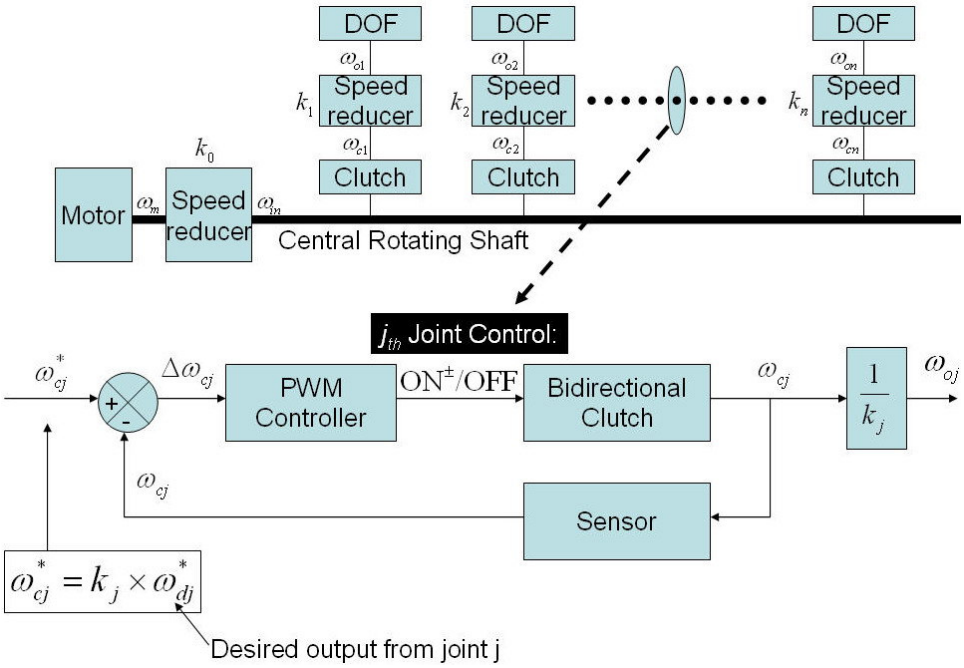

Figure 3.5 General Diagram of SMD Mechanism

3.3 Design of SMD

In this subsection, the design of a mechanical drive for the SMD mechanism is discussed. The mechanical drive consists of a gear train and two clutches to provide a controllable bidirectional motion from a unidirectional constant input. The mathematical models of the mechanical drive and clutches are presented here and the integrated model, as one of the contributions of this thesis, is presented later in detail in Chapter 5.

3.3.1 Gear Train Design

To implement the conceptual model shown in Section 3.2, a mechanical drive is needed to differentiate the unidirectional speed of the central rotating shaft into forward and reverse motions. For this purpose, the mechanical drive unit shown in Figure 3.6 was

designed. The unit consists of two sets of bevel gear mates (inner and outer), and two sets of perpendicularly crossing shafts (one set is for pivoting and the other is for twisting).

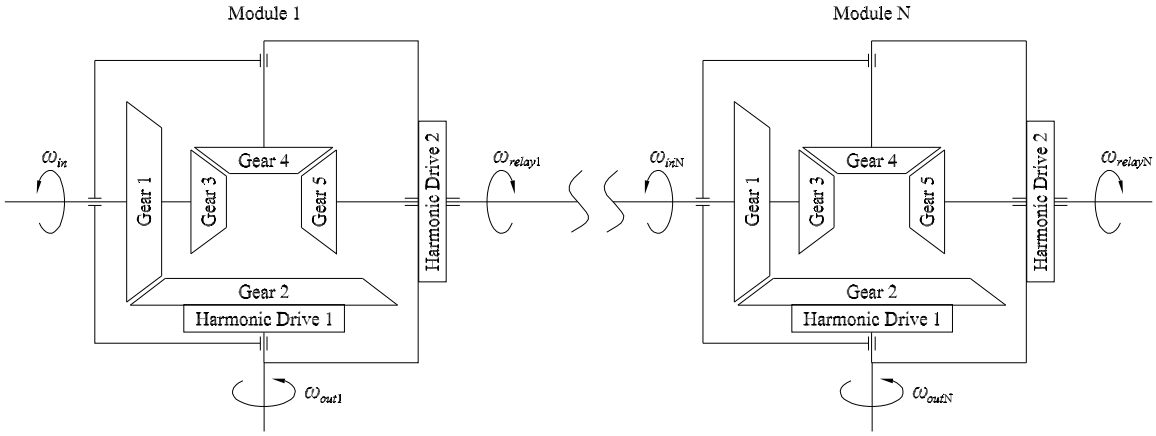

Figure 3.6 Schematic View of the Mechanical Drive

The outer bevel gear on the left hand side has one constant input – the rotational input velocity ω_{in}. With the gear ratio G_{ratio}=1/100 at every module (harmonic drive usually has large reduction ratio), the output velocity at "Output Shaft 1" is:

$$\omega_{out1} = G_{ratio} \cdot \omega_{in} \tag{3.6}$$

The velocity of "Relay Shaft 1" is:

$$\omega_{relay1} = -\omega_{in} \text{ if } \omega_{out1} = 0 \tag{3.7}$$

or

$$\omega_{relay1} = -(\omega_{in} + \omega_{out1}) = -(1 + G_{ratio}) \cdot \omega_{in} \text{ if } \omega_{out1} \neq 0 \tag{3.8}$$

Depending on the engagement status of "Joint 1" and "Output Shaft 1", the replayed velocity will be the same as input velocity with opposite direction. The rotation of "Joint 1" will affect the relayed velocity slightly as G_{ratio} is normally very small.

Suppose all of the N joints are engaged to respective output shaft, the last relay velocity is:

$$\omega_{relayN} = (-1)^N \cdot (1 + G_{ratio})^N \cdot \omega_{in} \tag{3.9}$$

Since G_{ratio} is usually very small, the following equation holds with acceptable tolerance[16]:

$$\omega_{relayN} \cong (-1)^N \cdot \omega_{in} \tag{3.10}$$

So every module in a Serial SMD mechanism can be considered has the same absolute velocity input. All odd modules have the same input velocity while even modules have a reverse velocity input.

With the gear reduction ratio G_{ratio}, the respective output velocity is:

[16] The dominant tolerance factor is $N \cdot G_{ratio}$.

$$\omega_{out}^{i} = (-1)^{i} \cdot F_{clutch}^{i} \cdot G_{ratio} \cdot \omega_{in} \tag{3.11}$$

in which F_{clutch}^{i} is the status of clutch in *i*th joint. If *i*th clutch is engaged, F_{clutch}^{i} is 1, and if unengaged F_{clutch}^{i} is 0.

According to the schematic view in Figure 3.6, a prototype mechanical drive unit has been fabricated in NTU/IVL. The gearing specifications are given in Table 3.2 and the velocities of the output shafts can thus be calculated from Equation (3.11) as

$$\omega_{out}^{i} = \begin{cases} -\omega_{in} & i \text{ is odd number} \\ \omega_{in} & i \text{ is even number} \end{cases} \tag{3.12}$$

Table 3.2 Specifications of the Mechanical Drive of the First SMD Mechanism

	No. of Tooth	Module	Press Angle	Material
Gear 1	16	0.75	20°	Plastic
Gear 2	40	0.75	20°	Plastic
Gear 3	20	0.5	20°	Steel
Gear 4	40	0.5	20°	Steel
Gear 5	20	0.5	20°	Steel
	Reduction Ratio			
Harmonic Drive 1	100			
Harmonic Drive 2	100			

3.3.2 Bidirectional Clutch Design

One key component in SMD mechanism is the specially designed bidirectional clutch. The bidirectional clutch used in this work is a modification of the PIC "Shaft Mounted Clutch" by means of attaching two identical clutches end-by-end. There are two voltage bores: 24 Volts and 90 Volts. For the consideration of safety, the former voltage bore is chosen.

A typical cross-section of the first bidirectional clutch prototype is shown in Figure 3.7. It mainly consists of an input shaft, an output shaft, an active armature, two coils and two rotors which connect a pulley and a spur gear respectively. The active armature always rotates with the input shaft. Once one coil is powered on, the active armature will be attracted to the corresponding rotor and will make it rotate too. With the help of pulleys and spur gears, bidirectional motion transmission is achieved. The whole clutch size is constrained in a space of 35x25x70mm.

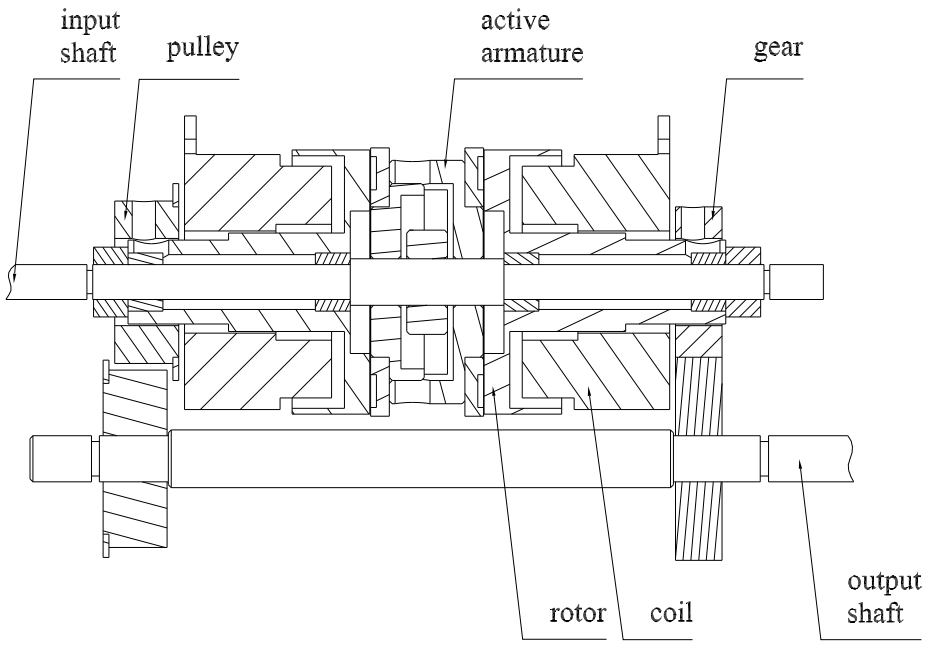

Figure 3.7 Typical Cross-section of Bidirectional Clutch

Therefore, with constant velocity input ω_{in}, the bidirectional clutch can have three stages of output:

$$\omega_{out} = \begin{cases} \omega_{in} \\ -\omega_{in} \\ 0 \end{cases} \tag{3.13}$$

3.3.3 Improved SMD Mechanism

The first SMD mechanism cannot invert its motion direction as long as the constant input velocity keeps on. This is only because the unidirectional clutch (normal clutch) mechanism is adopted. With the unidirectional clutches build in its two perpendicular crossed shafts, the mechanism can have only two states of operations: on and off, thus the output motion of each joint can only be either the coupled direction of input, or zero-movement – with the engagement of brakes in the mechanism. To invert the motion, as surely needed by robots, the constant input velocity must invert itself. To make the SMD mechanism really DOF-independent and dexterous, the unidirectional clutches are replaced by bidirectional clutches in the new version of SMD mechanism. Thus with the constant input motion keeps on, the output movement at every joint can be classified into three states: positive rotation, non-rotation, and negative rotation. Apparently this new SMD mechanism is more dexterous than the old one.

3.4 Feature and Function

In this section, the theory of variable structure systems and nonlinear PWM control as the background material for Chapter 5, and path planning methods and independent joint control of manipulators for Chapter 5 are built.

3.4.1 Sliding Mode Control and Variable Structure Systems

In this subsection, the sliding mode control for single-input and multi-input Variable Structure Systems (VSS) is discussed.

3.4.1.1 Single-input Variable Structure Control

Consider the *n*-dimensional variable structure system

$$\frac{dx}{dt} = uf_1(x) + (1-u)f_2(x) \tag{3.14}$$

$$u = \begin{cases} 1 & for \quad s(x) > 0 \\ 0 & for \quad s(x) < 0 \end{cases} \tag{3.15}$$

With $S=\{x:s(x)=0\}$ being a smooth $(n-1)$ dimensional manifold defined in the open set N of R^n, with gradient vector $\frac{\partial s}{\partial x} \neq 0$, for all x in S. A sliding regime is said to exist locally on the manifold S whenever the following conditions are satisfied [143]

$$\begin{cases} \lim_{s\to+0} \frac{ds}{dt} = \lim_{s\to+0}[ds, f_1(x)] < 0 \\ \lim_{s\to-0} \frac{ds}{dt} = \lim_{s\to-0}[ds, f_2(x)] > 0 \end{cases} \tag{3.16}$$

with $[ds,f_i]$ being a shorthand notation for the chain rule $\left(\frac{\partial s}{\partial x}\right)^T f_i(x)$.

- Proposition 1 [143]: If a sliding regime exists locally on S then, necessarily, for all $x \in S$ where the sliding regime exists, the following transversality condition is satisfied

$$[ds, f_1(x) - f_2(x)] < 0 \tag{3.17}$$

- Proof is obvious upon subtracting the expressions in (3.16) evaluated on S.

Being a necessary condition, (3.16) determines the extent of a region which properly contains the region of existence of a sliding regime on the surface S.

If a sliding motion exists locally on S, the state trajectories undergo a chattering motion about the switching (sliding) manifold. An idealized version of such a motion is obtained by assuming that the trajectories smoothly evolve on the sliding manifold. To

describe such an ideal sliding dynamic, two general methods have been proposed: Utkin's method, based on the equivalent control method [144], and the method of Filippov's geometric averaging [155].

The equivalent control method is based on defining a function, called the equivalent control denoted by $u_{eq}(x)$, locally defined on S for which the following invariance conditions are satisfied

$$\frac{ds}{dt} = 0 \quad on \quad s = 0 \tag{3.18}$$

Using shorthand notation, these conditions are expressed as

$$[ds, u_{eq}(x) f_1(x) + (1 - u_{eq}(x)) f_2(x)] = 0 \quad on \quad s = 0 \tag{3.19}$$

The geometric (Filippov's approach) interpretation of (3.19) should be clear: the smooth vector field $u_{eq}(x)f_1(x)+(1-u_{eq}(x))f_2(x)$ must be locally orthogonal to the surface gradient at every point $x \in S$ located in the region of existence of the sliding mode. From (3.19) one finds the unique value of the equivalent control for $x \in S$ as

$$u_{eq}(x) = \frac{-[ds, f_2(x)]}{[ds, f_1(x) - f_2(x)]} \tag{3.20}$$

To see that $u_{eq}(x)$ is indeed unique [155], assume $\mu(x)$ is a different function also satisfying (3.19) i.e. $[ds, \mu(x) f_1(x) + (1 - \mu(x)) f_2(x)] = 0$. Subtracting the expression with $\mu(x)$ from(3.19), yields

$$(u_{eq}(x) - \mu(x))[ds, f_1(x) - f_2(x)] = 0 \tag{3.21}$$

Since necessarily $[ds,f_1(x)-f_2(x)]<0$, it follows that $\mu(x)=u_{eq}(x)$, and thus $u_{eq}(x)$ is unique.

When (3.20) is formally substituted in place of the discontinuous control u in (3.14), the obtained dynamic, constrained to evolve on S, is known as the ideal sliding mode. Its explicit expression is readily obtained as follows

$$\frac{dx}{dt} = \frac{-[ds, f_2(x)] f_1(x) + [ds, f_1(x)] f_2(x)}{[ds, f_1(x) - f_2(x)]} \quad x \in S \tag{3.22}$$

- Theorem 1 [156]: Let the transversality condition (3.17) be locally satisfied on S. The necessary and sufficient condition for the local existence of a sliding regime of (3.14), (3.15) on S is that the equivalent control $u_{eq}(x)$ satisfies

$$0 < u_{eq}(x) < 1 \quad on \quad s = 0 \tag{3.23}$$

- Proof [156]: Suppose (3.23) is locally valid on S. Inverting (3.20) and considering (3.23), one obtains

$$\frac{-[ds, f_1(x) - f_2(x)]}{[ds, f_2(x)]} > 1 \quad x \in S \tag{3.24}$$

i.e.,

$$-\frac{[ds, f_1(x)]}{[ds, f_2(x)]} > 0 \tag{3.25}$$

Hence, $[ds, f_1(x)]$ and $[ds, f_2(x)]$ have opposite signs on S. According to the transversality condition (3.17), the numerator of expression (3.24) is negative; $[ds, f_2(x)]$ is then necessarily positive and hence (3.25) implies that $[ds, f_1(x)]<0$, locally on S. It follows that there exists locally an open neighborhood surrounding S where condition (3.16) or a sliding regime exists locally on S. To prove necessity, suppose a sliding regime exists locally on S and conditions (3.16) are locally valid on S. Then there exists a positive function $0<\mu(x)<1$, such that $\mu(x)[ds,f_1(x)]+(1-\mu(x))[ds,f_2(x)]=0$. Solving for $\mu(x)$ obtains the same expressions as in (3.20) for $\mu(x)$. By virtue of the uniqueness of the equivalent control $\mu(x) =\mu_{eq}(x)$, the result follows.

The following theorem expresses the implementation of Filippov's Geometric Averaging method [155] to sliding mode existence conditions.

- Theorem 2 [157]: A sliding regime exists locally on S for system (3.14) and (3.15) if and only if there exists a scalar function $0<\mu(x)<1$ defined on S such that S is a local integral manifold for the average dynamics $f_{av}(x)$, defined as

$$\frac{dx}{dt} = \mu(x) f_1(x) + (1-u(x)) f_2(x) = f_{av}(x) \tag{3.26}$$

It is clear that Filippov's convex combination function $\mu(x)$ is none other than the equivalent control and therefore, Filippov's Average dynamics coincides with the ideal sliding mode.

3.4.1.2 Multi-input Variable Structure Control

To study multi-input variable structure control, consider a dynamic system of the form

$$\begin{aligned} &\dot{x}(t) = f(x) + \sum_{i=1}^{m} g_i(x) u_i = f(x) + G(x)u \\ &u = (u_1, u_2, \ldots, u_m)^T \\ &G(x) = (g_1(x), g_2(x), \ldots, g_m(x)) \end{aligned} \tag{3.27}$$

where f, g_i, for $i=1,2,\ldots,m$, are smooth vector fields locally defined on an open neighborhood X or R^n. It is assumed that the rank of $G(x)$ is m with constant dimension. The sliding surface S is now defined as the intersection of m smooth $(n-1)$ dimensional manifolds, called *individual sliding manifolds* and denoted by s_i

$$S = \bigcap_{i=1}^{m} s_i = \bigcap_{i=1}^{m} \{x \in X : s_i(x) = 0\} =: \{x \in X : s(x) = 0\} \tag{3.28}$$

where $s(x)=(s_1(x), s_2(x),\ldots, s_m(x))^T$ with each s_i being a smooth function, $s_i: R^n \to R$. The set of functions s_i, for i=1,2,…,m, locally have functionally independent gradients denoted by ds_i; S is then locally an $(n\text{-}m)$-dimensional, constant rank, sub-manifold of X.

Similar to (3.15), the variable structure control law is defined component-wise as

$$u_i = \begin{cases} 1 & for \quad s_i(x) > 0 \\ 0 & for \quad s_i(x) < 0 \end{cases} \tag{3.29}$$

In multi-input systems, a wider range of possibilities is offered for the definition of a sliding motion. On the one hand, one may consider sliding motions on each individual surface s_i caused by the action corresponding to the ith controller input. If the sliding motion is made to coverage towards the intersection manifold S, where all controllers induce sliding motions in their individual surfaces, then the combination of "individual" sliding motions results in a "collective" sliding motion.

The sliding motion on a particular individual sliding surface s_i is defined in a manner similar to the single-input case, i.e. a sliding motion locally exists on S_i if, with u_i and all u_j $(j \neq i)$ given by (3.29), the following inequalities are satisfied [143]

$$\begin{cases} \lim_{s_i \to +0} [ds_i, f(x) + G(x)u] < 0 \\ \lim_{s_i \to -0} [ds_i, f(x) + G(x)u] > 0 \end{cases} \tag{3.30}$$

Contrary to the single-input case, condition (3.30) is only a sufficient condition since "collective" sliding motions may exist on S, and hence on s_i, without necessarily having (3.30) satisfied [143]. Now, the question is how to achieve sliding mode on S. In robotic applications of multi-input VSC, one may think about two strategies. The first is: if no particular path is defined for each joint, the ith controller regards the control input u_j $(j \neq i)$ as disturbances and attempts to achieve its individual sliding motion. The second is: the *method of hierarchy of controls* [143] which is resolving the possible conflict and imposing an arbitrary "queue" of the controllers for collective sliding motion. Each controller regards the inputs of those controllers higher in the hierarchy as already undergoing sliding motion on their respective surfaces, and takes the corresponding components of the equivalent control (to be defined as the ideal smooth control, turning S into an invariant manifold) as the applied input. Those controllers lower in the hierarchy are supposed to apply one of the two available feedback control options specified by (3.29). This method can be effective when a special path or priority is defined for the joints.

Now, assume that a sliding mode exists on S achieved by any of the conceptual solutions discussed above. The ideal motions on S, due to the smooth control vector known as the equivalent control, u_{eq}, renders the manifold S as a local integral (invariant) manifold of the controlled system. The equivalent control vector is defined by means of the invariance conditions

$$\begin{cases} s_i = 0 \\ [ds_i, f + Gu_{eq}] = \left(\dfrac{\partial s_i}{\partial x}\right)^T (f + Gu_{eq}) = 0 \quad i = 1,2,\ldots,m \end{cases} \tag{3.31}$$

Or, more briefly

$$\begin{cases} s = 0 \\ \left(\dfrac{\partial s}{\partial x}\right)^T (f(x) + G(x)u_{eq}(x)) = 0 \end{cases} \tag{3.32}$$

From (3.31), the equivalent control is given by

$$u_{eq}(x) = -\left[\left(\frac{\partial s}{\partial x}\right)G(x)\right]^{-1}\left[\left(\frac{\partial s}{\partial x}\right)f(x)\right] \tag{3.33}$$

The dynamic system $\dot{x} = f(x) + G(x)u_{eq}(x)$ is said to describe the ideal sliding dynamics. Further multi-input VSC theorems and lemmas can be found in [143] [144] and [158].

3.4.2 Nonlinear PWM Controller Design

In this section, a recent design method for the specification of stabilizing PWM feedback control for nonlinear dynamic systems is presented. This method is based on an infinite frequency average model and is extracted from [157]. The fundamental achievement in this method is proving that the infinite frequency average model of the PWM controlled system coincides with Filippov's geometrical average dynamics of the original discontinuous PWM system [155]. The average model captures the essential qualitative stability properties of the feedback controlled system and thus considerably simplifies the design task.

There are three classes of nonlinear controlled systems, which use discontinuous feedback control strategies. These are

- Variable Structure Systems (VSS) undergoing sliding regimes
- Plants regulated by PWM techniques
- Systems regulated by Pulse Frequency Modulation (PFM) controllers [159]

PWM controlled systems constitute a class of nonlinear periodlically sampled-data control systems. The sampled output error, being the difference between the desired and the actual plant output signals, is translated into a pulse control signal whose pulse width is proportional to the error signal. PWM controlled systems, as VSS in sliding mode, are typically robust with respect to plant parameter variations and external perturbation signals [157].

In general, PWM controlled systems are recognized by two different classes corresponding to ON-OFF or ON-OFF-ON controlled switches, in which the control variable can be made to take values in the discrete set {0, 1} or {-1, 0, 1}, respectively [142] [160]. DC to DC power convertors and joint positioning control in robotics are examples of ON-OFF and ON-OFF-ON systems, respectively.

In the following sections, first it is shown that in a VSS undergoing structural changes according to an ON-OFF PWM scheme, an infinite sampling frequency assumption reduces the feedback system model precisely to a Filippov's geometric average model of the discontinuous PWM system. This result is then extended to the class of output error feedback ON-OFF-ON PWM switched-controlled plants. The specification of the PWM controller is made on the basis of the average PWM model. The average model is obtained by formally replacing the discontinuous PWM regulator by a nonlinear, memory-less, piecewise smooth controller of the saturation type.

3.4.2.1 ON-OFF PWM Controlled Systems

Consider the nonlinear discontinuously controlled system

$$\frac{dx}{dt} = f(x) = \begin{cases} f_1(x) & for \quad t_k < t \le t_k + D(x(t_k))T \\ f_2(x) & for \quad t_k + D(x(t_k))T < t \le t_k + T \end{cases} \tag{3.34}$$

where $f_1(x)$ and $f_2(x)$ are smooth vector fields defined on R^n. t_k represents regularly spaced instants of time where an ideal sampling process takes place. The duty ratio function, $D(x)$, is determined in correspondence with the value of the sampled state vector, $x(t_k)$. This duty ratio function is assumed to take values in the bounded interval [0, 1]. The regions where $D(x)$ is fixed at either 0 or 1 constitute the saturation regions of the PWM controller. The sampling period T is assumed to be constant, and sufficiently small in comparison to the time constants associated with the dynamics of the controlled system.

In terms of an ideal switching function u, taking values in the discrete set {0, 1}, system (3.34) can be equivalently represented as system (3.14) with a switching control policy of the form

$$u = \begin{cases} 1 & for \quad t_k < t \le t_k + D(x(t_k))T \\ 0 & for \quad t_k + D(x(t_k))T < t \le t_k + T \end{cases} \tag{3.35}$$

Using the following lemma, the next important theorem will be proven.

➢ Lemma 3: Let f be smooth vector filed and let $I_f(t)=\int_0^t f(x(s))ds$. Then for any smooth and strictly positive function $\tau(x)$

$$\lim_{T\to 0, t_k \to t} \frac{(I_f(t_k + \tau(x(t_k))T) - I_f(t_k))}{T} = \tau(x(t)) f(x(t)) \tag{3.36}$$

The next theorem determines the smooth character of the infinite-frequency average dynamics of (3.14), (3.35) under non-saturating conditions.

➢ Theorem 3: In the regions where the PWM controller is not saturated, as the sampling frequency $1/T$ tends to infinity in system (3.34), the discontinuous system is substituted by Filippov's average model

$$\frac{dx}{dt} = D(x) f_1(x) + (1 - D(x)) f_2(x) = f_{av}(x) \tag{3.37}$$

In fact, the duty ratio $D(x)$ represents the convex combination function $\mu(x)$ in (3.26). Moreover, in such a region, a sliding regime is exhibited by the actual PWM controlled system (3.14), (3.35) about an integral manifold $S=\{x\in R^n: s(x)=0\}$ of (3.37).

➢ Proof: From (3.34), the state x at time t_k+T is exactly computed as

$$\begin{aligned} x(t_k + T) &= x(t_k) + \int_{t_k}^{t_k + D(x(t_k))T} f_1(x(\sigma))d\sigma + \int_{t_k + D(x(t_k))T}^{t_k + T} f_2(x(\sigma))d\sigma \\ &= x(t_k) + \int_{t_k}^{t_k + D(x(t_k))T} f_1(x(\sigma))d\sigma + \int_{t_k}^{t_k + T} f_2(x(\sigma))d\sigma \\ &\quad - \int_{t_k}^{t_k + D(x(t_k))T} f_2(x(\sigma))d\sigma \end{aligned}$$

Assuming that $D(x)$ takes a value between 0 and 1 in the region of interest, and using Lemma 3, one has

$$\begin{aligned} &\lim_{T\to 0, t_k \to t} \frac{x(t_k + T) - x(t_k)}{T} \\ &= \lim_{T\to 0, t_k \to t} \frac{\int_{t_k}^{t_k + D(x(t_k))T} f_1(x(\sigma))d\sigma + \int_{t_k}^{t_k + T} f_2(x(\sigma))d\sigma - \int_{t_k}^{t_k + D(x(t_k))T} f_2(x(\sigma))d\sigma}{T} \\ &= D(x) f_1(x) + (1 - D(x)) f_2(x) \end{aligned}$$

In other words, the infinite frequency model of (3.34) coincides with Filippov's average model in which the convex combination $\mu(x)$, defining the average vector field $f_{av}(x)$, is precisely taken as the duty ratio function $D(x)$.

From the results of Theorem 2, and the assumption that the duty ratio function is locally bounded in the open interval (0, 1), it follows that a sliding regime exists locally

on the manifold S for the VSS (3.34). The equivalent control $u_{eq}(x)$, associated with such a sliding regime, is simply obtained from the invariance conditions (3.19) for the ideal sliding mode taking place on S (see Equation (3.20)). It follows, from the uniqueness of the equivalent control that

$$D(x) = u_{eq}(x) = \frac{-[ds, f_2(x)]}{[ds, f_1(x) - f_2(x)]} \tag{3.38}$$

i.e., the equivalent control of the sliding motion associated with (3.34) is then, precisely, constituted by the duty ratio associated to the PWM control scheme. The corresponding ideal sliding dynamic is then represented by

$$\begin{aligned} \frac{dx}{dt} &= u_{eq}(x) f_1(x) + (1 - u_{eq}(x)) f_2(x) \\ &= D(x) f_1(x) + (1 - D(x)) f_2(x) \end{aligned}$$

which is just the average PWM model (3.37).

The region of existence of a sliding motion is determined by the region on S where conditions (3.16) are satisfied. From the results of Theorem 2 the portion of S on which $D(x)$ satisfies

$$0 < D(x) = u_{eq}(x) < 1$$

determines such an existence region. The duty ratio evidently satisfies the above condition, along the integral manifold S, in all regions of the state space where the PWM controller is not saturated.

- Corollary 1 [157]: Provided $0<D(x)<1$, Filippov's average model corresponding to a PWM controlled system of the form

$$\frac{dx}{dt} = f(x) + ug(x) \tag{3.39}$$

with u given as in (3.35), is obtained by formally substituting the discontinuous control variable u by the duty ratio function $D(x)$, i.e.

$$\frac{dx}{dt} = f(x) + D(x)g(x) = f_{av}(x) \tag{3.40}$$

Moreover, in such a non-saturation region, the actual controlled system (3.39), (3.35) exhibits a sliding motion about an integral manifold for $S=\{x: s(x) =0\}$ satisfying the condition $[ds, f_{av}(x)] =0$.

The proof is immediate upon letting $f_1(x) = f(x) + g(x)$ and $f_2(x) = f(x)$ and using the results of theorem 3.

3.4.2.2 ON-OFF-ON PWM Controlled Systems

Consider the nonlinear PWM controlled system

$$\frac{dx}{dt} = f(x) = \begin{cases} f_1(x) + f_2(x)\,\mathrm{sgn}(e(t_k)) & for \quad t_k < t \le t_k + D(x(t_k))T \\ f_1(x) & for \quad t_k + D(x(t_k))T < t \le t_k + T \end{cases} \tag{3.41}$$

where $f_1(x)$ and $f_2(x)$ are smooth vector fields and $e(x)$ is a known smooth scalar function of x. The above system can be expressed, in terms of a switch position function u taking values in the discrete set {-1, 0, 1}, as

$$\frac{dx}{dt} = f_1(x) + uf_2(x) \tag{3.42}$$

with

$$u = PWM_D(e(t_k)) \begin{cases} \mathrm{sgn}(e(t_k)) & for \quad t_k < t \le t_k + D(x(t_k))T \\ 0 & for \quad t_k + D(x(t_k))T < t \le t_k + T \end{cases} \tag{3.43}$$

It should be noted that for both $e(x)>0$ and $e(x)<0$ the PWM controlled system is an ON-OFF PWM controlled system of the form (3.39). It is easy to see, from the results of Corollary 1, that the average PWM model of (3.42)-(3.43), in the region where $0<D(x)<1$, is simply described by

$$\frac{dx}{dt} = f_1(x) + D(x)\,\mathrm{sgn}(e(x))\,f_2(x) \tag{3.44}$$

- Corollary 2 [157]: In those regions of the state space where $0<D(x)<1$, the state trajectories of the ON-OFF-ON PWM controller system (3.42)-(3.43) exhibit a sliding mode behavior about integral manifolds of the average PWM model (3.44).

3.4.2.3 Output Error Feedback PWM Controlled System

In Figure 3.8 a block diagram for a nonlinear PWM feedback controlled system is depicted. This system is described by

$$\begin{cases} \dfrac{dx}{dt} = f(x) + ug(x) \\ y = h(x) \\ e = y_d(t) - y \\ u = MPWM_D(e(t_k)) \end{cases} \tag{3.45}$$

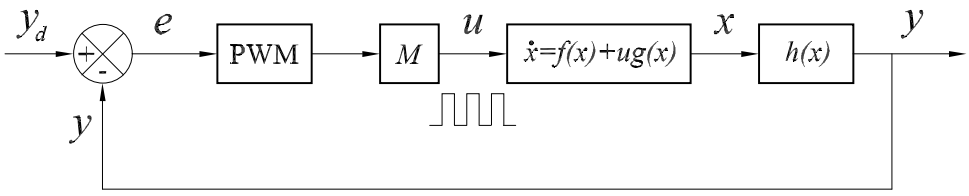

Figure 3.8 Nonlinear PWM Controlled System

with f and g being smooth vector fields, while h is smooth scalar output function. The control input u is a discontinuous scalar control function obtained as the output of a pulse width modulator excited by the output error e. The error signal e is obtained, at each

instant, as the difference between the desired output value $y_d(t)$ and the actual output value $y(t)$. The sampling process associated with the PWM process is assumed to take place at regularly spaced time intervals of fixed duration T, i.e., $t_{k+1}=t_k+T$. M is a positive constant gain representing the maximum allowable input magnitude.

The PWM control operator, $PWM_D(e)$, characterizing as ON-OFF-ON switch is defined as in (3.43) with $D(e(t_k))$ as the error dependent duty ratio function defined by

$$D(e(t_k))\begin{cases}\beta|e(t_k)| & for \quad |e(t_k)| \le 1/\beta \\ 1 & for \quad |e(t_k)| > 1/\beta\end{cases} \tag{3.46}$$

where β is a positive constant. It should be noted that

$$D(e(t_k))\,\mathrm{sgn}(e(t_k)) = sat(e(t_k),\beta) = \begin{cases}\beta|e(t_k)| & for \quad |e(t_k)| \le 1/\beta \\ \mathrm{sgn}(e(t_k)) & for \quad |e(t_k)| > 1/\beta\end{cases} \tag{3.47}$$

The basis of a design technique for the above class of PWM controlled systems, is given by the corollary bellow.

- Corollary 3 [157]: As the sampling frequency $1/T$ tends to infinity, the description of the nonlinear controlled system (3.45) coincides with

$$\begin{cases}\dfrac{dx}{dt} = f(x) + vg(x) \\ y = h(x) \\ e = y_d(t) - y \\ v = Msat(e,\beta)\end{cases} \tag{3.48}$$

As shown in Figure 3.9, the behavior of the infinite frequency sampled system is described by a nonlinear system which includes a continuous piecewise smooth control v, generated as the output of a memory-less nonlinear function of the saturation type. The saturation function is excited by the output error signal e. In other words, to evaluate the average behavior of the PWM controlled system, the PWM controller is simply substituted by a nonlinear memory-less saturating controller.

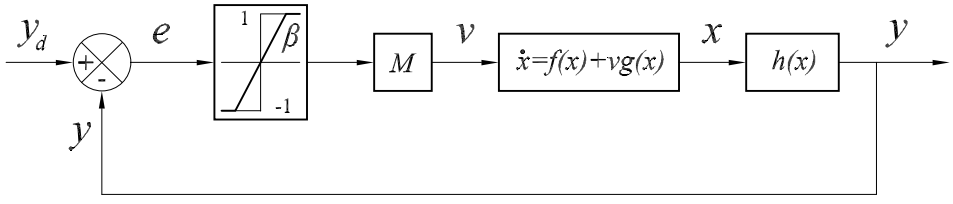

Figure 3.9 Average Model of ON-OFF-ON PWM Controlled System

A necessary and sufficient condition for asymptotic stability of the actual PWM system (3.45), toward the state space manifold represented by e=0, is given by the asymptotic stability of the average model towards the same manifold. Furthermore, the actual PWM controlled response can be made to follow, arbitrarily closely, in a sliding

mode fashion, the response of the average model [156]. This is accomplished by suitably increasing the sampling frequency of the PWM controller. If the response of the average model (3.48) is asymptotically stable to the zero error manifold, then the actual PWM controller system trajectories slide around the average trajectories toward such a manifold. The amplitude of the chattering motion decreases as the sampling frequency increases. The following theorems express the above concepts in a more mathematical form. The proofs of these theorems can be found in [157].

- Theorem 4: the closed loop PWM controlled system (3.45) is asymptotically stable toward the manifold e=0, if and only if the average PWM system (3.48) is asymptotically stable toward such a manifold.

At the sampling instant t_k, let $e^*(t_k)=x(t_k)-z(t_k)$ be the difference between the state x of the PWM controlled system (3.45) and the state z of the average model (3.48). Assuming the vector field $f(x)$ is globally Lipschitz[17] and the vector field $g(x)$ is globally bounded on R^n, i.e., there exist constants L_1 and G such that $\|f(x)-f(z)\| \le L_1\|x-z\|$ and $\|g(x)\| \le G$ for all x and z in R^n. Under the above assumptions the following theorem is expressed.

- Theorem 5: Given a small positive ε, there exists, for any arbitrary finite time interval, [0, NT], a sampling frequency $F_0=1/T_0$ such that, in the initial difference $e^*(t_0)=x(t_0)-z(t_0)$, of the initial states of systems (3.45) and (3.48) is norm bounded by a small positive quantity δ, then $e^*(t_0+\mathrm{NT})$ is norm bounded by $(1+\varepsilon)\delta$, for any sampling frequency $F>F_0$ and

$$\left\|e^*(t_0+NT)\right\| \le (2MNGT+\left\|e^*(t_0)\right\|)\exp(L_1NT) \tag{3.49}$$

The following transcendental equation, which is directly obtained from (3.49)

$$2MNGT+\delta=(1+\varepsilon)\delta\exp(-L_1NT) \tag{3.50}$$

has a unique solution for some $T=T_0>0$. This is due to the fact that the left hand side term monotonically increases with T from the value δ at T=0, while the right hand side term monotonically decreases with T from the value $(1+\varepsilon)\delta>\delta$ at T=0. Hence, given an initial error bound, $\|e^*(t_0)\|\le\delta$, and a small positive constant ε, a sampling frequency

---

[17] **Lipschitz Condition:**

A function $f(x)$ satisfies the Lipschitz condition of order α at x=0 if

$$\left|f(h)-f(0)\right| \le B|h|^{\beta}$$

for all $|h|<\varepsilon$, where B and β are independent of h, $\beta>0$, and α is an upper bound for all β for which a finite B exists.

$F_0=1/T_0$ exists for which a pre-assigned bound of the form $(1+\varepsilon)\delta$ can be obtained such that $\|e^*(t_0+NT)\|\leq(1+\varepsilon)\delta$. It follows, according to (3.49) that for any sampling frequency $F>F_0$ ($T<T_0$) the states error $e^*(t_0+NT)$, is strictly bounded by $(1+\varepsilon)\delta$.

Equation (3.50) may be solved iteratively for T (or for NT) once all its parameters have been identified from the system model. Since (3.50) does not depend on β, the task of finding an appropriate sampling frequency is thus independent of the problem of finding a stabilizing parameter β for the PWM controller.

3.4.2.4 High-gain Approach for Average PWM Controller Design

The design tasks are reduced to determining the average PWM operator gain, β, and an appropriate sampling frequency. The gain β is desired to stabilize the response of the average closed loop system toward the manifold $e=0$. The appropriate sampling frequency must be such that it makes the actual PWM controlled trajectory follow arbitrarily close to the designed average model.

Although a Lyapunov-based design approach can be sufficient to study the stability of (3.48) and determine the value of β, the following theorem allows one to establish an easily implemented design method based on the high-gain method [161].

- Theorem 6: If the control law $u=M\text{sgn}(e)$ creates a sliding regime locally around the manifold $e=y_d-y=y_d-h(x)=0$, then there exists a sufficiently high gain β of the average PWM operator such that the state trajectories of the average PWM system stabilize toward $e=0$.
- Proof [157]: Suppose such a sliding regime exists locally on $e=0$ and for simplicity let $y_d=0$. Then it follows that locally

$$\begin{cases} \lim_{e\to+0}\dfrac{de}{dt}=\lim_{e\to+0}-[dh,\ f+Mg]<0 \\ \lim_{e\to-0}\dfrac{de}{dt}=\lim_{e\to-0}-[dh,\ f-Mg]>0 \end{cases} \tag{3.51}$$

Subtracting these inequalities on $e=0$ one obtains $[dh,\ g]>0$ locally on the zero error manifold. It follows from the smoothness assumptions on h and g that there exists a boundary layer of width 2ε around $e=0$, with ε arbitrarily small, where locally $[dh,\ g]>0$. Taking $\beta>1/\varepsilon$ the control law $u=\beta e=-\beta y$ yields a controlled error of the form

$$\frac{de}{dt}=-[dh,\ f]+\beta y[dh,\ g] \tag{3.52}$$

It is evident that for sufficiently high β the controlled error dynamics exhibit a time scale separation property. Indeed, dividing by β and letting $\beta\to\infty$ one sees that since

$[dh, g]>0$ then $e=-y=0$ is a slow manifold of the controlled system. The corresponding fast subsystem, described in the fast time scale $\sigma=\beta t$ is given by

$$\frac{de}{d\sigma} = y[dh, g] = -e[dh, g] \tag{3.53}$$

which is locally asymptotically stable toward $e=0$. It follows from Tihonov's theorem [161] that $e=-y=0$ is an asymptotically stable manifold for the high gain controlled system.

As far as the parameter β is concerned, this result immediately suggests a method for the design of PWM controllers. First, the existence of a local sliding regime on the manifold $y=0$ is verified and then a high gain replacement for the discontinuous controller will be found. This entails finding an appropriate boundary layer along the sliding manifold. The slope of the linear portion of the high gain controller coincides with the needed stabilizing parameter β of the PWM system.

The high-gain approach to design of nonlinear feedback control systems is usually accompanied by the singular perturbation method. In Appendix A, the singular perturbation concept is introduced and some further references are provided.

3.4.3 Independent Joint Control

In the control of robotic manipulators, the joint inputs are determined to execute a commanded motion. The joint inputs may be joint forces/torques, or the inputs to the actuators such as commanded voltages. The commanded motion is typically specified as a sequence of end-effector positions and orientations.

There are many control techniques and methodologies used in the control of manipulators with which different performances may be observed. In addition, the mechanical design of the manipulator influences the type of control scheme needed. As an example, compare a robot actuated by permanent magnet DC motors with gear reduction to a direct-drive robot using high-torque motors with no gear reduction. In the first case, the motors' dynamics are linear and well understood and the effect of the gear reduction is largely to decouple the system by reducing the nonlinear coupling among the joints. However, the presence of the gears introduces friction, drive train compliance and backlash. In order to achieve high performance, the control designer would likely have to pay more attention to these latter effects than to nonlinear inertia, Coriolis forces, etc. In the case of a direct-drive robot, the problems of backlash, friction, and compliance due to the gears are eliminated. However, the nonlinear coupling between the links is now significant, and the dynamics of the motors themselves may be much more complex.

In order to design local controllers, here independent joint control is used. In this type of control, each axis of the manipulator is controlled as a single-input/single-output system. Any coupling effect due to the motion of the other links is either ignored or treated as a disturbance.

To formulate the design procedure for local controllers of SMD modular robots, we start by recalling the independent joint control method for regular manipulators in which their links are actuated by DC motors. The block diagram of a permanent magnet DC motor is shown in Figure 3.10. In this model the DC-motor is in series with a gear train with ratio 1: n (1/n=r) and is connected to a link of the manipulator, and τ_l is the load torque required by the manipulator at the associated joint. The input $V(s)$ and output $\theta_m(s)$ are DC motor voltage and motor angular position, respectively. Based on this block diagram, the equations of motion can be derived as

$$(Ls + R)I_a(s) = V(s) - K_b s\theta_m(s) \tag{3.54}$$

$$(J_m s^2 + B_m s)\theta_m(s) = K_i I_a(s) - r\tau_l(s) \tag{3.55}$$

where L, R and I_a are motor armature inductance, resistance and current, and K_b and K_i are back emf and torque constant, respectively. The inertia J_m and damping coefficient B_m represent both armature and gear train inertias and damping coefficients.

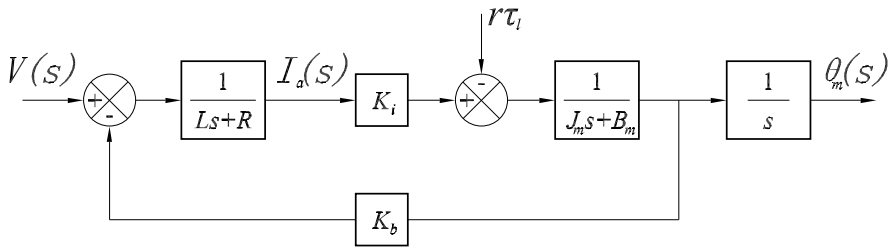

Figure 3.10: Block Diagram for a Linear DC Motor System

Frequently, it is assumed that the electrical time constant L/R is much smaller than the mechanical time constant J_m/B_m. This is a reasonable assumption for many electromechanical systems and leads to a reduced order model of the actuator dynamics. If we now divide numerator and denominator of (3.54) by R and neglect the electrical time constant by setting L/R equal to zero, the transfer function between θ_m and V becomes (with τ_l=0)

$$\frac{\theta_m(s)}{V(s)} = \frac{K_i / R}{s(J_m s + B_m + K_b K_i / R)} \tag{3.56}$$

Similarly the transfer function between θ_m and τ_l is

$$\frac{\theta_m(s)}{\tau_l(s)} = \frac{r}{s(J_m s + B_m + K_b K_i / R)} \tag{3.57}$$

In the time domain, Equations (3.56) and (3.57) represent, by superposition, the second order differential equation

$$J_m\ddot{\theta}(t)+(B_m+K_bK_i/R)\dot{\theta}(t)=\tau_m-r\tau_l \tag{3.58}$$

where $\tau_m=(K_i/R)V(t)$ is the generated torque by the motor. If the output side of the gear train is directly coupled to the link, then the joint variables q_k's and the motor variables are related by

$$q_k=r_k\theta_{m_k} \quad k=1,2,\cdots,n \tag{3.59}$$

where r_k is the kth gear ratio. Similarly, the joint torques and the actuator load torques τ_{l_k} are related by

$$\tau_{l_k}=\tau_k \quad k=1,2,\cdots,n \tag{3.60}$$

Then the equation of motion of the manipulator can be written as [50]

$$\sum_{j=1}^{n} d_{jk}(q)\ddot{q}_j+\sum_{i,j=1}^{n} c_{ijk}(q)\dot{q}_i\dot{q}_j+g_k(q)=\tau_k \tag{3.61}$$

$$J_m\ddot{\theta}_{m_k}+(B_m+K_bK_i/R)\dot{\theta}_{m_k}=\tau_{m_k}-r_k\tau_k \quad k=1,2,\cdots,n \tag{3.62}$$

Equation (3.62) represents the actuator dynamics and (3.61) represents the nonlinear inertial, centripetal, Coriolis, and gravitational coupling effects due to the motion of the manipulator. The simplest approach to the control of the above system is to consider the nonlinear term τ_k entering (3.62) and defined by (3.61) as an input disturbance to the motor and design an independent controller for each joint according to model (3.62) are linear. Notice that τ_k in (3.62) is proportional to the gear reduction r_k. This is an important observation. The effect of the gear ratio is to reduce the coupling nonlinearities represented by (3.61), which adds to the validity of the above approach to control. However, for high speed motion, or for manipulators without gear ratio at the joints, the coupling nonlinearities have a much larger effect on the performance of the system. Treating the nonlinear coupling terms represented by τ_k simply as a disturbance, and using classical controllers such as PD compensator will generally cause large tracking error.

4 Analysis and Design of EA Mechanism

The key idea of elastic actuation (EA) is to place a compliant spring between mechanical rotation source and load. By measuring the deflection of the spring, the torque in the spring and thus the torque in robot joint can be inferred. Closed loop feedback control then modulates the actuation system to obtain the desired output torque. This technique is termed Elastic Actuation.

This chapter discusses the fundamental principle of elastic actuation. By systematic analysis of its requirement, a concept model is produced. Based on that model, some features and functions of EA are derived.

4.1 Feasibility Analysis

4.1.1 Back lash in SMD Mechanism

As described in previous chapter, SMD itself can "run" a mechanism in both articulated form and parallel form with simple position/trajectory controller. However there is a fatal weakness for nearly all motion system – the "back lash" caused by the physical component in that system.

Back lash is one of the main principal causes of positional uncertainty in a motion system. Simply stated, all mechanical devices, even a bar of solid steel, have some elasticity. Thus, a small torque and rotation can be applied to the output of a device (or one end of the bar) and be absorbed in the windup of the device or bar, with no movement at the input (or other end of the bar).

In gearbox backlash describes the condition in which an input to a mechanism yields no corresponding displacement at the output. Backlash is the amount by which the width of a gear's tooth space exceeds the thickness of an engaging tooth measured at the pitch circle of the gears, as shown in Figure 4.1.

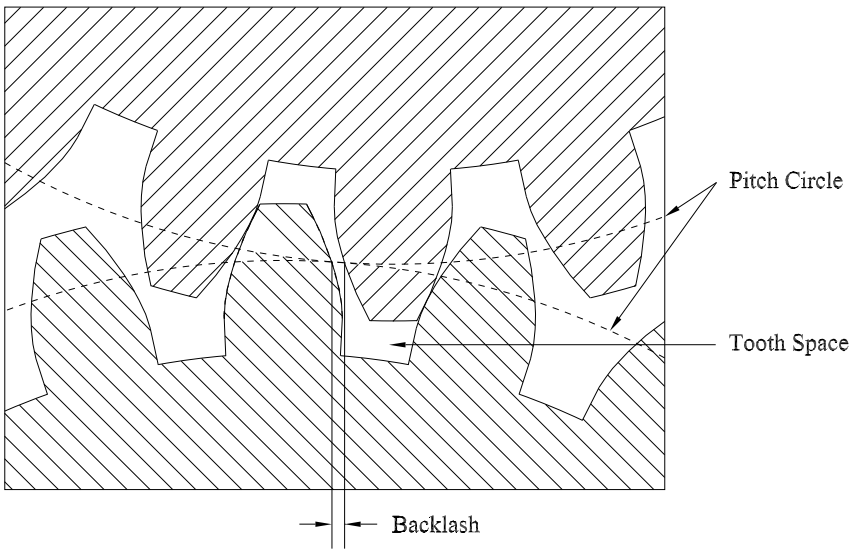

Figure 4.1 Backlash is Inherent in Gear Mate

The error caused by backlash can be accumulated to very large scale in large gear train system. Unfortunately, SMD is such kind of mechanism. The end-effector shaking and jerk of SMD arm has been noticed long time. It seems improvement of SMD design and fabrication alone cannot solve this inherent problem.

To minimize the effects of back lash in SMD, here is one solution from the outer side of SMD itself. Spring is a widely used device which can translate physic motion into force/torque variation. By using torsion spring with the gear mate, uncontrollable back lash can be translated into controllable torque variation, and nonlinear contact force pulse can be converted to linear torque variation. The problem of back lash is minimized by adding an elastic feature with SMD.

Fortunately, the elastic feature with spring just has more merits than this. They are discussed in next subsection.

4.1.2 Other Merits of Elastic Actuation

The vast majority of commercial robot applications consist of tasks that control the position[18] or trajectory of each robot's degree of freedom. Traditional robots can do this with great speed, endurance and accuracy. Robots have been used in this commercial niche because repetitive tasks which require endurance and accuracy are difficult and tedious for humans.

On the other hand, there are many tasks in which robot competence is inferior to that of biological counterparts. Despite extensive research, actions such as walking, running, swimming, catching, grasping and manipulation, considered easy to most able-

[18] The term position is the generalized position / orientation vector.

bodied humans, are difficult for robots. These tasks all required interacting with the real world.

Since our world is kinematically and inertially constrainted, it is important for a robot to be able to sense and control the interaction forces between itself and the environment. This is typically referred to as Force Control[19]. There are two aspects to successful force control. The first is to use an algorithm and sensory information to determine the desired robot joint torques in order to place the proper forces on the robot's environment. The second aspect of successful force control is to generate accurate forces at the robot joints. This chapter deals with the second aspect of force control and specifically on the actuation mechanism that create the forces.

Present-day actuation technology is typically poor at generating and maintaining accurate forces. Using local closed-loop control of actuator forces can improve the quality of force output by rejecting disturbances. Furthermore, it has also been shown that using a compliant load sensor in a configuration called Elasticity (Linear or Torsion), increases an actuator's ability to generate accurate forces.

The focus of this chapter is to analyze and quantify the effects of load sensor compliance for closed-loop actuator force control. There are some unifying principles of series elasticity that can be captured in a general mathematical model. These general principles are further developed with specific models and physical prototypes for situation that EA and SMD, as two complementary actuation methods, are combined together to form a brand new actuation approach in the research field of biped robot.

4.1.3 Ways to Elastic Actuation

The torque output capabilities of a standard actuator such as an electric motor with gear reduction or a hydraulic piston can be dramatically improved by using a load sensor as feedback for a closed-loop control system. This technique has been used for many years on both actuator closed-loop torque control and robot endpoint force control.

Standard load sensors are designed to be as stiff as possible for a given load. This allows the sensor to transmit power interactions with no internal storage of energy. Unfortunately, a stiff load cell in series with an already stiff actuator means that the open-loop gain of the actuator is very high. This in turn implies that to maintain actuator control stability, control gains must be kept low. Low control gains typically indicate poor overall closed loop performance. Low control gains, high impedance actuators and stiff

[19] The term force denotes a gernalized force / torque vector.

sensors make a system such deficient that it cannot handle shock loads from the environment or filter out friction and other transmission non-linearities inherent in real systems.

To overcome these deficiencies, several investigators including Howard [89] and Pratt and Williamson [90] [91] experimented with a closed-loop control of an electro-magnetic motor and gear reduction in series with a compliant spring. Information about torque in the spring is obtained by measuring the spring strain or deflection. Pratt and Williamson named this actuator configuration a Series Elastic Actuator.

Series elastic actuators are topologically similar to any motion actuator with a load sensor and closed-loop control system. However, there are two significant differences resulting from the compliant element. First, there is increased energy storage in the spring that cannot be neglected. Second, integration of a compliant load-bearing sensor within a compact actuator can prove challenging. Nevertheless, compact designs have been successfully developed.

The primary advantage of series elasticity is that the compliant load bearing sensor lowers the loop gain of the closed-loop system. The control gain can be proportionally increased to maintain the overall loop gain of the actuator at desired stability margins. This allows series elastic actuators to have low output impedance, be tolerant to shock loading and robust to changing loads. In addition, the increased controller gain greatly reduces the effects of internal stiction and other transmission non-linearities to give the actuators clearn torque output.

Many other research and commercial groups have recognized that purposeful compliance in actuators can be beneficial for force control. (Several of these ideas and implementations in both standalone actuators and complete robots are described in Chapter 2.) For the most part, in the past, the advantages of compliance in actuators, including series elastic actuators, have been explained with intuitive reasoning and not with mathematical demonstration.

In the following section, quantitative understanding for closed-loop control of elastic actuation is built. Performance measures for the actuator are also given. These measures include closed-loop bandwidth, large torque bandwidth, output impedance, and inertial loading effects. These performance measures can be used to help guide actuator design, especially in choosing the stiffness of the elasticity.

4.2 Concept Model

As described before, the main idea behind EA is to generate actuation torque for robot with low torque output impedance, while avoid using bulky EM motor at every joint. In this thesis, the mechanism of Elastic Actuation is to convert pure rotational motion (income) into pure torque (outcome). Figure 4.2 shows the main components of an EA mechanism with the round corner box indicating the division between power domain and signal domain. Its main elements are: Elasticity, Control System, Actuation, and System Inputs.

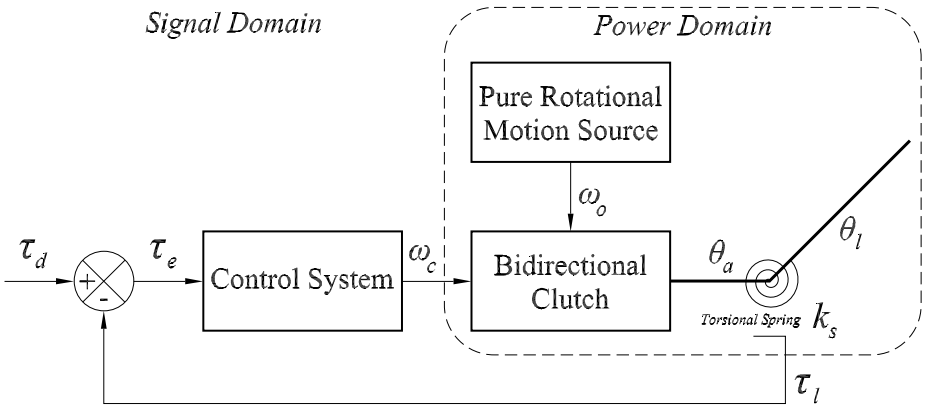

Figure 4.2 Concept Model of EA

This concept model is almost the same as any conventional robot joint with closed loop force control except two differences in Power Domain:

- Mechanical energy comes from a Pure Rotational Motion Source and modulated by Bidirectional Clutch. (PWM control of bidirectional clutch is presented in Chapter 3)
- Mechanical energy is delivered to robot link via Torsion Spring with relatively small stiffness k_s.

4.2.1 Elasticity

The elasticity can be thought of two parts. One part is the spring which is in the power domain. The other part is the deflection sensor which is in the signal domain.

The elasticity is produced by a linear torsion spring with a spring constant k_s between the mechanical power output (output end of bidirectional clutch) and load (link). Depending on the spring stiffness, the deflection can be significant in order to cover the full torque output range.

The sensor measures the deflection in the spring which is a representation of the torque τ_l, generated by the spring. Normal torsion spring has no hysteresis and therefore the relationship between torque and spring deflection is defined by Hooke's Law [162]:

$$\tau_l = k_s \theta_s \tag{4.1}$$

where θ_s is the spring deflection, defined by the difference between the output shaft angle of bidirectional clutch θ_a and the link position θ_l:

$$\theta_s = \theta_a - \theta_l \tag{4.2}$$

It is possible to measure both θ_a and θ_l and take the difference for the measurement, but there may be uncorrelated noise between these two measurements due to transmission dynamics and other non-liberalities, and thus not a good idea. In order to reduce noise from the compliant sensor, it is much better to make a single direct measurement of the spring deflection θ_s. Since the torsion spring has a good linearity between torque and deflection, the measurement of spring deflection is a very good representation of the torque output of the spring.

4.2.2 Control System

The spring strain measurement θ_s implies the load torque τ_l or torque in the spring and is used for feedback in a control system. Given that there is some desired torque τ_d for the joint, the error between these two signals will define the input to the controller τ_e:

$$\tau_e = \tau_d - \tau_l \tag{4.3}$$

For the simplicity of analysis, the control system is represented by the controller gain K. Therefore the control law for the EA concept model is:

$$\omega_c = K \tau_e \tag{4.4}$$

K has the proper units to convert torque error to desired angular velocity.

With further controller development, improvements in overall system performance can be realized. However, a proportional control law K clearly demonstrates the closed-loop effects of the elastic actuation. Premature introduction of complex control systems would make the underlying issues hard to understand. There are ample methods for controller design once the basic concepts of the plant characteristics are clarified [163] [164].

4.2.3 Actuation Mechanism

The actuation mechanism relays the mechanical torque and motion generated by the single energy source – EM motor – usually mounted in the biped robot's trunk. For the

consideration of energy efficiency, there are two sets of speed reduction in the mechanism: one just after the motor output and the other at each joint. Therefore the actuation mechanism in the concept model is also assumed to be a high impedance velocity source and has a simple relationship between controller input ω_c and actuation output ω_a.

$$\omega_a = K_a \omega_c \tag{4.5}$$

where K_a is the gain of the actuation mechanism.

In equation (4.5) the mass of actuation mechanism is neglected because by means of proper controller, the single motor can generate the required constant source angular velocity, or pure velocity, no matter how much the mass or inertia is[20]. The theory model of this actuation mechanism is graphically depicted in Figure 4.3.

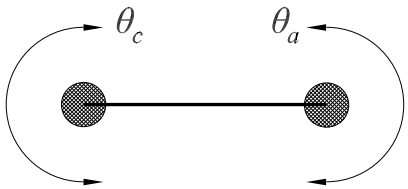

Figure 4.3 Graphical Representation of the Actuation Mechanism
which neglects mass or inertia and thus has an instantaneous limit of torque and velocity

Since the torque in the spring is a function of its deformation or the position difference of two ends, which are defined by the actuation mechanism and link position, the position of the actuation mechanism is the time integral of the actuation velocity:

$$\theta_a = \int \omega_a(t) \tag{4.6}$$

It can be written in the Laplace form:

$$\Theta_a = \frac{\Omega_a}{s} \tag{4.7}$$

Substituting equation (4.5) into equation (4.7) and solving for the actuation position output Θ_a, creates a transfer function relating controller velocity to actuation position:

$$\Theta_a = \frac{K_a}{s}\Omega_c \tag{4.8}$$

Typical actuation system should be designed to be low impedance devices when used in torque control situations. However in this case it is actually advantageous to have a high impedance actuation mechanism modulating the position of the spring for two reasons:

[20] Many commercial EM motor amplifiers can do this.

- The causality of the spring dictates that it should have a position input to give a torque output. The better the actuation mechanism can modulate the spring position, the cleaner the torque output of the spring.
- It is easier to control the velocity and thus the position's output of a real rotation mechanism than it is for the force. This is due to the fact that real rotation mechanism including transmissions has non-linearity such as backlash and friction that create torque noise in the system.

4.2.4 System Inputs

There are two system inputs or boundary conditions:

- τ_d – desired output torque.
- θ_l – rotational motion from the load or robot link.

The desired torque is in the signal domain. The value of τ_d is generated by a higher level controller. Ideally, the output torque of the mechanism equals τ_d with one-to-one correspondence in magnitude and phase over the frequency spectrum.

The motion of the load, θ_l, is in the power domain. Since the actuation is in torque control, the mechanism may be either directly in contact with the environment or it may be connected to a freely moving inertial load. When in contact with the environment, the load position can be considered a position source either fixed or moving. However, an inertial load moving in free space defines the load position as a function of the torque in the spring and the load inertia. There is energy interaction between the spring and the load that must be taken into account.

4.3 Feature and Function

4.3.1 Linear Model of EA

With each of the main elements of elastic actuation defined, the linear model can now be derived. Figure 4.4 shows the model in both time and frequency domain representation.

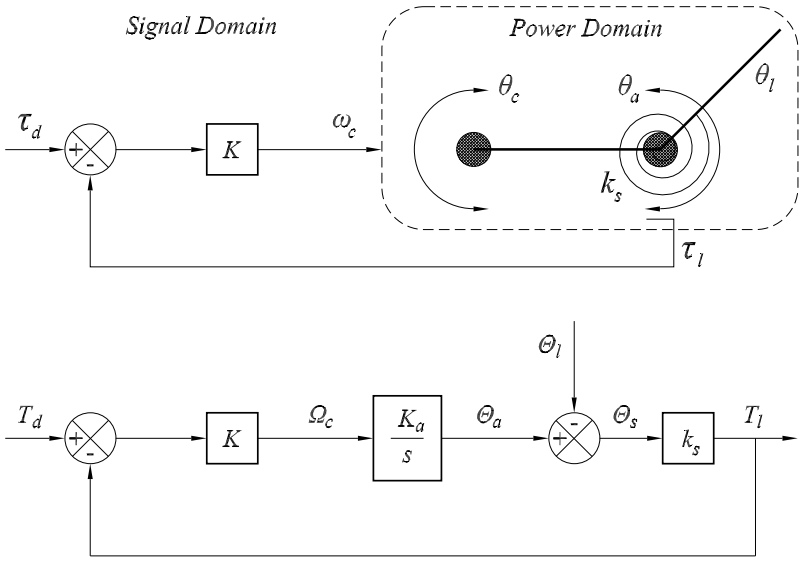

Figure 4.4 General Model and Block Diagram for an Elastic Actuation Mechanism

The goal of EA is to control the torque in the spring, T_l. The model of this figure is used to derive the linear dynamic equation for T_l as a function of the two inputs T_d (desired input force) and Θ_l (position of the load/link).

4.3.1.1 General Power Domain Open Loop Model

The torque T_l in the spring is directly proportional to the spring's deformation or displacement Θ_s, as described in equation (4.1). Θ_s is a function of the actuation mechanism Θ_a and the boundary condition for position of the load Θ_l, as described in equation (4.2). Substituting equation (4.2) into equation (4.1) for Θ_s:

$$T_l = k_s \Theta_s = k_s (\Theta_a - \Theta_l) \tag{4.9}$$

Subsequently putting equation (4.8) into the result for Θ_a yields the open loop dynamics for the torque in the spring of a general elastic actuation system:

$$T_l = k_s (\frac{K_a}{s} \Omega_c - \Theta_l) \tag{4.10}$$

Equation (4.10) shows that the open loop power domain model for the torque in the torsion spring, T_l, is a function of the input from the controller and the position of the load.

4.3.1.2 General Closed Loop Model

The closed loop dynamic equation can be derived by including feedback and a control law. From equation (4.4) the input velocity signal to the actuation mechanism Ω_c is proportional to the error difference between the desired torque and load torque:

$$\Omega_c = K(T_d - T_l) \tag{4.11}$$

Combining the open loop power domain model equation (4.10) with the control law equation (4.11) gives:

$$T_l = k_s(\frac{K_a}{s}\Omega_c - \Theta_l) = k_s(\frac{K_a}{s}K(T_d - T_l) - \Theta_l) \tag{4.12}$$

Solving the equation for T_l, the closed loop dynamic equation of a general elastic actuation mechanism is:

$$T_l(s) = \frac{k_s K K_a T_d(s) - k_s s\Theta_l(s)}{s + k_s K K_a} \tag{4.13}$$

The inputs for equation (4.13) are, as described in the previous section, the desired torque T_d and the motion of the load Θ_l.

4.3.2 Two Environments of EA

There are two inputs to the elastic actuator, desired torque T_d, and load motion Θ_l. By looking at the effects of each of these two inputs independently, the closed loop bandwidth and output impedance can be understand as two separate cases: fixed load motion, and forced load motion.

4.3.2.1 Fixed Load Motion

The first case has fixed load motion where Θ_l is constant (Figure 4.5). Rewriting equation (4.13) with this constraint defines the closed loop bandwidth. The relative values of the control gain, K, and the spring stiffness of the sensor, k_s, play an important role in defining the actuator bandwidth. In the control of an elastic actuation mechanism, a decrease in spring stiffness is compensated for an increase in control gain in order to maintain a high closed loop bandwidth.

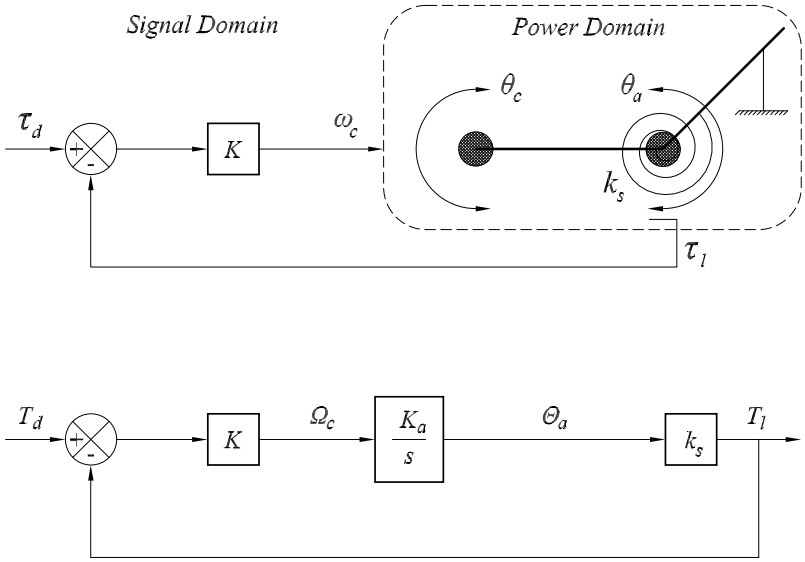

Figure 4.5 Fixed Load Motion Model and Block Diagram

Under the same condition of fixed load motion, large torque bandwidth can also be investigated. Large torque bandwidth is defined as the ability of the mechanism to oscillate at a full steady state output torque level. Torque and velocity saturation limits of the mechanism and the low stiffness of the spring, reduce the ability of the mechanism to output large torques at increased frequency. Low torques can be generated to the full closed loop bandwidth. However, the large torque bandwidth is typically smaller and is limited by the open loop dynamics of the system.

4.3.2.2 Forced Load Motion

In this case (Figure 4.6), the load end is forced to follow a specific trajectory and the desired torque is held constant (T_0). Rewriting equation (4.13) under this constraint defines the output impedance which is a measure of how well the system responds to external disturbances. In other words, the output impedance defines how well the internal dynamics of the actuation mechanism are decoupled from load motion. Spring stiffness, k_s, plays an important role in minimizing output impedance.

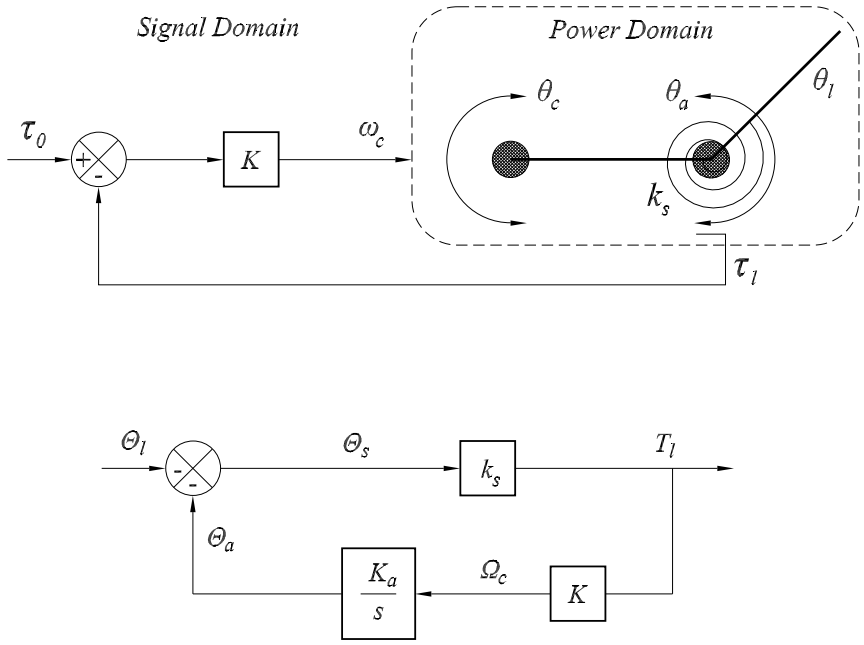

Figure 4.6 Forced Load Motion Model and Equivalent Block Diagram.

(Top) The desired torque is fixed constant, $\tau_d = \tau_0$, and the load motion is defined externally. The relationship between load motion and output torque is defined as the output impedance.

(Bottom) The block diagram shows that the feedback system and actuation mechanism dynamics are in the feedback loop.

Impact tolerance has to do with the ability of the actuation mechanism to handle impact loading. This is a function of the external motion constraint in the general model and the output impedance described later. Soft spring (small stiffness) in the sensor and

an increased controller gain help the actuation mechanism lengthen the time of impact that in turn minimize peak impact torques.

4.3.3 Features of EA

By assuming a fixed load, $\Theta_l=\Theta_0$ where Θ_0 is a constant (Figure 4.6), the closed loop forward transfer function relating the load torque T_l to desired torque T_d is:

$$G_{cl}(s)=\frac{T_l}{T_d}=\frac{k_s KK_a}{s+k_s KK_a} \tag{4.14}$$

For low frequencies, this transfer function is unity. There is a one-to-one correspondence between the desired torque and measured output torque. As frequency increases, the actuation mechanism response begins to drop off (bandwidth). Since this is a first order model, the controlled bandwidth, ω_{ctrl}, can be defined as:

$$\omega_{ctrl}=k_s KK_a \tag{4.15}$$

It is a function of the spring constant k_s, controller gain K, and rotor[21] gain K_a.

4.3.3.1 Moving System Gain

There are various factors that limit the actuation mechanism bandwidth. Depending on the design and configuration, one of the limitations will be dominant. Increasing closed-loop bandwidth is an optimization problem between all of the potential limitations, however the spring stiffness k_s is not one of the limits. k_s may represent high or low stiffness, but the fundamental bandwidth limit is independent of k_s.

Spring constant k_s and the control gain K are always together in the loop gain. Spring itself is very compliant in comparison to the stiffness of a load cell, therefore, it is possible to increase the control gain a proportional amount and maintain the same bandwidth of the actuation mechanism (Figure 4.7, (4.15)).

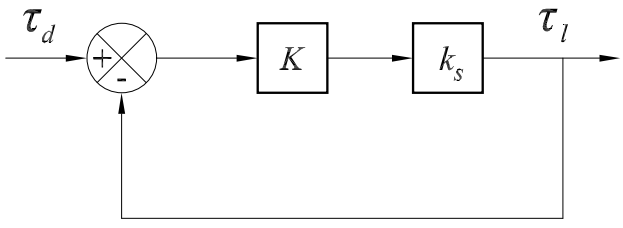

Figure 4.7 Moving System Gain.

Spring constant k_s is reduced, but by increasing controller gain K, the bandwidth ω_{ctrl} of the actuation mechanism can be maintained constant.

[21] An actuation mechanism, though has no EM motor for SMD, do have rotational shaft, or rotor.

4.3.3.2 Internal Motion Error Rejection

A real EM motor doesn't have perfect velocity output and always have some position or motion error. This error is scattered to every joint via the SMD mechanism, as well as errors generated by SMD mechanism itself like the backlash in the gear train and so on. The final motion error before the spring, x_n, is depicted in Figure 4.8.

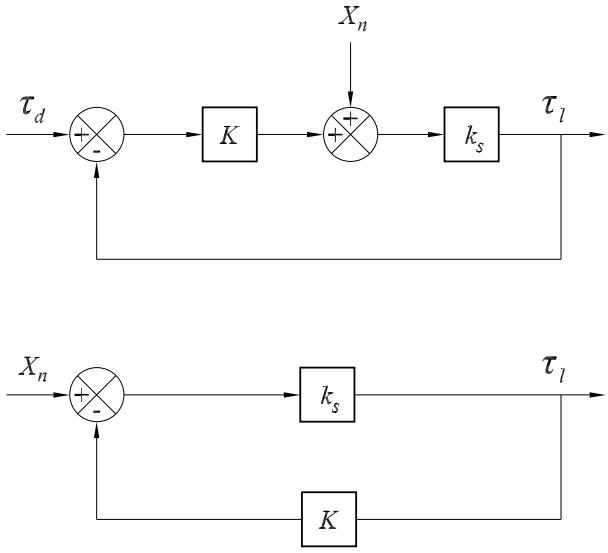

Figure 4.8 Internal Motion Error Rejection

If the desired torque is held constant, the reduction in sensitivity of the internal position noise on the output torque of the actuation mechanism can be written as:

$$\frac{\tau_l}{x_n} = \frac{k_s}{1 + k_s K} \tag{4.16}$$

It is clearly that the position noise (motion error x_n) is reduced by $1/K$. Using a compliant spring and increasing the control gain K dramatically reduces the effect of motion errors generated by EM motor and mechanical transmission chain. The high control gain helps the actuation mechanism to generate clean torque output.

4.3.3.3 Large Torque Bandwidth

As described before, one of the two application scenario of elastic actuation is the "Fixed Load Motion" in which the output end of the actuation mechanism is fixed (Figure 4.5). In order to generate large torques, there must be a large elastic deformation in the torsion spring. At steady state, the mechanism can produce the maximum torque output T_{sat}. Large torque bandwidth is defined as the frequency range over which the mechanism can oscillate at a torque amplitude equivalent to T_{sat}. Because of the compliance, the mechanism can only modulate the maximum torque over a certain frequency range, called large torque bandwidth, ω_0. The mechanism can still provide torque above frequency ω_0 but maximum torque capability decreases with increased frequency.

The input motion source, SMD mechanism, has limited input rotational velocity ω_a, thus there is a limit to the frequency at which the actuation mechanism can oscillate at maximum torque. Decreasing the stiffness of the spring means that the amount of the input shaft angle must increase, therefore cost more time for an actuation variation period, or result in a small torque bandwidth. Increasing the stiffness results in short period time or large bandwidth.

Let $T_{lmax}(\omega)$ denotes the maximum amplitude the actuation mechanism can oscillate at any given frequency ω:

$$\tau_l(t) = T_{l\max}(\omega)\sin(\omega t) = k_s\theta_a(t) \tag{4.17}$$

Its first order derivative is related to the input velocity:

$$\dot{\tau}_l(t) = T_{l\max}(\omega)\omega\cos(\omega t) = k_s\omega_a(t) \tag{4.18}$$

4.3.3.4 Low Output Impedance

The second case of interest is when the load is free to move and the desired torque is fixed T_d=T_0 (Figure 4.6). With T_d fixed, the dynamics due to the desired torque are eliminated. Therefore, the transfer function relating the change in load torque T_l due to the load position θ_l can be written as

$$Z(s) = \frac{T_l}{\theta_l} = \frac{k_s s}{s + k_s K K_a} \tag{4.19}$$

This equation is referred to as the output impedance. T_l has been adjusted to be centered on T_0. Therefore, this is the impedance around the constant desired torque T_0. However, often it is important to know the impedance of the actuator when T_0=0.

As described before, mechanical impedance is adapted from the idea of impedance in electrical circuits [165]. Output impedance is a measure of the stiffness of a system for a given load motion. For example, the impedance of a spring is its spring constant because the spring constant relates an input position to output force/torque. For robot actuators, low impedance is desirable.

The output impedance in Equation (4.19) is minimal at low frequency. At high frequencies, the impedance is equal to the spring stiffness of the physical spring in the sensor. Very low impedance at low frequencies is equivalent to having a zero rate spring connected to the load. Any load inertia will move around, and reaction to the actuator torque is almost entirely decoupled from the dynamics of the actuation mechanism itself.

There are two factors that reduced the impedance of the EA mechanism, one passive and one active. The first is the fact that the spring stiffness k_s is greatly reduced

from that of a stiff load cell. This is a passive effect and the lower spring stiffness may reduce the impedance by several orders of magnitude by itself.

The second effect in reducing output impedance is due to the active control system. Note that the characteristic equation for both closed-loop forward transfer function (Equation (4.14)) and closed-loop output impedance (Equation (4.19)) is the same.

$$s + k_s K K_a = 0 \tag{4.20}$$

The argument previously given in case 1 (Fixed Load) for increasing the control gain K proportional to the reduction of spring stiffness k_s holds for the impedance as well. Therefore, not only is there a passive impedance reduction with the compliant spring, but the control system has an increased gain which further extends the low impedance range.

The output impedance has an active physical equivalent at low frequencies. Given that the load motion is slow enough or has low frequency content then the impedance looks like a physical damper.

$$T_l = b_{eq} s \theta_l \tag{4.21}$$

where the equivalent damping coefficient is:

$$b_{eq} = \frac{1}{K K_a} \tag{4.22}$$

The impedance of the actuation mechanism is graphically depicted in Figure 4.9. It shows the equivalent damper in series with the physical spring. The damping effect is strongest at low frequencies and the passive impedance of the spring dominates at higher frequencies.

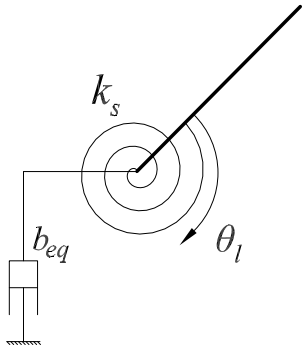

Figure 4.9 Equivalent Impedance for the General EA Mechanism.

The active impedance of the actuation mechanism can be thought of as an equivalent damper in series with the physical spring. At low driving frequencies, the actuation mechanism appears to be a damper. At high frequencies, the impedance is the stiffness of the spring.

Depending on the actuation mechanism dynamics and the control system, the impedance can take on other physical equivalents at low frequencies such as an

equivalent inertia, I_{eq}, although the impedance is always equal to the spring stiffness at high frequencies.

The closed-loop bandwidth of the system, ω_c, is the frequency at which the damping effect and the passive impedance of the spring are the same. Regardless of the impedance bode profile, the increased compliance in the sensor dramatically reduces the overall output impedance of the actuator.

4.3.3.5 Impact Tolerance

Whenever a robot works in unknown surroundings it makes and breaks contact with that environment. The interaction power at the system interface is subsequently transferred through the robot structure and can be significant. To minimize interaction power, most torque controlled robots move very slowly in anticipation of contact. If the impact power is too high, there is the potential for damage to the robot structure, actuators and to the environment. Elastic Actuation maximizes impact tolerance by the use of the load bearing compliant sensor and can operate at high speeds even in the presence of potential impacts.

While the energy transferred to the actuation mechanism is independent of spring stiffness, the spring and control system reduce the peak impact power to a range within the actuation mechanism output power capabilities. This power matching insures that the impact energy does not exceed the load capability of the actuation mechanism. The compliance allows the actuation mechanism to move out of the way of the impact while maintaining the proper desired torque.

As an example of the impact power in the actuation mechanism from an unexpected load, there is a sudden load motion v_l defined by the environment. The impact power, P_l, from the load is defined by the load torque and velocity at the spring output.

$$P_l = T_l v_l \tag{4.23}$$

The spring's deformation defines T_l.

Assuming that the desired torque in the actuator is T_d=0, the general model for impedance (4.19) can be redefined in terms of velocity rather than position.

$$\frac{T_l}{v_l} = \frac{k_s}{s + k_s K K_a} \tag{4.24}$$

Combining Equation (4.23) and Equation (4.24) gives the controlled impact power.

$$P_l = v_l^2 \frac{k_s}{s + k_s K K_a} \tag{4.25}$$

There are two parts in Equation (4.25). The first is v_l which is defined by the environment. There is no control over this constraint. Therefore, in order to minimize

interaction power, the focus should be on the second part of the equation which is due to the actuation mechanism.

The second part constrains information on the actuation mechanism characteristics, namely, spring stiffness, control gain, and bandwidth. Remember that this is the load interaction power regardless of the spring stiffness. The power contribution due to the actuation mechanism is at worst $1/KK_a$. As mentioned above, because of the sensor's compliance decreasing loop gain, the control gain K can be increased. Clearly from Equation (4.25), as control gain increases, the impact power decreases. The impact power spectrum rolls off at higher frequency with the break point at the controlled bandwidth of the actuation mechanism but this effect is secondary.

4.4 Design of EA Mechanism

The theoretical work just presented has a practical side too. The following discussion elaborates on design decisions made during the design and construction of the actuation mechanism prototype (Figure 1.1). Detailed engineering design will be presented in Chapter 5. The discussion in this section focuses on component selection, with particular emphasis on picking the correct elasticity. Experimental results are also given which help to quantify actuation capabilities.

4.4.1 General Structure

The design space for EA prototype is very large. Besides geometry and topology there are six major components: motor, amplifier, transmission, elasticity, sensor, and controller. Of all six components, choosing the spring elasticity is the only part of the actuation mechanism which requires unique perspective and is discussed in the next section.

The specifications for the motor, amplifier, and transmission need to be done based on the torque, speed, and power requirements for a given task. These design requirements are not unique to EA and would be done for any actuation system.

As a helpful aid to the final operation, the motor and transmission should be selected with the idea of keeping friction and motor saturation low. Motor friction b_m, same role as rotor friction b_a, is kept at a minimum in the prototype actuator by using a brushless DC motor[22]. The actuator design also reduces drive friction by designing the

[22] Motor friction b_m / rotor friction b_a is seen through the transmission with a multiplication of N^2.

centre of inertia, centre of friction, and centre of stiffness to be collinear along the ball bearing axis [166].

Transmission dynamics should also be kept to a minimum as these can be a primary limiting factor in using high feedback gain [37]. Thus a DC motor with build-in gear-head is used to minimize the coupling, or gears.

The other limiting component to achieve high feedback gain is the sensor. The sensor needs to directly measure the spring deflection. This insures that the feedback measurement is a representation of true torque. Noise in the sensor is also detrimental to operation.

4.4.2 Spring Constant

Selecting the spring constant for the sensor needs to be balanced when trading off the effects of large torque bandwidth with low impedance and error rejection. Some guidelines for choosing a spring constant are listed here:

- Select a motor and transmission based on the torque, speed, and power requirements for the given task. This will define the lumped rotor inertia, damping, and saturation characteristics seen through the reduction.
- Define an operation bandwidth, ω_o, for which the actuator will need large torques. In other words, define a required large torque bandwidth profile. This profile is independent of controller and depends solely on ω_n and B[23]. This places a lower bound on k_s. Most likely, the operational bandwidth may be a little greater but close to the selected natural frequency.
- Minimizing impedance places an upper bound on k_s. This is a function of the controller values κ and Γ (See Section 4.5.2.1). Insure that the controller gains can be raised to acceptable levels of stiction and impedance reduction.
- It may be necessary to iterate. Better value of k_s can be obtained after several times of try.

[23] B is a dimensionless item defined later in Equation (4.36).

4.5 Study of EA

4.5.1 Model Derivation

There are four main parts to the EA actuator as seen in Figure 4.10.

- System Inputs
- Motion Source and Transmission
- Compliant Sensor
- Control System

The system inputs and the compliant sensor are the same as the general model. Specifically there are two system inputs. T_d is the desire output torque and Θ_l is the motion of the load. Also, identical to the general model, the compliance of the sensor is defined by the linear spring constant k_s.

While the system inputs and sensor are the same as in the general model, Figure 4.10 shows that Motion Source / Transmission model and the control system are different. Therefore, this section will focus on the discussion on these differences.

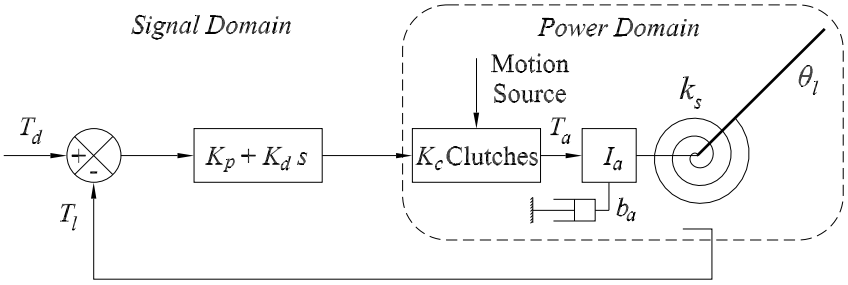

Figure 4.10 EA Mechanism Model

4.5.1.1 Motion Transmission Model

The motion transmission in the power domain consists of a constant motion source, inertial mass (rotational body), and a viscous friction element.

The motion source provides motion on the inertial mass given a signal from the controller. For the initial linear analysis of the mechanism, two assumptions about the motion sources are made:

- The motion source can provide any desired output motion up to the motion saturation limits.
- The controller dynamics are small enough that they are assumed to be negligible.

In the physical prototype actuator (Figure 1.1), the clutch gain K_c, which relates the desired torque (controlled by clutch-engage-time) to torque on the rotor inertial mass

(output torque), is unity. K_c is therefore lumped into the controller gain and eliminated throughout the section to reduce equation complexity.

The lumped inertial mass I_a includes the dynamic rotor mass and the mass of the transmission elements as seen through the transmission. This reflected inertia is N^2 the actual mass value where N is the transmission reduction ratio.

The rotor friction b_a is also seen through the transmission. It is N^2 of its actual value. Even so, depending on rotor and transmission construction, the viscous friction can be very low.

There are two modes of operations for an EA device, torque control and velocity control. In this model, the torque control is chosen. Velocity control, to some degree, masks the effect of rotor mass which happens to be very important in defining the large torque bandwidth for the EA device. Therefore, while torque control is perhaps the more difficult method of controlling an EA device, it is done in order to highlight effects of the rotor mass that makes the mechanism inherently a second order system.

4.5.1.2 Control System

Feedback control of the mechanism is closed by measuring the deflection of the spring which implies the torque output, T_l, of the device. PD controller was used on the error of the signal with gains K_p and K_d for the proportional and derivative terms respectively. Since the system is already of second order, no integral term is used. By assuming the amplifier to be ideal, the torque on the rotor mass, T_a, is determined by

$$T_a = (T_d - T_l)(K_p + K_d s) \tag{4.26}$$

The mechanism can be controlled with proportional control alone. However, it is helpful to have a damping term as well to help reduce the natural resonance on the mass and spring in the sensor.

It would be very easy to use a feed-forward term in the controller and attempt to keep the set point of the system always centered on the desired torque. This would allow the control system to focus on controlling the error in the spring rather than requiring a large error signal just to compress the spring at high torque. However, in order to keep the control system complexity to a minimum, feed-forward is not included.

4.5.1.3 Power Domain Model

Figure 4.11 shows the model for the power domain for an EA device. The two constitutive equations for the power domain are defined by the torque in the spring and the motion of the rotor mass:

$$T_l = k_s(\theta_a - \theta_l)$$
$$I_a\ddot{\theta}_a + b_a\dot{\theta}_a = T_a - T_l \tag{4.27}$$

These equations can also be written with Laplace variables:

$$T_l = k_s(\Theta_a - \Theta_l)$$
$$\Theta_a = \frac{T_a - T_l}{I_a s^2 + b_a s} \tag{4.28}$$

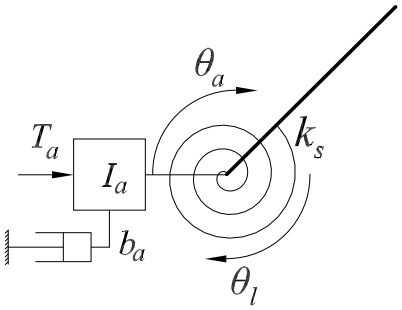

Figure 4.11 EA Power Domain Model

By combining the two equations of (4.28), the torque in the spring, T_l, can be written as a function of two variables: the torque input from the motion source, T_a, and the relative position of the load, Θ_l. This relationship is derived to be:

$$T_l(s) = \frac{T_a(s) - (I_a s^2 + b_a s)\Theta_l(s)}{\frac{I_a}{k_s}s^2 + \frac{b_a}{k_s}s + 1} \tag{4.29}$$

This is the open-loop dynamic equation for the torque T_l in the spring as a function of the rotor torque and the load motion.

4.5.1.4 Close-loop Model

As shown in Figure 4.10 the open-loop power domain is modulated by a torque feedback loop. Combining power domain model (4.29) and the feedback signal commands from the controller (4.26) yields the closed-loop dynamic equation for the torque through the spring:

$$T_l(s) = \frac{(K_d s + K_p)T_d(s) - (I_a s^2 + b_a s)\Theta_l(s)}{\frac{I_a}{k_s}s^2 + \frac{b_a + k_s K_d}{k_s}s + (K_p + 1)} \tag{4.30}$$

The closed-loop dynamic equation for the torque T_l in the spring is a function of the desire torque T_d, and load motion, Θ_l.

4.5.1.5 Two Input Cases

As mentioned in the early section, it is helpful to write the torque in spring, T_l, in the power domain model and the closed-loop model as a function of isolated input variables. For the first case, the load end is fixed eliminating the load motion. The second case is

with load end free to move and the desired torque fixed. The second case eliminates the dynamics due to desired torque modulation.

➢ Case 1: Fixed Load

By eliminating the load motion, the transfer function between rotor torque input and mechanism output can be taken from equation (4.29) and written explicitly as:

$$\frac{T_l(s)}{T_a(s)} = \frac{1}{\frac{I_a}{k_s}s^2 + \frac{b_a}{k_s}s + 1} \tag{4.31}$$

Equation (4.31) will be referred to as the open-loop transfer function.

By imposing the fixed end condition again and using the closed-loop dynamic equation (4.30), the close-loop forward transfer function for case one, which relates the desired torque to the output torque, is

$$\frac{T_l(s)}{T_d(s)} = \frac{K_d s + K_p}{\frac{I_a}{k_s}s^2 + \frac{b_a + k_s K_d}{k_s}s + (K_p + 1)} \tag{4.32}$$

Depending on the magnitude of K_p, at low frequency, this transfer function is close to unity. In the limit at high frequency it goes to zero. The zero in the numerator is an artifact of the taking the derivative of the desired torque via the error signal.

For EA device, K_p is typically very high. It is at least an order of magnitude greater than 1 if not more. Therefore, $K_p+1 \approx K_p$.

➢ Case 2: Free End with Zero Torque

With the desired torque fixed constant, the torque in the spring due to the load motion under closed-loop torque control can be written from Equation (4.30) as:

$$\frac{T_l(s)}{\Theta_l(s)} = \frac{-(I_a s^2 + b_a s)}{\frac{I_a}{k_s}s^2 + \frac{b_a + k_s K_d}{k_s}s + (K_p + 1)} \tag{4.33}$$

This is the output impedance. The impedance at low frequency is ideally equal to zero. At high frequency, it is equal to k_s, the spring constant of the physical spring.

Whenever, either of the closed-loop equations is used in the rest of the section, it is assumed that $K_p+1 \approx K_p$. Even though this assumption is not technically and mathematically precise, it is accurate enough.

4.5.2 Model Analysis

This section will discuss EA with respect to the following characteristics:

- Saturation

- Closed-loop bandwidth
- Output impedance
- Error rejection

4.5.2.1 Saturation

In order to clarify saturation at the most basic level in the EA mechanism, the load is fixed as in Case 1 (Figure 4.12). Obviously, saturation is affected by load motion. Depending on the frequency and phase of the load motion, it can either help or hinder the mechanism. However, by fixing the load, there is a fixed point of reference for understanding saturation.

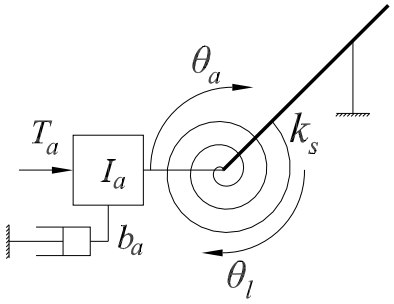

Figure 4.12 EA Model with a Fixed Load

Assuming no velocity saturation for the moment, the clutches can produce large rotor torque over a wide frequency range. However, in order to create large torque in the spring, the torque from the clutch must rotate the rotor inertial mass. The torque from the clutch is independent of the torque in the spring. For the clutch with a transmission in series with an elastic element, the mass-spring resonance of the rotor inertial and torsion spring define the plant dynamics. Therefore, the ability of the device to produce large torques is limited in frequency by these dynamics independent of control system. The frequency at which the open-loop characteristics of the plant begin to fall off is defined as the saturation frequency ω_0:

$$\omega_0 = \sqrt{\frac{k_s}{I_a}} \tag{4.34}$$

Since the sensor spring is very compliant, ω_0 can be low. Typically, it may be a few hertz to tens of hertz depending on the reflected inertia as seen through the transmission [24]. The saturation bandwidth is well within the controlled bandwidth discussed later. The device still operates and can generate torques at frequencies above ω_0. It is simply limited in the magnitude of large torque at high frequency.

[24] Estimated number based on the first prototype.

Other saturation effects, such as viscous friction, also play a role in defining the large torque bandwidth profile near the saturation frequency ω_0. These effects are explained after reformulating the open and closed-loop transfer functions in dimensionless terms.

➢ Dimensionless Formulation

Both the open and closed loop transfer function, Equation (4.31) and Equation (4.32), and the output impedance, Equation (4.33), can be written in dimensionless form.

There are two natural frequencies in the dynamic equations. The first is the saturation frequency of the rotor inertial mass and spring just described ω_0. The second is the controlled natural frequency ω_c.

$$\omega_0 = \sqrt{\frac{k_s}{I_a}}$$

$$\omega_c = \sqrt{\frac{k_s K_p}{I_a}} \tag{4.35}$$

Both the open and closed loop equations of Case 1 and the impedance of Case 2 can be non-dimensionalized using these two frequencies and the following dimensionless groups:

$$\begin{cases} S = \dfrac{s}{\omega_o} \\ \kappa = \dfrac{\omega_c}{\omega_o} = \sqrt{K_p} \\ B = \dfrac{b_m}{k_s}\omega_o \\ \Gamma = K_d \omega_o \end{cases} \tag{4.36}$$

S normalizes the equation to the saturation frequency or the natural resonance of the rotor mass-spring system of the mechanism.

κ represents the gain in the system and is a measure of the increase in controlled bandwidth above the saturation frequency. Definition of κ assumes that K_p>>1.

B is a scaled natural damping term due to viscous friction physically present in the construction of the prototype.

Γ represents the scaled controller damping gain.

The dimensionless open-loop, closed-loop, and output impedance transfer functions are:

$$G_{ol}(S) = \frac{T_l(S)}{T_a(S)} = \frac{1}{S^2 + BS + 1} \tag{4.37}$$

$$G_{cl}(S) = \frac{T_l(S)}{T_d(S)} = \frac{\Gamma S + \kappa^2}{S^2 + (\Gamma + B)S + \kappa^2} \tag{4.38}$$

$$Z_{cl}(S) = \frac{T_l(S)}{k_s \theta_l(S)} = \frac{-S(S+B)}{S^2 + (\Gamma + B)S + \kappa^2} \tag{4.39}$$

4.5.2.2 Bandwidth

The controlled bandwidth is significantly higher than the saturation bandwidth for the EA mechanism. In the previous section, several things that can potentially limit the bandwidth of the mechanism are outlined. None of those limitations were a function of the compliance in the sensor. Therefore, the loop gain reduction from sensor compliance can be proportionally increased in the controller. This essentially takes the gain out of the spring and into the control system.

- Controller Gains

Using the closed-loop characteristic equation (denominator of Equation (4.38) and (4.39))

$$S^2 + (\Gamma + B)S + \kappa^2 = 0 \tag{4.40}$$

In conjunction with the dimensionless groups (Equation (4.36)), the controller gain values for a PD controller can be explicitly defined to get a desired closed loop natural frequency ω_c and damping ratio ζ_c.

The proportional gain is found from the definition of κ:

$$\kappa^2 = K_p$$

$$\Rightarrow K_p = \frac{\omega_c^2}{\omega_o^2} \tag{4.41}$$

The derivative gain is found from the damping term of the characteristic equation.

$$2\zeta_c \kappa = B + \Gamma$$

$$\Rightarrow K_d = \frac{2\zeta_c \omega_c I_a - b_a}{k_s} \tag{4.42}$$

4.5.2.3 Impedance

Equation (4.39) shows the dimensionless form of output impedance. For convenience, it is rewritten here as:

$$Z_{cl} = \frac{T_l(S)}{k_s \theta_l(S)} = \frac{-S(S+B)}{S^2 + (\Gamma + B)S + \kappa^2}$$

At low frequencies the impedance is small. As input frequency increases, the impedance increases accordingly. In the limit, the output impedance level off and is equal to the spring constant, k_s, of the torque sensor.

As mentioned previously, at frequencies above the controlled natural frequency ω_c, the mechanism's output impedance is the spring constant of the sensor. All high frequency disturbances and shock load are filtered through the spring.

There are three ways to decrease the output impedance for the EA mechanism.

- Increase the control gain. This drives the impedance resonance further away from the operational bandwidth.
- Decrease the spring constant. This linearly lowers the impedance profile.
- Increase the derivate gain. The major contribution is to reduce impedance resonance at the controlled natural frequency.

It is important to emphasize that the key benefit of EA mechanism is low impedance. Controlled bandwidth can remain constant by increasing control gain proportionally to the reduction in spring stiffness. Impedance however, is dramatically reduced when the spring stiffness is lowered.

4.5.2.4 Torque Error Rejection

As described in early section, Coulomb friction and stiction are dramatically affected by the introduction of the spring into the joint. The compliant spring allows for an increase in controller gain. Stiction is one of the main reasons why the normal actuator cannot respond to low torques and thus reduces dynamic range.

Because of stiction, the lumped inertia mass will not move until

$$T_a - T_l = T_a - T_d + T_e = T_s \tag{4.43}$$

where T_e is the feedback torque error and T_s is the torque due to stiction. Since stiction is a low frequency phenomenon, the derivative term of the controller is negligible. The torque to the rotor due to the error then becomes

$$T_a \approx K_p T_e + T_d \tag{4.44}$$

Using Equations (4.43) and (4.44) the torque error T_e can be solved:

$$T_e \approx \frac{1}{K_p + 1} T_s \tag{4.45}$$

This shows that the torque error due to stiction is related by the dimensionless group κ:

$$T_e \approx \frac{1}{\kappa^2} T_s \tag{4.46}$$

κ is an approximate ratio between the resonant frequency of the mass-spring system, ω_0, and the controlled natural frequency, ω_c. Increasing κ reduces the effect of stiction. There are two ways to effectively reduce stiction:

- Increase ω_c by increasing the gain, or
- Decrease ω_0 by reducing the spring constant.

The relationship is inverse parabolic. Theoretically, to eliminate stiction soft spring should be used. However, part of the design is to evaluate an acceptable level of stiction reduction.

As the gain is increased, there is a rapid decrease in the noticeable stiction torque in the system. For example, if the controlled natural frequency is set 5 times greater than the mass-spring resonance (K_p=25), the apparent stiction is reduced to 5% of its original value[25].

4.5.3 Effect of Load Inertia

Even though EA mechanisms have variable load condition due to intermittent contact with the environment, it is helpful to analyze the dynamics of an inertia load moving in free space (Figure 4.13). Ideally the inertia load is decoupled from the actuation mechanism dynamics such that the mechanism looks like a pure torque source. Given the load has some minimum inertia, the mechanism can be considered as a pure torque source within its close-loop bandwidth capabilities.

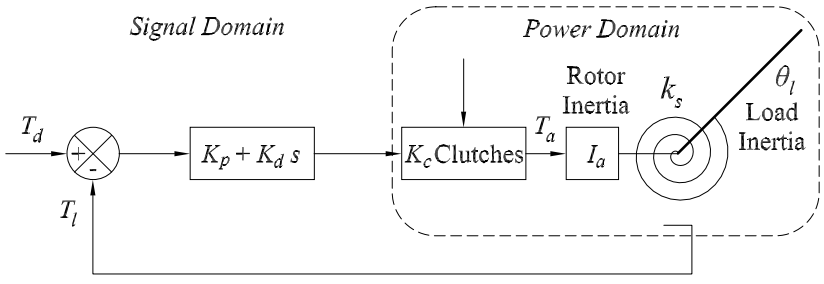

Figure 4.13 EA Model with Load Inertia Moving in Free Space.

The load inertia defines the load motion θ_l.

4.5.3.1 Load Torques

Consider the torque balance relationships for torque in spring, T_l, and rotor inertia motion, θ_a, derived previously from the Laplace domain (Equation (4.28)).

[25] Result from simulation.

$$T_l = k_s(\Theta_a - \Theta_l)$$

$$\Theta_a = \frac{T_a - T_l}{I_a s^2} \tag{4.47}$$

With the load inertia moving in free space, the load motion can be written in Laplace domain, Θ_l. It is solely a function of the torque in the spring, T_l.

$$\Theta_l = \frac{T_l}{I_l s^2}$$

For enhanced clarity and understanding, the viscous damping on the rotor is eliminated. Also emphasize that the rotor torque T_a is a function of the control system.

$$T_a = (K_p + K_d s)(T_d - T_l)$$

Substitute the controller into the equation for Θ_a. Then use this result and the equation for Θ_l to solve for the torque in the spring, T_l as a function of desired torque T_d.

$$\frac{T_l}{T_d} = \frac{K_d s + K_p}{\frac{I_a}{k_s} s^2 + K_d s + \left(K_p + 1 + \frac{I_a}{I_l} \right)} \tag{4.48}$$

With two exceptions, Equation (4.48) is the same as the closed-loop dynamic transfer function for the fixed load case (Equation (4.32)). The first exception is the elimination of the viscous damping term. Only controller damping remains. The second difference is in the s^0 term of the characteristic equation in the denominator. Instead of just being K_p+1, there is an additional term I_a/I_l that is the ratio of the rotor mass to the load mass.

There are two important things to emphasize about the s^0 term. The first is that K_p>>1. The proportional gain is high due to the fact that k_s is low. As mentioned before, $K_p+1 \approx K_p$. This leads to the second important point. The additional term, I_a/I_l, is only significant for the case where there is very little load inertia in comparison to the rotor inertia. Fortunately, this is hardly ever true.

Typically these elastic actuation mechanisms are used in robots with articulated joints. Practical experience with using the similar actuators on robots have shown that $I_l \approx I_a$ [167]. Therefore again K_p dominates and I_a/I_l can be assumed small in comparison. At low frequency, the mechanism has good torque response.

Remember that the load inertia resonates with the spring at a frequency $\omega_l = \sqrt{\frac{k_s}{I_l}}$

and that ω_l is part of the non dimensionless group L where

$$L = \frac{\omega_l}{\omega_o}$$

The load torque equation can be written in non-dimensional terms as

$$\frac{T_l(S)}{T_d(S)} = \frac{\Gamma S + \kappa^2}{S^2 + (\Gamma + B)S + \kappa^2 + L^2} \tag{4.49}$$

This situation is depicted in Figure 4.14. At low frequency, there is a small reduction in the output magnitude due to the load torque. However, the torque is in phase and in close to the actual desired value. I_{eq} is some fraction of the reflected rotor inertia I_a defined by the controller gain.

$$I_{eq} = \frac{I_a}{K_p} = \frac{I_a}{\kappa^2} \tag{4.50}$$

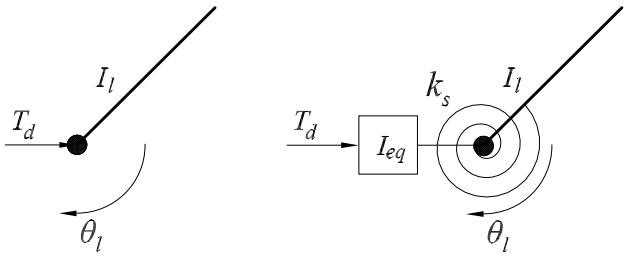

Figure 4.14 Control Abstraction for the EA Mechanism.

At frequencies below the controlled bandwidth, the actuator can be considered a pure torque source. Above the controlled bandwidth, the dynamics of the equivalent inertia I_{eq} and the spring come into play.

4.5.3.2 Load Motion

Assuming that the load inertia is significant, with refer to the load motion in Equation (4.47), the load motion, as a function of the desired input torque, can be written as:

$$\frac{\theta_l}{T_d} = \frac{1}{I_l s^2} \cdot \frac{K_d s + K_p}{\frac{I_a}{k_s} s^2 + K_d s + \left(K_p + 1 + \frac{I_a}{I_l} \right)} \tag{4.51}$$

There are two parts in Equation (4.51). The first part is just the dynamics of the load inertia as a function of a simple torque $T_d = I_l s^2 \Theta_l$. The second part of the transfer function comes from Equation (4.48) and represents the closed-loop characteristics of the mechanism. Equation (4.51) verifies that the actuation mechanism performs well as pure torque source over its closed-loop bandwidth as long as load inertia is significant.

In summary, a load inertia feels a pure torque at low frequency for the EA mechanism. As drive frequency increases, the dynamics of the mechanism begin to contribute to the torque on the load. In the very simplest model, it is presented by the

diagram in Figure 4.14. The mechanism dynamics are a small equivalent inertia, I_{eq} (Equation (4.50)) and the physical elasticity followed the load inertia.

5 Design and Experiment of PEJ

SMD an EA, the two complementary actuation methods for future robots, are presented and analyzed in detail in Chapter 3 and Chapter 4 respectively. In this chapter, they will be integrated together to form a new type robot joint which has the attributes of both SMD and EA. The new type robot joint is currently termed as Purposeful Elastic Joint (PEJ).

5.1 Design of PEJ

To produce the first PEJ prototype in the world, the design work is mostly concentrated on the concept validation and verification, but engineering implementation and optimization are also exercised as the main part of consideration.

5.1.1 Concept

The PEJ is supposed to generate desired controllable torque from a constant rotational velocity input. The generated torque is then acted on the payload – usually the robot link. From the top-down view, the desired PEJ should have such key properties:

- Input: Constant rotational velocity (one direction movement)
- Output: Measurable and controllable Torque from the joint on the payload (link)
- Must Have: Torsion spring to generate controllable torque and measurable deformation
- Must Have: Bidirectional clutch as the controllable component
- DOF definition: One joint (one link) to verify the concept idea

5.1.2 Schematic Deployment

With the concept model stated previously, a final schematic deployment of PEJ's key components has come out as shown in Figure 5.1.

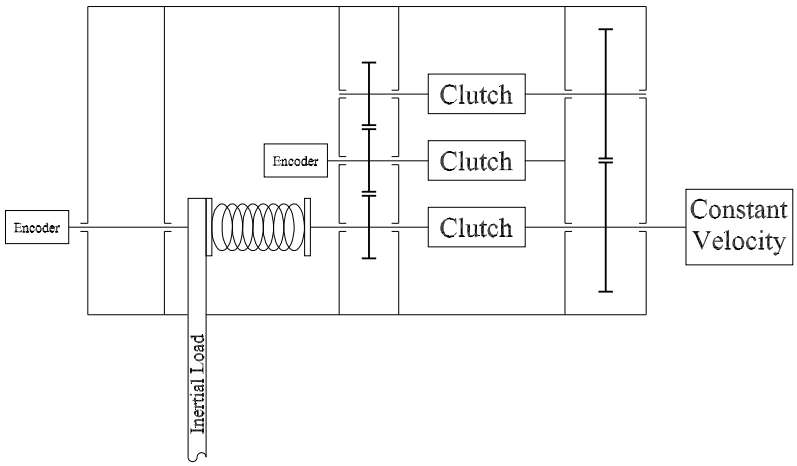

Figure 5.1 Schematic Deployment of Key Parts of PEJ

It can be treated as a combination of four "sub-assembly":

- Constant velocity source (right hand side)
- Bidirectional Clutch II (the group with five gears and three normal unidirectional clutches)
- A normal robot joint (link) with torsion spring
- Two encoders for the sake of feedback control

The bidirectional clutch II (BCII) is different from the bidirectional clutch (BCI) described in Chapter 3. BCI has one gear mate at one side and one pulley mate at the other side (Figure 3.7). Therefore, with the same rotation of one shaft, the other shaft of the mates can generate opposite rotation direction. This is because of the fact that two shafts have different rotation direction for a gear mate but same for a pulley mate. BCI functions well as a bidirectional clutch for the robot hand described in Chapter 3, but it uses pulley and pulley belt and therefore has a little elastic property. In PEJ the whole elasticity is concentrated on the torsion spring in the joint, and for the validity of experiment results no other elasticity is needed in the whole mechanical transmission. As a result of the limitations of BCI here comes the BCII, which purely consists of gears and normal unidirectional clutches, and therefore is a "rigid" bidirectional clutch.

5.1.3 Key Component Selection and Design

In order to keep the prototype cost as low as possible, most parts of PEJ are chosen from standardized catalogue of various vendors. The BOM of final standard components is listed in Appendix B. The drawings of other fabricated components are presented in Appendix C. Most of the parts are made of stainless steel, except the frame and Inertial Load, which are made of aluminum.

5.1.3.1 Clutch

Clutches are standardized parts and are chosen directly from PIC-Design product catalogue. For the safety consideration, 24VDC type is chosen. Another key parameter of the clutch is its shaft bores. The five shafts, which are also standardized parts and will be presented later, all have metric diameter of 6mm. So the ¼ inch bore clutches are chosen as the final choice (part number: RW1-333). Its drawing is shown in Figure 5.2. Its main dimensions are listed in Table 5.1.

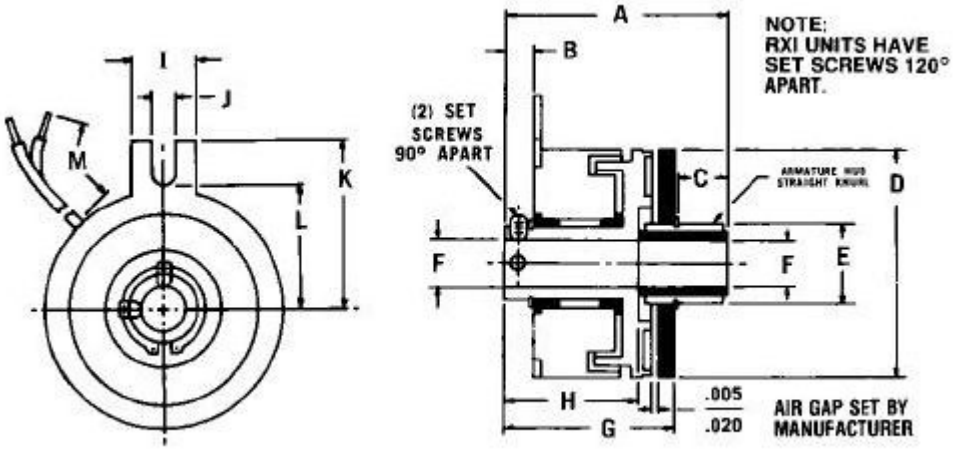

Figure 5.2 The Inch-bore Shaft Mounted Clutch

Table 5.1 Dimensions of Clutch RW1-333 (in inch)

A	B	C	D	E	G	H	I	J	K	L	M
1.370	.191	.410	.903	.506	.874	.763	.305	.094	.625	.445	12.00

5.1.3.2 Shaft

The shaft is the modification of MISUMI shaft. The "Female thread, both end" stainless steel shaft was chosen to make modifications – two Spanner Grooves to provide the set points for setting screws of other components like clutches, gears, and so on. The original drawing is shown in Figure 5.3. The main dimensions are listed in Table 5.2, and the drawings of five shafts which show the detailed modifications are presented in Appendix C.

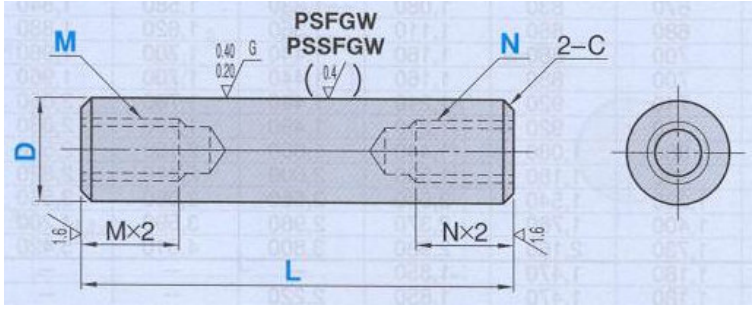

Figure 5.3 Shafts – Female thread, both end

Table 5.2 Dimensions of Shafts (in mm)

C	D	L	M	N
0.5	6	Modified, see Appendix C	3	3

5.1.3.3 Bearing

Two type of bearings are use, the "T shape" type (Figure 5.4) and the "Direct fixing" type (Figure 5.5). Their dimensions are listed in Table 5.3 and Table 5.4 respectively.

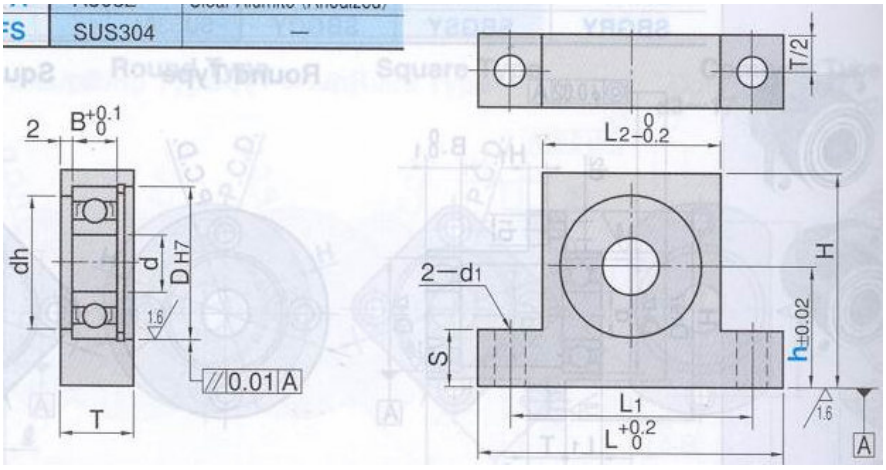

Figure 5.4 T-shape Bearing

Table 5.3 Dimensions of T-shape Bearing (in mm)

h	d	D	dh	B	H	L	L1	L2	T	S	d1
25	6	17	13	6	h+13	47	35	23	12	10	5.5

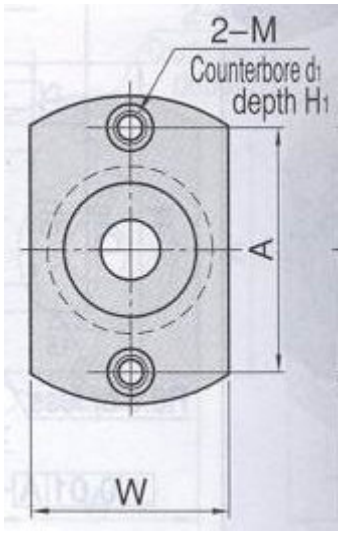

Figure 5.5 Direct Fixing Type Bearing

Table 5.4 Dimensions of Direct Fixing Type Bearing (in mm)

A	M	W
29	4	23

5.1.3.4 Gear

As shown in Figure 5.1, there needs two big gears and three small gears. The pitch diameter of the bigger gear d_1 should be two times of that of the smaller gear d_2:

$$d_1 = 2 \times d_2 \tag{5.1}$$

There isn't too much torque requirement for PEJ at this moment, so the gear module is chosen as 0.75. Consider the dimensions of bearings, pitch diameter 48mm and 24mm are chosen for d_1 and d_2 respectively. Another diameter to be considered is the hub diameter since it must let the shaft with 6mm diameter get through. The details of two gears are listed in Table 5.5.

Table 5.5 Details of Gears

	m	*N*	*d* (mm)	Material	*S*
Big Gear	0.75	48	48	Steel	M3
Small Gear	0.75	24	24	Steel	M3

where,

m =gear module

N =Number of teeth

d =Pitch diameter, d_1 for bigger gear and d_2 for smaller gear

M =Material

S =Setting screw type

5.1.3.5 Spring

Spring is the key component to generate torque. We chose the torsion spring from "Associated Spring" catalogue. The spring's drawing and dimensions are shown in Figure 5.6 and Table 5.6 respectively.

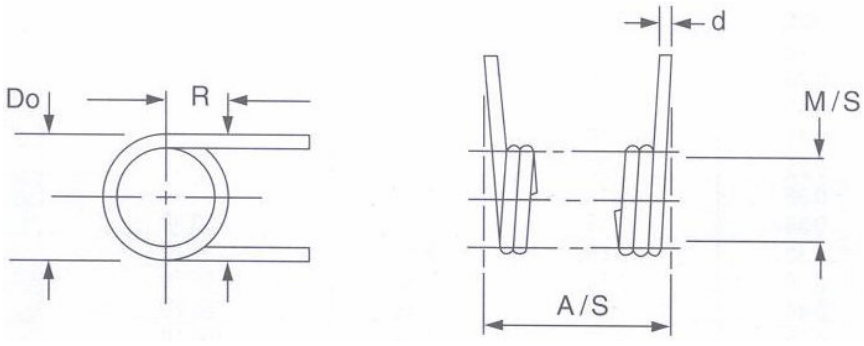

Figure 5.6 Torsion Spring

Table 5.6 Dimensions of Spring

d (mm)	*Do* (mm)	*T*(N·mm)	*R* (mm)	*M*/*S*(mm)	*E* (mm)	*A*/*S* (mm)
0.64	8.64	42.40	12.70	5.54	25.40	5.23

where,

d =Wire diameter

Do =Outside diameter

T =Torque

R =Loaded position

M/S =Recommended Mandrel size

E =Leg Length (from centerline)

A/S =Min Axle Length

The spring constant k_s can be got from product catalogue or by the method provide in Appendix D. More information of torsion spring can be found there either.

5.1.3.6 Screw and Other Standard Components

Choosing of other standardized components like screw and washer is also part of the design work. They all come from catalogues provided by local vendors, and their details are listed in Appendix B.

5.1.3.7 Fabricated Parts

Some parts however cannot be found in catalogue and have to be designed and fabricated separately. They are the base (1 part), the supporting plate (5 parts), the motor racket (1 part), the clutch connector (3 parts), the brake base (1 part), the end for spring (1 part), and the link (1 part) which also serves as another end for the spring. Their detailed drawings are presented in Appendix C.

5.1.4 First Prototype

The finished first prototype of PEJ is shown in Figure 5.7. It has the dimension of 250mm×130mm×59mm and totally weights about 2kg including the base. This is the original device for the experiment results presented later.

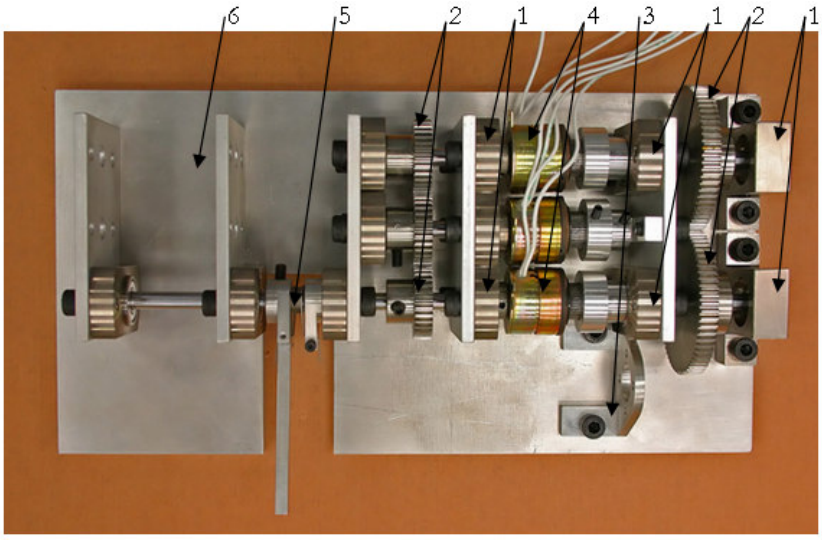

Figure 5.7 The First Prototype of PEJ.

Labels: 1-Bearing, 2-Gear, 3-DC Motor Bracket, 4-Clutch, 5-Torsion Spring, 6-Base/Frame

5.2 Modeling of PEJ

The key element of PEJ is the close coiled torsion spring, which has one end attached to the link (output) and the other end attached to the output shaft of BCII which is directly connected to the ring of clutch (control ring). A stationary coil (solenoid) is used to engage the clutch by drawing the control ring against the collar on the input shafts. Friction between the control ring and input shaft causes the output rotation of BCII which in turns rotates one end of torsion spring. After the electric current is interrupted, the magnetic field is removed causing the stationary coil to disengage the two ends of clutch. This joint relies on the relative rotation between the input and output shafts for outputting joint torque, thus the slower the speed, the longer the build up time for required torque.

To model a PEJ, its three main elements: magnetic circuit, control ring motion and clutch function should be considered. In the following subsection these elements are discussed and complete model of a PEJ is developed.

5.2.1 Compact Model

A compact model of a PEJ is shown in Figure 5.8. In this model, translational and rotational motions of the control ring are considered to be independent. For each motion, a mass-spring-damper mechanism is considered. As in the real system, both motions have limited travel. In the model, the control ring is connected to the output by a torsion spring (k_r) and to the ground by a translational spring (k_l). Its maximum translational and rotational motions are x_g and φ_g, respectively. For both independent translational and

rotational movement of the control ring, absolute and relative viscous frictions are considered.

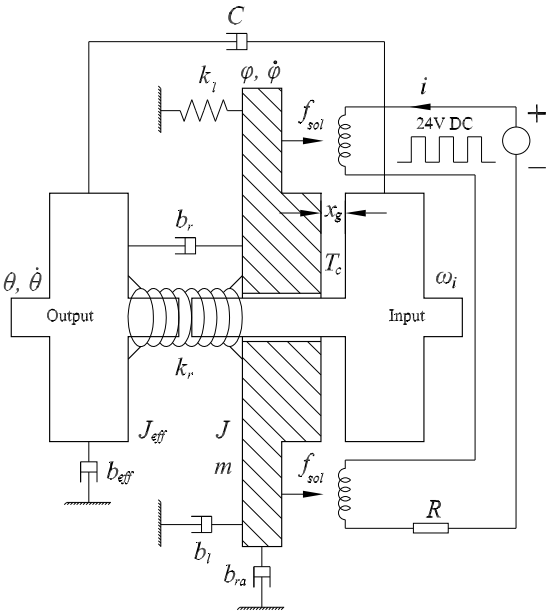

Figure 5.8 Compact Model for PEJ.

As a voltage is applied to the solenoid, the magnetic force f_{sol} is applied to the control ring. When the control ring moves by x_g, it comes in contact with the input shaft, and the Coulomb friction between the two generates the torque T_c to wrap the torsion spring. This torque can be calculated from

$$T_c = \mu f_{sol} r \tag{5.2}$$

where μ and r are the Coulomb friction coefficient and average force arm, respectively. As the spring wraps, the generated torque will drive the output shaft which is rigidly connected with the link/load. As a result, when the relative rotation of the spring is φ_g the output velocity becomes equal to the input velocity. The torsion spring will not be deformed anymore and a constant torque will be acted on the load.

To calculate the solenoid force in Equation (5.2) it is noticed that the coil is wound around both the control ring and input shaft. When the solenoid is energized, the resulting magnetic flux pulls the control ring and input shaft together. Using Faraday's law, the flux (assuming fringing and leakage flux are negligible [168]) is calculated from

$$\dot{\Phi} = \frac{v_{sol} - iR}{N_s} \tag{5.3}$$

where Φ, v_{sol}, i, R, and N_s are magnetic flux, solenoid voltage, current, resistance, and number of turns, respectively. To obtain the solenoid current the following is used

$$i = \frac{f_{mm}}{N_s} \tag{5.4}$$

where f_{mm} is the magneto-motive force [168]. The magneto-motive force is broken up into components for the steel and air gap. Although the majority of the circuit's reluctance is concentrated at the air gap, the nonlinear properties of the steel components such as saturation and hysteresis can limit performance. The magneto-motive force is

$$f_{mm} = f_{mma} + f_{mms} \tag{5.5}$$

where f_{mma} and f_{mms} are the magneto-motive forces in the air gap and steel and are calculated in terms of magnetic field intensity, from

$$f_{mma} = H_{air}(x_g - x) \tag{5.6}$$

$$f_{mms} = H_{steel} L_{steel} \tag{5.7}$$

where H_{air} and H_{steel} are field intensities. $(x_g\text{-}x)$ and L_{steel} are circuit lengths in the air gap and steel, respectively.

The field intensity H_{steel} is a nonlinear function of the flux density B, and dependent upon the material properties, while H_{air} is a linear function of B. These functions are

$$H_{steel} = \zeta(B) \tag{5.8}$$

$$H_{air} = \frac{B}{\mu_0} \tag{5.9}$$

where ζ represents a nonlinear function for which the curves can be found for different materials in [168], and μ_0 is the permeability of air. If assuming that the area A, which relates the magnetic flux Φ and B at the air gap, remains uniform for the steel path then

$$B = \frac{\Phi}{A} \tag{5.10}$$

By backward substitution of Equation (5.3) through (5.10), a nonlinear differential equation is derived in terms of magnetic flux Φ, and by solving this equation, B is obtained from Equation (5.10). The solenoid force f_{sol} can then be calculated from the energy method [169] as

$$f_{sol} = \frac{0.5B^2 A}{\mu_0} \tag{5.11}$$

Using (5.11), (5.10) and (5.3), a nonlinear differential equation can be obtained as

$$\dot{f}_{sol} = k(v_{sol} - iR) f_{sol}^{\frac{1}{2}} \tag{5.12}$$

where $k = \dfrac{\sqrt{2A\mu_0}}{A\mu_0 N_s}$.

In a PEJ as the torsion spring wraps, the output torque increases linearly according to the Hooke's Law (4.1) in a short period of time and the output velocity finally becomes equal to the input velocity. To model this, a variable viscous friction is assumed acting between the input and output shafts. In this manner, as the torsion spring (see Figure 5.8) wraps ($\varphi \approx \varphi_g$), the viscous coefficient c increases according to an arctan function of ($\varphi - \varphi_g$) and as a result, the torque rapidly accelerates the output until the input and output velocities are equal. The general form of the assumed arctan function is

$$c = k_0 + k_1 \arctan(k_2(\varphi - \varphi_g)) \tag{5.13}$$

where k_0, k_1 and k_2 are constant parameters. By tuning these parameters, the engagement of the clutch can be simulated. For example, by tuning k_1 and k_2, the slope and magnitude of the torque can be regulated to adjust the engagement time. It should be noted that modeling the clutch engagement using a continuous function as Equation (5.13) will result in a computationally stable model, which is important for numerical simulations. Any other discontinuous model may result in crashing the simulation and keep asking for smaller step size during the numerical computation.

In order to limit linear and rotational movements of the control ring, variable stiffness for k_r, k_l are considered. These parameters are almost constant for the travel distance of x_g and φ_g, but increase exponentially towards the travel limit to present hard stops. Based on the above assumption, the equations of motion for the PEJ model become

$$\begin{cases} m\ddot{x} + b_l\dot{x} + k_l x = f_{sol} & \text{if} \quad 0 \le x < x_g \qquad (5.14) \\ J\ddot{\varphi} + b_r(\dot{\varphi} - \dot{\theta}) + k_r(\varphi - \theta) + b_{ra}\dot{\varphi} = T_c & \text{if} \quad x = x_g, 0 \le \varphi < \varphi_g \qquad (5.15) \\ J_{eff}\ddot{\theta} + b_r(\dot{\theta} - \dot{\varphi}) + k_r(\theta - \varphi) + b_{eff}\dot{\theta} = c(\omega_i - \dot{\theta}) & \text{if} \quad \varphi = \varphi_g \qquad (5.16) \end{cases}$$

where m, J, J_{eff}, b_l, b_r, b_{ra} and b_{eff} are the mass, moment of inertia, and viscous friction coefficient shown in Figure 5.8. θ, φ, ω_i are the clutch output and control ring angular displacement, and clutch input angular velocity, respectively. Equation (5.14) gives the forced linear motion of the control ring that is actuated by the magnetic force. Equation (5.15) represents the forced rotational motion of the control ring that is actuated by the torque from Equation (5.2). Finally, Equation (5.16) shows the forced rotational motion of the output that is actuated by virtual nonlinear viscous friction. In the overall model of the mechanical drive unit, J_{eff} and b_{eff} represent the inertia and friction of the gear train.

Since Equation (5.16) represents the dynamic of the actuated link as well, by its modification the overall model of the PEJ can be derived.

5.3 Control of PEJ

In this section, using the theory of variable structure systems and nonlinear PWM controller reviewed in Chapter 3, the local controllers for the PEJ are designed. The experimental results are analyzed and effect of multiple sampling periods on the quality of control is studied in the end of this section.

5.3.1 Design of Local Controllers

In Figure 5.9, a proposed control scheme for the SMD mechanism is presented. As shown in this figure, a motor mounted at the base feeds all mechanical drives with constant ω_{in}. Drive torque for the module is tapped from a central rotating shaft using clutch. The position and velocity of the modules are regulated by controlling the engagement time of the clutches using the Pulse Width Modulation (PWM) technique. The mechanical drives power the modules and their outputs are controlled by local controllers. The inputs and output of a local controller are the position and velocity of its module, and a tuned PWM signal respectively. While the local controller are used to control each module, a path planner is needed to supervise all local controllers to accomplish the robot's main task and also to deal with redundancy in the robot for energy minimization, obstacle or singularity avoidance.

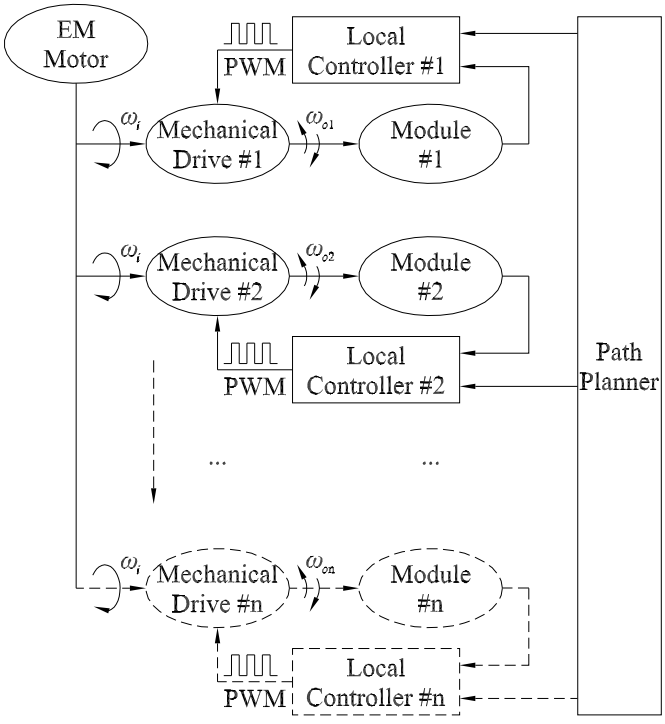

Figure 5.9 Control Scheme for the SMD Mechanism

In this subsection, the local controllers of SMD mechanism are designed based on the proposed control structure in Figure 5.9. This design is achieved using the existing similarity between ON-OFF-ON PWM and the PEJ model obtained in last section.

5.3.2 Output Error Feedback PWM for Local Controllers

In order to build an output error feedback PWM for local controllers, as depicted in Figure 3.9, it starts with the state space model of (5.14)-(5.16). The solenoid force, f_{sol} can be related to the PWM signal, u by a nonlinear first order differential equation (5.12) as

$$\dot{x}_1 = F_{sol}(u, x_1) \tag{5.17}$$

where x_1=f_{sol}. Considering (5.2), the torque T_c is proportional to f_{sol}, then the state space model is obtained as:

$$\dot{x} = f(x) = \begin{pmatrix} F_{sol}(u, x_1) \\ x_3 \\ \frac{1}{k_1}x_1 - \frac{k_3}{k_1}x_2 - \frac{k_2}{k_1}x_3 \\ x_5 \\ \frac{k_8}{k_4}x_1 - \frac{k_6}{k_4}x_4 - \frac{(k_7+k_5)}{k_4}x_5 + \frac{k_6}{k_4}x_6 + \frac{k_5}{k_4}x_7 \\ x_7 \\ \frac{k_6}{k_9}x_4 + \frac{k_5}{k_9}x_5 - \frac{k_6}{k_9}x_6 - \frac{(k_5+k_{10}+k_{11})}{k_9}x_7 + \frac{k_{11}}{k_9}r\omega_i - \frac{l}{k_9} \end{pmatrix} \tag{5.18}$$

where l and r are considered as an external constant load and the mechanical drive gear ratio, respectively, and $k_{1\sim11}$ are the mechanical drive and the robot parameters. The definitions of the states in (5.18) are

$x_1 =$ Solenoid force (f_{sol})
$x_2 =$ Translational displacement of the control ring (x)
$x_3 =$ Translational velocity of the control ring ($\dot{x}$)
$x_4 =$ Angular displacement of the control ring (φ)
$x_5 =$ Angular velocity of the control ring ($\dot{\varphi}$)
$x_6 =$ Angular displacement of the load (θ)
$x_7 =$ Angular velocity of the load ($\dot{\theta}$)

Assuming that while the PWM signal is off (u=0), the dominant dynamic of the system is reduced to the free motion of the slider, $f_1(x)$, the ON-OFF-ON PWM model in (3.41) can be applied to (5.18) as

$$f_1(x)=\begin{pmatrix} 0 \\ 0 \\ 0 \\ 0 \\ 0 \\ x_7 \\ -\dfrac{k_{10}}{k_9}x_7-\dfrac{l}{k_9} \end{pmatrix} \tag{5.19}$$

$$f_2(x)=\begin{pmatrix} F_{sol}(u,x_1)\,\mathrm{sgn}(e) \\ x_3\,\mathrm{sgn}(e) \\ \left(\dfrac{1}{k_1}x_1-\dfrac{k_3}{k_1}x_2-\dfrac{k_2}{k_1}x_3\right)\mathrm{sgn}(e) \\ x_5\,\mathrm{sgn}(e) \\ \left(\dfrac{k_8}{k_4}x_1-\dfrac{k_6}{k_4}x_4-\dfrac{(k_7+k_5)}{k_4}x_5+\dfrac{k_6}{k_4}x_6+\dfrac{k_5}{k_4}x_7\right)\mathrm{sgn}(e) \\ 0 \\ \left(\dfrac{k_6}{k_9}x_4+\dfrac{k_5}{k_9}x_5-\dfrac{k_6}{k_9}x_6-\dfrac{(k_5+k_{11})}{k_9}x_7\right)\mathrm{sgn}(e)-\dfrac{k_{11}}{k_9}r|\omega_i| \end{pmatrix} \tag{5.20}$$

then $f_1(x)+f_2(x)\mathrm{sign}(e)$ represents the dynamic of the system when the PWM signal is on (u=1). The direction of the motion is determined by the sign of the error signal.

Using the average ON-OFF-ON PWM model (3.44), the output error feedback PWM control structure introduced in (3.45) and (3.48) can be applied to (5.19) and (5.20) with M=1. Also the proposed diagram is as shown in Figure 3.9.

5.3.3 Sampling Frequency

Using Theorem 5 of Chapter 3, inequality (3.49), and model (5.19) and (5.20) a prediction for the chattering amplitude can be made. As understood from (3.49), this amplitude depends on the PWM frequency, the initial difference ε between the states of actual and average systems, and constants G and L_1, such that it satisfies some norm conditions. Using (5.19) and (5.20), the following can be obtained

$$\left\| \begin{array}{c} F_{sol}(u,x_1)\,\mathrm{sgn}(e) \\ x_3\,\mathrm{sgn}(e) \\ \left(\frac{1}{k_1}x_1-\frac{k_3}{k_1}x_2-\frac{k_2}{k_1}x_3\right)\mathrm{sgn}(e) \\ x_5\,\mathrm{sgn}(e) \\ \left(\frac{k_8}{k_4}x_1-\frac{k_6}{k_4}x_4-\frac{(k_7+k_5)}{k_4}x_5+\frac{k_6}{k_4}x_6+\frac{k_5}{k_4}x_7\right)\mathrm{sgn}(e) \\ 0 \\ \left(\frac{k_6}{k_9}x_4+\frac{k_5}{k_9}x_5-\frac{k_6}{k_9}x_6-\frac{(k_5+k_{11})}{k_9}x_7\right)\mathrm{sgn}(e)-\frac{k_{11}}{k_9}r\left|\omega_i\right| \end{array} \right\| \le G \tag{5.21}$$

One can simply consider the supremum of norm 2 over the operational interval, for example, and having all the parameters, the value of G can be found. On the manifold e=0, an estimate of the Lipschitz constant L_1 is simply given by the quantity $|\lambda|$ [157].

5.3.4 High-gain Approach

According to Theorem 6 of Chapter 3 (page 68), the high-gain design method [161] is available if the control law u=sgn(e) creates a sliding regime locally around the manifold $e=y_d-y=y_d-h(x)=0$. The value of β then has to be greater than $1/\varepsilon$ and 2ε is the width of a boundary layer where locally $[d_h, f_2]>0$. For instance, considering y_d=0 and selecting $h(x)$ in (3.48) as

$$h(x) = \lambda(x_{6d} - x_6) + (x_{7d} - x_7) \tag{5.22}$$

where λ, x_{6d} and x_{7d} are a positive constant, the desired values for the position, and the velocity of the slider, respectively. In the sliding regime, the state trajectory moves toward the desired point on the sliding line with a time constant equal to $1/\lambda$. Considering (5.22), dh is obtained as

$$dh = \begin{pmatrix} 0 \\ 0 \\ 0 \\ 0 \\ 0 \\ -\lambda \\ -1 \end{pmatrix} \tag{5.23}$$

The condition of existence of a sliding regime (3.51) has to be satisfied locally. Then

$$\lim_{e\to+0}\frac{de}{dt}=\frac{k_6}{k_9}x_4+\frac{k_5}{k_9}x_5-\frac{k_6}{k_9}x_6+\left(\lambda-\frac{k_5+k_{10}+k_{11}}{k_9}\right)x_7-\frac{l}{k_9}-\frac{k_{11}}{k_9}r|\omega_i|<0 \tag{5.24}$$

$$\lim_{e\to-0}\frac{de}{dt}=\frac{k_6}{k_9}x_4+\frac{k_5}{k_9}x_5-\frac{k_6}{k_9}x_6+\left(\lambda-\frac{k_5+k_{10}+k_{11}}{k_9}\right)x_7-\frac{l}{k_9}+\frac{k_{11}}{k_9}r|\omega_i|>0$$

Knowing the parameters of the system and working range of the state variables, one is able to come up with a designed range for ω_i where local existence of a sliding mode regime is guaranteed. Furthermore, considering Corollary 1 of Chapter 3, the transversality condition (3.17), and equivalent control method (3.38) are respectively obtained as

$$[dh,f_2]>0 \quad D(x)=-\frac{[dh,f_1]}{[dh,f_2]} \tag{5.25}$$

Substituting from (5.19) and (5.20) into (5.25), returns

$$-\left(\frac{k_6}{k_9}x_4+\frac{k_5}{k_9}x_5-\frac{k_6}{k_9}x_6-\frac{(k_5+k_{11})}{k_9}x_7\right)\mathrm{sgn}(e)+\frac{k_{11}}{k_9}r|\omega_i|>0 \tag{5.26}$$

$$D(x)=\frac{\left(\frac{k_{10}}{k_9}-\lambda\right)x_7+\frac{l}{k_9}}{\left(\frac{k_6}{k_9}x_4+\frac{k_5}{k_9}x_5-\frac{k_6}{k_9}x_6-\frac{(k_5+k_{11})}{k_9}x_7\right)\mathrm{sgn}(e)-\frac{k_{11}}{k_9}r|\omega_i|} \tag{5.27}$$

Using (5.26), and a constant ω_i, one is able to find a width of the boundary layer or sliding manifold, e=0, where the transversality condition is satisfied and hence the lower bound of β is obtained. Using (5.26) one is also able to find the PWM duty ratio based on the equivalent control method and state variable values.

A similar result would be obtained by using so-called integral control [164]. In this case, instead of using (5.22), $h(x)$ is defined as

$$h(x)=(x_{7d}-x_7)+2\lambda(x_{6d}-x_6)+\lambda^2\int_0^t(x_{6d}-x_6)d\tau \tag{5.28}$$

and then dh will be obtained as

$$dh=\begin{pmatrix}0\\0\\0\\0\\0\\-2\lambda-\lambda^2x_6\\-1\end{pmatrix} \tag{5.29}$$

Equation (5.26) remains the same and Equation (5.24), and (5.27) are changed accordingly

$$\lim_{e\to+0}\frac{de}{dt} \tag{5.30}$$
$$=\frac{k_6}{k_9}x_4+\frac{k_5}{k_9}x_5-\frac{k_6}{k_9}x_6+\left(2\lambda+\lambda^2x_6-\frac{k_5+k_{10}+k_{11}}{k_9}\right)x_7-\frac{l}{k_9}-\frac{k_{11}}{k_9}r|\omega_i|<0$$
$$\lim_{e\to-0}\frac{de}{dt}$$
$$=\frac{k_6}{k_9}x_4+\frac{k_5}{k_9}x_5-\frac{k_6}{k_9}x_6+\left(2\lambda+\lambda^2x_6-\frac{k_5+k_{10}+k_{11}}{k_9}\right)x_7-\frac{l}{k_9}+\frac{k_{11}}{k_9}r|\omega_i|>0$$

$$D(x)=\frac{\left(\frac{k_{10}}{k_9}-2\lambda-\lambda^2x_6\right)x_7+\frac{l}{k_9}}{\left(\frac{k_6}{k_9}x_4+\frac{k_5}{k_9}x_5-\frac{k_6}{k_9}x_6-\frac{(k_5+k_{11})}{k_9}x_7\right)\mathrm{sgn}(e)-\frac{k_{11}}{k_9}r|\omega_i|} \tag{5.31}$$

5.4 Experimental Results

In this section, the experimental results of the closed loop response of the proposed SMD+EA mechanism will be studied. This investigation is conducted using the PEJ shown in Figure 5.7. To evaluate the performance of the designed control system against changes in parameters such as PWM frequency, gain of controller β, input speed, and load, four different types of tests have been performed.

These tests have been conducted on the elastic joint to validate the results presented in Chapter 3 and this chapter for the design of the local controllers. In all these tests, position control is the goal of the control system and as a result the $x_6(t)$ is demanded and measured. The structure used for feedback control is the output error feedback PWM which was introduced in Figure 3.9. The amplitude of the chattering depends on the PWM frequency for a constant input speed. This is investigated in the first test. The effects of different controller gains β on the quality of the closed loop response are studied in the second test. In the third and fourth tests, the investigation focus is on the effects of input speed and load on the closed loop response.

5.4.1 First Test – Frequency and Chattering Phenomenon

In the first test, the relationship between PWM frequency and the chattering phenomenon is shown for constant parameter values of the controller gain, 0.25, input speed, 230 rpm, and load, 10^{-3}Nm. The experimental results of this test are shown in Figure 5.10 and Figure 5.11. In general, chattering is unavoidable since the implementation of the

associated control switching is imperfect and is not instantaneous. Also, chattering is undesirable, since it involves high control activity, and furthermore may excite high-frequency dynamics neglected in the course of modeling. However, it is possible to eliminate chattering by modifying the switching control laws [164].

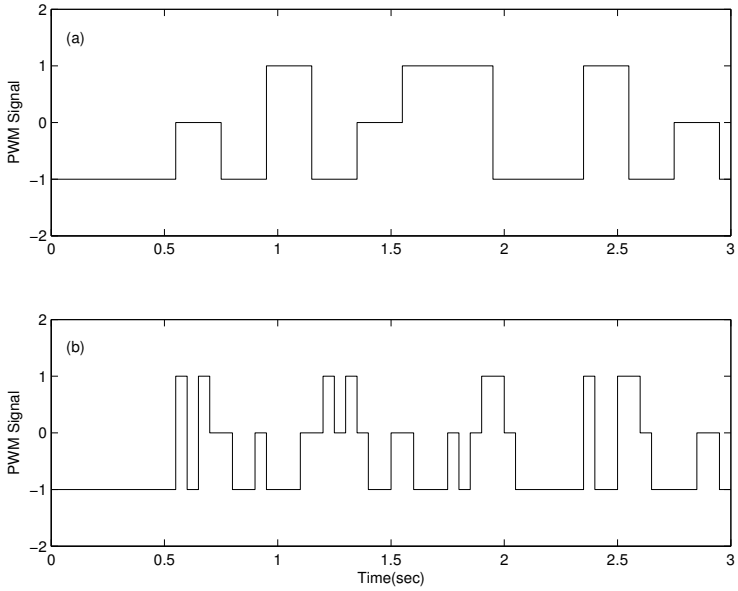

Figure 5.10 PWM Signals with Different Frequencies
a) 5Hz, b) 20Hz

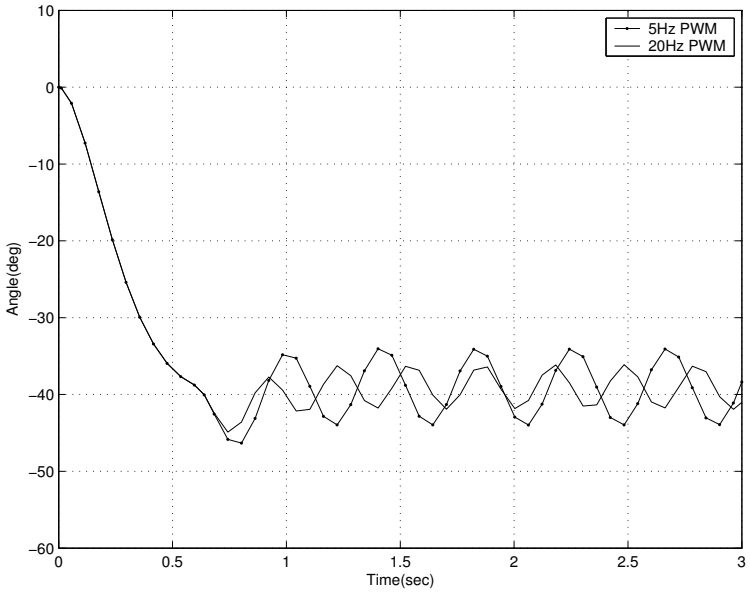

Figure 5.11 Chattering Amplitude Reduced by Increasing PWM Frequency

In Figure 5.11, the 40° step response of the closed loop system is shown for two different PWM frequencies. Considering Equation (3.49), as the frequency increase, the difference between states of the actual and average system decreases. This fact has been verified in this figure since the chattering amplitude is substantially decreased by increasing the frequency from 5Hz to 20Hz. The associate PWM signals are shown in Figure 5.10 (a) and (b).

5.4.2 Second Test – Controller Gain

In the second test, the quality of the closed loop system response is assessed by using three different controller gains, β. First the condition of existence of sliding mode should be verified for this case. Because the error signal is formed based only on position, dh is found as

$$dh = \begin{pmatrix} 0 \\ 0 \\ 0 \\ 0 \\ 0 \\ -\lambda \\ 0 \end{pmatrix} \tag{5.32}$$

therefore the condition (5.24) become

$$\begin{aligned} \lim_{e \to +0} \frac{de}{dt} &= \lambda x_7 < 0 \\ \lim_{e \to -0} \frac{de}{dt} &= \lambda x_7 > 0 \end{aligned} \tag{5.33}$$

but x_7 is the velocity of the slider, which is immediately matched to the input speed, $r\omega_i$, once direction switching occurs. The control system is programmed to have a switching strategy such that the sign of ω_i is set to the opposite sign of the error. Therefore, conditions (5.33) are satisfied and the existence of a sliding regime is guaranteed. Then, based on Theorem 6, a high-gain design method is available. Considering (5.19), (5.20), and (5.32), one has $[dh, f_2]=0$ which shows a singular point, and no lower bound is assigned to β. It means that there is no upper bound for the width of boundary layer ε, to invalidate the existence of a sliding mode regime.

The experimental results of the second test are shown in Figure 5.12 and Figure 5.13. In this test, the constant parameter values are: PWM frequency, 20Hz, load 10^{-3}Nm, and input speed 230rpm. In Figure 5.13, the 40° step response of closed loop system is shown for three different β. It can be seen that, as β increases, the actual PWM response approaches the desired average value and the steady state error decreases. Theoretically, there is no upper bound for β in this case. However, large β results in larger chattering amplitude. In Figure 5.12 (a), (b), and (c) the associated PWM signals are depicted. When the value of β is high enough, a symmetrical chattering is seen about the zero error.

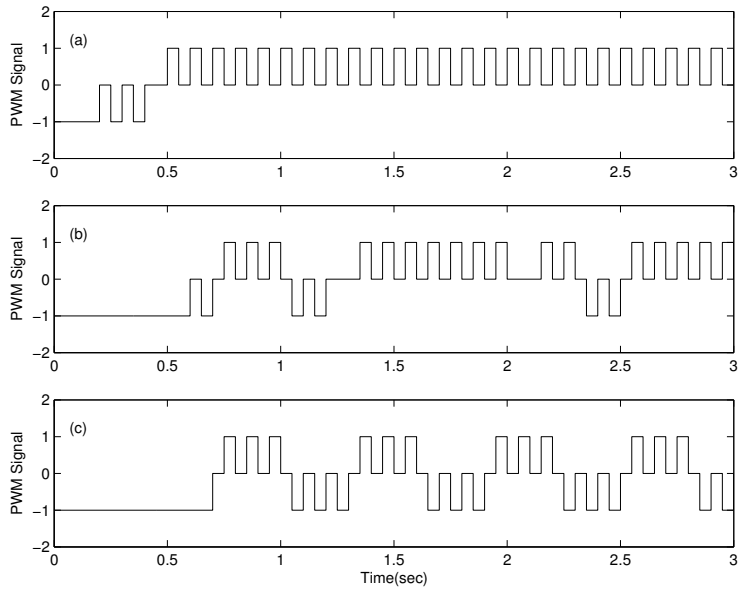

Figure 5.12 The Effects of Different Gains on 20Hz PWM Signals
a) gain=0.05, b) gain=0.1, c) gain=0.2

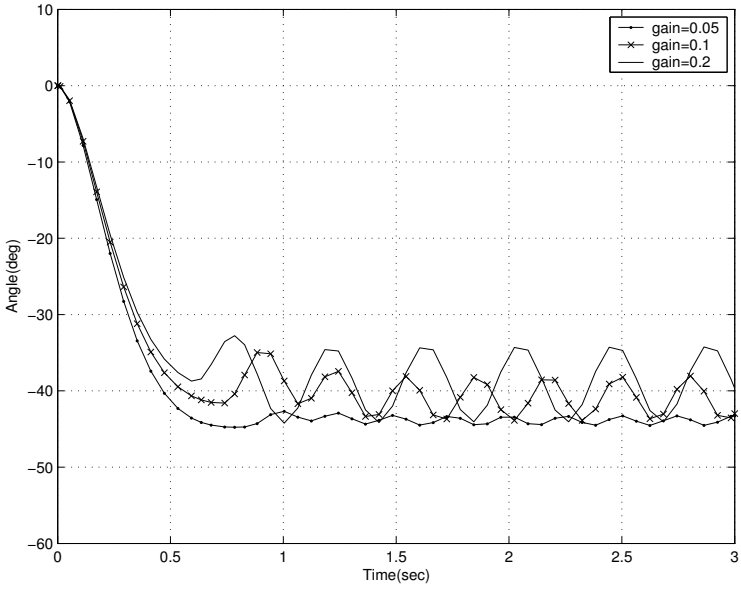

Figure 5.13 Steady State Error Reduction in the Controlled Response Due to Increasing Gain

5.4.3 Third Test – Input Speed

In the third test, the investigation focus is on the effect of input speed on the closed loop response. In this test, the input speed is varied and the constant parameter values are: PWM frequency, 20Hz, load 10^{-3}Nm, and controller gain, 0.25. The experimental results of the third test are shown in Figure 5.14 and Figure 5.15. In Figure 5.15 the 40° step response of closed loop system is shown for three different ω_t. It can be seen that, by increasing ω_t, the rise time decreases but the chattering amplitude increases. This behavior can be explained using (3.49) where G appears on the right-hand side. Considering (5.21), as ω_t increases the vector norm, and therefore G, increases. As a result

of this, the chattering is amplified according to (3.49). In general, using (5.24) and (5.25), the value of ω_t is important for both stability and control response quality. In Figure 5.14 (a), (b), and (c) the associated PWM signals are depicted. For larger ω_t, PWM signals perform wider pulses and from this point of view, increasing ω_t and β has the same result in chattering.

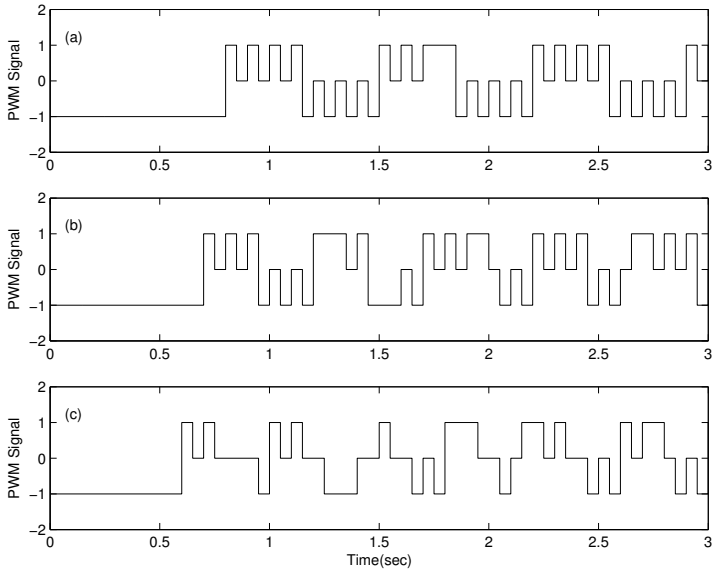

Figure 5.14 The Effects of Different Input Speeds on 20Hz PWM Signals
a) 173 rpm, b) 230 rpm, c)288 rpm

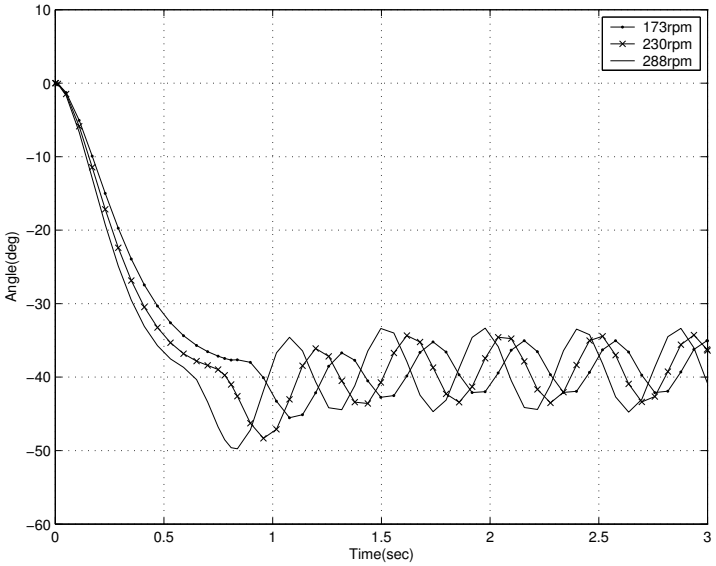

Figure 5.15 The Effects of Input Speed on Both Chattering Amplitude and Final Value of PWM Controlled System

5.4.4 Fourth Test - Load

In the fourth test, the investigation focus is on the effect of load on the closed loop response. The experimental results of this test are shown in Figure 5.16 and Figure 5.17. The constant parameter values are: PWM frequency, 20Hz, controller gain 0.25, and input

speed, 230 rpm. In Figure 5.17, the 40° step response of the closed loop system is shown with three different loads. It can be observed that, by tripling the load from 10^{-3}Nm to $3*10^{-3}$Nm, the control system still provides the same response. The amount of load has some effect on the conditions of existence of sliding mode through (5.24) and theoretically no effects on chattering phenomena since it does not appear in (3.49). However, this result is valid in the case where the amount of load is negligible compared to the torque capacity of the motor. This result verifies the robustness of the designed control system against changes in parameters and modeling uncertainties which is a heritage feature because of the sliding mode base structure controller. In Figure 5.16 (a), (b), and (c), the associated PWM signals are shown. They show the same behavior for the different cases and this again verifies the consistency of the control system performance.

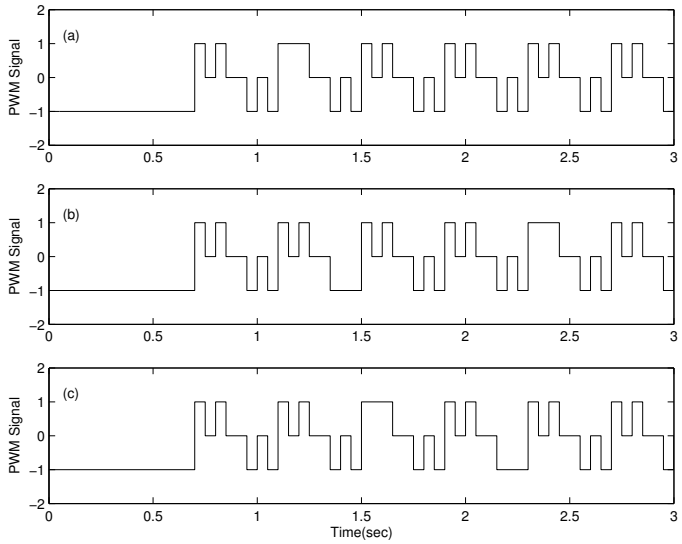

Figure 5.16 The Effects of Different Loads on 20Hz PWM Signals
a) 10^{-3}Nm, b) $2*10^{-3}$Nm, c)$3*10^{-3}$Nm

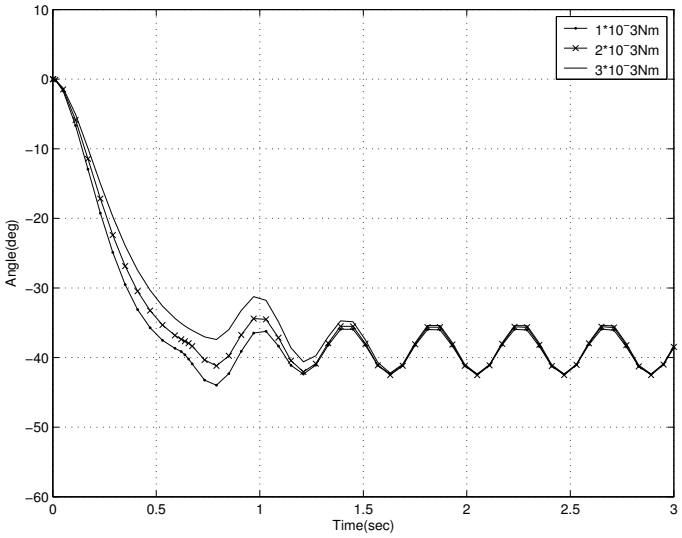

Figure 5.17 The Effects of Changing in the System Parameters (load) on Both Chattering Amplitude and Final Value of PWM Controlled System Response

5.4.5 More Tests

More results for position and tracking control have been obtained when weight is not an issue. For this case, the input speed to the mechanical drive and PWM frequency are set at 288rpm and 10Hz, respectively. In Figure 5.18 the response of the closed loop system to the ±40° position step is plotted. As seen in the figure, the steady state error is small (about 0.05°) and by looking at the details, no chattering is detected. In Figure 5.19, the set point is a sinusoidal wave with 150° amplitude, for which the control system demonstrates a promising tracking response with maximum error of ±2.5°.

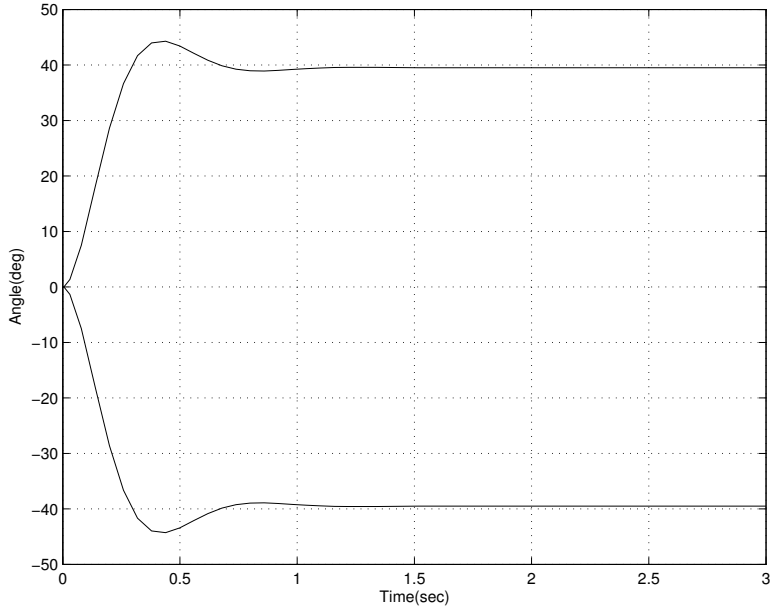

Figure 5.18 Closed Loop System Response to the Step Input with Proportional Controller

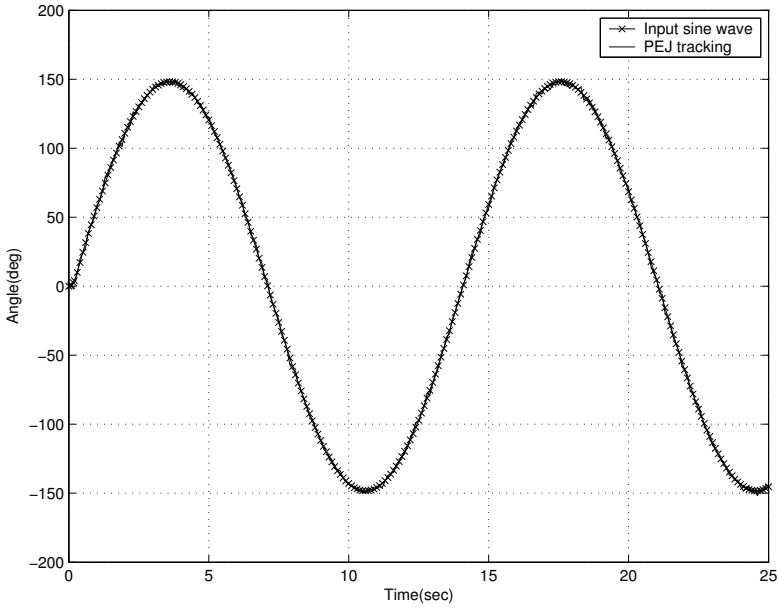

Figure 5.19 Tracking Control of the PEJ

Using the integral control (5.28) introduced earlier in this chapter, results in better position control performance. In Figure 5.20, the 40° step response of the PEJ with

integral control is depicted. In this test, the constant parameters are PWM frequency, 20Hz, load, 10^{-3}Nm, and input speed, 230rpm. This figure shows that the control system can regulate the position in less than 1 second without any considerable fluctuation.

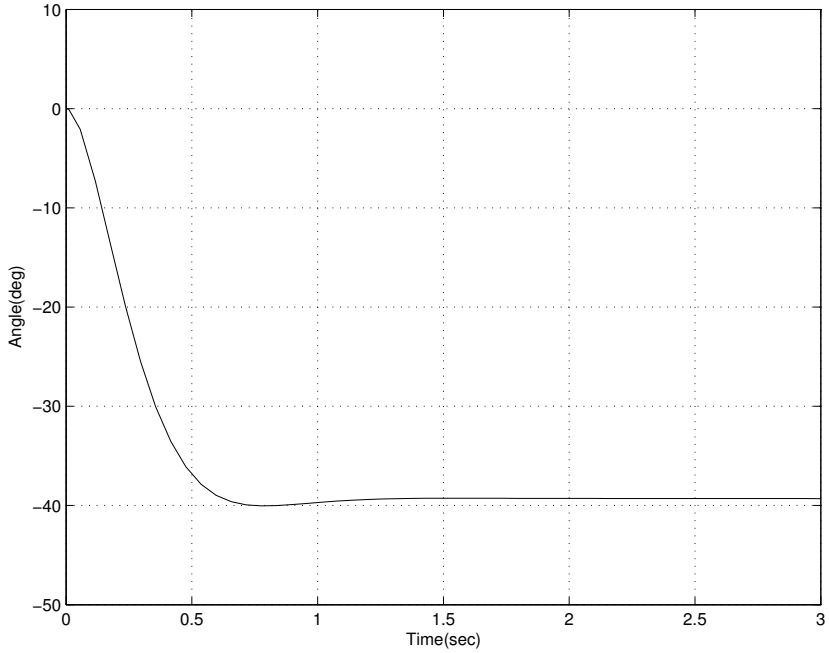

Figure 5.20 Step Response of PEJ with Integral Control

5.4.6 The Effect of Multiple Sampling Periods on Control Algorithm

Generally, when using computers to control a process, the chosen sampling period T_s, can have a significant impact on its performance. The sample period can affect the stability of the system and its speed of response to disturbances. It is usually desirable to make the sample period as short as possible in order to achieve rapid response and minimize the adverse effects of the period on stability. On the other hand, calculations must be performed by the control computer every sample period, and the shorter the sample period, the greater the computational load laced on the control computer.

In a PWM controlled system, the PWM period (T_{PWM}) is a crucial parameter that has to be selected. In previous sections, some effects of this parameter on the quality of the PWM controlled system were revealed. One of the important results was obtained when one could derive an average model (3.37) from an actual PWM system (3.34), while the PWM sampling period was small enough. From there, one could build a common nonlinear feedback control system as shown in Figure 3.9 and discuss its stability and gain design method. To keep this result valid, the PWM sampling period must be kept as small as possible. On the other hand, in the PEJ, the time constant of the clutches limits the lower bound of the PWM sampling period, and beyond this limit the clutches do not respond.

In the PWM controlled system shown in Figure 3.9, the control law is somehow designed to establish a sliding regime around a zero error manifold and therefore the sampling period T_s cannot affect the stability of the closed loop system; however, by selecting a large value of T_s, the quality of the response can be degraded.

In Figure 5.21, the two sampling periods are compared (T_s is considered to be smaller than T_{PWM}). In the PWM controlled system shown in Figure 3.9, the controller updates the duty ratio every T_{PWM} based on the error signal. This task has to take place between point A and B on Figure 5.21. In this particular application, the computation time required is very small compared to T_{PWM}; the question that arises is how small T_s should be and what is the effect of this parameter on the quality of control for different controllers, for example on a proportional and PID controller. To answer these questions we first need to define a criterion to evaluate the control system quality. For this purpose, different performance indices can be used. Some of these indices are

$$IAE = \int_0^\infty |e(t)|dt \tag{5.34}$$

$$ISE = \int_0^\infty e(t)^2 dt \tag{5.35}$$

$$ITAE = \int_0^\infty t|e(t)|dt \tag{5.36}$$

$$ITSE = \int_0^\infty te(t)^2 dt \tag{5.37}$$

where *IAE*, *ISE*, *ITAE*, and *ITSE* stand for Integral of Absolute Error, Integral of Squared Error, Integral of Time multiplied by Absolute Error, and Integral of Time multiplied by Squared Error, respectively. Because it is assumed that the input to the mechanical drive is time invariant and the response time of the system depends on this parameter, the *IAE* or *ISE* will adequately reflect the assessment of control quality.

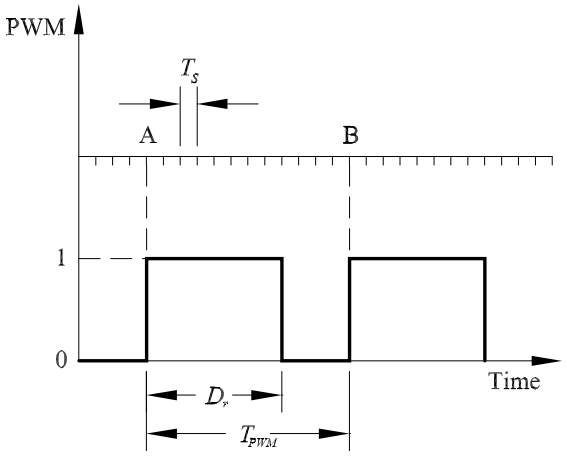

Figure 5.21 Multiple Sampling Periods on PWM Controlled Systems
Computer Sampling Period T_s and PWM Sampling Period T_{PWM}

To evaluate the quality of the PEJ, the *IAE* criterion is selected. The variation of this performance index, as a function of sampling period ratio T_s/T_{PWM}, is also studied. For this purpose, the position response of the PEJ is considered and the constant parameters are PWM frequency, 20Hz, load 10^{-3}Nm, and input speed, 230 rpm. In Figure 5.22, the variation of *IAE* with respect to T_s/T_{PWM} is shown for the proportional and PID controllers. For the PID controller case, the saturation and proportional blocks in Figure 3.9 are replaced by a saturation and a PID block, respectively.

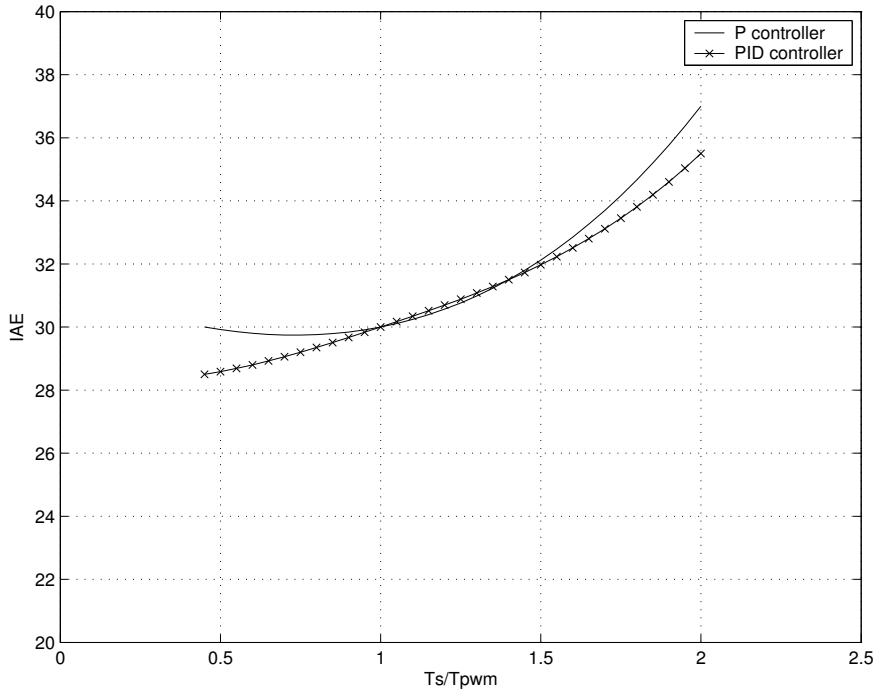

Figure 5.22 Integral of Absolute Error versus T_s/T_{PWM} for Proportional and PID Controllers

It can be seen in Figure 5.22, that in the case of proportional control, the performance of the control system is not affected by increasing T_s in the range of $T_s<T_{PWM}$, but for $T_s>T_{PWM}$ the control system performance is degraded. This behavior can be explained by understanding the time independent nature of the proportional controller. Proportional control action does not depend on previous information and as long as this action takes place between point A and B or $T_s<T_{PWM}$, the control system exhibits similar behavior. However, for the PID controller the results are quite different and the *IAE* monotonously decreases with smaller T_s resulting in better control performance. This behavior appears because the control action is based not only no information at the sample instant, but also on information from previous samples for the derivation part of the controller. Thus, as T_s decreases, the control action is closer to the action of continuous control and therefore results in a better performance.

5.5 PEJ Characteristics Analysis

The experiments of PEJ show the physical characteristics as following.

- Open-loop Dynamics

By fixing the load end of the actuator and forcing the mass with motor torque, PEJ exhibits second order behavior. The natural frequency of PEJ is dominated by dynamic mass and spring constant. This frequency is the one at which large torque performance of the actuator begins to drop off. There are signal filters on the feedback from the sensor; however, they are set high enough that their effects are not noticeable.

- Saturation

Because of the mass-spring resonance, PEJ is limited in its ability to control large torques. The resonance defines the frequency at which the actuator begins to decrease in large torque performance. This constraint is independent of control system. PEJ can still produce some fraction of the maximum output torque at high frequency as the controller commands however its peak to peak magnitude will be limited due to saturation.

- Bandwidth

Closed-loop bandwidth of PEJ can be found by assuming small torques with fixed load and sweeping the frequency spectrum. The derivative term of the controller always introduces a zero into the system that represents the apparent resonance in the closed loop system. Controlled bandwidth remains constant while control gain increases proportionally to the reduction in spring stiffness. Impedance however, is dramatically reduced when the spring stiffness is lowered.

- Power Density

The desired torque in PEJ is set to just balance the gravity of the aluminum link in -40° position from level plane. By oscillating the desired torque around the equilibrium point, the link moves up when it has greater torque and drops when it has less. Current design of PEJ has a bulky size and heavy weight (about 2kg including the base) as compared with commercial product of DC motor. The design optimization of PEJ subcomponents especially of bidirectional clutch is one of the future works of this research topic, which potentially has big commercial value.

6 Simulation of SMD Biped Walking

Although the combined feature of SMD mechanism and EA mechanism is presented as PEJ in the previous chapter, it is still a one-joint device and can hardly be termed as a "robot", not mention a biped robot. However, it's a big challenge to design a multi-link/multi-joint biped robot that has both SMD and EA feature fulfilled. Instead of concentrate in the engineering design chaos, this chapter will present a biped robot built with in ADAMS. In other words, this chapter will not discuss the engineering details of building a biped robot that has SMD and EA feature (can come to world in 5 years?), but present the simulation of a virtual biped robot mathematically and dynamically.

For simple demonstration, some simulation preconditions are defined:

- Only link mass and inertia will be considered.

This is based on the fact that for SMD robot, its actuation units are reduced to as minimum as possible and therefore its link mass and inertia account for the majority part of total mass and inertia. Other parts like those in SMD mechanism do not dominant the biped walking performance so much.

- Mechanical parts deployment will be simplified as normal robot.

There is no robot in the world at this moment that has more than two joints with the combined feature of SMD and EA (PEJ has only one joint), however its "birth" is only a matter of time related to the mechanical engineering and other aspects of technology and engineering progress. We predict the new generation of biped robot with SMD and EA will have the same mechanical deployment for its links and joints just like the one presented in Figure 3.1, except the fact how they are engineeringly designed.

Figure 6.1 is the schematic view of SMD biped used in this chapter. As discussed in Chapter 3 the input velocity ω_{in} for every module/joint will be the same with acceptable tolerance when the number of module/joint is not too big – in this scheme it is 3. Three joint outputs ω_{hip}, ω_{knee}, and ω_{ankle} will have continuous value between $-\omega_{in}$ and ω_{in} including 0. By means of bidirectional clutch and its PWM control, the independent joints have independent rotational output values although their input values are the same. This output variation is the key reason why SMD biped robot can walk. Independent joints have independent joint profiles therefore have independent control signals. For one case study these control signals will be presented in Figure 6.7.

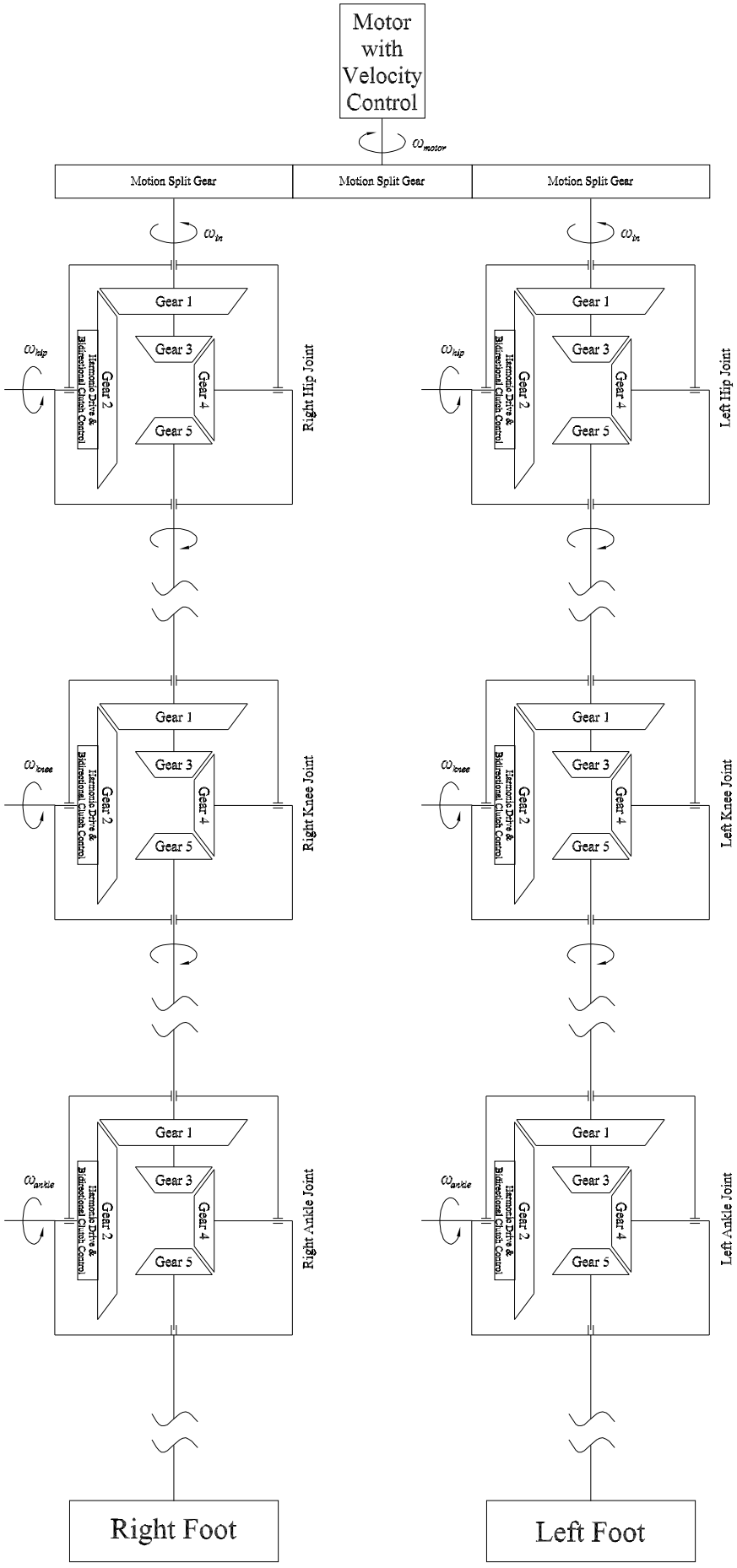

Figure 6.1 Schematic View of SMD Biped Robot

6.1 Gait Planning

The SMD biped robot model in Figure 6.2 (a) is simulated in this chapter. It was build up in MATLAB and ADAMS, in both mathematical and dynamic environment. The SMD mechanism was fully integrated into the walking model. Even the smallest gear mate/ratio was modeled and simulated in terms of SMD mechanism [Figure 6.2 (b)].

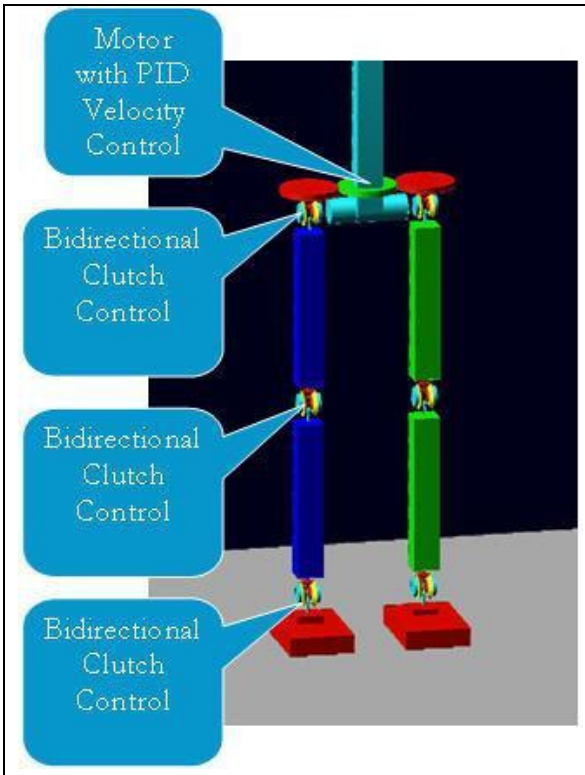

(a) SMD Biped Robot Control

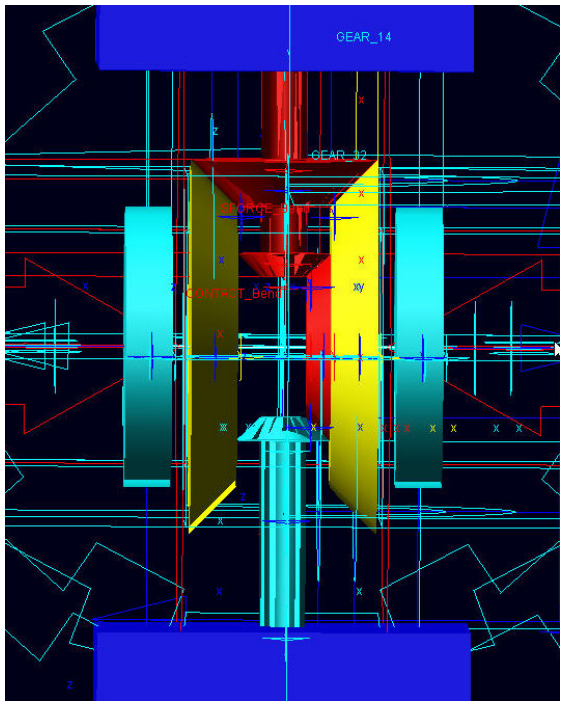

(b) SMD Joint Model

Figure 6.2 SMD Biped Robot Model in ADAMS

6.1.1 Walking Cycle

Biped walking is a periodic phenomenon. A complete walking cycle is composed of two phases: a double-support phase and a single-support phase. During the double-support phase, both feet are in contact with the ground. This phase begins with the heel of the forward foot touching the ground, and ends with the toe of the rear foot leaving the ground. During the single-support phase, while one foot is stationary on the ground, the other foot swings from the rear to the front.

Many studies on gait planning have assumed that the double-support phase is instantaneous. But in such a case, the hip has to move super fast in the extreme short period of double-support phase. In order to maintain its stability, the robot's center of gravity, in the case of static stability or the ZMP [3] in the case of dynamic stability, must

be transferred from the rear foot to the front foot during the short double-support phase. On the other hand, if the interval of the double-support phase is too long, it is difficult for the biped robot to walk at high speed. The interval of the double-support phase in human locomotion is about 20% [170] [171], so we used this value as the basis for the simulation.

If both foot trajectories and the hip trajectory are known, all joint trajectories of the biped robot will be determined by kinematic constraints. The walking pattern can therefore be denoted uniquely by both foot trajectories and the hip trajectory. When the robot moves straightforward, the lateral positions of both feet are constant. The lateral hip motion can be obtained similarly as the sagittal hip motion as discussed later in Section 6.1.3. In the following sections, only trajectories in the sagittal plane are discussed (Figure 6.3).

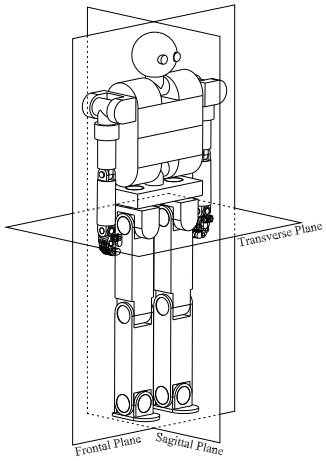

Figure 6.3 Three Analysis Planes of Biped Walking

In sagittal plane, each foot trajectory can be denoted by vector $X_a = [x_a(t), z_a(t), \theta_a(t)]^T$, where $[x_a(t),\ z_a(t)]$ is the coordinate of the ankle position, and $\theta_a(t)$ denotes the absolute angle of foot. The hip trajectory can be denoted by vector $X_h = [x_h(t), z_h(t), \theta_h(t)]^T$, where $[x_h(t),\ z_h(t)]$ denotes the coordinate of the hip position and $\theta_h(t)$ denotes the angle of hip. The detailed walking parameters are shown in Figure 6.4.

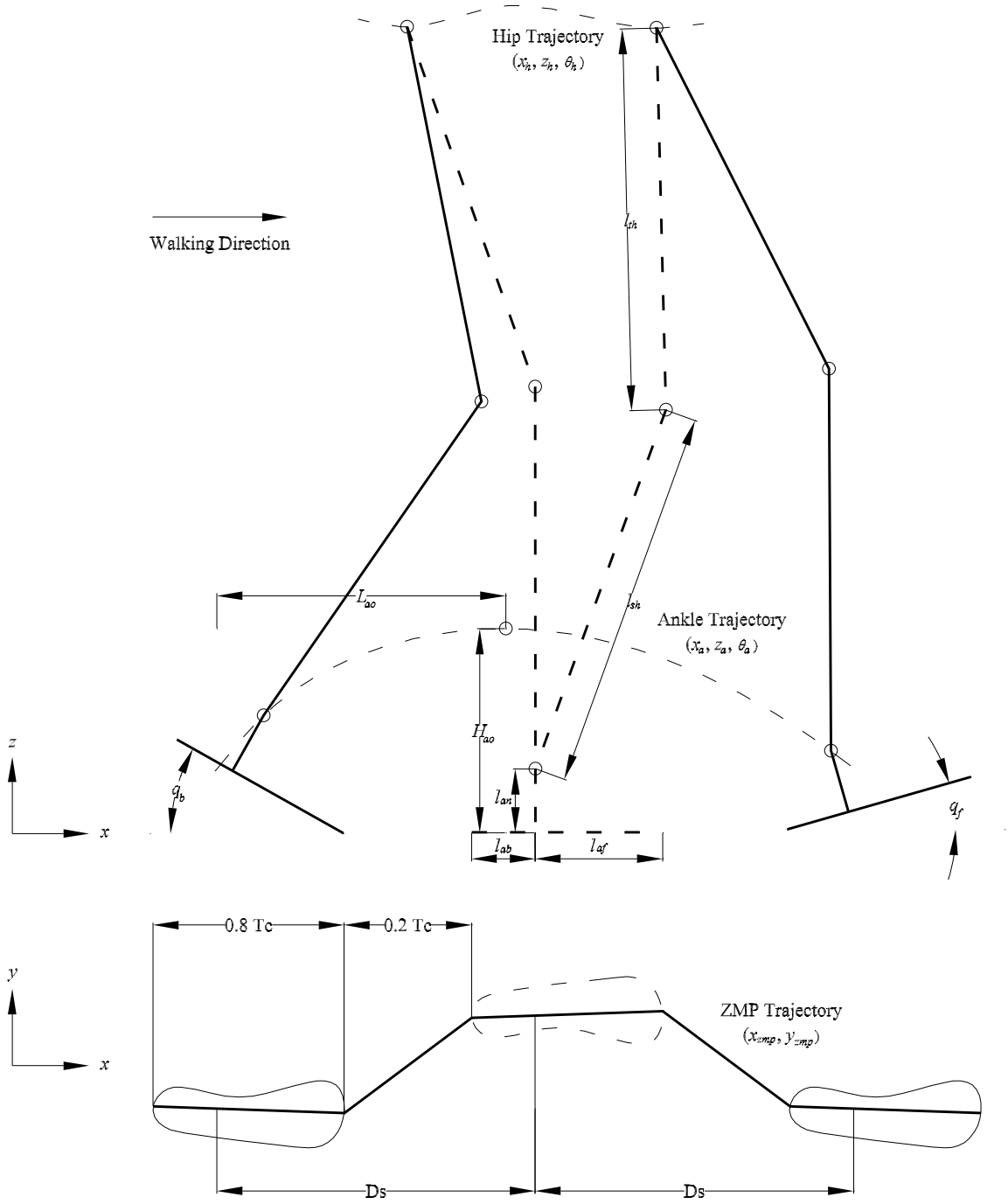

Figure 6.4 Walking Parameters at Single-support Phase

6.1.2 Foot Trajectories

Assuming that the period necessary for one walking step is T_c, the time of the kth step is from kT_c to $(k+1)T_c$, $k=1,2,\ldots,K$, K is the total number of steps. To simplify the analysis, we define the kth walking step to begin with the heel of the right foot leaving the ground at $t=kT_c$, and to end with the heel of the right foot making first contact with the ground at $t=(k+1)T_c$. In the following analysis, only the right foot trajectory generation is discussed. The left foot trajectory is same as the right foot trajectory except for a T_c delay.

Most previous studies have defined foot trajectories in which the feet are always level with the ground, that is, the foot angle $\theta_a(t)$ is always zero. Since the robot cannot touch the ground first by the heel of the forward foot and leave the ground finally by the toe of the rear foot, these kinds of foot trajectories are not useful for high-speed walking. Additionally, from the viewpoint of natural human locomotion and aesthetics, it is undesirable that the sole surface always be parallel with ground surface.

Letting q_b and q_f be the designated angles of the right foot as it leaves and lands on the ground, respectively. Assuming that the entire sole surface of the right foot is in contact with the ground at $t=kT_c$ and $t=(k+1)T_c+T_d$, the following constraints hold:

$$\theta_a(t)=\begin{cases}0 & t=kT_c\\ q_b & t=kT_c+T_d\\ -q_f & t=(k+1)T_c\\ 0 & t=(k+1)T_c+T_d\end{cases} \tag{6.1}$$

where T_d is the interval of the double-support phase. Here flat ground condition is assumed therefore before leaving and after contact of foot with ground the ankle joint angles are both 0.

Because there are always obstacles on the walking path, it is necessary to lift the swing foot high enough to negotiate obstacles. Letting (L_{ao}, H_{ao}) be the position of the highest point of the swing foot (Figure 6.4), from Equation (6.1) and kinematic constraints, the following two equations (constraints) must be satisfied:

$$x_a(t)=\begin{cases}kD_s & t=kT_c\\ kD_s+l_{an}\sin(q_b)+l_{af}(1-\cos(q_b)) & t=kT_c+T_d\\ kD_s+L_{ao} & t=kT_c+T_m\\ (k+2)D_s-l_{an}\sin(q_f)-l_{ab}(1-\cos(q_f)) & t=(k+1)T_c\\ (k+2)D_s & t=(k+1)T_c+T_d\end{cases} \tag{6.2}$$

$$z_a(t)=\begin{cases}l_{an} & t=kT_c\\ l_{af}\sin(q_b)+l_{an}\cos(q_b) & t=kT_c+T_d\\ H_{ao} & t=kT_c+T_m\\ l_{ab}\sin(q_f)+l_{an}\cos(q_f) & t=(k+1)T_c\\ l_{an} & t=(k+1)T_c+T_d\end{cases} \tag{6.3}$$

where D_s is the length of one step, kT_c+T_m is the time when the right foot is at its highest point, l_{an} is the height of the foot, l_{af} is the length from the ankle joint to the toe, l_{ab} is the length from the ankle joint to the heel (Figure 6.4).

Since the entire sole surface of the right foot is in contact with the ground at $t=kT_c$ and $t=(k+1)T_c+T_d$, the following derivative constraint must be satisfied:

$$\begin{cases} \dot{\theta}_a(kT_c) = 0 \\ \dot{\theta}_a((k+1)T_c + T_d) = 0 \end{cases} \tag{6.4}$$

$$\begin{cases} \dot{x}_a(kT_c) = 0 \\ \dot{x}_a((k+1)T_c + T_d) = 0 \end{cases} \tag{6.5}$$

$$\begin{cases} \dot{z}_a(kT_c) = 0 \\ \dot{z}_a((k+1)T_c + T_d) = 0 \end{cases} \tag{6.6}$$

To generate a smooth trajectory, it is necessary that the first derivative or velocity terms $\dot{x}_a(t)$, $\dot{z}_a(t)$, and $\dot{\theta}_a(t)$ be differential, the second derivative or acceleration terms $\ddot{x}_a(t)$, $\ddot{z}_a(t)$, and $\ddot{\theta}_a(t)$ be continuous at all time t, including all breakpoints $t=kT_c$, kT_c+T_d, kT_c+T_m, $(k+1)T_c$, $(k+1)T_c+T_d$.

To satisfy constraint from equations (6.1) to (6.6), and the continuity conditions of the first derivative and the second derivative, the order of the polynomial will be too high and its computation is difficult using polynomial interpolation. Therefore the foot trajectory is calculated as third-order spline interpolation. In this case, $x_a(t)$, $z_a(t)$, and $\theta_a(t)$ are characterized by third-order polynomial expressions, and the second derivatives $\ddot{x}_a(t)$, $\ddot{z}_a(t)$, and $\ddot{\theta}_a(t)$ are always continuous. With different foot trajectory specification on q_b, q_f, H_{ao} and L_{ao}, different foot trajectory can be produced.

6.1.3 Hip Trajectory

From the viewpoint of stability, it is desirable that hip motion parameter $\theta_h(t)$ is constant when there is no waist joint; in particular, $\theta_h(t)=0.5\pi$ rad on level ground. Hip motion $z_h(t)$ hardly affects the position of the ZMP, so it can be specified constant, or varying within a fixed range. Assuming that the hip is at its highest position H_{hmax} at the middle of the single-support phase, and at its lowest position H_{hmin} at the middle of the double-support phase during one walking step, $z_h(t)$ will be constrained by the following equation:

$$z_h(t) = \begin{cases} H_{h\min} & t = kT_c + 0.5T_d \\ H_{h\max} & t = kT_c + 0.5(T_c - T_d) \\ H_{h\min} & t = (k+1)T_c + 0.5T_d \end{cases} \tag{6.7}$$

The trajectory of $z_h(t)$ that satisfies equation (6.7) and the second derivative continuity condition also can be obtained by third-order spline interpolation.

The change of $x_h(t)$ is the main factor that affects the stability of a biped robot walking in a sagittal plane. A complete walking process is composed of three phases: a starting phase in which the walking speed varies from zero to a desired constant velocity,

a steady phase with a desired constant velocity, and an ending phase in which the walking speed varies from a desired constant velocity to zero. First, the hip motion $x_h(t)$ of the steady phase is obtained with the following procedure.

During a one-step cycle, $x_h(t)$ can be described by two functions: one for the double-support phase and one for the single-support phase. Letting x_{sd} and x_{ed} denote distances along the x-axis from the hip to the ankle of the support foot at the start and end of the single-support phase, respectively, the following equation can be got:

$$x_h(t) = \begin{cases} kD_s + x_{ed} & t = kT_c \\ (k+1)D_s - x_{sd} & t = kT_c + T_d \\ (k+1)D_s + x_{ed} & t = (k+1)T_c \end{cases} \tag{6.8}$$

To obtain a smooth periodic $x_h(t)$ of the steady phase, the following derivative constraints must be satisfied:

$$\begin{cases} \dot{x}_h(kT_c) = \dot{x}_h(kT_c + T_c) \\ \ddot{x}_h(kT_c) = \ddot{x}_h(kT_c + T_c) \end{cases} \tag{6.9}$$

Using third-order periodic spline interpolation, suitable $x_h(t)$ can be got which satisfieds constraints (6.8) and (6.9), and the second derivative continuity condition is given by:

$$x_h(t) = \tag{6.10}$$

$$\begin{cases} kD_s + \dfrac{D_s - x_{ed} - x_{sd}}{T_d^2(T_c - T_d)}[(T_d + kT_c - t)^3 - (t - kT_c)^3 \\ -T_d^2(T_d + kT_c - t) + T_d^2(t - kT_c)] & t \in (kT_c, kT_c + T_d) \\ + \dfrac{x_{ed}}{T_d}(T_d + kT_c - t) + \dfrac{D_s - x_{sd}}{T_d}(t - kT_c) \\ kD_s + \dfrac{D_s - x_{ed} - x_{sd}}{T_d(T_c - T_d)^2}[(t - T_d - kT_c)^3 - (T_c + kT_c - t)^3 \\ +(T_c - T_d)^2(T_c + kT_c - t) - (T_c - T_d)^2(t - T_d - kT_c)] & t \in (kT_c + T_d, kT_c + T_c) \\ + \dfrac{D_s - x_{sd}}{T_c - T_d}(T_c + kT_c - t) + \dfrac{D_s + x_{ed}}{T_c - T_d}(t - kT_c - T_d) \end{cases}$$

By defining different value for x_{sd} and x_{ed} a series of smooth $x_h(t)$ according to equation (6.10) can be got. Normally x_{sd} and x_{ed} vary within a fixed range, in particular the following range:

$$\begin{cases} 0 < x_{sd} < 0.5D_s \\ 0 < x_{ed} < 0.5D_s \end{cases} \tag{6.11}$$

Based on equation (6.10) and (6.11) and the ZMP calculation (Section 6.3.1), a smooth trajectory of $x_h(t)$ with the largest stability margin can be got.

Determining $x_h(t)$ of the steady phase also specifies the final constraints of the starting phase and the initial constraints of the ending phase. The initial constraints of the starting hpase, such as $\dot{x}_h(t_b)=0$, and the final constraints of the ending phase, such as $\dot{x}_h(t_e)=0$, are known. Therefore $x_h(t)$ of the starting phase and ending phase can be obtained by third-order spline interpolation.

6.2 Ground Reaction Force

6.2.1 Foot-Ground Contact Model

Ground reaction forces include normal pressure force F_z (normal to ground surface) and friction forces F_x and F_y (inside ground surface). The ground can be represented by a flat rigid surface while the two feet (soles) can be represented by an elastic material with stiffness coefficient k and damping coefficient c. Therefore the normal reaction force F_z is modeled as following function:

$$F_z = \begin{cases} \max(0,\ -kd_z - cv_z) & d_z < 0 \\ 0 & d_z \geq 0 \end{cases} \tag{6.12}$$

where:

d_z – contact penetration displacement along z axis

v_z – contact penetration velocity along z axis, $v_z = \dot{d}_z$

Damping coefficient c is a non-linear function of ground penetration d_z:

$$c = \begin{cases} c_{\max}\left|\frac{3}{h^2}d_z^2 - \frac{2}{h^3}d_z^3\right| & d_z < h \\ c_{\max} & d_z \geq h \end{cases} \tag{6.13}$$

where:

h, c_{max} – constant values

According to different materials of sole and ground, stiffness k, damping parameters h and c_{max} have different values. The contact penetration d_z corresponds to the deflection of foot/sole during walking. The chosen level of damping is high enough to prevent the foot from bouncing after hitting the ground, agreed with the commonsense that human foot/sole is very soft. The choosing of parameters k, c_{max} and h is not crucial as it was observed that their changing within range of 20% does not affect the model behavior very much.

The friction force, or tangent force, T is represented in terms of pseudo-Coulomb friction model. In pseudo-Coulomb friction model, there is no stiction, i.e. the bodies are

moving relative each other at a negligibly small velocity. The sliding velocity between foot/sole and ground v_p is

$$v_p = \sqrt{v_x^2 + v_y^2} \tag{6.14}$$

where:

v_x – x component of sliding velocity inside ground surface

v_y – y component of sliding velocity inside ground surface

The friction force can be calculated by

$$T = \mu' F_z \tag{6.15}$$

where:

μ' – non-constant friction coefficient

μ' is dependent on v_p:

$$\mu' = \mu \frac{2}{\pi} \arctan \frac{v_p}{\lambda} \tag{6.16}$$

where:

μ – constant Coulomb friction coefficient

λ – constant value

Finally the friction force components are given by

$$\begin{cases} F_x = -T \dfrac{v_x}{v_p + \varepsilon} \\ F_y = -T \dfrac{v_y}{v_p + \varepsilon} \end{cases} \tag{6.17}$$

where:

ε – small constant value

The parameter λ has no physical meaning but is used only for numerical reasons. The typical Coulomb friction model introduces some discontinuities into the model, because it consists of two separate models for the stiction phase and for the sliding phase. The discontinuities are responsible for difficulties with the convergence of numerical integration of the differential-algebraic equations that describe the multibody system. The pseudo-Coulomb friction model is an approximation of the Coulomb model: instead of stiction phase, small velocity sliding is assumed. Both models are equivalent when the parameter λ tends to infinity, however if an extreme small value of the parameter is chosen, numerically stiff equations will result. For a relative velocity high enough the magnitude of T approaches the value - μF_z give by the typical Coulomb friction model.

Parameter ε was added in order to avoid division by zero when v_p tends to zero. It has been found that the biped model behavior sensitivity to the parameter λ and ε is low.

6.2.2 Ground Reaction Force Distribution

Considering the two legs together, the motion of the biped's CoM can be written as:

$$m_{cm}a_{cm} = F_L + F_R + m_{cm}g \tag{6.18}$$

where:

m_{cm} – total mass of the biped

a_{cm} – acceleration of the CoM

During the single-support phase, the foot force is obtained directly from the above equation as one of f_L or f_R will be zero. During the double-support phase, however, only the total reaction force is known. According to the criteria of minimizing the internal force, some methods have been proposed to find the force distribution between two supporting legs [172] [173]. Unfortunately, these methods do not consider the motion of contact point on the sole. Further, smooth transition of the reaction forces before and after full contact, or touch and leave, is not satisfied.

During the double-support phase, the normal reaction force, which is along the z-axis, is determined by:

$$\begin{cases} y_L F_{Lz} + y_R F_{Rz} = y_{zmp}(F_{Lz} + F_{Rz}) \\ x_L F_{Lz} + x_R F_{Rz} = x_{zmp}(F_{Lz} + F_{Rz}) \end{cases} \tag{6.19}$$

where:

x_L, y_L – world coordinates of left foot contact point

x_R, y_R – world coordinates of right foot contact point

x_{zmp}, y_{zmp} – world coordinates of ZMP point

F_{Lz} – normal reaction force on left foot

F_{Rz} – normal reaction force on right foot

x_L, y_L, x_R, y_R, x_{zmp}, and y_{zmp} can be produced by gait planning in Section 6.1. Sum of F_{Lz} and F_{Rz} (F_{Lz}+F_{Rz}) can be obtained from the third equation of (6.18). Then the respective value of F_{Lz} and F_{Rz} can be obtained.

The friction forces in double-support phase are constrained by the first two equations of (6.18). With considering the contact model in Section 6.2.1 and the criteria of minimizing the internal force, their respective value can be obtained from the following optimization problem [174]:

- Minimize $-d_1-d_2$
- Subject to

$$\begin{cases} F_{Lx} + F_{Rx} = m_{cm} a_{cmx} \\ F_{Ly} + F_{Ry} = m_{cm} a_{cmy} \\ P\begin{bmatrix} F_{Lx} & F_{Ly} & F_{Rx} & F_{Ry} \end{bmatrix}^T + d_1 I < b \\ \dfrac{(p_L - p_R)^T}{\|p_L - p_R\|}(F_L - F_R) + d_2 < 0 \\ \dfrac{-(p_L - p_R)^T}{\|p_L - p_R\|}(F_L - F_R) + d_2 < 0 \\ d_1, d_2 > 0 \end{cases}$$

where:

$$P = \begin{bmatrix} 1 & 0 & 0 & 0 \\ -1 & 0 & 0 & 0 \\ 0 & 1 & 0 & 0 \\ 0 & -1 & 0 & 0 \\ 0 & 0 & 1 & 0 \\ 0 & 0 & -1 & 0 \\ 0 & 0 & 0 & 1 \\ 0 & 0 & 0 & -1 \end{bmatrix},\ b = \begin{bmatrix} -\mu F_{Lz} \\ -\mu F_{Lz} \\ -\mu F_{Lz} \\ -\mu F_{Lz} \\ -\mu F_{Rz} \\ -\mu F_{Rz} \\ -\mu F_{Rz} \\ -\mu F_{Rz} \end{bmatrix},\ I = \begin{bmatrix} 1 \\ 1 \\ 1 \\ 1 \\ 1 \\ 1 \\ 1 \\ 1 \end{bmatrix},\ F_L = \begin{bmatrix} F_{Lx} \\ F_{Ly} \\ F_{Lz} \end{bmatrix},\ F_R = \begin{bmatrix} F_{Rx} \\ F_{Ry} \\ F_{Rz} \end{bmatrix},$$

p_L and p_R, both in form of $(p_x \quad p_y \quad 0)^T$, are the position of left foot contact point and right foot contact point respectively. μ is the constant Coulomb friction coefficient defined before. The scalar d_1 physically represents the contact stability margin, while d_2 is in inverse proportion to the internal force.

By solving the optimization problem, ground friction force distribution between two supporting feet can be got. These values maximize the biped stability but minimize the internal force during the double-support phase. The smooth transition of the foot forces during the "reach" and "leave" stage are also ensured.

6.3 ZMP Processing

For a robot with four or more supporting legs, it is possible to consider static stability using the center of gravity. But for a biped robot, it is necessary to take into account dynamic stability. To evaluate dynamic stability, the most "popular" concept is the Zero Moment Point (ZMP) first introduced by Vukobratovic and Juricic [3].

6.3.1 Dynamic ZMP Calculation

The ZMP is defined as the point on the ground about which the sum of all the moments of active forces is equal to zero. If the ZMP is inside the contact polygon between the foot and the ground, the biped robot is stable. The ZMP can be computed by the following equations:

$$x_{zmp} = \frac{\sum_{i=1}^{n} m_i(\ddot{z}_i + g)x_i - \sum_{i=1}^{n} m_i \ddot{x}_i z_i - \sum_{i=1}^{n} I_{iy}\ddot{\Omega}_{iy}}{\sum_{i=1}^{n} m_i(\ddot{z}_i + g)} \tag{6.20}$$

$$y_{zmp} = \frac{\sum_{i=1}^{n} m_i(\ddot{z}_i + g)y_i - \sum_{i=1}^{n} m_i \ddot{y}_i z_i - \sum_{i=1}^{n} I_{ix}\ddot{\Omega}_{ix}}{\sum_{i=1}^{n} m_i(\ddot{z}_i + g)} \tag{6.21}$$

where m_i is the mass of link i, $(I_{ix}, I_{iy})^T$ is the inertial vector of link i, $(\Omega_{ix}, \Omega_{iy})^T$ is the angular velocity vector of link i, g is the gravity acceleration, $(x_{zmp}, y_{zmp}, 0)$ is the world coordinate of the ZMP, and (x_i, y_i, z_i) is the coordinate of the CoM of link i on the absolute Cartesian coordinate system.

m_i, $(I_{ix}, I_{iy})^T$, g are all constant if the biped robot is fabricated out, or modeled out. $(\Omega_{ix}, \Omega_{iy})^T$ and (x_i, y_i, z_i) can be got once the gait has been planned out. Therefore every set of planned gait corresponds to one set of the ZMP trajectory $(x_{zmp}, y_{zmp}, 0)$.

Due to both the measurement inaccuracy and additional operations (like those making it symmetric and periodical) the gait pattern suffers from relatively big errors. When gait patterns for joints are precisely realized the absolute motion of the trunk is left uncontrolled. If the biped stared to fall the control system would not react. The only way to control the absolute motion of the trunk is to apply a control algorithm, which instantaneously modifies the prescribed joint motions (gait) in order to prevent the biped from losing its stability. This procedure is termed ZMP optimization.

6.3.2 ZMP Optimization

Since the ZMP is a point on the two dimensional ground surface, its trajectory can be controlled by controlling the motion of two orthogonal joints with horizontal axes. For example, the simplest choice of two such joints is the waist joint [175]. It is known that periodic motions are most appropriate for trajectory planning and control of underactuated mechanisms. Moreover, since human locomotion is an almost periodic process, it is desirable to have this characteristic in the robot locomotion for naturality. Since finite energy periodic signals can be represented through the sine and cosine function (Fourier series), the corrective motion is represented in the following form:

$$\delta\theta_i = \sum_{i=1}^{n} [a_{in} \sin(n\omega_{wi} t) + b_{in} \cos(n\omega_{wi} t)] \tag{6.22}$$

where, $\delta\theta_i$ is the corrective motion at ith joint, a_{in} and b_{in} represent the amplitude, and ω_{wi} is the frequency of the corrective motion. The ZMP, being a point on the ground plane, has two degrees of freedom. However, the Fourier expansion of the corrective signals may involve a large number of unknown coefficients. This allows us to formulate an optimization problem to determine the unknown coefficients for obtaining a good match between the actual and the desired ZMP trajectories as follows:

$$Minimize \quad J = \int \left\| p_{zmp} - p_{zmp}^{d} \right\|^2 dt \tag{6.23}$$

where p_{zmp} and p_{zmp}^{d} represent the measured and desired ZMP trajectory respectively.

6.4 Simulation Results

The optimized gait was generated in MATLAB 7 according to the algorithm in Section 6.1 and the result was exported into ADAMS 2003 in which the simulation model was built. The physical properties of the biped robot are same as those presented in author's First Year Report [176]. The biped's walking parameters are described in Figure 6.4. The walking speed was 1.0 km/h with the step length D_s of 250 mm/step and the step period T_c of 0.9 sec/step, a little slower than human being walking speed. The total simulation time is 4.5 seconds with 5 steps, in which the first step is from static standing to steady walking and the rest 4 steps are all steady walking. Figure 6.5 is the first two steps walking frame capture, from time 0 to time 1.8 seconds.

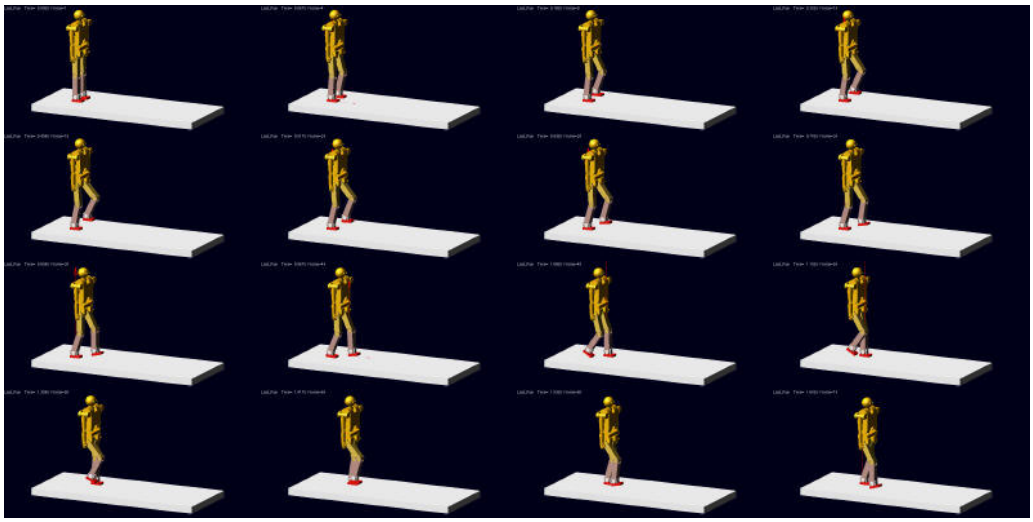

Figure 6.5 Two Step Walking Frame Capture
Sequence from left to right, top to down.

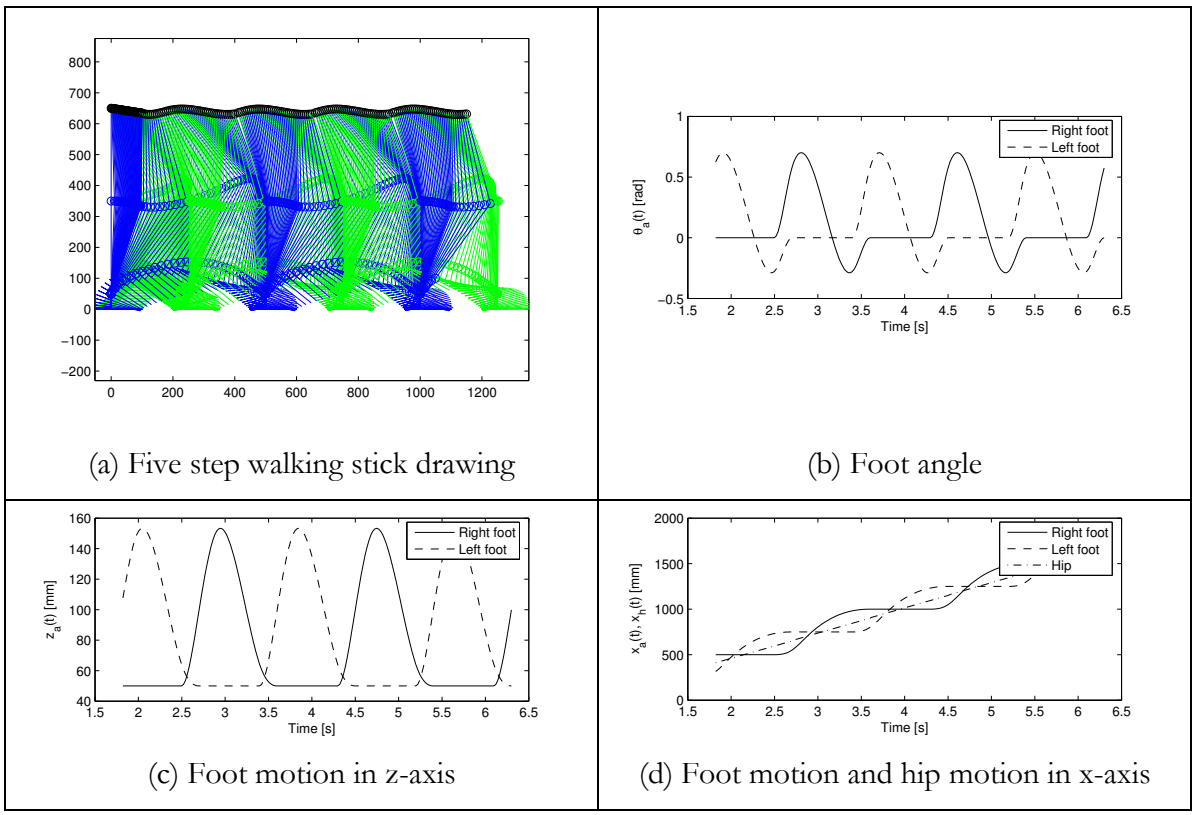

(a) Five step walking stick drawing

(b) Foot angle

(c) Foot motion in z-axis

(d) Foot motion and hip motion in x-axis

Figure 6.6 Simulation Results Drawing

q_b=30deg, q_f=15deg, L_{ao}=0.2125m, H_{ao}=0.15m

6.4.1 Walking Parameter Review

Figure 6.6 shows the walking parameter simulation results drawing. From the stick figure [Figure 6.6 (a)] and the foot angle [Figure 6.6 (b)] we can see both feet leave and land on the ground with the desired angles. Also, both foot trajectories [Figure 6.6 (a)-(d)] and the hip trajectory [Figure 6.6 (d)] are smooth.

6.4.2 Joint Position Profile

As demonstrated in Figure 6.1, the SMD biped robot has two sets of real time control – the control of single DC motor rotation (velocity control), and the control of bidirectional clutch engagement at every local joint (force control, but only its direction). For the motor rotation velocity control, PID controller is used. While the desired rotation velocity is set to 60000deg/sec (about 166.7rpm), in the whole 5-step walking period the maximum velocity fluctuation observed is 25 deg/sec. This velocity fluctuation (error) is less than 0.05% of the desired value, therefore the DC motor rotation is quite "smooth" and its velocity output can be thought of constant.

For the local joint bidirectional clutch control, a simple closed-loop proportional controller with threshold is used. The controller compares the desired and measured

position trajectory and outputs two-stage control signal – positive *F* or negative *F*, which represent the positive and negative magnetic force in bidirectional clutch. By adjusting the friction parameters between bidirectional clutch mate pair, the controlled joint position trajectory can be very close to the desired one. The right leg's desired and measured joint positon profiles, as well as their conresponding control signal of bidirectional clutches, are presented in Figure 6.7. The left leg is the same case, but for sake of space reason, its figures are not presented in this thesis.

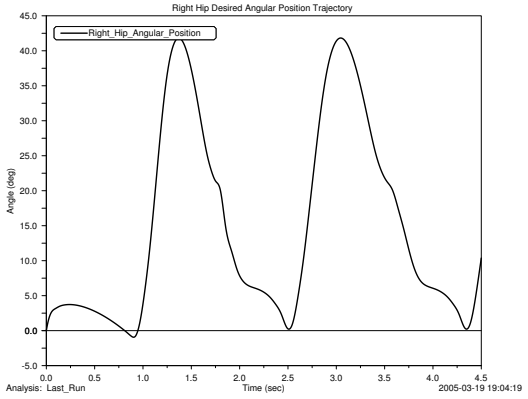

Right Hip's Desired Position Trajectory

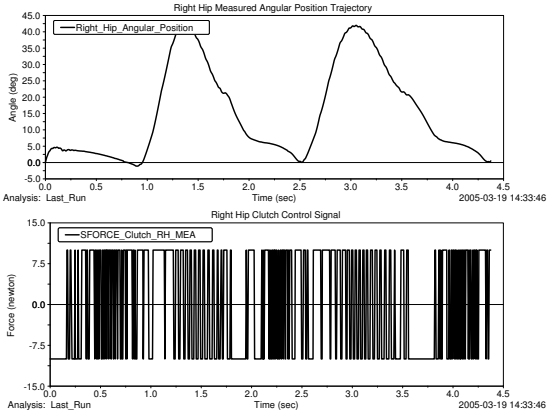

Right Hip's Measured Position & Control

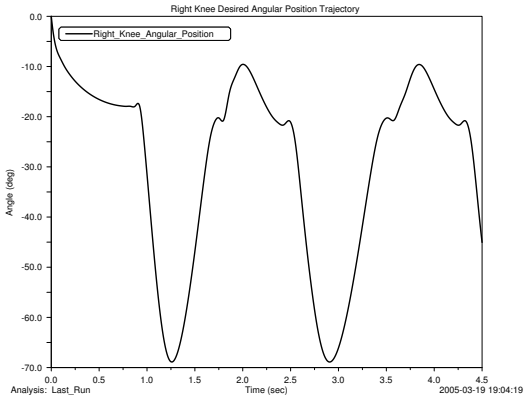

Right Knee's Desired Position Trajectory

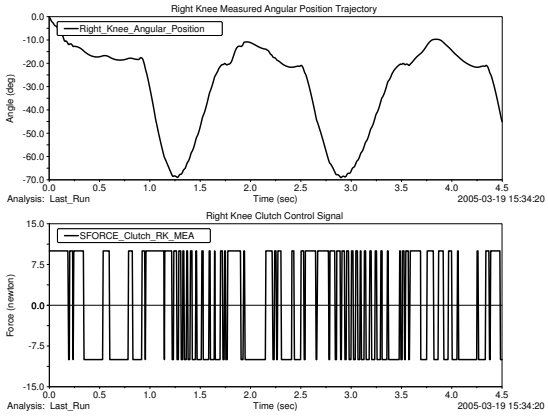

Right Knee's Measured Position & Control

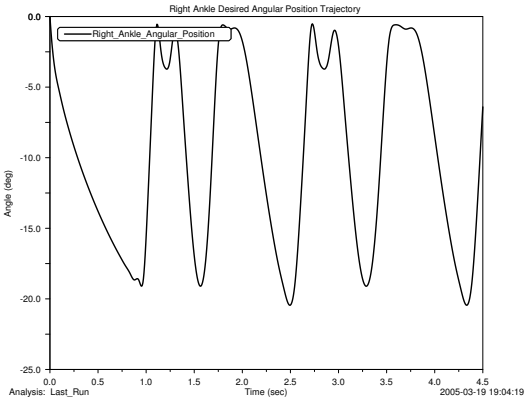

Right Ankle's Desired Position Trajectory

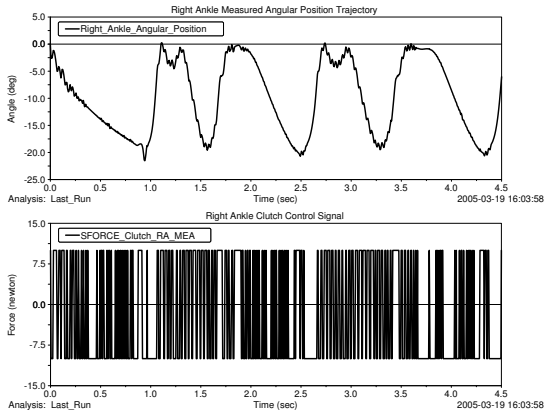

Right Ankle's Measured Position & Control

Figure 6.7 Right Leg's Desired and Measured Joint Position Profile as well as Control Signal

Hip, knee and ankle joint velocity continuously vary between $-\omega_{tn}$ and ω_{tn}. By means of bidirectional clutch and respective PWM control independent joints have independent rotational output values although their input values are the same. Joint angle trajectory as the integration of joint velocity trajectory therefore gets very close to the desired one. This happens to all six joints of SMD biped robot therefore its stable dynamic walking is achieved.

In Figure 6.7 different clutch engagement frequencies were observed. Knee joint's clutch has relatively low frequency of engagement than hip and knee joints'. This is due to the fact that during the walking knee's amplitude of joint variation is relatively small.

6.4.3 Joint Torque Profile

Although DC motor can be modeled that its output torque is proportional to its input electrical current, it is extremely difficult to measure the real working torque in the joint because of the existence of speed reduction mechanism. One of the advanced SMD's merits is that the real working torque in joint can be got directly from measuring the deformation of spring. If the spring coefficient is constant, the relationship between the measured spring deformation and the real working joint torque is linear.

Figure 6.8 shows the six joint torque profiles of the SMD biped robot in the 4.5 seconds walking time. All six joints have huge torque peak which is periodical and supposed to be caused by the sudden contact of foot and ground. In the simulation environment, all material are steel, including the sole and the ground. Using soft and elastic material as sole, just like the Honda Humanoid Robot [1], these torque peaks can be greatly reduced. But soft contact between sole and ground will introduce new problem including more complicated gait optimization and control, which is beyond the scope of this thesis.

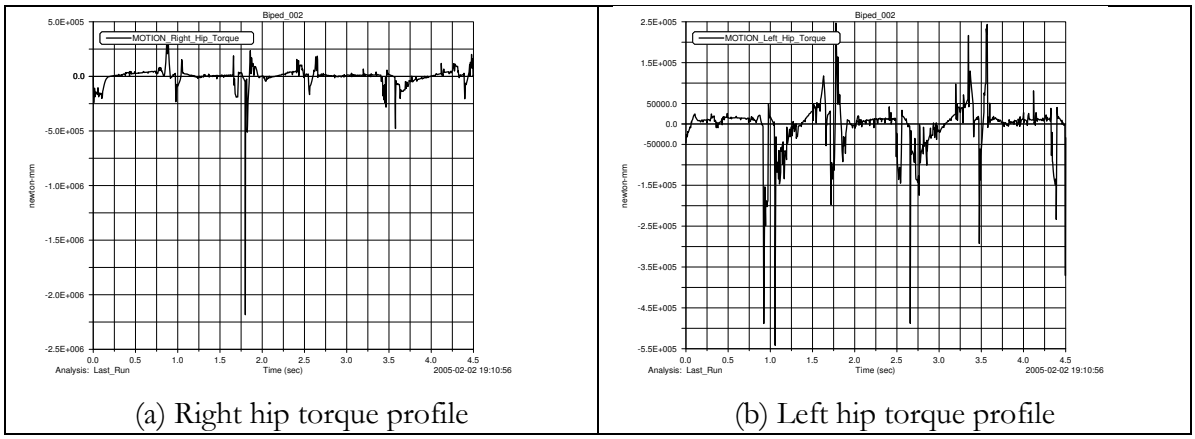

(a) Right hip torque profile (b) Left hip torque profile

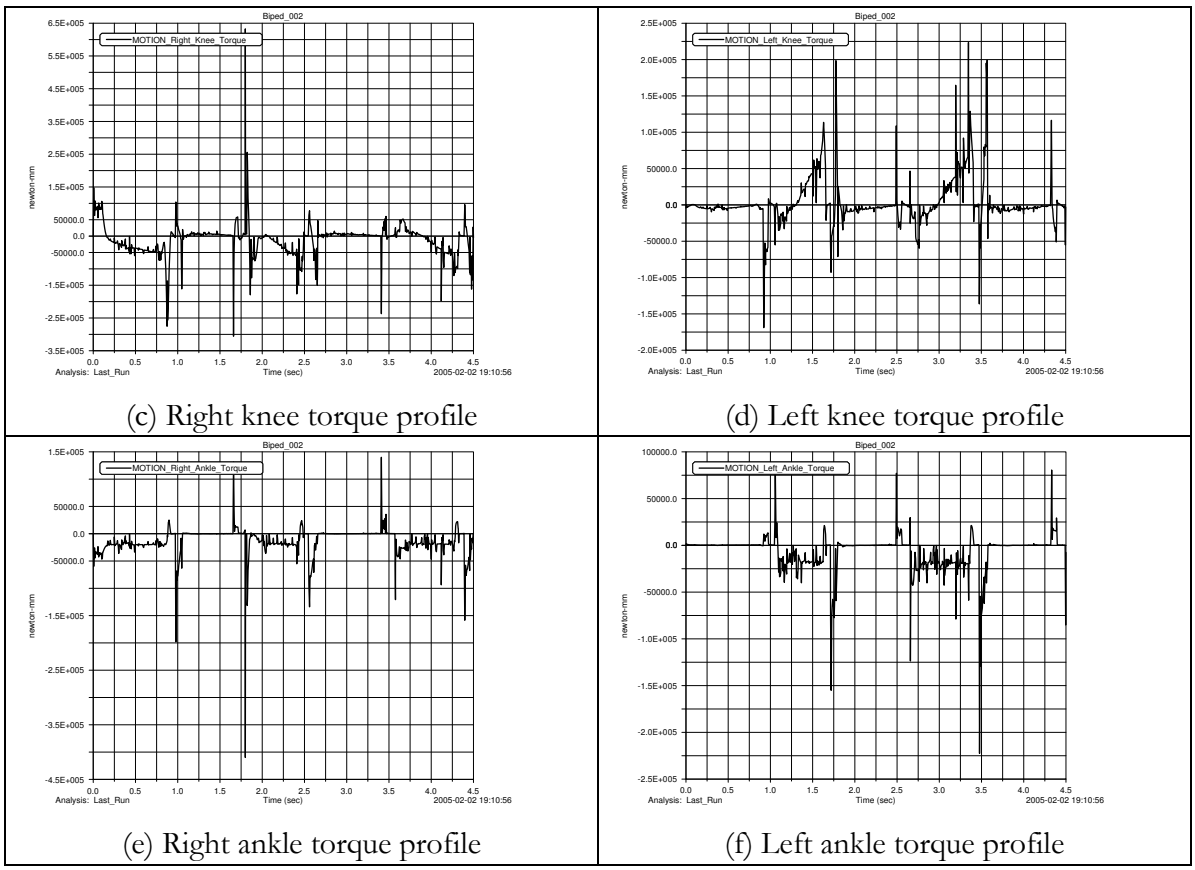

(c) Right knee torque profile

(d) Left knee torque profile

(e) Right ankle torque profile

(f) Left ankle torque profile

Figure 6.8 Torque Profile of SMD Biped Robot Joint

7 Conclusion

7.1 Thesis Summary

In this thesis, a single-motor-driven biped robot concept is prompted first. Two complementary actuation technologies to approach this goal are investigated. They are Single Motor Driven (SMD) and Elastic Actuation (EA).

First, a new design for modular robots (SMD modular robot) was demonstrated from an intuitive comparison between mechanical system and electrical system. The new modular robot benefits from much lighter modules due to the Single Motor Driven concept. The main element of an SMD modular robot is a mechanical drive capable of providing a variable bidirectional rotation speed from a constant unidirectional input rotation speed.

Second, the Elastic Actuation (EA) was introduced based on the fact that SMD mechanism can only transmit and distribute mechanical power but cannot modulate and therefore control the mechanical power. Elastic actuator is not new in the robot research field. However it is quite different from the so called term Elastic Actuation, which is the newly developed complementary actuation technology for SMD, rather than a special kind of actuator.

Then, by adding the EA feature into SMD mechanism, a new kind of actuation method was developed. It circumvents the inherent "back lash" problem but presents measurable and controllable torque and thus makes it suitable for torque/force control which is essential for biped robots always interacting with human being and environment. This combined actuation technology has no precedent in the world at the time this thesis was written. Therefore, as a pioneer research work, this thesis presented a physical prototype that has only one joint featured in both SMD and EA – Purposeful Elastic Joint (PEJ). The experiment results of PEJ verified the new actuation technology, as well as its unique control algorithm.

It's hard to term a one joint mechanism a "robot". However at current technological and engineering status, plus the financial problem, for a first trying PhD work, it's a big problem to design and fabricate a biped robot that has both SMD and EA feature built in. Instead of being entangled by the engineering chaos, this thesis builds an

SMD biped robot in ADAMS and presents its simulation mathematically and dynamically. The simulation results verified the idea of Single Motor Driven biped robot, and also reveal its energy efficient property.

Having completed this thesis, there is an encouraging potential to continue the research for the next stage which would be the design and fabrication of a real SMD biped robot prototype with every joint featured in EA. In this case, the performance of SMD biped walking can be evaluated in the face of more common tasks. To do this job, some steps have to be taken first. These steps are listed in the Future Work section after the Thesis Contribution section.

7.2 Thesis Contribution

7.2.1 Inspiration and Exploration

- Single Motor Driven Biped Robot Scheme

One energy source is ubiquitous in electrical domain, as well as in some mechanical system like automobile and lathe. However, no previous research has ever touched this issue in biped robot. By simple comparison of mechanical system and electrical system, we brought out the scheme of single-motor-driven biped robot.

- Combined Actuation Approach

Single Motor Driven (SMD) and Elastic Actuation (EA) are not brand new concept in robotics research; however, they are usually presented in different research and different application. No precedent research has ever combined them together, or discussed any relationship between them.

With the finding of "back lash" problem in SMD mechanism, we are inspired to avoid this problem by integrating EA feature into SMD. Fortunately, EA feature has more merits than just a remedy function to SMD. These merits include the feasibility of torque control and the property of shock tolerance, which in turn augment the safety level for biped robot.

- The Prototype and Experiments

This PhD work also presented a prototype to verify the research goal and approach. PEJ is a one-joint actuator that has both SMD and EA feature built in. Its prototype and mathematical model are developed. Local controller is developed and validated by several experiments:

The first experiment shows that the amplitude of the chattering depends on the PWM frequency for a constant input speed. The effects of different controller gains on the quality of the closed loop response are studied in the second experiment. In the third and fourth experiments, the investigation focus is on the effects of input speed and load on the closed loop response. All the experimental results match the models and theories well.

7.2.2 Improvements and Enhancements

- Improved Bidirectional Clutch - Bidirectional Clutch II

Normal clutch can produce two stages, ON and OFF, or 1 and 0 ratio of input motion. The bidirectional clutch however can produce additional ratio of -1. With different shaft arrangement, bidirectional clutch can be classified into two categories: coaxial bidirectional clutch and non-coaxial bidirectional clutch. Consider the transmission inside "bidirectional clutch". If it has compliant component like "belt" then it is termed as "compliant bidirectional clutch". If all the transmission are rigid (like gear mate) then it is termed as "rigid bidirectional clutch". It makes the main difference of Bidirectional Clutch I and Bidirectional Clutch II. The later is designed and used in the PEJ prototype.

- Improved SMD Mechanism

The first SMD mechanism cannot invert its motion direction as long as the constant input velocity keeps on. This is only because the unidirectional clutch (normal clutch) mechanism is adopted. With the unidirectional clutches build in its two perpendicular crossed shafts, the mechanism can have only two states of operations: on and off, thus the output motion of each joint can only be either the coupled direction of input, or zero-movement – with the engagement of brakes in the mechanism. To invert the motion, as surely needed by any robot, the constant input velocity must invert itself. To make the SMD mechanism really DOF-independent and dexterous, the unidirectional clutches are replaced by bidirectional clutches. This is the main feature of new SMD mechanism.

- Finding and Solving of the Back Lash Problem in SMD

The end-effector shaking and jerk of SMD arm has been noticed long time. We find that the main reason is the inherent back lash in the large gear train system. It seems improvement of SMD design and fabrication alone can not solve the problem.

To minimize the effects of back lash in SMD, this thesis proposed one solution from the outer side of SMD itself. Spring is a widely used device which can "translate" physic motion into force/torque variation. By using torsion spring with the gear mate,

uncontrollable back lash can be translated into controllable torque variation, and nonlinear contact force pulse can be converted to linear torque variation. The problem caused by back lash is avoided by adding the elastic feature with SMD. This is why the EA is termed "complementary" to SMD.

7.2.3 Other Contribution

Other important contributions of this thesis are:

- A presentation of a minimal model for elastic actuation that aids in understanding the fundamental principles of the new actuation method
- The development of linear model for PEJ
- Several unique feature of PEJ like the large bandwidth limits, small impedance, and impact/shock tolerance are described in detail
- Development of a control structure including local controllers and path planner suitable to manipulate and supervise the SMD mechanism
- Development of a design methodology for local controllers by developing a mathematical model for SMD mechanism and implementing this on the PEJ prototype
- Biped walking simulation in ADAMS which is more suitable for 3D dynamic robot walking simulation than other mathematical software like MATLAB/Simulink

7.3 Limitations, Recommendations and Future Works

Though the idea of single-motor-driven biped robot scheme sounds quite simple, the way to this goal has not been fully discovered. The combined actuation approach presented in this thesis is just a first try to the goal. There are still many topics that deserve further investigation. Here presents only those topics that relate to the understanding and design of SMD and EA for biped robot:

7.3.1 Topics in SMD Aspect

Generally, in order to design and build a modular robot, a standardized modular architecture must be developed. For this purpose, it is important to identify the basic mechanical elements of a robotic system. These are:

- Base unit for robot attachment

- Joints with one or more degrees of freedom
- Links with actuator and electronics enclosure capability
- End-effector for tool and payload handling

This list divides the robot into functional elements and may be used as a basis for module development. The basic approach then becomes the design of each of the modules in different scales that fit the biped robot application.

To add the SMD feature to the above modular robot, the following important design tasks would be considered:

- Mechanical drives with optimum dimension and gear ratio according to the required power distribution
- Energy tapping mechanism for connecting the central rotating shaft to the mechanical drives
- Optimum connecting mechanism between the modules to extend the central rotating shaft from one module to the next one

More future work also includes:

- Development of a general path planning and control strategy for the path planner
- Sophisticated SMD module design and prototype (with EA feature) for the new coming research problems.

7.3.2 Topics in EA Aspect

- Strategy of Combination

This thesis has presented two complementary actuation technologies for biped robot, but does not explain how to use them in different joint of biped robot. For example, at low torque and position requirements situation (like the ankle joint in swing phrase) it may be that a simple drive mechanism, with no elasticity, can complete the task. Using simple feed-forward current control may be sufficient for that case. When the torque and position requirements increase to a certain precision level, a combined mechanism is required.

- Investigation of Springs

Springs are at the core of the elastic actuation. This thesis focused attention only on linear springs. However, in order to more fully understand the actuation method, the springs themselves need to be investigated. Spring hysteresis, materials, nonlinear

stiffening springs, space constraints, geometry and life cycle are all important. Here is the brief discussion on the first two.

Hysteresis and Materials – Most physical springs have some hysteresis. The die compression springs used in this thesis have very little hysteresis and were assumed to be linear in the control. It is suspected that with increased spring hysteresis, the EA mechanism becomes more difficult to control. For example rubber springs are often used for vibration isolation because of inherent hysteresis and damping properties. Air springs are often used for high force applications. However, they too have thermodynamic hysteresis properties. Quantifying the effects of hysteresis would be an important step to use new materials and springs in the EA design.

Non-linear Stiffening Springs – Biological springs (tendons) are stiffening. One theory behind this is that at low torques or during contact tasks the low stiffness helps maintain stability. At much higher torques, low stiffness is unnecessary and may be even undesirable.

Some initial theoretical and experimental work has been done previously in applying non-linear stiffening springs to the actuators in fixed base robots [177] [178] [179]. In this thesis, it is shown that there is a fundamental trade off between large torque bandwidth and impedance when choosing spring stiffness. Low impedance requires a soft spring whereas a soft spring reduces the large torque bandwidth. Using a non-linear stiffening spring may be a bridge between these requirements.

Stable control of EA with non-linear springs may be as simple as using a scheduling control gain that is a function of spring deflection. As the spring stiffness increases, the control gain decreases proportionally. This keeps the loop gain of the system constant and within stability margins.

- Control System Design

This thesis focused attention on simplicity of control system design. P, PI and PD controller operating on the torque error signal adequately demonstrated the properties of the prototype.

There exist many other more complex control systems that could incrementally enhance EA performance. Proper use of state feedback could eliminate the zeros in the closed-loop system. The use of feed-forward could help further eliminate internal errors such as stiction. Adaptive control could be used to better understand load conditions and accommodate for load variations. New experiments and simulation with new controllers are also necessary.

7.3.3 Other SMD Solution

The bevel gear train formed SMD mechanism presented in this thesis is not the only solution to "Single Motor Driven" requirement. Instead of gear train, some kind of flexible shaft can be used to transmit/relay input motion. This will lead to other kind of SMD mechanism which is totally different from that presented in this thesis.

At the end of the thesis we are able to answer the question prompted in Chapter 1 – It is not only possible, but also promising, to power a biped robot with only one EM motor.

7.3.4 SMD Mechanism Outlook

The SMD mechanism in small DOF system such as biped robot, which normally has 6 DOFs in leg, has limited advantage of total weight saving. However when the number of DOF increases, the property of weight saving will be prominent. This situation includes the robotic arms used in space station, airplane refueling in the sky, ship/plant inspection and so on… All these applications require large number of DOFs/joints. For example, Canadarm2 [Figure 7.1 (a)] has 7 motorized joints. The "dexterous hand" mounted on this arm has 15 more DOFs. Even it's mainly build up with carbon fiber tube and aluminum interfaces, its total weight reaches 1640 kg. The European Robotic Arm [Figure 7.1 (b)], benefited from its relatively small size, still weights 630 kg.

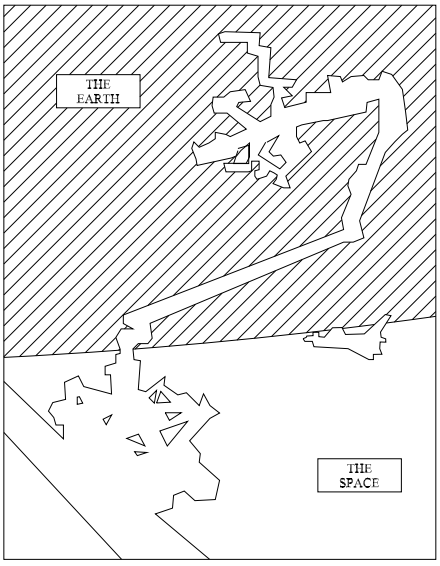

a) Canadarm2

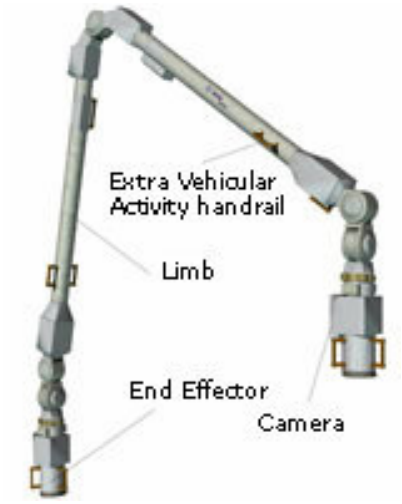

b) European Robotic Arm

Figure 7.1 Example of Robotic Arm in Space

Appendix A – Singular Perturbations

While the perturbation method applies to state equations that depend smoothly on a small parameter ε (the reader is referred to [180] for further detail on perturbation methods), the singular perturbation problem is characterized by discontinuous dependence of system properties on the perturbation parameter ε. In this appendix the so-called standard singular perturbation is introduced with the model give by

$$\dot{x} = f(t, x, z, \varepsilon) \tag{A.1}$$

$$\varepsilon\dot{z} = g(t, x, z, \varepsilon) \tag{A.2}$$

where setting ε=0 causes a fundamental and abrupt change in the dynamic properties of the system, as the differential equation $\varepsilon\dot{z} = g$ degenerates into the algebraic or transcendental equation

$$0 = g(t, x, z, 0) \tag{A.3}$$

The essence of the theory developed in the literature for dealing with the singular perturbation problem is that the discontinuity of solutions caused by singular perturbations can be avoided if analyzed in separated time scales. This multi-time scale approach is a fundamental characteristic of the singular perturbation method [180].

- The Standard Singular Perturbation Model

The singular perturbation model (A.1)-(A.2) of a dynamic system is a state model where the derivatives of some of the states are multiplied by a small positive parameter ε. It is assumed that the function f and g are continuously differentiable in their arguments for

$$(t, x, z, \varepsilon) \in [0, t_1] \times D_x \times D_z \times [0, \varepsilon] \tag{A.4}$$

where $D_x \in R^n$ and $D_z \in R^m$ are open connected sets. When set ε=0 in (A.1) and (A.2), the dimension of the state equation reduces from (n+m) to n because the differential Equation (A.2) degenerates into Equation (A.3). The model (A.1)-(A.2) is in standard form if (A.3) has $k \geq 1$ isolated real roots

$$z = h_i(t, x) \quad i = 1, 2, \ldots, k \tag{A.5}$$

for each $(t,\ x) \in [0,\ t_1] \times D_x$. This assumption ensures that a well-defined n-dimensional reduced model will correspond to each root of (A.3). Substituting (A.5) into (A.1), the ith reduced model is obtained at ε=0 as

$$\dot{x} = f(t, x, h(t, x), 0) \tag{A.6}$$

This model is sometimes called a quasi-steady-state model, because z, whose velocity $\dot{z} = g/\varepsilon$ can be large when ε is small and $g \neq 0$, may rapidly converge to a root of (A.3), which is the equilibrium of (A.2). The model (A.6) is also known as the slow model. The two-time-scale property of (A.1)-(A.2) will be discussed further in this appendix.

Modeling a physical system in the singularly perturbed form may not be easy. It is not always clear how to pick the parameters to be considered as small. Fortunately, I many applications, people's knowledge of physical processes and components of the system set them on the right track. Two different typical ways of choosing parameter ε are discussed here.

One way is that ε be chosen as a small time constant. This is the most popular source of singularly perturbed models and, historically, the case that motivated interest in singular perturbations. Small time constants, masses, capacitances, and similar parasitic parameters that increase the order of a model are quite common in physical systems. In the interest of model simplification, these parasitic parameters are usually neglected to reduce the order of the model. Singular perturbations legitimize this ad hoc model simplification and provide tools for improving oversimplified models. Another way is that the parameter ε be chosen as the reciprocal of a high-gain parameter in a feedback system. The use of high-gain parameters or more precisely, parameters that are driven asymptotically toward infinity, in the design of feedback systems is quire common. A typical approach to the analysis and design of high-gain feedback systems is to model them in the singularly perturbed form. The following example illustrates this important source of singularly perturbed models.

Consider the feedback control system of Figure A.1. The inner loop represents an actuator control with high-gain feedback. The high-gain parameter is the integrator constant k_1. The plant is a single-input-single-output nth-order system represented by the state-space model $\{A, B, C\}$. $\psi(\cdot)$ is a first and third-quadrant nonlinearity which satisfies

$$\psi(0) = 0 \quad and \quad y\psi(y) > 0, \quad \forall y \neq 0 \tag{A.7}$$

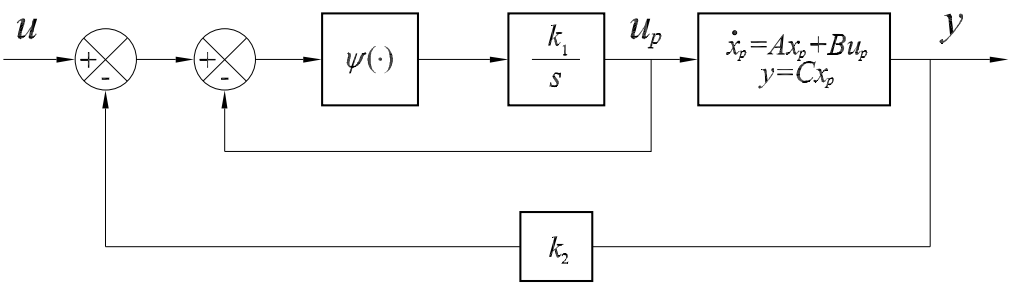

Figure A.1 Actuator Control with High-gain Feedback

The state equation for the closed-loop system is

$$\dot{x}_p = Ax_p + Bu_p \tag{A.8}$$
$$\frac{1}{k} = \dot{u}_p = \psi(u - u_p - k_2 C x_p)$$

With $\varepsilon=1/k_1$, $x_p=x$, and $u_p=z$, the model takes the form (A.1) and (A.2). Setting $\varepsilon=0$, or equivalently $k_1=\infty$, the following solved

$$\psi(u - u_p - k_2 C x_p) = 0 \tag{A.9}$$

to obtain

$$u_p = u - k_2 C x_p \tag{A.10}$$

which is the unique root since $\psi(\cdot)$ vanishes only at its origin. The resulting reduced model is

$$\dot{x}_p = (A + Bk_2 C)x_p + Bu \tag{A.11}$$

The block diagram of this model is shown in Figure A.2, where the whole inner loop of Figure A.1 is replaced by a direct connection (unit gain).

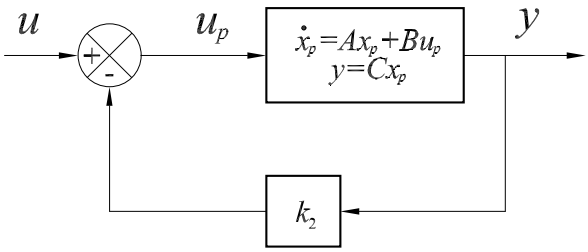

Figure A.2 Simplified Block Diagram of Figure A.1

➢ Time-scale Properties of the Standard Model

Singular perturbations cause a multi-time scale behavior of dynamic systems characterized by the presence of slow and fast transients in the system's response to external stimuli. Loosely speaking, the slow response is approximated by the reduced model (A.6), while the discrepancy between the response of the reduced model and that of the full model (A.1)-(A.2) is the fast transient. The time-scale decomposition mentioned above is used to analyze the stability of equilibrium via Lyapunov's method [180].

Appendix B – BOM of PEJ

Suppliers			Parts		Part Number	Quantity
Company	Sales	Contact No.	Name	Brand		
Isatech	Karen	67478946	Clutch	PIC	RW1-333	3
Tripod Trading Pte. Ltd.		62950933	Gear	KG Stock Gear	S75SU 32B +0606	3
					S75SU 64B +0606	2
					S75SU 16B +0805	1
Associated Spring Raymond	Stephanie Seah	68635635	Spring		T025-270-218	1
Misumi Corporation	Lilian Lim	67337211	Bearing		BGHK 606ZZ 25	2
					BGCN 606ZZ	10
			Shaft		PSSFGW 6 59 M3 N3 WSC0 X17	2
					PSSFGW 6 81 M3 N3 WSC26 X13	2
					PSSFGW 6 89 M3 N3 WSC21 X26	1
					PSSFGW 6 71 M3 N3 SC57	1
			Screw		CB 2 - 5	8 10
					CB 2 - 8	20 25
					CB 3 - 5	10 15
					CB 4 - 6	5 10
					CB 5 - 12	24 30
					CB 5 - 20	4 10
					SCBS 3 - 8	6 10
			Washer		WSSB 10 - 4 - 2	5 10
Servo Dynamics	Irenaeus	97836641	DC Motor	Maxon		1
			Gear	Maxon		1
			Encoder	Maxon		1
			Motor Control	Maxon		1

Appendix C – Drawings of PEJ

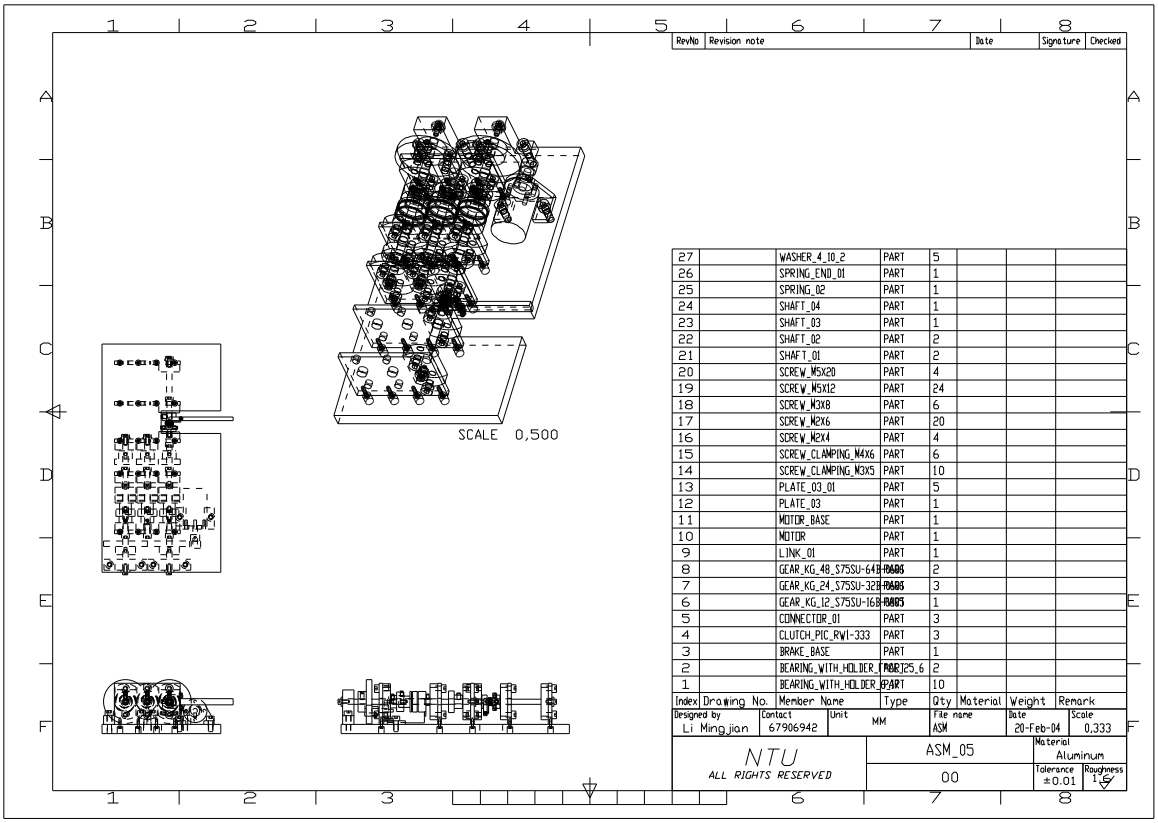

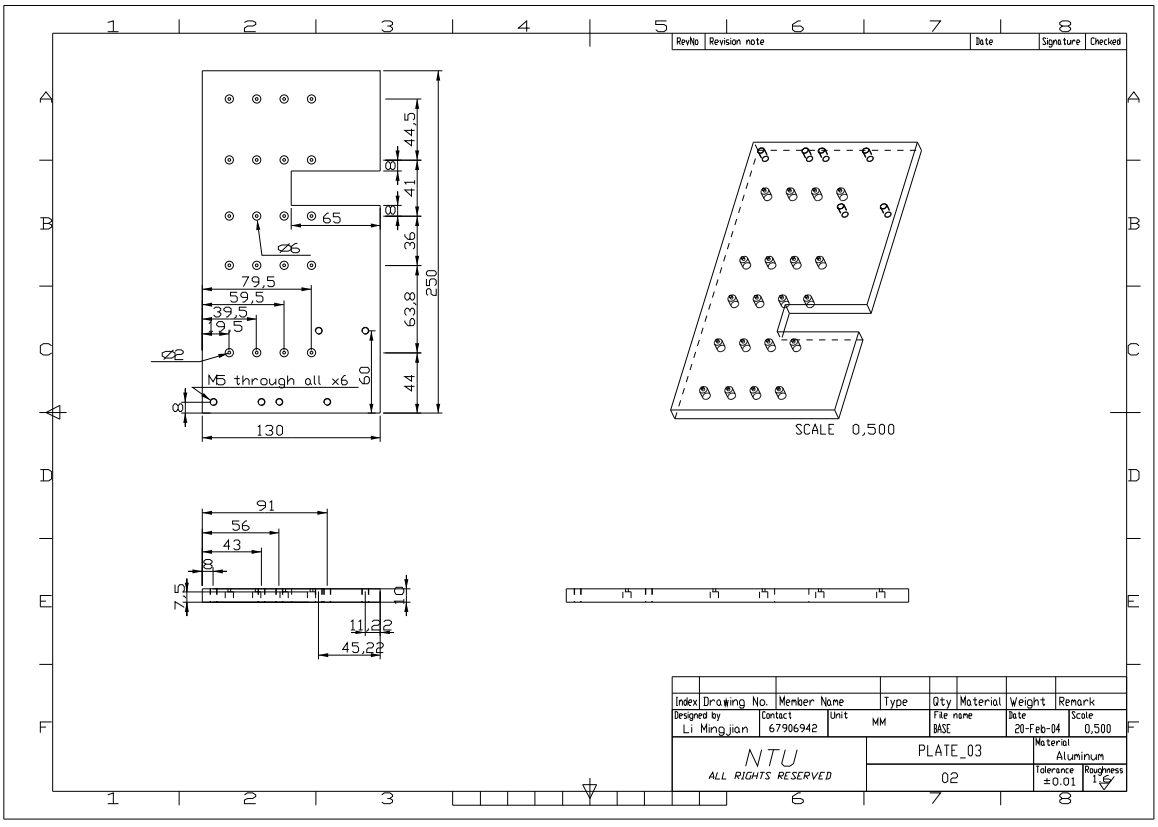

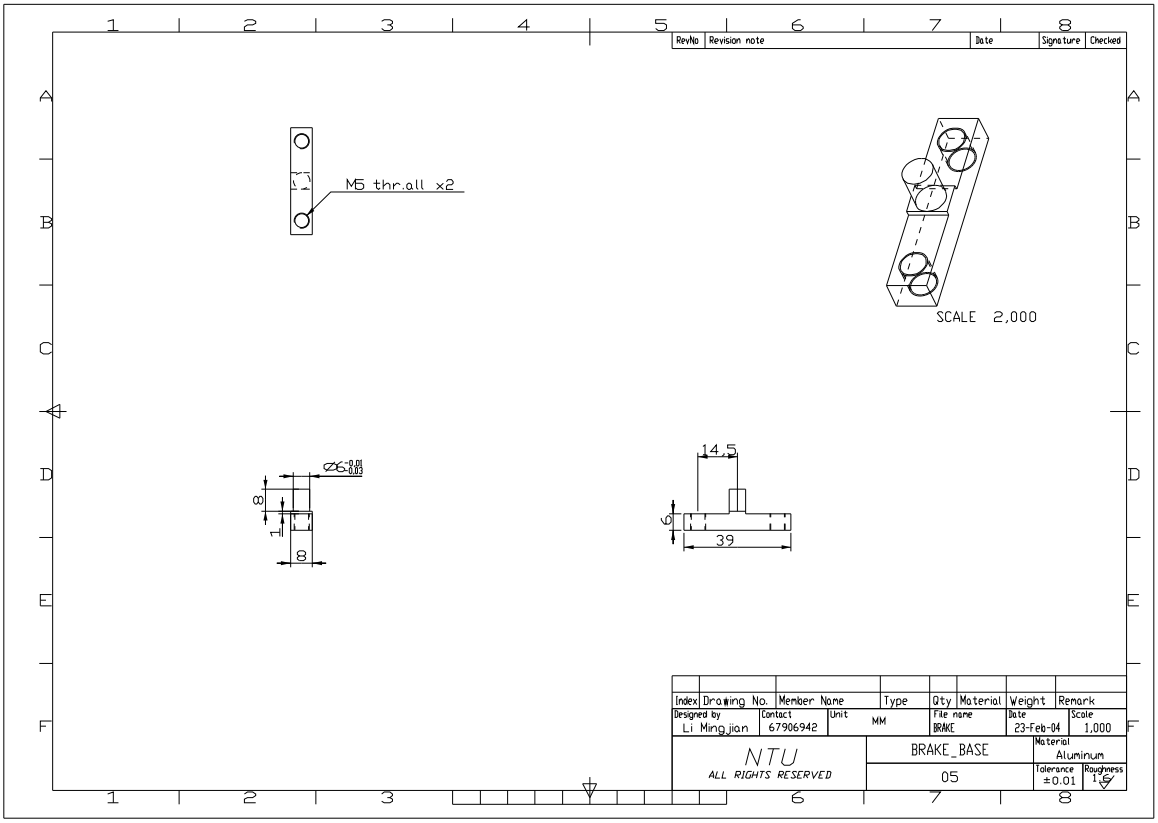

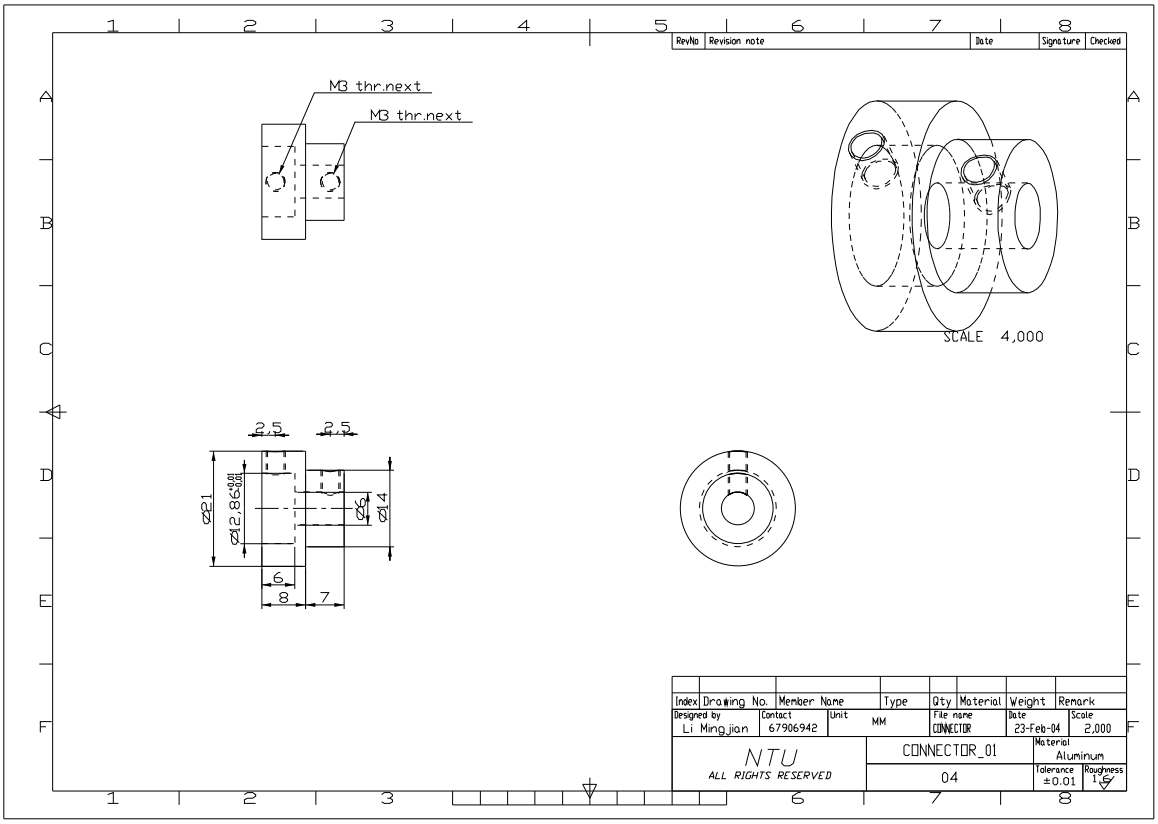

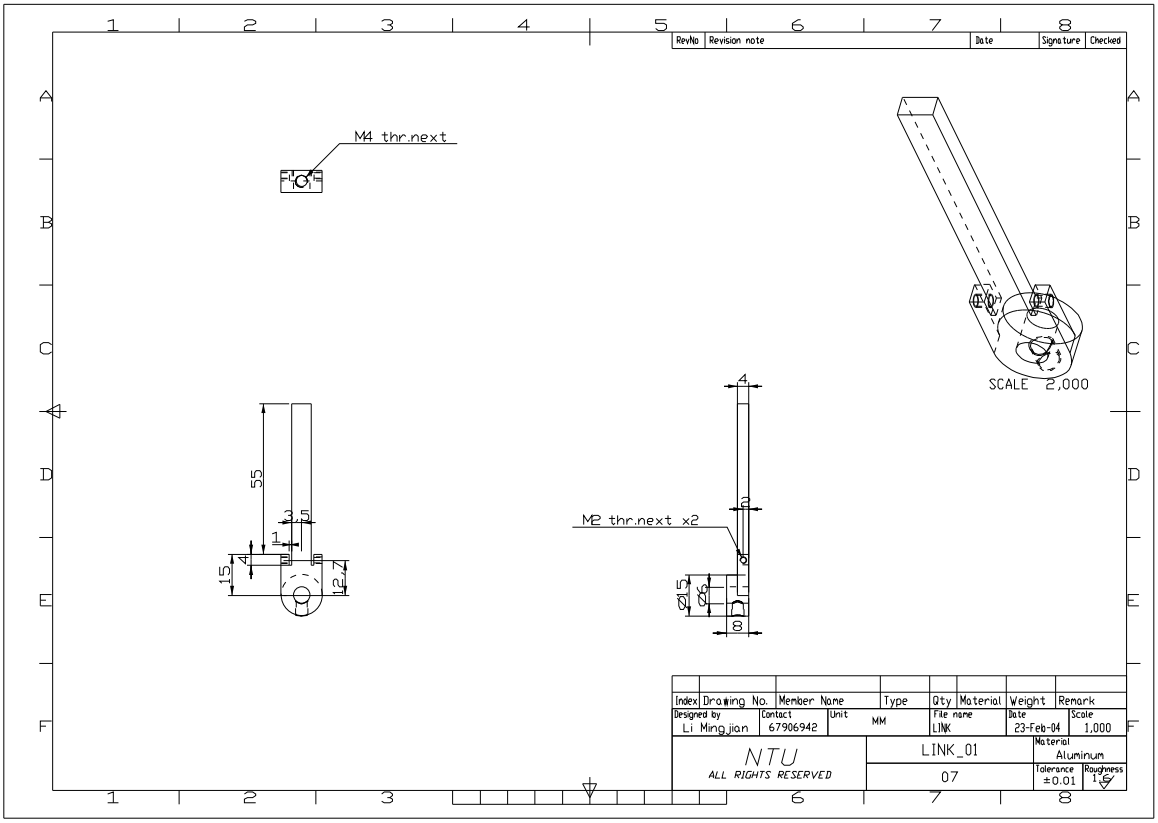

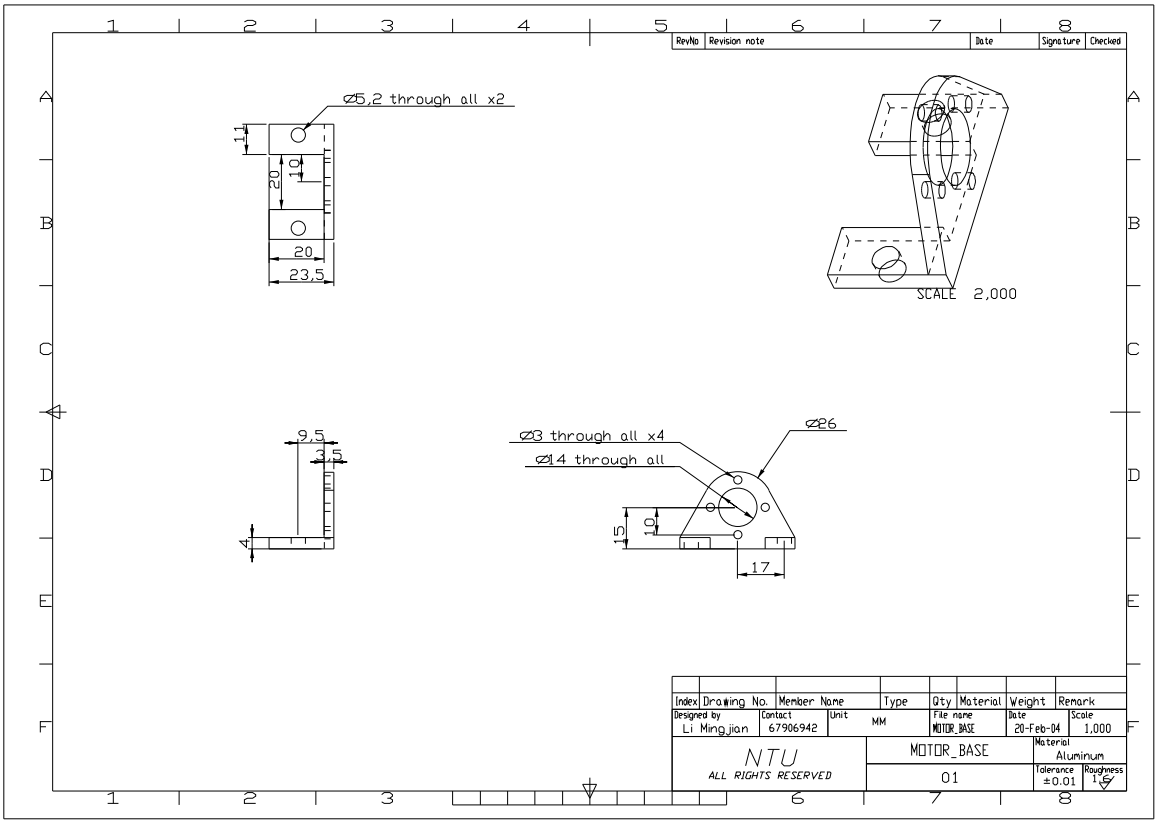

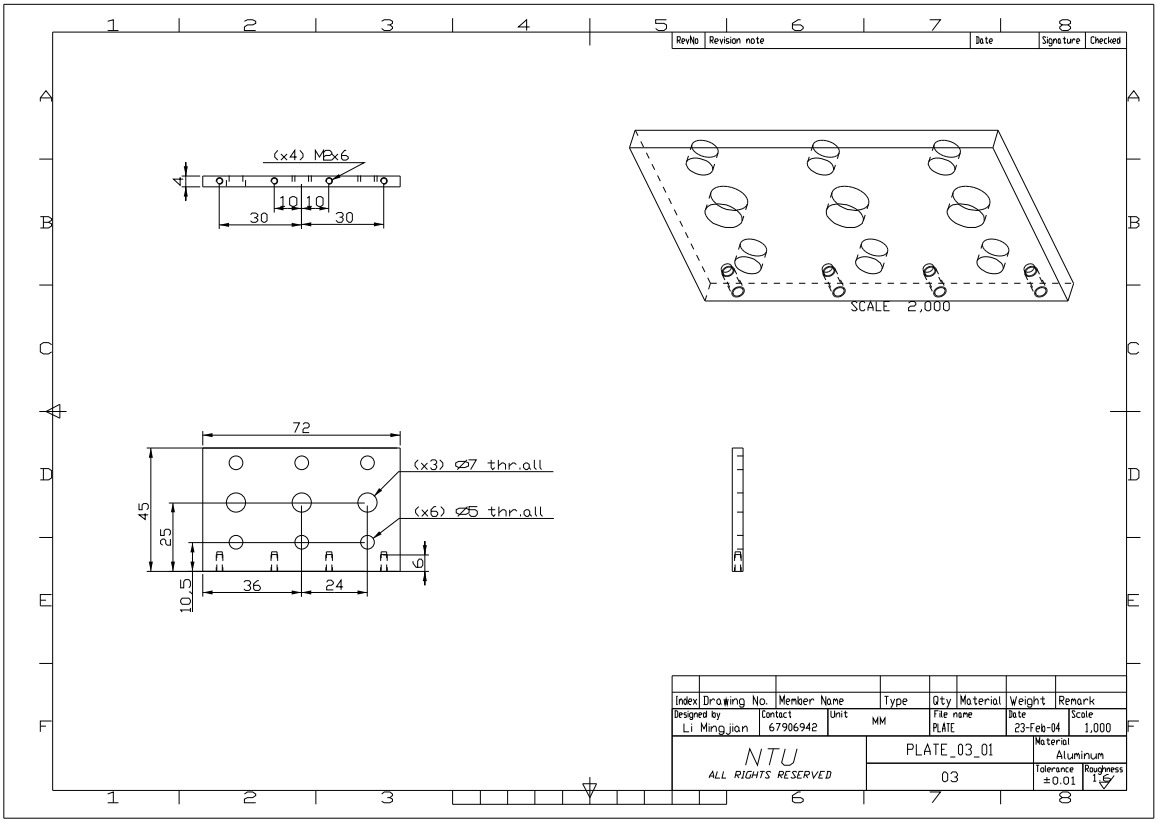

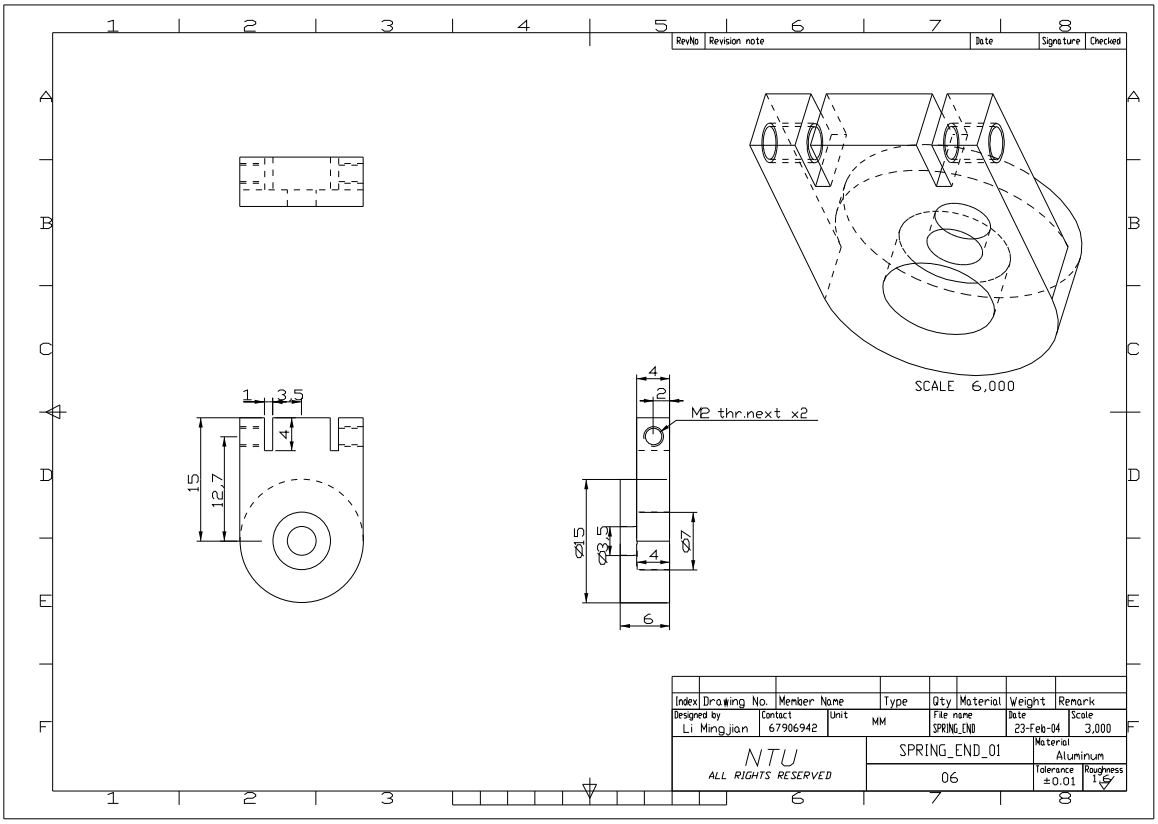

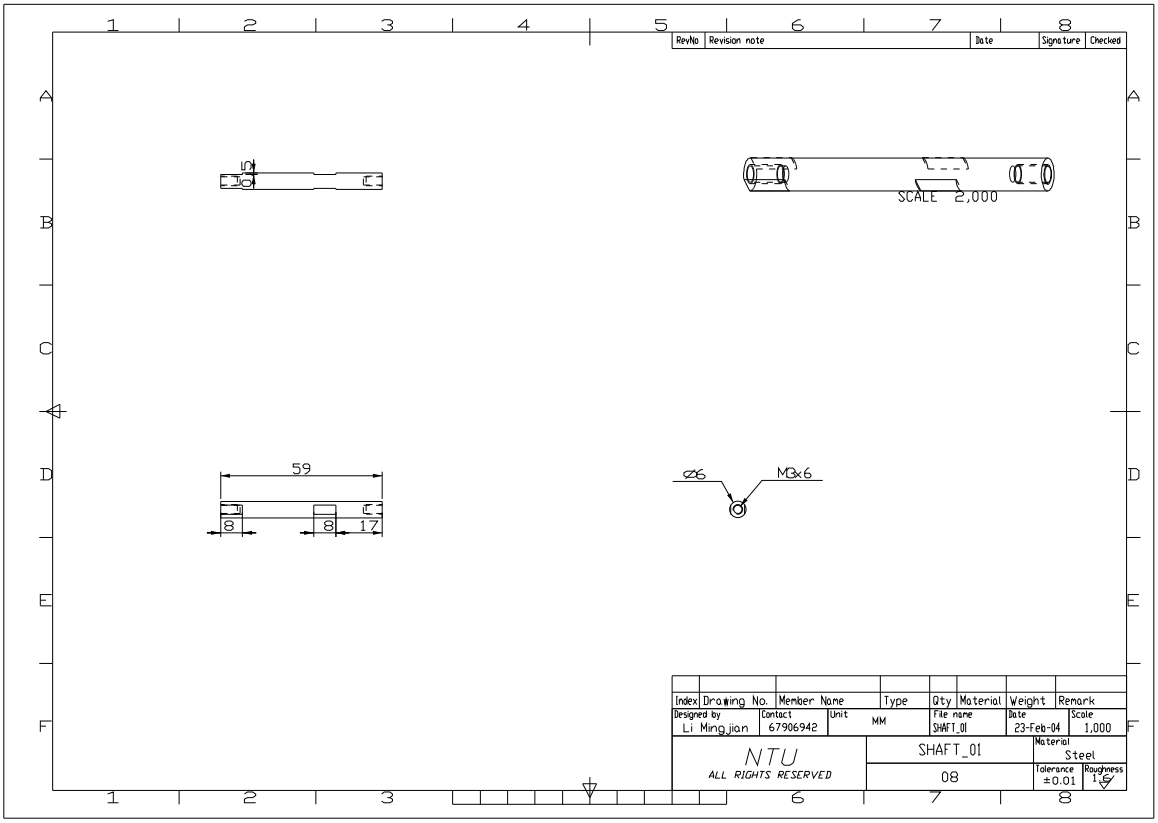

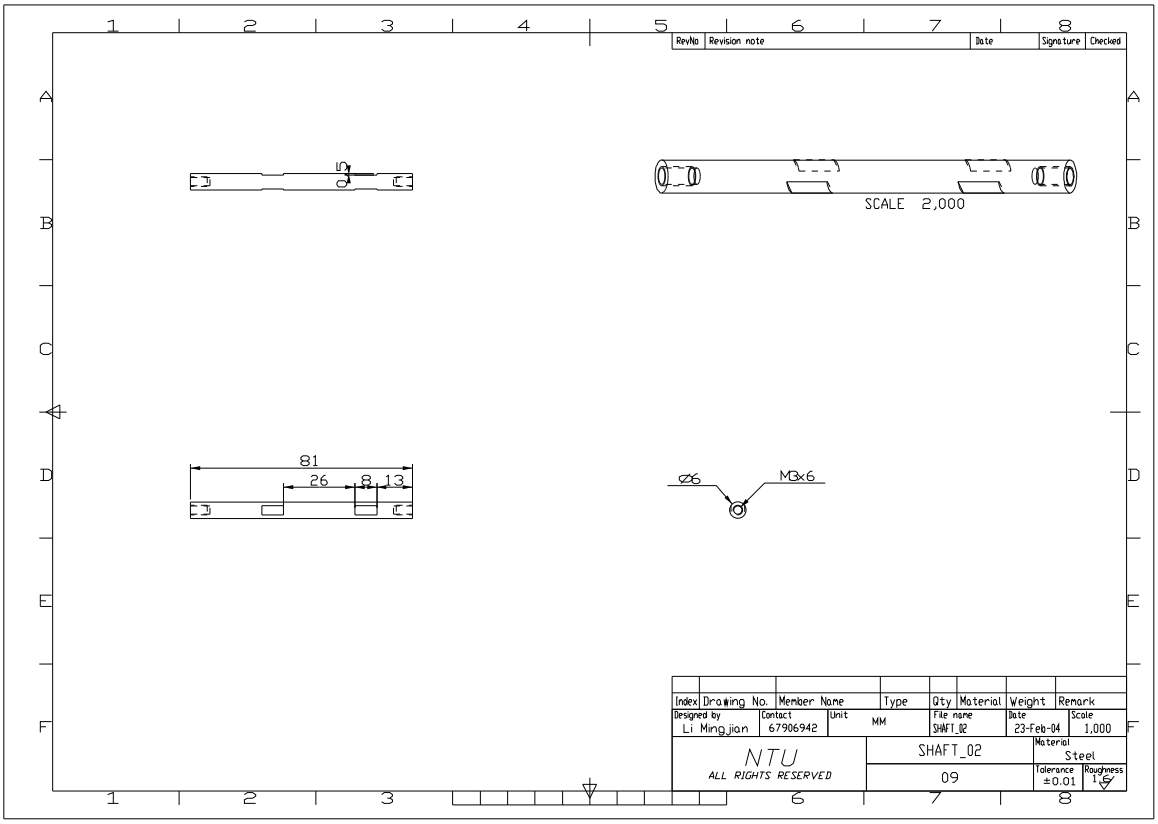

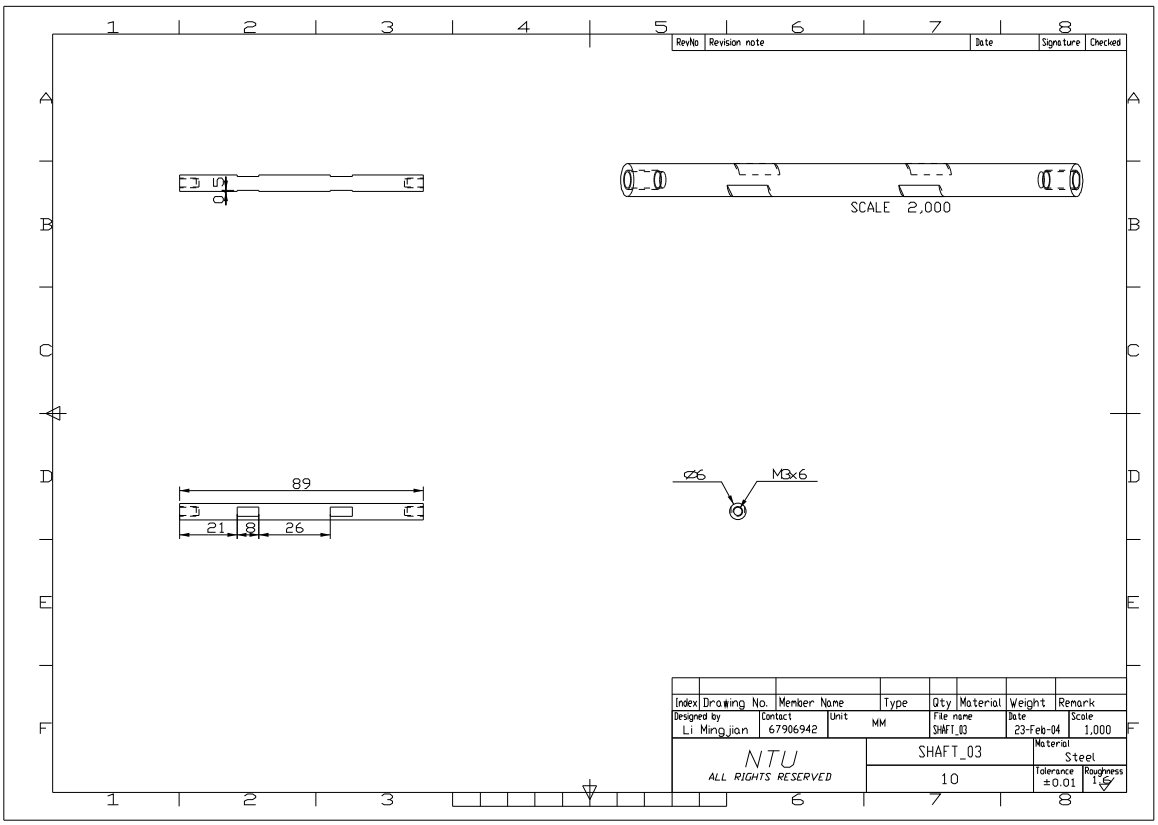

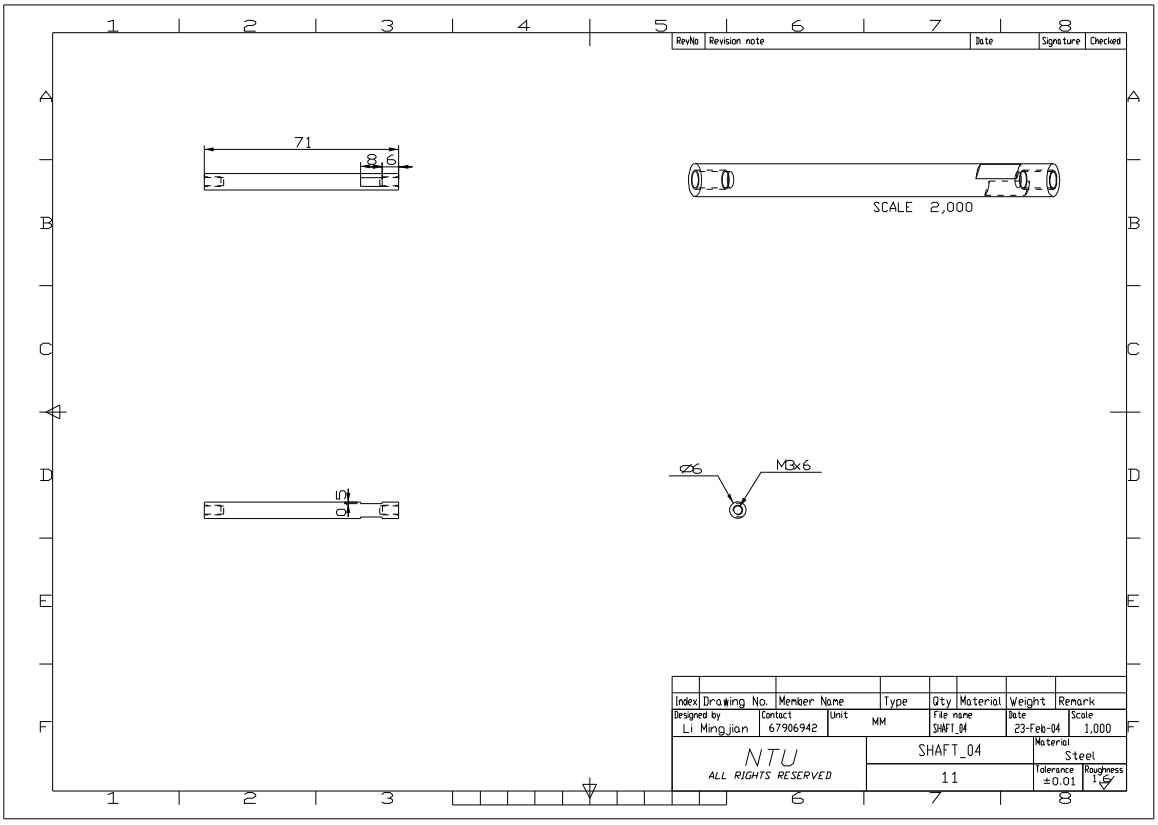

Appendix D – Torsion Spring

➢ Selecting a Torsion Spring

First, determine the torque the spring will be expected to develop. The torque (or moment) is simply the applied force (pounds) pushing perpendicularly on a leg or leg extension times its distance (inches) to the centerline of the spring body. A typical example is depicted below:

$$TORQUE = LOAD \times L$$

Next, determine the angular deflection (degree of motion) through which the spring leg is required to rotate. Divide the torque by this angle to obtain the spring constant (rate) required:

$$Rate = \frac{Torque}{Degrees} \quad \left(\frac{In.-Lbs.}{Deg.} \right)$$

Or, if the torque required to rotate the spring through a given angle is required:

$$Torque = Rate \times Degrees$$

Next, scan down the inventory's "Rate" column or a spring with an acceptable rate. When found, observe the spring's "Inside Diameter" (*I.D.*) and "Body Width" (Length) columns for size compatibility with the application.

The "Suggested Maximum Deflection" column reflects limits (degree) that should produce a long service life with average cycling. These values can be increased by as much as 20% for static (non-oscillatory) applications. Near-infinite service life can be possible using values of about 35% of those listed.

The initial unloaded relative-leg-angle orientation is determined by the number of coil in the spring body.

If it takes the right hand and index finer to simulate the spring's end view then it would be a right-hand wound spring.

The body (solid) lengthening due to deflection increases approximately by one wire diameter for each complete leg revolution (360 degrees).

The body Inside Diameter (*I.D.*) decreases according to

$$I.D. = \frac{N}{N + REVs} \times I.D.(unloaded)$$

where *N* is the number of coils and *REVs* is the number of leg revolutions.

Once the inside diameter of the load-contracted spring body is determined, the supporting mandrel's maximum diameter is usually set to about 90% of this value.

➢ Design Information

The spring rate and stress for helical, round-wire torsion springs can be calculated from:

$$R = \frac{PL}{\theta} = \frac{Ed^4}{3888DN} \qquad S = \frac{32PLK}{\pi d^3}$$

where:

P =Load, lb.

L =Moment arm, inches

θ =Angle of deflection, degrees

E =30×10^6, (28×10^6 for stainless) Young's Modulus

d =Wire diameter, inches

D =Body mean diameter (O.D.-d), inches

$O.D.$ =Outside diameter, inches

N =Number of coils

K =Stress correction factor (can be found in product catalogue)

R =Rate (Constant), In.-Lbs./deg.

S =Stress (in bending), p.s.i.

Bending deflection of long legs under load must be considered for some applications and added to the total angular deflections. The uncorrected stress can be used for static applications. The suggested maximum-allowable-stress value (S) for a torsion spring is considered to be 75% of the material's minimum tensile strength (MTS). MTS values are a function of the wire diameter and can be found in catalog.

Bibliography

[1] K. Hirai, M. Hirose, Y. Haikawa, and T. Takenaka, "The development of the honda humanoid robot", *The 1998 IEEE International Conference on Robotics and Automation*, 1998.

[2] I. Kato and H. Tsuiki, "The hydraulically powered biped walking machine with a high carrying capacity", *The Fourth Symposium on External Extremities*, Dubrovnik, Yugoslav, 1972.

[3] M. Vukobratovic and D. Juricic, "Contribution to the synthesis of biped gait", *IEEE Transaction on Bio-Medical Engineering*, vol. 16, pp. 1-6, 1969.

[4] M. Vukobratovic, Yu. Stepanenko, "On the Stability of Anthropomorphic Systems", *Mathematical Biosciences*, vol. 15, pp 1-37, 1972.

[5] A. Goswami, "Postural stability of biped robots and the foot rotation indicator (FRI) point", *International Journal of Robotics Research*, vol. 18, pp. 523-533, 1999.

[6] J. Furusho and M. Masubuchi, "Control of a dynamical biped locomotion system for steady walking", *Journal of Dynamic Systems, Measurements, and Control*, vol. 108, pp. 111-118, 1986.

[7] M.-Y. Cheng and C.-S. Lin, "Genetic algorithm for control design of biped locomotion", *The IEEE International Conference on Robotics and Automation*, 1995.

[8] J. Pettersson, H. Sandholt, and M. Wahde, "A flexible evolutionary method for the generation and implementation of behaviors in humanoid robots", *The IEEE-RAS International Conference on Humanoid Robots*, 2001.

[9] P.C. Breedveld, “Fundamentals of Bond Graphs”, *IMACS Annal of Computing and Applied Mathematics*, Vol. 3: Modelling and Simulation of Systems, Basel, 1989, pp. 7-14.

[10] P.B.T. Weustink, T.J.A. de Vries, and P.C. Breedveld, “Object Oriented Modelling and Simulation of Mechatronic Systems with 20-sim 3.0”, J. Adolfson, J. Karlsen, editors, *Mechatronics 98*, Elsevier Science Limited, 1998.

[11] S. Tosunoglu, “Fault Tolerance for Modular Robots”, *Proceedings of the 1993 International Conference fo the IEEE Industrial Electronics Society and SICE of Japan on Industrial Electronics, Control and Instrumentation – IECON’93*, Lahaina, Maui, Hawaii, Vol. 3, pp. 1910-1914, November 15-19, 1993.

[12] K.H. Wurst, “The Conception and Construction of a Modular Robot System”, *Proc. Of 16th ISIR*, pp. 37-44, Brussels, 1986.

[13] D. Schmitz, P. Khosla, and T. Kanade, *The CMU Reconfigurable Module Manipulator System*, Technical Report, Carnegie-Mellon University, CMU-RI-TR-88-7, 1988.

[14] T. Matsumaru, “Design and Control of the Modular Robot System: TOMMS”, *IEEE International Conference on Robotics & Automation*, 21-27 May 1995.

[15] M. Sack, N. Elkmann, T. Felsch, and T. Bohme, "Intelligent Control of Modular Kinematics – The Robot Platform SIRIUS", *IEEE International Symposium on Intelligent Control*, Vancouver, Canada, October 27-30, 2002.

[16] R. Cohen, M.G. Lipton, M.Q. Dai, and B. Benhabib, "Conceptual Design of a Modular Robot", *ASME Journal of Mechanical Design*, Vol. 114, pp. 117-125, 1992.

[17] R. Bryngelson and S. Tosunoglu, "On The Design of A Seven-Axis Modular Robot", *20th International Conference on Industrial Electronics, Control and Instrumentation*, 5-9 Sept. 1994.

[18] B. Gombert, G. Hirzinger, G. Plank, and M. Schedl, "Modular Concept for a New Generation of Light Weight Robots", *20th International Conference on Industrial Electronics, Control and Instrumentation*, Vol. 3, 5-9 Sept. 1994.

[19] G. Hirzinger, A. Albu-Schaffer, M. Hahnle, I. Chaefer, and N. Sporer, "On a New Generation of Torque Controlled Light-Weight Robots", *IEEE International Conference on Robotics and Automation*, Vol. 4, 21-26 May 2001.

[20] G. Hirzinger, N. Sporer, A. Albu-Schaffer, M. Hahnle, R. Krenn, A. Pascucci, and M. Schedl, "DLR's Torque-Controlled Light Weight Robot III – Are We Reaching The Technological Limits Now?", *IEEE International Conference on Robotics and Automation*, Vol. 2, 11-15 May 2002.

[21] M. Xie, *Fundamentals of Robotics*, World Scientific 2003.

[22] J. M. Hollerbach, "A comparative analysis of actuator technologies for robotics", *Robotics Review*, pages 298-342, 1991.

[23] H. Inoue, "Whither Robotics: Key Issues, Approaches and Applications", *IROS'96*, pp.9-14, Osaka, Japan, Nov. 1996.

[24] R. Brooks, "Behaviour Based Humanoid Robotics", *IROS'96*, pp.1-8, Osaka, Japan, Nov. 1996.

[25] Darwin G. Caldwell, N. Tsagarakis, D. Badihi, and G. A. Medrano-Cerda, "Pneumatic Muscle Actuator Technology a light weight power system for a Humanoid Robot", *Proceedings of the 1998 IEEE International Conference on Robotics & Automation*, Leuven, Belgium, May 1998.

[26] K. Hirai, "The Honda Humanoid Robot", Plenary Presentation, *IROS'97*, Grenoble, France, 1997.

[27] M. Inaba, T. Igarashi, S. Kagami, and H. Inoue, "A 35 DOF Humanoid that can Co-ordinate Arms and Legs in Standing up, reaching and Grasping and Objects", *IROS'96*, 23-28, Osaka, Japan, 1995.

[28] S. C. Jacobsen, B. K. Iverson, D. F. Knutti, R. T. Johnson, and K. B. Biggers, "Design of the Utah/MIT Hand", *IEEE International Conference on Robotics And Automation*, pp.1520-1532, San Francisco, 1986.

[29] D. G. Caldwell, G. A. Medrano-Cerda, and M. J. Goodwin, "Control of Pneumatic Muscle Actuators", *IEEE Control Systems Journal*, Vol.15, no.1, pp.40-48, Feb. 1995.

[30] R. A. Schulte, "The Characteristics of the McKibben Artificial Muscle", *In the Application of External Power in Prosthetics and Orthetics*, Publ. 874, Nas-RC, pp.94-115, 1962.

[31] M. Inaba *et al*., "Vision-based Adaptive and Interactive Behaviors in Mechanical Animals using the remote Brained Approach", *Robotics and Autonomous Systems*, Vol.17, p.35-52, 1996.

[32] M. Minsky, M. Ouh-young, O. Steele, F. P. Brooks and M. Behensky, "Feeling and Seeing: Issues in Force Display", *Computer Graphics*, Vol.24, no.2, pp.235-243, 1990.

[33] K. Pimentel and K. Teixeira, *Virtual Reality through the new looking glass*, Intel/McGraw-Hill, New York, 1992.

[34] R. Holmberg, S. Dickert, and O. Khatib, "A New Actuation System for High-Performance Torque-Controlled Manipulators", *Proceedings of the Ninth CISM-IFToMM Symposium on the Theory and Practice of Robots and Manipulators*, pp. 285-292, Udine, Italy, Sept 1992.

[35] H. Asada and J. J. Slotine, *Robot Analysis and Control*, John Wiley and Sons, New York, 1985.

[36] H. Paynter, *Analysis and Design of Engineering Systems*, MIT Press, Cambridge, MA, 1960.

[37] S. Eppinger, *Modeling Robot Dynamic Performance for Endpoint Force Control*, PhD thesis, Massachusetts Institute of Technology, Mechanical Engineering, 1998.

[38] M. Hirose *et al*., *Legged mobile robot and a system for controlling the same*, United States Patent, (#5,455497), Issued October 3, 1995.

[39] K. Hirai, M. Hirose, Y. Haikawa, and T. Takenaka, *The Development of Honda Humanoid Robot*, International Conference on Robotics and Automation, 1998.

[40] R. Alexander, *Elastic Mechanisms in Animal Movement*, Cambridge University Press, 1988.

[41] S. Drake, *Using compliance in lieu of sensory feedback for automatic assembly*, PhD thesis, Massachusetts Institute of Technology, Mechanical Engineering 1978.

[42] M. Mason, "Compliant motion", *Robot Motion: Planning and Control*, pages 305-322, MIT Press, 1982.

[43] D. E. Whitney, "Historical Perspective and State of the Art in Robot Force Control", *International Journal of Robotics Research*, 6(1), 1987.

[44] K. Salisbury, "Active Stiffness Control of a Manipulator in Cartesian Coordinates", *19th IEEE Conference on Decision and Control*, pages 83-88, Dec. 1980.

[45] N. Hogan, "Impedance control: An approach to manipulation: Part i - theory, part ii - implementation, part iii – applications", *Journal of Dynamic Systems, Measurement and Control*, 107:1-24, 1985.

[46] M. H. Raibert and J. J. Craig, "Hybrid position/force control of manipulators", *Journal of Dynamic Systems, Measurement, and Control*, 102, 1981.

[47] O. Khatib, "Dynamic Control of Manipulators in Operational Space", *6th IFToMM Congress on Theory of Machines and Mechanisms*, New Delhi, 1983.

[48] H. Asada and J. J. Slotine, *Robot Analysis and Control*, John Wiley and Sons, New York, 1985.

[49] M. Mason, "Compliance and force control for computer controlled manipulators", *IEEE Transactions on Systems, Man, and Cybernetics*, SMC-11(6):419-426, June 1981.

[50] M. W. Spong and M. Vidyasagar, *Robot Analysis and Control*, John Wiley & Sons, 1989.

[51] J. Pratt, *Virtual Model Control of a Biped Walking Robot*, Master's thesis, Massachusetts Institute of Technology, Electrical Engineering and Computer Science, May 1995.

[52] J. Pratt, A. Torres, P. Dilworth, and G. Pratt, "Virtual Actuator Control", *IROS*, Osaka, Japan, Nov. 3-9, 1996.

[53] J. Pratt and G. Pratt, "Intuitive Control of a Planar Bipedal Walking Robot", *ICRA*, 1998.

[54] H. Asada, "Manufacturing Robotics: Basic Issues and Challenges", *IFAC*, pages 319-330, San Francisco, CA, 1996.

[55] M. L. Aisen, H. I. Krebs, N. Hogan, F. McDowell, and B. T. Volpe, "The Effect of Robot-assisted Therapy and Rehabilitative Training on Motor Recovery Following Stroke", *Archives of Neurology*, 54:443-6, 1997.

[56] T. B. Sheridan, "Telerobotics", *Automatica*, 9(5):487-507, 1989.

[57] T. B. Sheridan, *Telerobotics, Automation, and Human Supervisory Control*, MIT Press, Cambridge, MA, 1992.

[58] G. Niemeyer, *Using Wave Variables in Time Delayed Force Reflecting Teleoperation*, PhD thesis, Massachusetts Institute of Technology, Aeronautics and Astronautics, 1996.

[59] J. K. Salisbury, "The Heart of Microsurgery", *Mechanical Engineering*, pages 46-51, Dec. 1998.

[60] J. K. Salisbury and M. A. Srinivasan, *Proceedings of The First PHANToM User's Group Workshop*, MIT AI Laboratory, 1996.

[61] J. K. Salisbury, "Making Graphics Physically Tangible", *Communications of the ACM*, 42(8):75-81, August 1999.

[62] M. H. Raibert, *Legged Robots That Balance*, MIT Press, Cambridge, MA., 1986.

[63] W. Hong, *Robotic Catching and Manipulation Using Active Vision*, Master's thesis, Massachusetts Institute of Technology, Mechanical Engineering, September 1995.

[64] M. S. Triantafyllou and G. S. Triantafyllou, "An Efficient Swimming Machine", *Scientific American*, 272(3):64-70, March 1995.

[65] B. Hannaford and J. Winters, "Actuator Properties and Movement Control: Biological and Technological Models", In Winters and Woo, editors, *Multiple Muscle Systmes: Biomechanics and Movement Organization*, pages 101-120, Springer-Verlag, 1990.

[66] J. Hollerbach, I. Hunter, and J. Ballantyne, "A Comparative Analysis of Actuator Technologies for Robotics", *Robotics Review 2*, pages 299-342, MIT Press, 1991.

[67] L. C. Hale and A. H. Slocum, "Design of Anti-backlash Transmissions for Precision Position Control Systems", *Precision Engineering*, 16(4):244-258, 1994.

[68] H. Asada and K. Youcef-Toumi, *Direct Drive Robots: Theory and Practice*, pp. 39, MIT Press, Cambridge, 1987.

[69] F. Aghili, M. Buehler, and J. M. Hollerbach, "Sensing the Torque in a Robot's Joints", *Mechanical Engineering*, pages 66-69, Sept. 1998.

[70] W. T. Townsend and J. K. Salisbury, "Mechanical Bandwidth as a Guideline to High-performance Manipulator Design", *IEEE International Conference on Robotics and Automation*, pages 1390-1395, Scottsdale, AZ, 1989.

[71] J. K. Salisbury, W. T. Townsend, B. S. Eberman, and D. M. DiPietro, "Preliminary Design of a Whole-arm Manipulation System (wam)", *Proceedings of 1988 IEEE International Conference on Robotics an d Automation*, Philadelphia, PA, April 1988.

[72] T. H. Massie, *Design of a Three Degree of Freedom Force-reflecting Haptic Interface*, Undergraduate Thesis, Massachusetts Institute of Technology, 1993.

[73] D. S. Barrett, *Propulsive Efficiency of a Flexible Hull Underwater Vehicle*, PhD thesis, Massachusetts Institute of Technology, Ocean Engineering, May 1996.

[74] M. S. Triantafyllou and G. S. Triantafyllou, "An efficient swimming machine", *Scientific American*, 272(3):64-70, March 1995.

[75] A. J. Madhani, *Design of Teleoperated Surgical Instruments for Minimally Invasive Surgery*, PhD thesis, Massachusetts Institute of Technology, Mechanical Engineering, 1998.

[76] D. Vischer and O. Khatib, "Design and Development of High-performance Torque-controlled Joints", *IEEE Transactions on Robotics and Automation*, 11(4):537-544, 1995.

[77] B. E. Berlinger, "Evoloid – A New Concept in High Ratio Gearing", *AGMA Paper*, 5(109.37), Oct. 1975.

[78] Electro-Craft Engineering Handbook. DC Motors, Speed Controls, and Servo Systems.

[79] J. M. Hollerbach, "A Recursive Lagrangian Formulation of Manipulator Dynamics and a Comparative Study of Dynamics Formulation Complexity", *IEEE Transactions on Systems, Man, and Cybernetics*, pages 730-736, November 1980.

[80] C. J. Murray, "All-in-one Hydraulics", *Design News*, pages 84-89, Nov. 15, 1999.

[81] F. Conrad and C. Jensen, "Design of Hydraulic Force Control Systems with State Estimate Feedback", *IFAC*, pages 307-312, Munich, Germany, 1987.

[82] A. Alleyne, "Nonlinear Force Control of an Electro-hydraulic Actuator", *Japan/USA Symposium on Flexible Automation*, 1:193-200, 1996.

[83] M. Pelletier and M. Doyon, "On the Implementation and Performance on Impedance Control on Position Controlled Robots", *IEEE Conference on Robotics and Automation*, pages 1228-1233, Atlanta, GA, 1994.

[84] B. Heinrichs, N. Sepehri, and A. B. Thornton-Trump, "Position-based Impedance Control of an Industrial Hydraulic Manipulator", *IEEE Control Systems Magazine*, 17(1):46-52, 1997.

[85] G. K. Klute, J. M. Czerniecki, and B. Hannaford, "Mckibben Artificial Muscles: Pneumatic Actuators with Biomechanical Intelligence", *IEEE/ASME Conference on Advanced Intelligent Mechatronics*, Atlanta, GA, Sept. 19-22, 1999.

[86] D. Brock and W. Lee, "Dynamic Model of a Linear Actuator Based on Polymer Hydrogel", *Journal of Intelligent Material Systems & Structures*, 5(6):764-771, Nov. 1994.

[87] R. Pelrine, R. Kornbluh, Q. Pei, and J. Joseph, "High-speed Electrically Actuated Elastomers with Strain Greater Than 100%", *Science*, 287:836-839, 4 February 2000.

[88] R. M. Alexander, *Elastic Mechanisms in Animal Movement*, Cambridge University Press, 1988.

[89] R. D. Howard, *Joint and Actuator Design for Enhanced Stability in Robotic Force Control*, PhD thesis, Massachusetts Institute of Technology, September 1990.

[90] G. A. Pratt and M. M. Williamson, "Series Elastic Actuators", *IEEE International Conference on Intelligent Robots and Systems*, 1:399-406, 1995.

[91] M. M. Williamson, *Series Elastic Actuators*, Master's thesis, Massachusetts Institute of Technology, June 1995.

[92] R. A. Brooks, C. Breazeal, M. Marjanovic, B. Scassellati, and M. Williamson, "The Cog Project: Building a Humanoid Robot", *Springer-Verlag Lecture Notes in Computer Science Volume*, 1999.

[93] M. M. Williamson, *Robot Arm Control Exploiting Natural Dynamics*, PhD thesis, Massachusetts Institute of Technology, June 1999.

[94] B. T. Krupp, *Design and Control of a Planar Robot to Study Quadrupedal Locomotion*, Master's thesis, Massachusetts Institute of Technology, Mechanical Engineering, 2000.

[95] J. B. Morrell, *Parallel Coupled Micro-macro Actuators*, PhD thesis, Massachusetts Institute of Technology, Mechanical Engineering, 1996.

[96] H. Hanafusa and H. Asada, "A Robotic Hand with Eleastic Fingers and Its Application to Assembly Process", *IFAC Symposium on Information and Control Problems in Manufacturing Technology*, pages 127-138, Tokyo, 1977.

[97] T. Sugar and V. Kumar, "Design and Control of a Compliant Parallel Manipulator for a Mobile Platform", *ASME Design Engineering Technical Conference*, September 13-16, Atlanta, GA, 1998.

[98] S. Sugano, S. Tsuto, and I. Kato, "Force Control of the Robot Finger Joint Equipped with Mechanical Compliance Adjuster", *International Conference on Intelligent Robots and Systems*, pages 2005-2012, 1992.

[99] J. K. Hodgins and M. H. Raibert, "Biped Gymnastics", *International Journal of Robotics Research*, September 13 1989.

[100] S. C. Jacobsen, C. C. Smith, D. K. Backman, and E. K. Iversen, "High Performance, High Dexterity, Force Reflective Teleoperator I", *ANS Topical Meeting on Robotics and Remote Systems*, 2:180-185, Washington, DC, November 1990.

[101] D. L. Wells, E. K. Iversen, C. C. Davis, and S. C. Jacobsen, "An Investigation of Hydraulic Actuator Performance Trade-offs Using a Generic Model", *IEEE International Conference on Robotics and Automation*, pages 2168-2173, May 13-18, 1990.

[102] J. J. Craig, *Introduction to Robotics*, Addison-Wesley Publishing, 1986.

[103] H. Asada and T. Kanade, "Design of Direct Drive Mechanical Arms", *ASME Journal of Vibration, Acoustics, Stress, and Reliability in Design*, 105(3):312-316, 1983.

[104] Y. Koren, *Robotics for Engineers*, McGraw-Hill Book Co., 1987.

[105] M. Zinn, O. Khatib, B. Roth, and J.K. Salisbury, "A New Actuation Approach for Human Friendly Robot Design", *Proceeding of the International Symposium on Experimental Robotics*, Sant'Angelo d'Ischia, Italy, 2002.

[106] J. B. Morrel, *Parallel Coupled Micro-Macro Actuators*, PhD thesis, Massachusetts Institute of Technology, Cambridge, MA, 1996.

[107] K. J. Waldron and A. Kumar, "The Dexterous Workspace", *ASME Paper No. 80-DET-108*, Presented at the ASME Mechanisms Conference, Los Angeles, 1980.

[108] K. C. Gupta and B. Roth, "Design Considerations for Manipulator Workspace", *ASME Paper No. 81-DET-79*, 1981.

[109] S. Chiaverini, "Singularity-robust Task-Priority Redundancy Resolution for Real-time Kinematic Control of Robot Manipulators", *IEEE Transactions on Robotics and Automation*, 13:398-410, 1997.

[110] R. G. Roberts, "Singularities, Stable Surface, and the Repeatable Behavior of Kinematically Redundant Manipulators", *International Journal of Robotics Research*, 13(1):70-81, 1994.

[111] A. McLean and S. Cameron, "The Virtual Springs Method: Path Planning and Collision Avoidance for Redundant Manipulators", *International Journal of Robotics Research*, 15:300-319, 1996.

[112] S. Hirose, "Connected Differential Mechanism and Its Applications", *Proceedings of '85 International Conference on Advanced Robotics*, Tokyo, 1985.

[113] K. J. Waldron and J. Reidy, "A Study of a Kinematically Redundant Manipulator Structure", *Proceedings of the IEEE International Conference on Robotics and Automation*, San Francisco, pages 1-8, 1986.

[114] C. Chen and C. Lin, "Motion Planning of Redundant Robots", *Journal of Robotics Systems*, 14(12):839-850, 1997.

[115] J. D. English and A. A. Maciejewski, "Fault Tolerance for Kinematically Redundant Manipulators Anticipating Free-swinging Joint Failures", *IEEE International Conference on Robotics and Automation*, Minneapolis, pages 460-467, 1996.

[116] H. S. Lee and M. Tomizuka, "Robust Motion Controller Design for High-accuracy positioning Systems", *IEEE Transactions on Industrial Electronics*, 12:543-552, 1996.

[117] J. M. Hollerbach and K. C. Suh, "Redundancy Resolution of Manipulators through Torque Optimization", *IEEE International Conference on Robotics and Automation*, St. Louis, pages 1016-1021, 1985.

[118] P. Chiacchio, S. Chiaverini, L. Sciavicco, and B. Siciliano, "Closed-loop Inverse Kinematic Schemes for Constrained Redundant Manipulators with Task Space Augmentation and Task Priority Strategy", *International Journal of Robotics Research*, 10:410-425, 1991.

[119] C. A. Klein and K. Kee, "The Nature of Drift in Pseudoinverse Control of Kinematically Redundant Manipulators", *IEEE Transactions on Robotics and Automation*, 5:231-234, 1989.

[120] C. A. Klein and C. H. Hung, "Review of the Pseudoinverse for Control of Kinematically Redundant Manipulators", *IEEE Transactions on Systems, Man and Cybernetics*, 1983.

[121] H. Ashrafiuon and F. Maghami, "Analysis of Hyper-redundant Manipulators", *Proceeding of the ASME Design Engineering Technical Conferences*, Las Vegas, Nevada, pages 1-12, September 1999.

[122] J. Lenarcic, "On Hyper-redundant Multiple-link Robots", *Laboratory Robotics and Automation*, John Wiley Inc., 1996.

[123] G. S. Chirikijian and J. W. Burdick, "An Obstacle Avoidance Algorithm for Hyper-redundant Manipulators", *IEEE International Conference on Robotics and Automation*, Cincinnati, OH, 1990.

[124] R. Ambrose, *Design, Construction and Demonstration of Modular, Reconfigurable Robots*, PhD Thesis, University of Texas at Austin, U.S.A., 1991.

[125] I.-M. Chen and G. Yang, "Configuration Independent Kinematics for Modular Robots", *IEEE Conference on Robotics and Automation*, pages 1440-1445, 1996.

[126] R. Cohen, M. Lipton, M. Dai, and B. Benhabib, "Conceptual Design of a Modular Robot", *ASME Journal of Mechanical Design*, (114):117-125, March 1992.

[127] T. Fukuda and S. Nakagawa, "Dynamically Reconfigurable Robotic System", *IEEE International Conference on Robotics and Automation*, pages 1581-1586, 1988.

[128] C. Paredis, H. Brown, R. Casciola, J. Moddy, and P. Khosla, "A Rapidly Deployable Manipulator System", *International Workshop on Some Critical Issues in Robitics*, Singapore, pages 175-185, 1995.

[129] K. Wurst, "The Conception and Construction of a Modular Robot System", *International Symposium on Industrial Robotics*, pages 37-44, 1986.

[130] T. Matsumaru, "Design and Control of the Modular Robot System: TOMMS", *IEEE International Conference on Robotics and Automation*, pages 2125-2131, 1995.

[131] D. Schmitz, P. Khosla, and T. Kanade, "The CMU Reconfigurable Modular Manipulator System", *Technical Report CMU-RI-TR-88-7*, Carnegie Mellon University, 1988.

[132] M. Li and M. Xie, "A New Light Weight Robot Arm and Its Design Philosophy", *The Second International Conference on Computational Intelligence, Robotics and Autonomous Systems*, Singapore, 2003.

[133] Y. Ishii, T. Fukuzawa, Y. Ichikawa, M. Suzuki, S. Naito, and N. Iwatsuka, "A Joint Connection Mechanism and Control System for a Reconfigurable Manipulator", *SICE'92*, pages 1095-1098, 1992.

[134] M. Yim, "A Reconfigurable Modular Robot with Many Modes of Locomotion", *Proceeding of the JSME International Conference on Advanced Mechatronics*, Tokyo, Japan, pages 283-288, 1993.

[135] I.-M. Chen and J. W. Burdick, "Determining Task Optimal Modular Robot Assembly Configurations", *Proceedings of the IEEE International Conference on Robotics and Automation*, pages 132-137, 1995.

[136] I.-M. Chen and G. Yang, "Automatic Generation of Dynamics for Modular Robots with Hybrid Geometry", *Proceedings of the IEEE International Conference on Robotics and Automation*, Albuquerque, New Mexico, pages 2288-2293, April 1997.

[137] I.-M. Chen and G. Yang, "Inverse Kinematics for Modular Reconfigurable Robots", *Proceedings of the IEEE International Conference on Robotics and Automation*, Leuven, Belgium, pages 1647-1652, May 1998.

[138] T. T. Kadota and H. C. Bourne, "Stability Conditions of Pulse-width-modulated Systems through the Second Method of Lyapunov", *IRE Transactions on Automatic Control*, 6:266-276, September 1961.

[139] F. R. Delfeld and G. J. Murphy, "Analysis of Pulse-width-modulated Control Systems", *IRE Transactions on Automatic Control*, 6:283-292, September 1961.

[140] G. J. Murphy, "A Stability Criterion for Pulse Width Modulated Feedback Control Systems", *IEEE Transactions on Automatic Control*, 10:434-441, 1964.

[141] R. A. Skoog, "On the Stability of Pulse-width-modulated Feedback Systems", *IEEE Transactions on Automatic Control*, AC-13(5):532-538, October 1968.

[142] R. A. Skoog and G. L. Blankenship, "Generalized Pulse-modulated Feedback Systems; Norms, Gains, Lipschitz Constants, and Stability", *IEEE Transactions on Automatic Control*, AC-15(3):300-315, June 1970.

[143] H. Sira-Ramirez, "Differential Geometric Methods in Variable-structure Control", *International Journal of Control*, 48(4):1359-1390, 1988.

[144] H. Sira-Ramirez, "Sliding-mode Control on Slow Manifolds of DC-to-DC Power Converters", *International Journal of Control*, 47(5):1323-1340, 1988.

[145] H. Sira-Ramirez, M. Zribi, and S. Ahmad, "Pulse Width Modulated Control of Robotic Manipulator", *International Journal of Systems Science*, 24(8):1423-1437, 1993.

[146] S. Choi and D.-W. Cho, "Control of Wheel Slip Ratio Using Mode Controller with Pulse Width Modulation", *Journal of Vehicle System Dynamics*, (32):267-284, 1999.

[147] S.-S. Han, S.-B. Choi, and C.-C. Cheong, "Position Control of x-y Table Mechanism Using Electro-rheological Clutches", *Journal of Mechanism and Machine Theory*, (35):1563-1577, 2000.

[148] S. P. Monckton, *Multi-agent Manipulator Control*, PhD Thesis, Department of Mechanical Engineering, The University of British Columbia, 1997.

[149] D. Cherchas and S. Monckton, "Jacobian Transpose Control: A Foundation for Multi-agent Manipulator Control", *IEEE Transactions on Systems, Man and Cybernetics*, pages 3391-3396, October 1995.

[150] O. Khatib, "Real Time Obstacle Avoidance for Manipulators and Mobile Robots", *Proceedings IEEE International Conference on Robotics and Automation*, 1985.

[151] H. Karbasi, J. P. Huissoon, and A. Khajepour, "Experimental and Theoretical Analysis of a Uni-drive Modular Robot: Design and Modeling", *Proceedings of DETC/CIE 27th ASME Biennial Mechanisms and Robotics Conference*, Montreal, Canada, 29 September –2 October 2002.

[152] H. Karbasi, A. Khajepour, J. P. Huissoon, and S. J. Park, "A New Modular Robot: Uni-drive with Pulse Width Modulation Control", *Proceedings of the IASTED International Conference on Robotics and Applications*, (ISBN: 0-88986-313-x):101 –105, November 2001.

[153] S. L. Chang and L. W. Tsai, "Synthesis and Analysis of Geared Robotic Mechanisms", *Proceddings of the 1989 IEEE International Conference on Robotics and Automation*, 2, pp. 920-927, Scottsdale, AE, USA, 1989.

[154] C. C. Lin and L. W. Tsai, "The Development of an Atlas of Beverl-gear-type Spherical Wrist Mechanisms", *Proceddings of the First National Conference on Applied Mechanisms and Robotics*, paper No. 89AMR-2A-3., Cincinnati, OH, USA

[155] A. F. Filippov, "Differential Equations with Discontinuous Right-hand Sides", In F. M. Arscott, editor, *Mathematics and Its Applications*, Kluwer Academic Publishers, 1988.

[156] H. Sira-Ramirez, "A Geometric Approach to Pulse-width Modulated Control in Nonlinear Dynamical Systems", *IEEE Transactions on Automatic Control*, 34(2):184-187, February 1989.

[157] H. Sira-Ramirez, "Nonlinear Pulse-Width-Modulation Controller Design", Capitulo 3, pp. 33-58, *Variable Structure Control for Robotics and Aerospace Applications*, Edited by K. K. Young, Elsevier Science Publishers, Amsterdam, Holland, 1993.

[158] V. I. Utkin, "Variable Structure Systems with Sliding Mode", *IEEE Transactions on Automatic Control*, AC-22(2):212-222, 1977.

[159] H. Sira-Ramirez, "Pulse-frequency-modulation Control of Nonlinear Systems", *Control Theory and Advanced Technology*, 9(4):935-945, 1993.

[160] M. La Cava, G. Paletta, and C. Picardi, "Stability Analysis of PWM Feedback Control Systems with PID Regulators", *International Journal of Control*, 39(5):987-1005, 1984.

[161] R. Marino, "High-gain Feedback in Non-linear Control Systems", *International Journal of Control*, 42(6):1369-1385, 1985.

[162] J. M. Gere and S. P. Timoshenko, *Mechanics of Materials*, PWS-KENT Publishing Company, Boston, MA., 1990.

[163] K. Ogata, *Modern Control Engineering*, Prentice Hall, 1990.

[164] J.-J. E. Slotine and W. Li, *Applied Nonlinear Control*, Prentice-Hall, Cambridge, MA., 1991.

[165] N. Hogan, "Impedance Control: An Approach to Manipulation: Part I – Theory, Part II – Implementation, Part III – Applications", *Journal of Dynamic Systems, Measurement and Control*, 107:1-24, 1985.

[166] A. H. Slocum, *Precision Machine Design*, Society of Manufacturing Engineers, 1992.

[167] D. W. Robinson, *Design and Analysis of Series Elasticity in Closed-loop Actuator Force Control*, PhD thesis, MIT, June 2000.

[168] G. R. Slemon and A. Straughen, *Electric Machines*, Addison-Wesley, 1980.

[169] G. R. Slemon, *Electric Machines and Drives*, Addison-Wesley, 1992.

[170]T. A. McMahon, *Muscles, Reflexes, and Locomotion*, Princeton, NJ: Princeton Univ. Press, 1984.

[171] V. T. Inman, H. J. Ralston, and F. Todd, *Human Walking*, Baltimore, MD: Willams & Wilkins, 1981.

[172] C. Chevallereau and B. Perrin, "Computed Torque Control Law Under Constraints for Single and Double Support Motion of Plannar Biped Robot", *4th ECPD International Conference on Advanced Robot, Intelligent Automation and Active Systems*, Moscow, Russia, 1998.

[173] J. F. Gardner, K. Srinivasan, and K. J. Waldron, "A Solution for the Force Distributio Problem in Redundantly Actuated Closed Kinematic Chain", *Journal of Dynamic Systems, Measurement, and Control*, vol. 112, pp. 523-526, 1990.

[174] A. Dasgupta and Y. Nakamura, "Making Feasible Walking Motion of Humanoid Robots From Human Motion Capture Data", *IEEE International Conference on Robotics and Automation*, Detroit, US, 1999.

[175] Q. Li, A. Takanishi, and I. Kato, "Learning Control of Compensative Trunk Motion for Biped Walking Robot based on ZMP Stability Criterion", *Journal of the Robotics Society of Japan*, Vol. 11, No. 4, pp. 77-83, 1993.

[176] M. Li, *Study of Augmented Robot Mobility with Humanoid and Two-wheeled Vehicle*, PhD First Year Report, Nanyang Technological University, 2002.

[177] A. Katz, *The Design and Applications of a Non-linear Series Compliance Actuator for Use in Robotic Arms*, Master's thesis, MIT, Mechanical Engineering, September 1999.

[178] J. K. Salisbury, *Kinematic and Force Analysis of Articulated Hands*, PhD thesis, Standford University, Deparment of Mechancial Engineering, May 1982.

[179] V. K. Shah, *Design and Control of a Nonlinearly Compliant Robotic Finger*, Master's thesis, MIT, Mechancial Engineering, September 1997.

[180] H. K. Khalil, *Nonlinear Systems*, Prentice-Hall Inc., Upper Saddle River, NJ 07458, USA, Third Edition, 2002.